ABSTRACT

IN-BEAM γ-RAY SPECTROSCOPY OF EXCITED STATES

IN ODD-MASS N=80 NUCLEI

By

Rahmat Aryaeinejad

The level structure of the N=80 nuclei, ^{143}Eu, ^{141}Pm, and ^{139}Pr have been studied using the techniques of in-beam γ-ray spectroscopy. The data were obtained by measuring γ-ray singles spectra, excitation functions (in ^{143}Eu case), prompt and delayed γ-γ coincidences, and angular distributions of the γ-rays, following the $(p,2n\gamma)$ and $(\alpha,4n\gamma)$ reactions. In all of these experiments, high resolution Ge(Li) detectors were used. For most of the levels in these nuclei, spin and parity values could unambiguously be attributed on the basis of the angular distribution data from this work and inputs from previous β-decay data (conversion electron data and logft values).

Levels in ^{143}Eu were populated by the ^{144}Sm$(p,2n\gamma)^{143}$Eu reaction. A total of 37 γ-rays deexciting from 30 states was assigned in ^{143}Eu. The calculations were performed to explain the resulting level structure in ^{143}Eu in terms of a triaxial weak-coupling model for both prolate and oblate deformations. These calculations indicate that ^{143}Eu has a slight oblate deformation.

The $(p,2n\gamma)$ and $(\alpha,4n\gamma)$ reactions were used to investigate the excited states in ^{141}Pm and ^{139}Pr. The half-life of the 628.6 keV isomeric state ($^{11}/_{2}^{-}$) in ^{141}Pm was measured to be 0.63±0.02 μs. In addition,

another isomeric state was found in ^{141}Pm at 2530.9 keV from (α,4nγ) reaction. The accurate measurement of the half-life for this state was not possible from present work, but estimated to be more than 2 μs.

The resulting level structure observed in ^{141}Pm and ^{139}Pr are explained quite satisfactorily within the limits of a triaxial weak-coupling model.

Finally, a survey was made of all of the energy state systematics of the low energy levels (below 3 MeV) of odd-mass N=80 isotones. From these observations, some predictions and suggestions for future experiments have been made.

IN-BEAM γ-RAY SPECTROSCOPY OF EXCITED STATES IN ODD-MASS N=80 NUCLEI

By

Rahmat Aryaeinejad

A DISSERTATION

Submitted to

Michigan State University

in partial fulfillment of the requirements

for the degree of

DOCTOR OF PHILOSOPHY

Department of Chemistry

1980

ACKNOWLEDGEMENTS

I sincerely wish to thank Dr. Wm. C. McHarris for suggesting this region of study. His expert guidance and patience during the experimental work and preparation of this thesis are greatly appreciated.

I also wish to thank Dr. A. Galonsky for his careful review of this thesis and his helpful suggestions.

Dr. Richard B. Firestone deserves my sincerest gratitude for his never-ending words of encouragement and his special advice.

I further wish to acknowledge Dr. Philip Walker for providing many useful discussions and advice during the latter part of this study.

Mr. W. H. Bentley has provided stimulating discussions and advice throughout the data acquisition and analysis.

Finally, I particularly wish to thank Judy Schmidt for typing the final copy of this thesis under the usual pressure of a deadline and for her editorial suggestions.

TABLE OF CONTENTS

Page

LIST OF TABLES..... vii

LIST OF FIGURES..... viii

CHAPTER

I. INTRODUCTION..... 1

II. THEORETICAL CONSIDERATION..... 3

2.1. Description of the Total Hamiltonian..... 4

2.2. Properties of the Triaxial Core..... 7

2.3. The Model Parameters and Their Determination..... 11

III. EXPERIMENTAL APPARATUS AND METHOD..... 14

3.1. Singles Experiments..... 14

3.2. Coincidence Experiments..... 15

3.3 Angular Distribution Experiments..... 18

IV. CHAPTER IV..... 21

4.1. Experimental Details and Results for the $(p,2n\gamma)$ Reaction..... 21

4.1.1. Target and Reaction..... 21

4.1.2. γ-Ray Singles Spectra..... 24

4.1.3. Excitation Functions..... 24

4.1.4. Coincidence Spectra..... 28

4.1.5. γ-Ray Angular Distributions..... 33

4.1.6. The ^{143}Eu Level Scheme..... 33

4.2. Triaxial Calculations and Discussion..... 44

4.2.1. Single-Particle States..... 44

Page

4.2.2. Negative-Parity Collective States..... 45

4.2.3. Positive-Parity Collective States..... 48

V. ^{139}Pm EXPERIMENTAL RESULTS AND DISCUSSION..... 51

5.1. Experimental Details and Results for the $(p,2n\gamma)$ Reaction..... 51

5.1.1. Target and Reaction..... 51

5.1.2. γ-Ray Singles Spectra..... 51

5.1.3. Coincidence Spectra..... 52

5.1.4. γ-Ray Angular Distributions..... 57

5.2. Experimental Details and Results for the $(\alpha,4n\gamma)$ Reaction..... 60

5.2.1. Target and Reaction..... 60

5.2.2. γ-Ray Singles Spectra..... 62

5.2.3. Coincidence Spectra..... 67

5.2.4. γ-Rays Angular Distributions..... 67

5.3. Construct of the ^{141}Pm Level Scheme and Comparison..... 70

5.3.1. Level Scheme and Spin-Parity Assignments from $(p,2n\gamma)$ Reaction..... 70

5.3.2. Level Scheme and Spin-Parity Assignments from $(\alpha,4n\gamma)$ Reaction..... 78

5.3.3. Comparison Between the $(p,2n\gamma)$ and $(\alpha,4n\gamma)$ Reaction and with Other Experimental Results.... 85

5.4. Discussion of Level Configurations..... 88

5.4.1. Single-Quasiparticle States..... 88

5.4.2. Negative-Parity Collective States..... 88

5.4.3. Positive-Parity Collective States..... 89

VI. CHAPTER VI

6.1. Experimental Details and Results for the $(p,2n\gamma)$ Reactions..... 91

Page

6.1.1. Target and Reaction..... 91

6.1.2. γ-Ray Singles Spectra..... 92

6.1.3. Coincidence Spectra..... 92

6.1.4. γ-Ray Angular Distributions..... 97

6.2. Experimental Details and Results for (α,4nγ) Reaction...101

6.2.1. Target and Reaction.....101

6.2.2. γ-Ray Singles Spectra.....101

6.2.3. Coincidence Spectra.....103

6.2.4. γ-Rays Angular Distributions.....108

6.3. Construct of the ^{139}Pr Level Scheme and Comparison.....113

6.3.1. Level Scheme and Spin-Parity Assignments from (*p*,2nγ) Reaction.....113

6.3.2. Level Scheme and Spin-Parity Assignment for (α,4nγ) Reaction.....119

6.3.3. Comparison Between the (*p*,2nγ) and (α,4nγ) Reaction and with Other Experimental Results....122

6.4. Discussion of Level Configurations.....122

6.4.1. Single-Quasiparticle States.....122

6.4.2. Negative-Parity Collective States.....125

6.4.3. Positive-Parity Collective States.....126

VII. SYSTEMATICS OF THE ODD-MASS *N*=80 NUCLEI.....128

VIII. SUMMARY AND CONCLUSIONS.....132

BIBLIOGRAPHY.....134

APPENDICES.....138

A. Gated Coincidence Spectra of Transitions in ^{143}Eu.....138

B. Angular Distribution Plots of ^{143}Eu Transitions.....144

C. Gated Coincidence Spectra of Transitions in ^{141}Pm from (*p*,2nγ) Reaction.....149

Page

D. Angular Distribution Plots of ^{141}Pm Transitions from (p,2$n\gamma$) Reaction.....154

E. Gated Coincidence Spectra of Transitions in ^{141}Pm from (α,4$n\gamma$) Reaction.....161

F. Angular Distribution Plots of ^{141}Pm Transitions from (α,4$n\gamma$) Reaction.....167

G. Gated Coincidence Spectra of Transitions in ^{139}Pr from (p,2$n\gamma$) Reaction.....173

H. Angular Distribution Plots of ^{139}Pr Transitions from (p,2$n\gamma$) Reaction.....179

I. Gated Coincidence Spectra of Transitions in ^{139}Pr from (α,4$n\gamma$) Reaction.....185

J. Angular Distribution Plots of ^{139}Pr Transitions from (α,4$n\gamma$) Reaction.....206

LIST OF TABLES

Table		Page
4-1.	Energies, relative intensities, angular distribution coefficients, and multipolarities for γ transitions in ^{143}Eu from $(p,2n\gamma)$ reactions	26
4-2.	Summary of coincidence results for the ^{144}Sm$(p,2n\gamma)$ ^{143}Eu reaction	31
5-1.	Energies, relative intensities, angular distribution coefficients, and multipolarities for γ transitions in ^{141}Pm from $(p,2n\gamma)$ reactions	55
5-2.	Summary of coincidence results for the ^{142}Nd$(p,2n\gamma)$ ^{141}Pm reaction	58
5-3.	Energies, relative intensities, angular distribution coefficients, and multipolarities for γ transitions in ^{141}Pm from $(\alpha,4n\gamma)$ reactions	65
5-4.	Summary of coincidence results for the ^{141}Pr$(\alpha,4n\gamma)$ ^{141}Pm reaction	68
6-1.	Energies, relative intensities, angular distribution coefficients, and multipolarities for γ transitions in ^{139}Pr from $(p,2n\gamma)$ reactions	94
6-2.	Summary of coincidence results for the ^{140}Ce$(p,2n\gamma)$ ^{139}Pr reaction	99
6-3.	Energies, relative intensities, angular distribution coefficients, and multipolarities for γ transitions in ^{139}Pr from $(\alpha,4n\gamma)$ reactions	105
6-4.	Summary of coincidence results for the ^{139}La$(\alpha,4n\gamma)$ ^{139}Pr reaction	110

LIST OF FIGURES

Figure

Page

2-1. Vector diagram of a particle coupled to a rotating core..... 5

2-2. Irrotational moments of inertia as functions of γ..... 8

2-3. Low-energy spectrum of an even triaxial core as a function of γ..... 10

3-1. "FAST-SLOW" coincidence diagram..... 16

3-2. The goniometer facility, showing the activation chamber and detector mounting..... 19

4-1. Excitation functions calculated by the evaporation code ALICE for p's on a ^{144}Sm target. Note that there are two curves for each of the Pm isotopes, one for the evaporation of an α particle, the other for evaporation of $2n + 2p$..... 22

4-2. In-beam singles γ-ray spectrum from the reaction, ^{144}Sm$(p,2n\gamma)^{143}$Eu, taken with the 10%-efficient Ge(Li) detector placed at 125°..... 25

4-3. Excitation functions for seven of the more prominent ^{143}Eu γ rays..... 29

4-4. In-beam γ-γ coincidence spectra for the reaction, ^{144}Sm$(p,2n\gamma)^{143}$Eu. The integral coincidence spectrum ("all events") is shown at the top, and three representative smoothed gated spectra are shown underneath..... 30

4-5. Four representative angular distributions of ^{143}Eu γ rays, together with their fits calculated by the code GADFIT. The points correspond to 90° and the backward angles, 100°, 110°, 125°, 140°, and 155°..... 34

4-6. ^{143}Eu level scheme as determined by the ^{144}Sm$(p,2n\gamma)$ ^{143}Eu reaction. The asterisks before $^{\pi}$ assignments indicate that we relied heavily on the ^{143}Gd^{m+g} β^+/ε decay [Fi78] for these assignments. Also, the dashed γ transitions are weak transitions seen in ^{143}Gd^{m+g} decay but not seen in our in-beam studies; however, they originate from levels seen in the in-beam studies. It should be noted that there are two 1059.3-keV transitions in this level scheme..... 36

Figure

Page

4-7. Decay schemes of $^{143}Gd^{g}$ and $^{143}Gd^{m}$ from Ref. [Fi78] for comparison with our in-beam studies..... 37

4-8. Energies of calculated excited negative-parity states in ^{143}Eu compared with our experimental findings. We calculated these energies using a triaxial weak-coupling model, coupling the $\pi h_{11/2}$ state to a deformed core. Results for both prolate and two different oblate deformations are shown; a slight oblate deformation seems indicated. Spins are shown in $2J$..... 47

4-9. Energies of calculated excited positive-parity states in ^{143}Eu compared with our experimental findings. We calculated these energies using a triaxial weak-coupling model, coupling both the $\pi d_{5/2}$ and $\pi g_{7/2}^{-1}$ states to an oblately deformed core. Spins are shown in 2 49

5-1. γ-ray singles spectrum of $^{142}Nd(p,2n\gamma)^{141}Pm$ taken with the 17%-efficient Ge(Li) detector placed at 125°..... 53

5-2. A detector efficiency curve for a 17%-efficient Ge(Li) detector with a source detector distance of 20 cm..... 54

5-3. Excitation functions for $^{141}Pr(\alpha,xn)$ reactions, calculated using the code CS8N..... 61

5-4. γ-ray singles spectrum of $^{141}Pr(\alpha,4n\gamma)^{141}Pm$ taken with 7.7%-efficient Ge(Li) detector placed at 125°..... 63

5-5. A detector efficiency curve for a 7.7%-efficient Ge(Li) detector with a source detector distance of 20 cm..... 64

5-6. Level scheme of ^{141}Pm obtained from $(p,2n\gamma)$ reaction..... 71

5-7. Level scheme of ^{141}Pm obtained from $(\alpha,4n\gamma)$ reaction..... 79

5-8. Delayed coincidence spectrum. This spectrum enhances those transitions that feed directly or indirectly into the 628.6-keV state ($t_{1/2}$ = 0.63 μsec) in ^{141}Pm..... 81

5-9. Time axis projection on a semi-logarithmic plot illustrating the half-life of 628.6-keV state in ^{141}Pm..... 82

Figure

Page

5-10. Energy levels of ^{141}Pm. Levels in columns 1 and 2 are from present work while levels in column 3 are from β-decay. Spins are shown in $2J$..... 86

6-1. γ-ray singles spectrum of ^{140}Ce$(p,2n\gamma)^{141}$Pm taken with the 17%-efficient Ge(Li) detector placed at 125°..... 93

6-2. Delayed coincidence spectrum. This spectrum enhances those transitions that feed into the 822.0-keV state ($t_{1/2}$ = 36 nsec) and 113.9-keV ($t_{1/2}$ = 2.6 nsec) in ^{139}Pr from $(p,2n\gamma)$ reaction..... 98

6-3. γ-ray singles spectrum of ^{139}La$(\alpha,4n\gamma)^{139}$Pr taken with 7.7%-efficient Ge(Li) detector placed at 125°.....102

6-4. Low energy γ-ray singles spectrum of ^{139}La $(\alpha,4n\gamma)^{139}$Pr taken with a small volume planar Ge(Li) detector placed at 90°.....104

6-5. Delayed coincidence spectrum. This spectrum enhances those transitions that feed into 822.0-keV state ($t_{1/2}$ = 36 nsec) in ^{139}Pr from $(\alpha,4n\gamma)$ reaction.....109

6-6. Level scheme of ^{139}Pr obtained from $(p,2n\gamma)$ reaction.....114

6-7. Level scheme of ^{139}Pr obtained from $(\alpha,4n\gamma)$ reaction.....120

6-8. Energy levels of ^{139}Pr. Levels in columns 1 and 2 are from present work while levels in column 3 are from β-decay [Be69, Bu71] and levels in column 4 are from scattering reaction [Go72]. Spins are shown in $2J$.....123

7-1. The position of known states in odd-mass N=80 isotones. The data for ^{133}I, ^{135}Cs, and ^{137}La are from β-decay or a combination of β-decay and in-beam studies. The ^{139}Pr, ^{141}Pm, and ^{143}Eu data are from the present in-beam study. The states in ^{139}Pr above 3 MeV from $(\alpha,4n\gamma)$ reaction are not shown in this figure. Also, spins are shown in $2J$.....129

A. Gated spectra of transitions in ^{143}Eu from $(p,2n\gamma)$ reaction. Background subtraction using the adjacent continuum has been

Figure

Page

included. The spectra are arranged according to increasing energy.....138

B. Angular distribution plots of ^{143}Eu transitions obtained from (p,2$n\gamma$) reaction. The data were taken in the 90-180° quadrant.....144

C. Integral coincidence and gated spectra of transitions in ^{141}Pm from (p,2$n\gamma$) reaction. Background subtraction using the adjacent continuum has been included. The spectra are arranged according to increasing energy.....149

D. Angular distribution plots of ^{141}Pm transitions obtained from (p,2$n\gamma$) reaction. The data were taken in the 90-180° quadrant.....154

E. Integral coincidence and gated spectra of transitions in ^{141}Pm from (α,4$n\gamma$) reaction. Background subtraction using the adjacent continuum has been included. The spectra are arranged according to increasing energy.....161

F. Angular distribution plots of ^{141}Pm transitions obtained from (α,4$n\gamma$) reaction. The data were taken in the 90-180° quadrant.....167

G. Integral coincidence and gated spectra of transitions in ^{139}Pr from (p,2$n\gamma$) reaction. Background subtraction using the adjacent continuum has been included. The spectra are arranged according to increasing energy.....173

H. Angular distribution plots of ^{139}Pr transitions obtained from (p,2$n\gamma$) reaction. The data were taken in the 90-180° quadrant.....179

I-1. Y-integral coincidence and Y-gated spectra (identifying high energy coincidences) of transitions in ^{139}Pr from (α,4$n\gamma$) reaction. Background subtraction using the adjacent continuum has been included. The spectra are arranged according to increasing energy.....185

I-2. X-integral coincidence and X-gated spectra (identifying low energy coincidences) of transitions in ^{139}Pr from (α,4$n\gamma$) reaction. Background subtraction using the adjacent continuum has been included. The spectra are arranged according to increasing energy.....197

Figure

Page

J. Angular distribution plots of ^{139}Pr transitions obtained from $(\alpha,4n\gamma)$ reaction. The data were taken in the 90-180° quadrant.....206

CHAPTER I

INTRODUCTION

One of the more interesting regions of the nuclidic chart for current study is the region immediately below the N=82 closed shell. Here long chains of isotones are amenable for study, encompassing both neutron-excess and neutron-deficient nuclei; a wealth of $M4$ and other isomers is available; and a large number of targets is available for cross-comparison in various in-beam experiments. The neutron-deficient N=80 isotones are among the most interesting of these nuclei because, although they lie close to the major closed shell, they lie at a considerable distance from stability. Thus, they are transitional nuclei: They contain many well-defined shell-model states, but they lie near the edge of the onset of deformation, so many of their higher-lying states can be characterized not only as multiple particle states, but also as (deformed) collective states. Also, the juxtaposition of the $h_{11/2}$ shell-model state with various low-spin states leads to a wealth of both high- and low-spin states in these nuclei.

The level structures of ^{143}Eu, ^{141}Pm, and ^{139}Pr have been investigated in this thesis, using the techniques of in-beam γ-ray spectroscopy. Levels in ^{143}Eu were populated by the $(p,2n\gamma)$ reaction only, whereas levels in ^{141}Pm and ^{139}Pr were populated by both $(p,2n\gamma)$ and $(\alpha,4n\gamma)$ reactions. These supplement and complement other previous studies of states in these same nuclides excited by β^+/ε decay. The in-beam experiments also tended to excite higher-spin states than those known from existing β-decay data.

High-resolution single γ-ray spectra, excitation functions for the various γ-rays (only in the case of ^{143}Eu), prompt and delayed γ-γ coincidences and angular distributions of the γ-rays in these nuclei were measured in an effort to elucidate their level schemes in as much detail as possible. This information would be of great value for the testing of existing nuclear models which could describe the resulting level structure of these nuclei. Generally, because of the weak deformation of the nuclei in this region, weak-coupling features of the level schemes are expected.

In the case of ^{143}Eu, calculations were performed to explain the resulting level structure in terms of a triaxial weak-coupling model for both prolate and oblate deformations. These calculations indicate that ^{143}Eu has a slight oblate deformation.

The structure of the thesis will be divided into eight chapters:

Chapter II discusses the theory of triaxial weak-coupling model, used in this study.

Chapter III describes the many types of experimental set-ups used during the course of present investigations.

Chapter IV describes the experimental and theoretical results of ^{143}Eu obtained from the $(p,2n\gamma)$ reaction.

Chapters V and VI describe the experimental results of ^{141}Pm and ^{139}Pr, respectively, obtained from both $(p,2n\gamma)$ and $(\alpha,4n\gamma)$ reactions.

In Chapter VII , the systematic behavior of some of the nuclear properties in the odd-mass N=80 region are discussed. Finally, the summary and conclusion will be found in Chapter VIII.

CHAPTER II

THEORETICAL CONSIDERATION

Since the collective model works so well for even-even nuclei in many regions of the periodic table, it is natural to attempt to extend it to odd-mass nuclei in these regions. If the properties of the even-mass isotopes are well explained by collective motions of all the particles, one would expect that the addition of an extra particle should lead to a behavior resembling that of the even-mass core but modified by the presence of the extra particle.

Some of the publications [He62] used an adiabatic approximation which considers the odd nucleon to be in a definite single-particle state. This approximation is certainly inadequate for weakly deformed nuclei, where the odd nucleon is coupled to the intrinsic shape. Pashkevich and Sardarian [Pa65] were the first to perform the calculation proposing that the model contains the weak-coupling limits as well as the strong-coupling limit and also could describe the various intermediate regions.

The model investigated in this study consists of an odd nucleon coupled to a rotating triaxial core. The odd nucleon is considered as a quasiparticle that represents either a particle or a hole or a superposition of both. For the most part the summary of the particle or hole-core coupling treatment follows a more detailed presentation of Meyer-ter-Vehn [Me75].

2.1. Description of the Total Hamiltonian

The angular momentum of odd-A deformed nuclei is due both to the rotational angular momentum of the core (or whole) and to the angular momentum of the odd nucleon. Figure 2-1 shows a vector diagram of an odd-A deformed nucleus consisting of a single particle coupled to a rotating core. According to this figure, a rotor with angular momentum $\vec{R}$, representing the core of the nucleus, is coupled to the angular momentum $\vec{j}$ of a single particle to form a total angular momentum $\vec{I}$. The total angular momentum $\vec{I}$ has the component M along the fixed axis Z and the component K along the nuclear symmetry axis 3. The projection of $\vec{j}$ on the nuclear symmetry 3-axis is Ω. In the axially-symmetric case, the core angular momentum $\vec{R}$ is perpendicular to the 3-axis, and the total angular momentum $\vec{I}$ has a projection K equal to Ω. In a rotating system like this, the total Hamiltonian can be written:

$$H = H_R + H_P \tag{1}$$

where H_R and H_P are the rotational and particle Hamiltonians, respectively. The rotational Hamiltonian may be written:

$$H_R = \frac{\hbar^2}{2\mathcal{I}_0} I^2 + \frac{\hbar^2}{2\mathcal{I}_0}(j_1^2 + j_2^2 - j_3^2) - \frac{\hbar^2}{2\mathcal{I}_0}(j_+ I_- + j_- I_+) \tag{2}$$

$\vec{I}$ and $\vec{j}$ are in different frames, so a (+) operator in one acts like a (-) operator in the other with the notation of $I_\pm = I_1 \pm iI_2$ and $j_\pm = j_1 \pm ij_2$. The first term depends only on the total angular momentum and is a constant of the motion. The second term represents a recoil energy of the rotor and depends only on the intrinsic variables (including the spin variables ℓ, j, and K). The third term is an effect of the Coriolis force on the particle in the rotating coordinate system and will be given the name "rotation-particle coupling." The total Hamiltonian is invariant

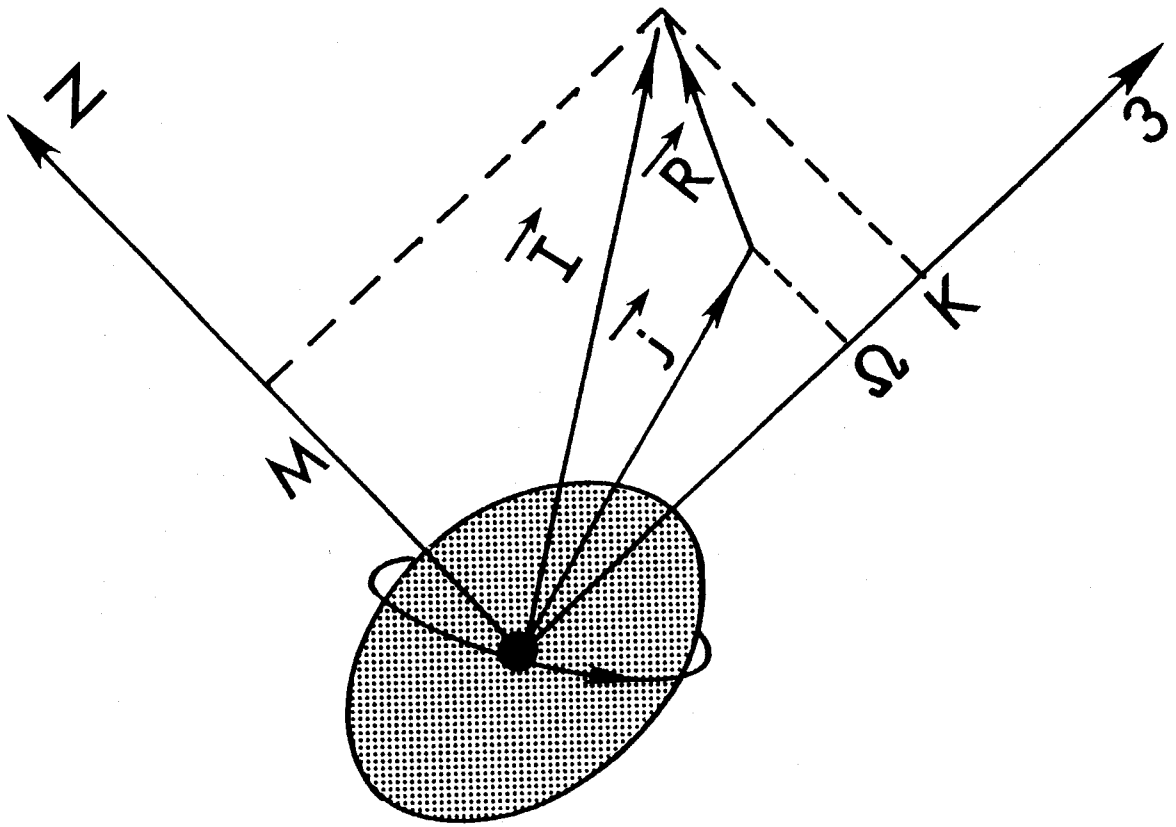

Figure 2-1. Vector diagram of a particle coupled to a rotating core.

under 180° rotations about the intrinsic axes (D_2 Symmetry group). These symmetries allow the wave function to be written in the form

$$\Psi_{IM,\alpha} = \sqrt{\frac{2I+1}{16\pi^2}} \sum_{K,\Omega,\tau}{}' C^{(I,j,\alpha)}_{K\Omega\tau} (D^{(I)}_{MK} \chi^{(j)}_{\Omega\tau} + (-)^{(I-j)} D^{(I)}_{M-K} \chi^{(j)}_{-\Omega\tau}), \tag{3}$$

where summation is restricted to $|K| \leq I$, $|\Omega| \leq j$, $(K + j)$ even, $(\Omega + j)$ even, and $\tau = \pm 1$; $D^{(I)}_{MK}$ denote rotational D-functions. The index τ distinguishes between particle and hole states, and α labels all states for a certain total angular momentum I. In this case, the energy can be simply diagonalized [Her50] and the various limits considered afterwards. The energy levels of the axially symmetric are characterized by a single particle energy and a set of rotational levels built upon the single particle state. The expression has been shown to be:

$$E_K(I) = E^{(0)}_K + E^{(1)}_K \left\{ I(I+1) + \delta_{K,1/2} a (-1)^{I+1/2} \left(I + \frac{1}{2}\right) \right\}, \tag{4}$$

where the parameter $E^{(1)}_K$ and the decoupling parameter a depend in some way on the nucleon configuration, and where $E^{(0)}_K$, a 0th order energy (an "ideal" energy before the perturbations set in) is conventionally chosen so that $E_K(I)$ will have the experimental energy. The second term in the braces, a so-called decoupling parameter, is actually a special case of the Coriolis shift operator. When K = 1/2, the wave function, symmetized with respect to ±K has a K = +1/2 and a K = -1/2 portion. These can be connected by the $I_{\pm} j_{\mp}$ shift operator. For this special case then, two halves of the wave function get scrambled among themselves. In other places $I_{\pm} j_{\mp}$ simply connects K and K ± 1 if the states lie close by.

The numerical solution of the energy spectrum of an odd nucleon coupled to a triaxial rotating core has been calculated as a function of the deformation β, the asymmetry γ, and the Fermi energy λ_f by Meyer-ter-Vehn [Me75].

The spectroscopic quadrupole moments and the magnetic moment can be written as:

$$Q_{I\alpha}^{(sp)} = \begin{pmatrix} I & 2 & I \\ -I & 0 & I \end{pmatrix} \langle I\alpha||Q||I\alpha\rangle, \tag{5}$$

$$\mu_{I\alpha} = g_R I + \begin{pmatrix} I & 1 & I \\ -I & 0 & I \end{pmatrix} \langle I\alpha||M||I\alpha\rangle, \tag{6}$$

and for the reduced *E2* and *M1* transition probabilities

$$B(\mathrm{E2}; I\alpha \to I\alpha') = \frac{5}{16\pi} |\langle I'\alpha'||Q||I\alpha\rangle|^2/(2I+1), \tag{7}$$

$$B(\mathrm{M1}; I\alpha \to I'\alpha') = |\langle I'\alpha'||M||I\alpha\rangle|^2/(2I+1). \tag{8}$$

Mixing ratios are defined as:

$$\delta(I\alpha \to I'\alpha') = \sqrt{0.7} E_\gamma \sqrt{\frac{5}{16\pi}} \frac{\langle I'\alpha'||Q||I\alpha\rangle}{\langle I'\alpha'||M||I\alpha\rangle}, \tag{9}$$

where $E_\gamma = (E_I - E_{I'})$ is the transition energy in MeV. The above expressions correspond to particles coupled to the rotor; the results for holes are obtained by applying the particle-hole transformations, which reverse the sign of $Q^{(sp)}$ and δ, but leave all other quantities unchanged (except for quasi-particles which are particle/hole combinations having all the B's reduced).

2.2. Properties of the Triaxial Core

The three moments of inertia can be written as:

$$\mathcal{I}_\kappa = \mathcal{I}_0 \tfrac{4}{3} \sin^2(\gamma - \tfrac{2}{3}\pi\kappa), \qquad \kappa = 1, 2, 3, \tag{10}$$

These moments of inertia are shown as function of γ in Figure 2.2 and the corresponding lowest states of the triaxial even rotor are given in

MSUX-80-208

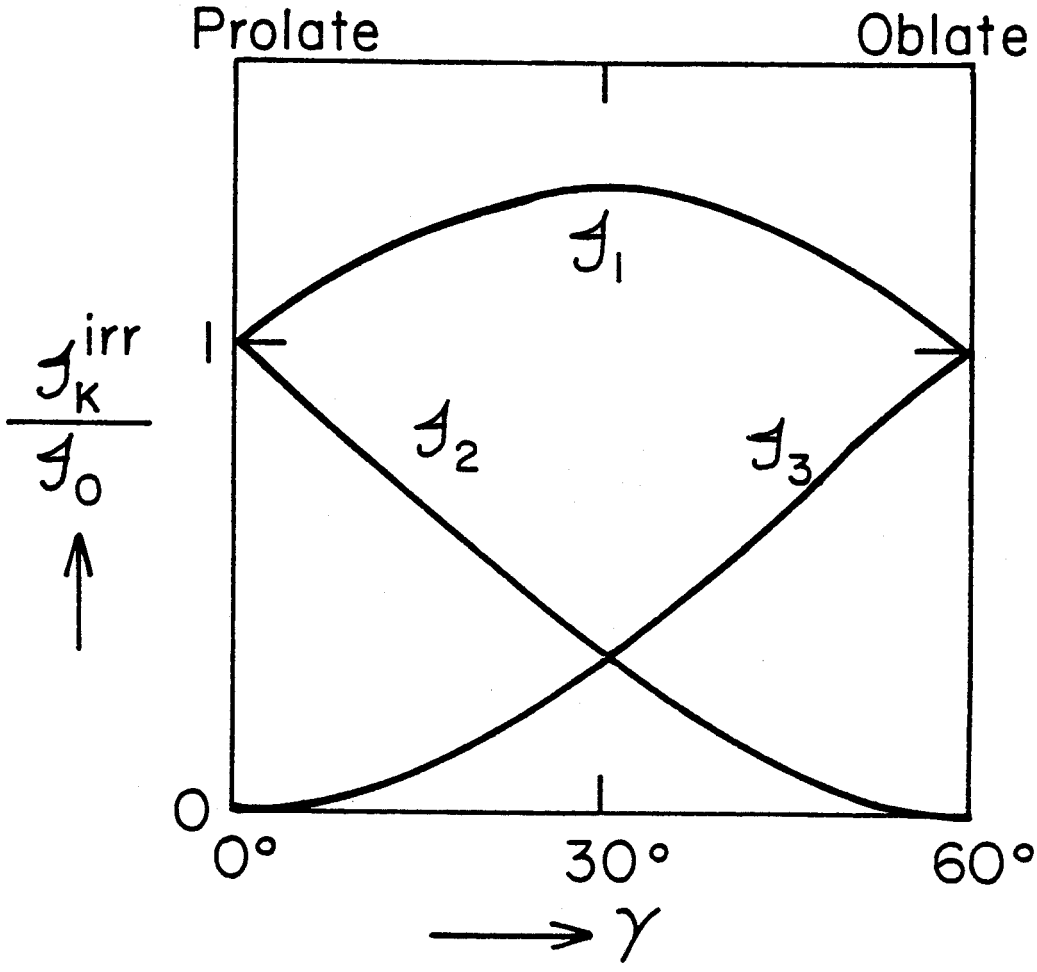

Figure 2-2. Irrotational moments of inertia as function of γ.

Figure 2-3. Besides the ground state rotational band, a second 2^+ state and other additional states are seen to come down in energy as a function of γ, marking the triaxial region. The energies of the first and second 2^+ states have been expressed analytically by Davydov et al. [Da58] as:

$$E_{2^+_{1,2}} = \frac{6\hbar^2}{2\mathcal{I}_0} \frac{9 \mp \sqrt{81 - 72\sin^2(3\gamma)}}{4\sin^2(3\gamma)}, \tag{11}$$

and the transition probabilities to the ground state as:

$$B(E2; 2^+_{1,2} \rightarrow 0^+) = \frac{5}{16\pi} Q_0^2 \frac{1}{10} \left[1 \pm \frac{3 - 2\sin^2(3\gamma)}{\sqrt{9 - 8\sin^2(3\gamma)}}\right], \tag{12}$$

where the upper sign refers to the 2^+_1 state and lower sign to the 2^+_2 state.

A general analytical solution for the even triaxial rotor at $\gamma = 30°$ has been given by Meyer-ter-Vehn [Me75]. Since two moments of inertia are equal $\mathcal{I}_2 = \mathcal{I}_3$ at $\gamma = 30°$, as seen in Figure 2-2, the Hamiltonian becomes axially symmetric about the $\hat{1}$-axis for $\gamma = 30°$ and can be written as

$$h_R = a[R_1^2 + 4(R_2^2 + R_3^2)], \tag{13}$$

with $a = 3\hbar^2/8\mathcal{I}_0$. Due to the symmetry, the angular momentum $\vec{R}$ has a sharp projection α on the $\hat{1}$-axis, α has to be an even integer. The energy spectrum is obtained as:

$$E_{I,\alpha} = a[\alpha^2 + 4(I(I+1) - \alpha^2)], \tag{14}$$

and the wave functions are:

$$\Psi_{IM,\alpha} = \sqrt{\frac{2I+1}{16\pi^2(1+\delta_{\alpha,0})}} (D^{(I)}_{M\alpha} + (-)^I D^{(I)}_{M-\alpha}). \tag{15}$$

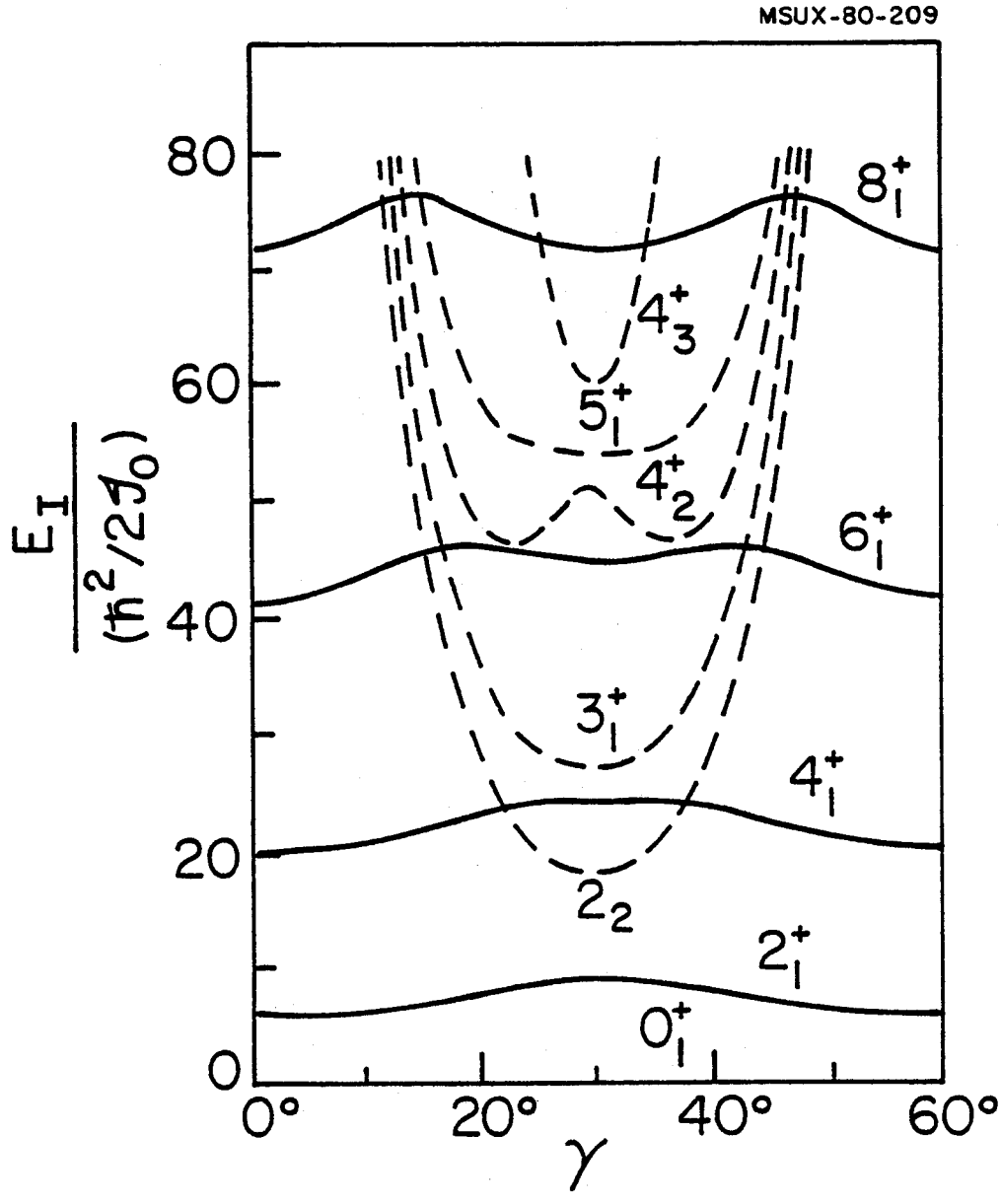

Figure 2-3. Low-energy spectrum of an even triaxial core as a function of γ.

In connection with the low-excited odd-A spectrum, one is interested in the lowest states of the core spectrum, in particular, in the first and second 2^+ state.

2.3. The Model Parameters and Their Determination

The free parameters of the model are β, γ, and λ_f. For a particular odd-A nucleus, β and γ will be determined from the lowest excited states of the adjacent even nuclei, and λ_f will be determined from the Nilsson level scheme. All other parameters are chosen as a smooth function of the mass A; e.g. k and Δ, or as a function of β and A, e.g. $\mathcal{J}_0$.

$$k = \int_0^\infty dr\, r^2 (f(r))^2 k(r) = 206/A^{\frac{1}{3}}\,(\mathrm{MeV}), \tag{16}$$

consistent with the splitting of the $h_{11/2}$ shell in the Nilsson level scheme. The inertia parameter $\mathcal{J}_0$ is determined by the relation,

$$\hbar^2/2\mathcal{J}_0 = 204/\beta^2 A^{7/3}\,(\mathrm{MeV}) \tag{17}$$

The pairing energy is chosen as:

$$\Delta = 135/A\ (\mathrm{MeV}) \tag{18}$$

consistent with odd-even mass difference in the mass region $100 < A < 200$.

The procedure to determine β, γ, and λ_f is ambiguous for several reasons:

i) The low-energy spectra of even transitional nuclei differ in general from those of a perfect triaxial rotor, and there are different ways to adjust β and γ.

ii) In a number of cases, the first excited energies of the even nuclei are rapidly changing with mass number so that the question arises which of the two neighbors or which average of them should be taken.

iii) Furthermore, there is evidence in some cases that the odd nucleon polarixes the core so that the parameters of the even neighbors are not quite applicable to the odd-A nucleus.

The parameter γ can be determined from the energy ratio of the second 2^+ state to the first 2^+ state, by using equation (11). For particle spectra (λ_f below j-shell), the (A-1) neighbor is chosen as reference nucleus and, for hole spectra (λ_f above the j-shell), the (A + 1) neighbor is chosen. Since the energy spectrum of the even triaxial rotor is symmetric about $\gamma = 30°$ (see Figure 2-3), this procedure cannot distinguish between prolate triaxial shapes $0° < \gamma < 30°$ and oblate triaxial shapes $30° < \gamma < 60°$. The information to which side a certain nucleus belongs has to be taken from the odd-A spectrum.

The parameter β is determined by average, $\bar{E}_{2^+} = [E_{2^+}^{(A-1)} + E_{2^+}^{(A+1)}]/2$, of the first 2^+ energies of the (A-1) and the (A+1) neighbor, and using the equation,

$$\beta = \left[\frac{1224}{A^{7/3}\, \bar{E}_{2^+}} \chi(\gamma) \right]^{1/2}, \qquad (19)$$

where $\bar{E}_{2^+}$ is taken in MeV, and the γ-dependent factor is equal to:

$$\chi(\gamma) = \frac{4\sin^2(3\gamma)}{9-[81-72\sin^2(3\gamma)]^{1/2}} \quad . \qquad (20)$$

The position of the Fermi energy λ_f relative to the j-shell on which the unique parity states are built determines the particle or the hole character of the system. For a given j-shell, λ_f is estimated from a Nilsson level scheme for $\gamma = 0°$. This estimate is sufficient as long as λ_f is located outside the j-shell level scheme. In cases where λ_f penetrates the j-shell appreciably, the fine adjustment of λ_f has been

performed by fitting approximately the first (j - 1) state of the odd-A spectrum. In this work, λ_f is given in the form $\bar{\lambda}_f = (\lambda_f - \varepsilon_1)/(\varepsilon_2 - \varepsilon_1)$ for particle spectra and $\bar{\lambda}_f = (\varepsilon_{(j+1/2)} - \lambda_f)/(\varepsilon_{(j+1/2)} - \varepsilon_{(j-1/2)})$ for hole spectra, where ε_ν with $\nu = 1, 2, \ldots . j + 1/2$ are the single-particle energies of the j-shell.

The computer program TRIAX, which was the modified program used by Meyer-ter-Vehn at Lawrence Berkeley Laboratory, was used for numerical calculations. This program calculates energies, wavefunctions, moments, and transition probabilities of the triaxial-rotor-plus-quasiparticle model.

CHAPTER III

EXPERIMENTAL APPARATUS AND METHOD

To arrive at the in-beam level scheme constructed during this investigation, both standard and new techniques of γ-ray spectroscopy were used.

This chapter describes in a general way the apparatus in current use at Michigan State University for γ-ray measurement. It has been divided into three sections in order to explain some significant general characteristics of the γ-ray spectrometers employed in this study for 1) singles, 2) coincidence, and 3) angular distribution experiments.

3.1. Singles Experiments

The basic components of the singles γ-ray spectrometer used in the present study were: a) a Ge(Li) detector cooled to liquid nitrogen temperature (77°K), b) a room temperature FET (field-effect transistor) preamplifier and bias supply, c) a pulse shaping amplifier with pole-zero compensation, d) an analog-to-digital converter (ADC) or multi-channel analyzer (MCA), and e) a data-readout system.

The data analysis in the present study was carried out on the Michigan State University Heavy Ion Laboratory's XDS Sigma-7 computer. Peak centroids and areas were determined off line by the peak-fitting code SAMPO [Ro69], which was especially useful in stripping unresolved multiplets.

Gamma-ray energy measurements were made by first computing least squares quadratic calibration equations from centroid channel numbers of well-known standard energies and then computing the energies of "unknown"

γ-rays from their measured centroids. Gamma-ray relative intensities were established with the aid of a detector efficiency versus photon energy curve for energies ranging from 30 keV to 2 MeV.

3.2. Coincidence Experiments

Coincidence spectra have played an important role in the present research. Since the vast majority of nuclear excited states have very short half-lives as compared with our ability to measure them, coincidence units with resolving times on the order of nano-seconds can be used to study those transitions which are in fast or "prompt" coincidence with one another. In this manner, coincidence spectra are a useful tool for determining the relationships of the observed γ transitions. By considering energy sums, relative intensities, excitation functions, and angular distribution functions, along with coincidence relationships among the various γ-rays, it was usually possible to construct a unique level scheme.

The most important and most extensive type of experimental data which were taken for this study consisted of three-parameter (E_γ x E_γ x t) coincidences. In such an experiment, two detectors were placed about 5 cm from the target at 180° with respect to each other. Gates could be set not only on gamma peaks, but also on any desired time intervals. Consequently, various half-lives could be determined and used efficiently in searching for unknown transitions or isomers.

A block diagram of the electronics set-up for the 3-dimentional coincidence experiments is shown in Figure 3-1. The γ-rays in a true coincidence event have a distinct relationship in time, which enables us to distinguish them from random chance coincidences. The necessary time

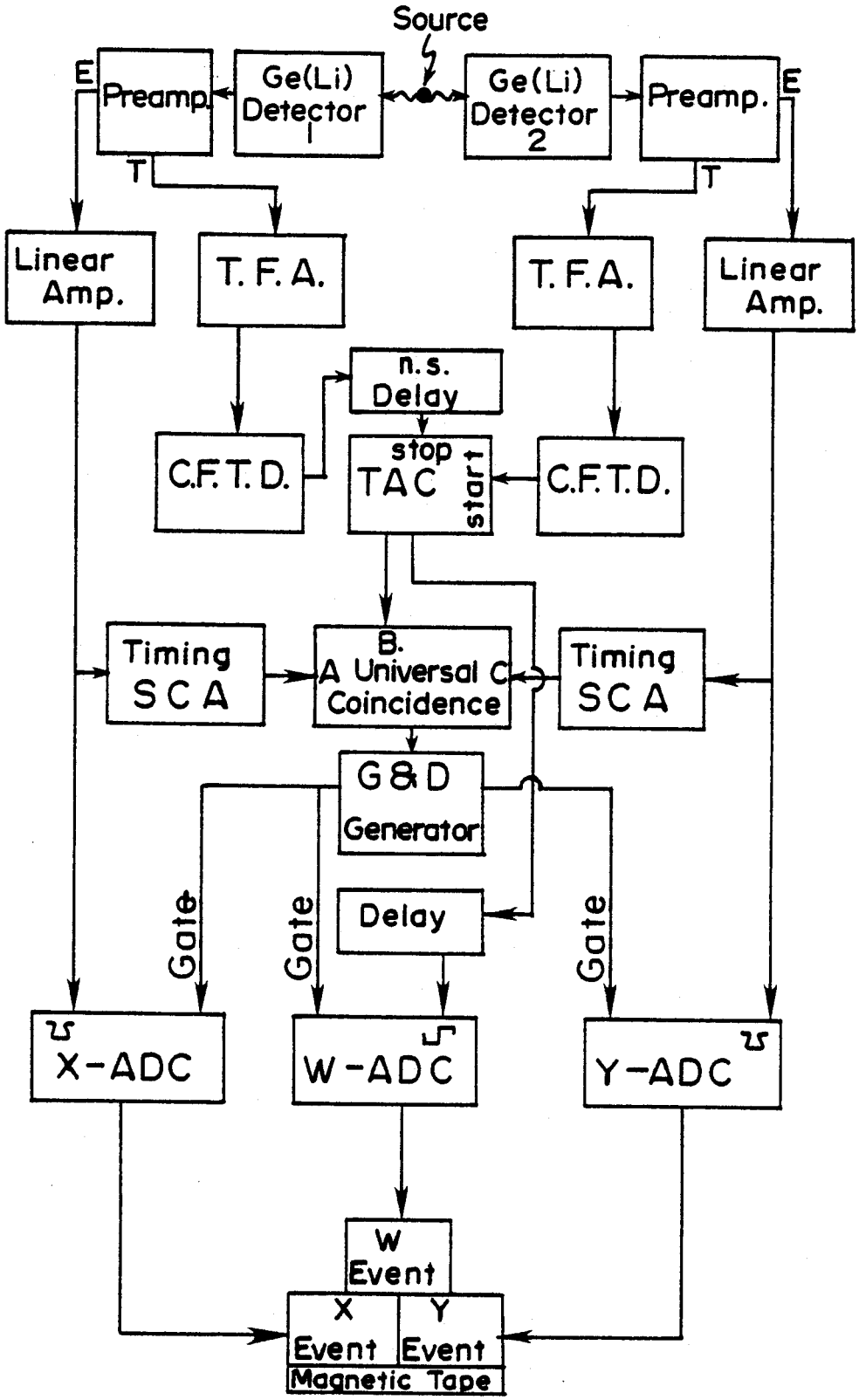

Figure 3-1. "FAST-SLOW" coincidence diagram.

selection can be accomplished by using a time-to-pulse-height converter (TAC). In order to measure elapsed time precisely, the TAC requires input pulses that provide accurate information concerning the time at which a particular nuclear event occurred. The spectroscopic amplifier distorts the shape of pulses from the preamp, decreasing rather than enhancing the steepness of the risetime of an incoming pulse. This in turn makes accurate timing measurements more difficult. For this reason, our timing signals are derived from the preamp pulses before they are passed through the spectroscopic amplifier. As the preamp pulses still need amplification, they are sent through a timing filter amplifier (TFA). It is found that the time for a peak to reach a set fraction of its maximum value is almost time-invariant. The constant fraction timing discriminator (CFTD) makes use of this invariance by setting an effective triggering threshhold at a fraction of the full height of the input pulse. In order to generate the proper pulse shape for this type of triggering, the input is branched into two paths. In one leg of the system, the input is attenuated to a fraction of its original height. In the other path the pulse is inverted and delayed by a time interval known as the shaping delay. Both signals are then added together to form a signal with a zero crossing. The constant fraction timing discriminator then uses a zero crossing discriminator to generate a logic pulse which is suitable for input into the TAC. The fast timing network generates the needed logic inputs for the TAC, but it also has a tendency to trigger on noise. This can prove to be a real problem if the energy range of pulses to be studied includes low energies. To eliminate these pseudocoincidences we make use of the ("slow") coincidence module. The slow timing network uses logic pulses generated from the energy signals (after amplification,

shaping and passing through a timing single channel analyzer [TSCA]) and from the corresponding TAC pulse to determine if a pair of γ-rays forms a true coincidence event. Then, for each true coincidence event, the slow timing opens a gate to the ADC's, allowing the TAC output and the γ-ray energy signals to be analyzed and then collected on magnetic tape under a computer program called IIEVENT [Au72]. By sorting the γ-rays into sequential time intervals, the prompt as well as the delayed γ-rays could be studied with chance or random background subtracted.

The data recorded on tape are recovered later, off-line, using a program called KKRECOVERY [KKREC]. The sorting process takes about 30 minutes per tape (3 million events) on the XDS Sigma-7 computer, and up to 120 spectra (2048-channel) can be generated in the sorting process.

3.3. Angular Distribution Experiments

One can obtain additional information about energy levels, spins, and transition multipolarities by measuring the angular distribution of γ-rays emitted from aligned states formed by nuclear reactions. When the incoming particles impinge upon the target nuclei with velocity $\vec{v}$, they align the nuclei such that the angular momentum vectors ($\vec{r} \times m\vec{v}$) are all predominantly in a plane perpendicular to the beam. As these nuclei decay by emitting electromagnetic radiation, they lose some of the original alignment with each transition. Although the mixing ratio of dipole and quadrupole radiation cannot be very precisely determined using these distributions, the qualitative information contained in the shapes of the curves can be helpful in confirming placement of γ-rays in the level scheme.

Figure 3-2 shows a portion of the goniometer chamber in one of its many experimental configurations, here used for angular distribution

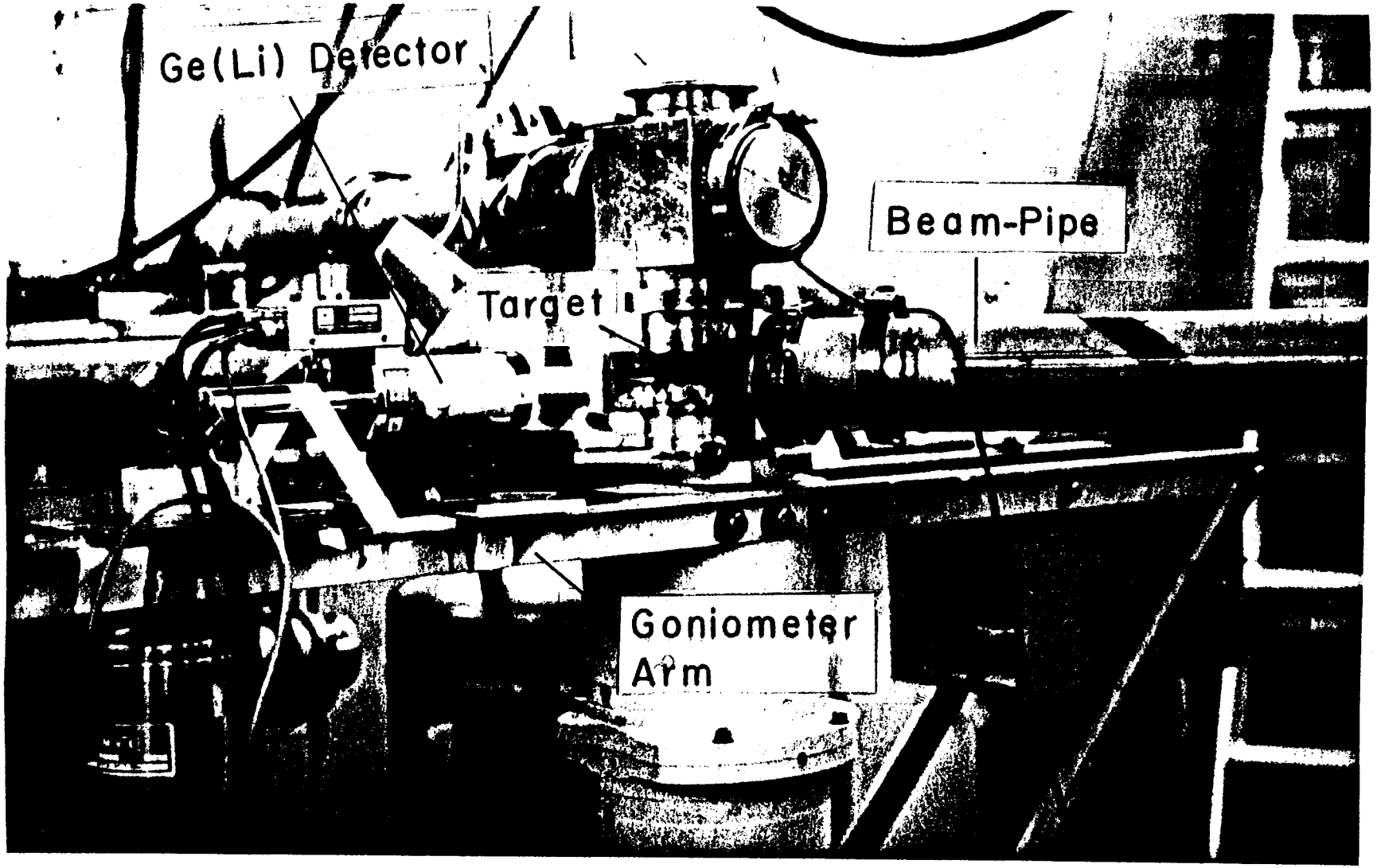

Figure 3-2. The goniometer facility, showing the activation chamber and detector mounting.

experiments in this study (The goniometer facility provides a number of other conveniences that are useful for γ-ray spectroscopy experiments). A large arm extends to both sides of the unit and provides a mounting for one or more detector packages (cryostat, dewar, preamp, etc.). This arm rotates about the vertical axis of the main body and is controlled either by the local control box or a remote control panel. The targets are held in a vertical ladder arrangement in the center of the chamber. Three 2.5- x 5.0-cm target frames can be mounted in this holder. Vertical movement of the ladder for target selection, as well as rotation of the target plane with respect to the beam, can be controlled remotely or locally.

Dead-time and amplifier pileup corrections, as well as run-to-run normalizations, were made by using the digitized output from a beam current integrator to trigger a Berkley Nucleonics Corporation model No. BH-1 tail-pulse generator. The pulser was in turn connected to the test input of both the angular distribution and the monitor detectors' preamplifiers. The resulting pulser peak in the γ-ray spectrum was placed so as not to interfere with γ-ray peaks.

CHAPTER IV

^{143}Eu EXPERIMENTAL AND THEORETICAL RESULTS

The $^{143}Gd^{m+g}$ β-decay has been used previously to study the excited states in ^{143}Eu [Va73, Wi76, Fi78].

The $^{144}Sm(p,2n\gamma)^{143}Eu$ reaction was used for this study in order to populate many high-spin states not populated by the β-decay. Many experiments such as γ-γ coincidences, excitation functions for the various γ-rays, and angular distributions were carried out in order to construct the level scheme. In the last sections, a triaxial weak-coupling model is used to explain the experimental level scheme.

4.1. Experimental Details and Results for the $(p,2n\gamma)$ Reaction

4.1.1. Target and Reaction

The states in ^{143}Eu were excited by the $^{144}Sm(p,2n\gamma)^{143}Eu$ reaction using a 30-MeV p beam from the MSU (50-MeV) sector-focused cyclotron. The target was prepared by vaporizing Sm enriched to 95.10% ^{144}Sm (obtained from Oak Ridge National Laboratory) onto a thin C backing. The target was 200-300 μg/cm^2 thick and the C backing 25 μg/cm^2 thick.

Excitation functions calculated by the compound-nucleus evaporation code [ALICE] are shown in Figure 4-1. From these it can be seen that the primary contaminants produced directly by the 30-MeV p beam were ^{144}Eu, ^{142}Sm, and to a lesser extent, ^{142}Eu. Their decays also produced readily identifiable γ rays from states in ^{144}Sm, ^{143}Sm, ^{143}Pm, ^{142}Sm, and ^{142}Nd. These predictions were observed in the experiments and accounted for.

Figure 4-1. Excitation functions calculated by the evaporation code ALICE for p's on a ^{144}Sm target. Note that there are two curves for each of the Pm isotopes, one for the evaporation of an α particle, the other for evaporation of $2n + 2p$.

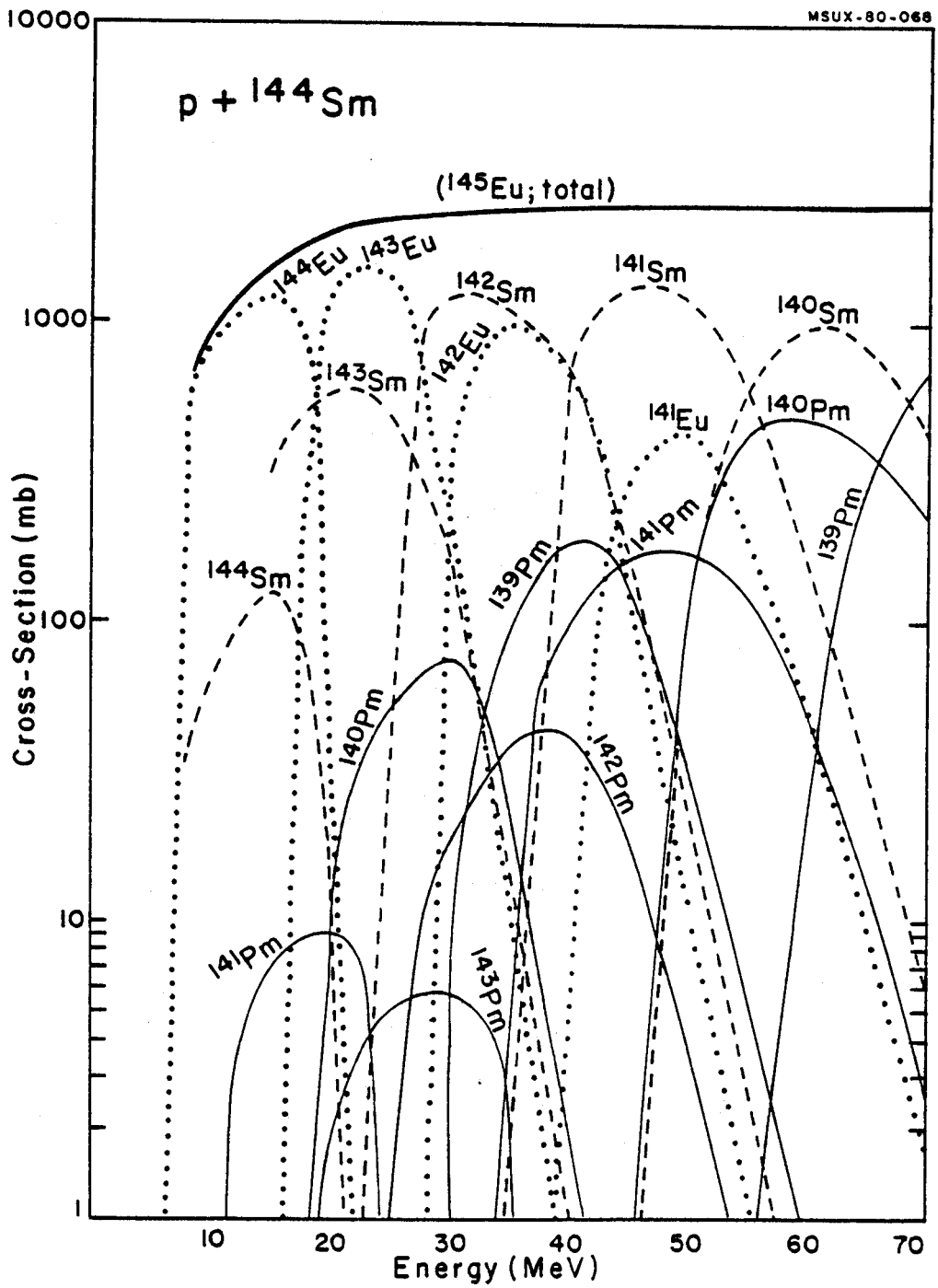
MSUX-80-068
p + 144Sm
(145Eu; total)
144Eu
143Eu
142Sm
141Sm
140Sm
143Sm
142Eu
141Eu
140Pm
139Pm
144Sm
139Pm
141Pm
140Pm
142Pm
141Pm
143Pm
Cross-Section (mb)
10000
1000
100
10
1
10
20
30
40
50
60
70
Energy (MeV)

4.1.2. γ-Ray Singles Spectra

The ^{143}Eu singles γ-ray spectra were taken with a 10%-efficient (with respect to a 7.6 x 7.6-cm NaI(Tℓ) detector for the ^{60}Co 1332.513-keV peak; source-to-detector distance, 25 cm) Ge(Li) detector having a resolution of 2.4 keV FWHM (for the ^{60}Co 1332.513-keV peak). They were normally taken at an angle of 125° from the beam direction [to minimize angular distribution effects, 125° being a zero of $P_2(\cos\theta)$]. Typically, a beam current of ≈2 nA was used and the detector was placed 20 cm from the target, resulting in a count rate of ≈6000-7000 cps. A singles γ-ray spectrum taken over a 2.5-*h* period is shown in Figure 4-2.

A total of 37 γ-rays was assigned to ^{143}Eu on the basis of singles spectra and the excitation and coincidence experiments discussed below. These are listed in Table 4-1 together with their relative intensities; also, Table 4-1 includes angular distribution coefficients and conversion coefficients which will be discussed later. The energy calibrations were performed by counting simultaneously with ^{60}Co, ^{226}Ra, and ^{116}Ho^{m} radioactive sources and also using some ^{143}Eu γ rays already characterized from ^{143}Gd β^+/ε decay [Fi78] as secondary standards. The errors quoted for the energies include estimated errors in the standards and are based primarily on the reproducibility of a peak and its height above background. Where the energies were known more precisely from ^{143}Gd decay, these values were adopted. The errors on the intensities are based primarily on the reproducibility of a given peak.

4.1.3. Excitation Functions

The γ-ray excitation functions were obtained with *p* beams having energies of 30, 35, and 40 MeV. The γ rays were detected with the 10%-efficient Ge(Li) at ≈90° from the beam direction and 5 cm from the target.

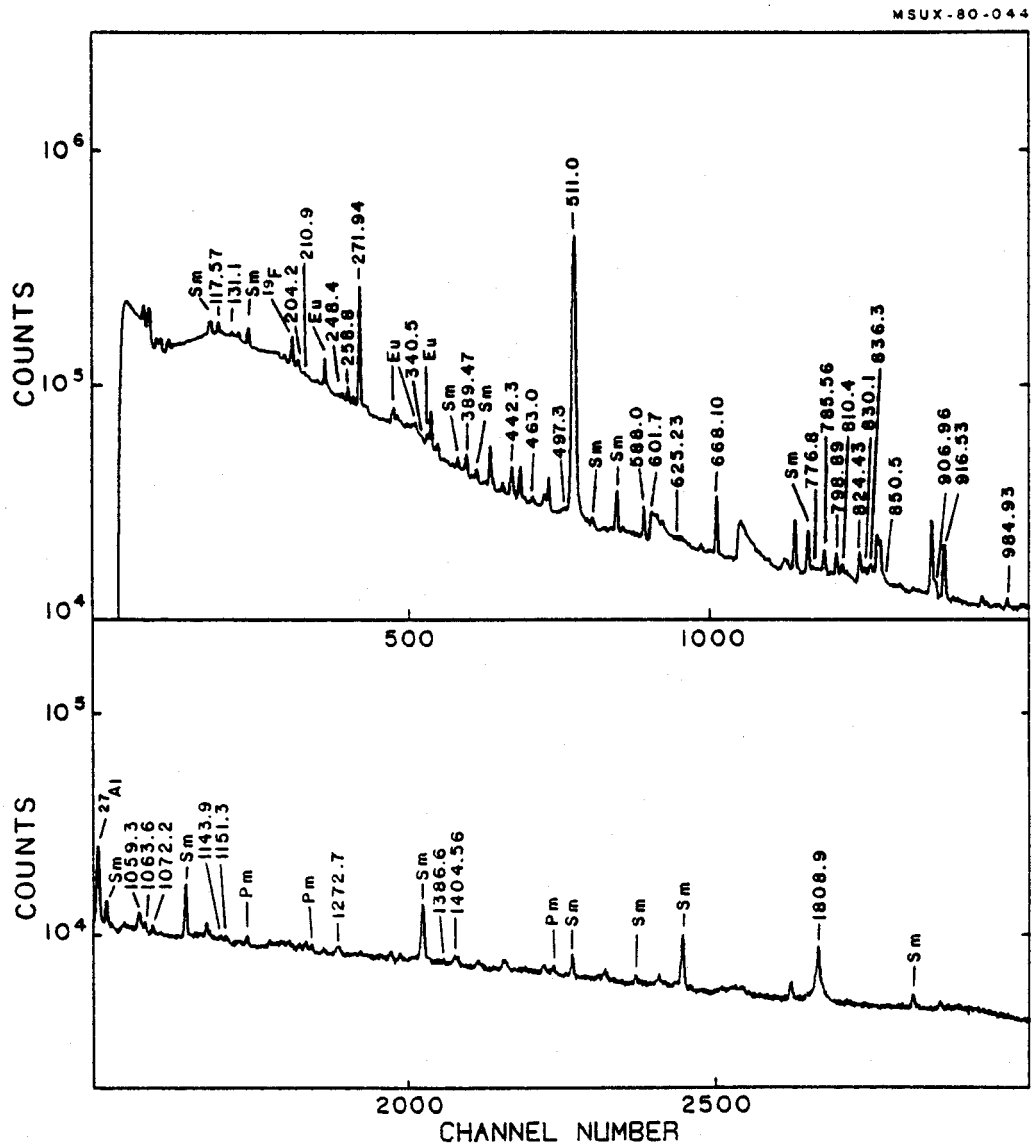

Figure 4-2. In-beam singles γ-ray spectrum from the reaction $^{144}Sm(p,2n\gamma)^{143}Eu$, taken with the 10%-efficient Ge(Li) detector placed at 125°.

Table 4-1. Energies, relative intensities, angular distribution coefficients, and multipolarities for γ transitions in ^{143}Eu from $(p,2n\gamma)$ reactions.

Energy E_γ (keV)	Relative Intensity I_γ	Angular Distribution Coefficients A_2/A_0	A_4/A_0	Multipolarity[a]
117.57±0.05[b]	3.7 ±0.2	isotropic	---	M2
131.1 ±0.1[b]	0.30±0.08	0.10±0.03	---	---
204.77±0.05[b]	5.0 ±0.4	isotropic	---	---
210.9 ±0.1[b]	1.1 ±0.3	-0.55±0.12	---	M1
248.4 ±0.1	1.6 ±0.2	-0.39±0.10	0.15±0.10	---
258.8 ±0.1	7.7 ±0.5	---	---	M1
271.94±0.03[b]	≡100	isotropic	---	M1
340.5 ±0.3	1.0 ±0.1	---	---	---
389.47±0.05[b]	1.5 ±0.2	isotropic	---	E3
442.3 ±0.1	11.9 ±0.8	---	---	---
463.0 ±0.1	2.8 ±0.2	---	---	---
497.3 ±0.1[b]	weak	---	---	---
588.00±0.03[b]	12.7 ±0.8	-0.41±0.02	0.03±0.02	M1+E2
601.7 ±0.2	7.5 ±0.7	0.90±0.40	---	---
625.23±0.08[b]	weak	---	---	---
668.10±0.03[b]	27.3 ±1.6	-0.68±0.03	-0.02±0.04	M1+E2
776.8 ±0.1[b]	weak	---	---	M1 or E3
785.56±0.06[b]	8.7 ±0.5	0.23±0.06	-0.04±0.03	E2
798.89±0.06[b]	8.2 ±0.5	-0.22±0.01	0.09±0.02	E2
810.4 ±0.2	1.6 ±0.3	---	---	---

Table 4-1. (cont'd.).

Energy E_γ (keV)	Relative Intensity I_γ	Angular Distribution Coefficients A_2/A_0	A_4/A_0	Multipolarity[a]
824.43±0.09[b]	10.3 ±0.6	0.09±0.02	-0.02±0.06	E2
830.1 ±0.1[b]	weak	---	---	---
836.3 ±0.1[b]	4.2 ±0.3	---	---	---
850.5 ±0.1	1.8 ±0.3	---	---	---
906.96±0.06[b]	5.6 ±0.6	---	---	E2
916.53±0.05[b]	2.4 ±0.4	0.31±0.03	-0.03±0.04	E2
984.93±0.05[b]	3.9 ±0.3	0.15±0.08	0.06±0.10	M1+E2
1059.3 ±0.1[b,c]	8.3 ±0.5	0.24±0.04	-0.07±0.05	---
1063.6 ±0.1	3.2 ±0.3	0.39±0.10	---	---
1072.2 ±0.1	2.4 ±0.3	0.27±0.14	---	---
1143.9 ±0.1	2.0 ±0.2	---	---	---
1151.3 ±0.1	2.4 ±0.3	---	---	---
1272.7 ±0.2	2.3 ±0.3	-0.15±0.10	0.08±0.06	---
1386.7 ±0.6	0.20±0.05	---	---	---
1404.56±0.07[b]	3.6 ±0.3	---	---	---
1807.14±0.07[b]	19.6 ±1.3	0.72±0.48	---	---

[a]Transition multipolarity assignments taken from conversion electrons, ref. [Wi76].

[b]These γ-rays were also seen in the decay of ^{143}Gd where the precision in energy was greater. The in-beam studies yielded essentially the same energies, so we have adopted the more precise energy values from [Fi78].

[c]There are two 1059.3-keV transitions in the level scheme; see text.

The beam intensity was held as constant as possible (±20%) from experiment to experiment, the integrated beam-current was recorded, and a pulser was included in the spectra to allow reliable normalization of the spectra from one experiment to another. The results for seven prominent γ-rays are shown in Figure 4-3, where the intensities have been normalized to the intensity from the 30-MeV reaction. (It should be mentioned that this excitation function procedure was also very useful in eliminating impurity γ-rays from competing reactions.)

4.1.4. Coincidence Spectra

The γ-γ coincidence spectra were obtained with a 30-MeV *p* beam. The 10%-efficient Ge(Li) detector and a 7.7%-efficient Ge(Li) detector (energy resolution 1.9 keV FWHM) were used. A standard three-parameter (E_γ x E_γ x *t*) fast-slow coincidence set-up with constant-fraction timing was used. The coincidences were recorded event-by-event on magnetic tape for off-line sorting with background subtraction. (For more details, cf. section 3-2).

Some coincidence spectra are shown in Figure 4.4. The integral coincidence spectrum (all coincidence events as displayed from the 10% Ge(Li) detector) is at the top, and three representative gated spectra are shown below it. Because of the relatively larger backgrounds that had to be subtracted from these gated spectra, they were smoothed (three-channel) to enhance the peaks. The raw spectra and the complete set of gated spectra are shown in Appendix A . A summary of the coincidence data is given in Table 4-2.

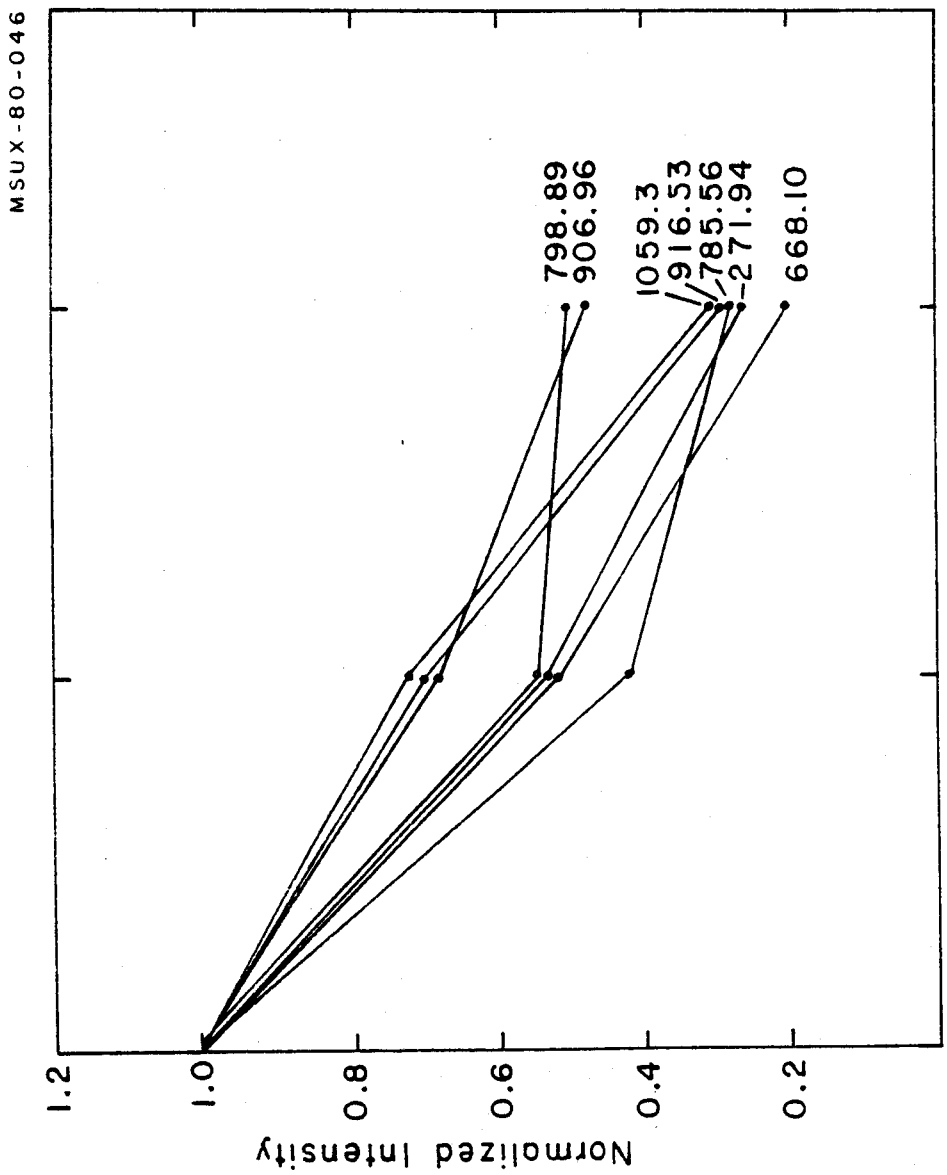

Figure 4-3. Excitation functions for seven of the more prominent ^{143}Eu γ rays.

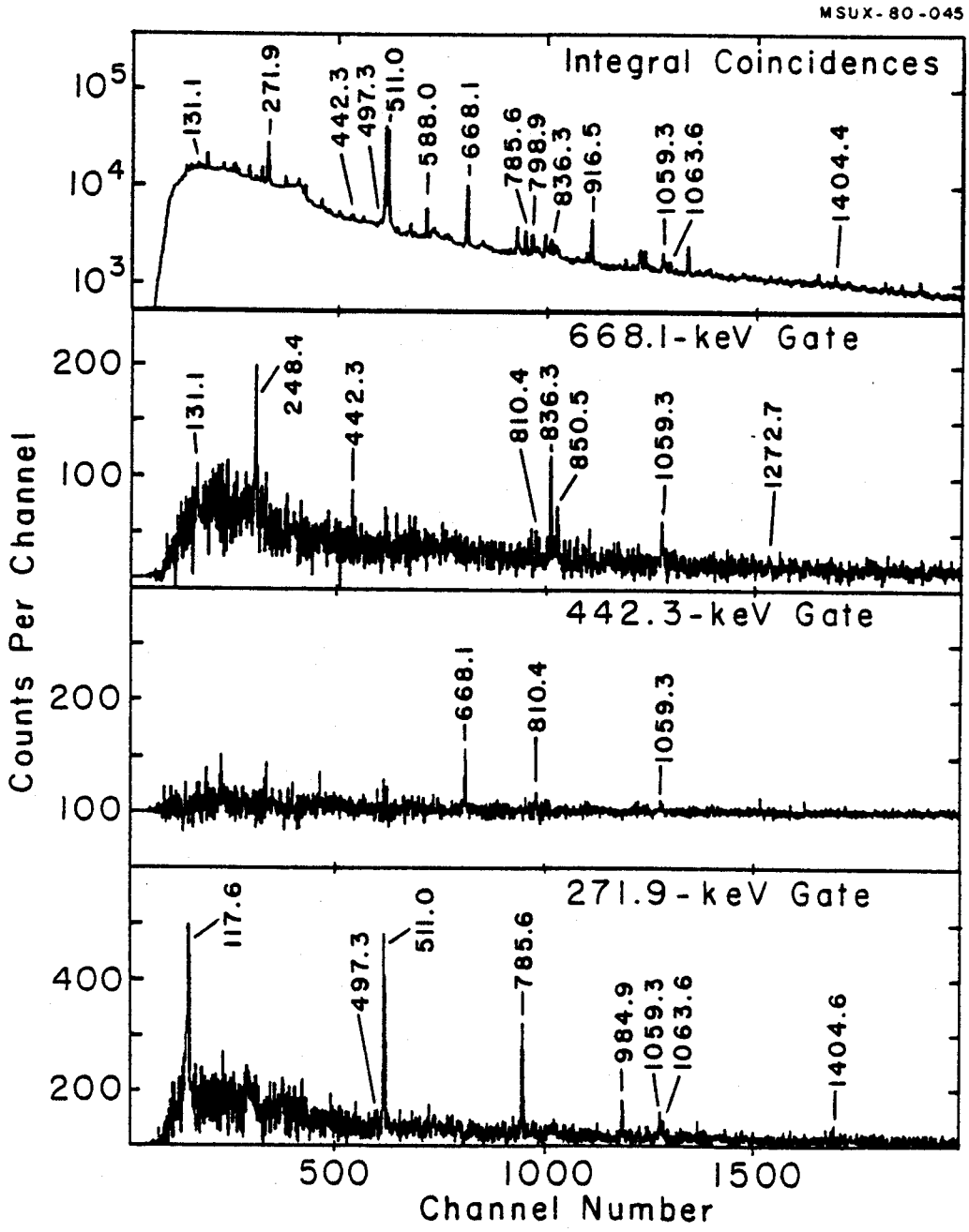

Figure 4-4. In-beam γ-γ coincidence spectra for the reaction, $^{144}Sm(p,2n\gamma)^{143}Eu$. The integral coincidence spectrum ("all events") is shown at the top, and three representative smoothed gated spectra are shown underneath.

Table 4-2. Summary of coincidence results for the $^{144}Sm(p,2n\gamma)^{143}Eu$ reaction.

Gated γ-Ray (keV)	Coincident γ-Rays (keV)
117.57	271.94
131.1	668.10
204.2	258.8, 340.2
210.9	588.00
248.4	668.10
258.8	204.2, 340.2
271.94	117.57, 497.3, 785.56, 984.93, 1059.3, 1063.6, 1404.56
340.2	204.2, 258.8, 463.0
389.47	---
442.3	668.10, 810.4, 1059.3
463.0	340.2
497.3	271.94, 984.93
588.00	210.9, 625.23, 776.8
601.7	916.53
625.23	588.00
668.10	131.1, 248.4, 442.3, 810.4, 836.3, 850.5, 1059.3, 1272.7
776.8	588.00
785.56	271.94, 1063.6
798.89	830.1
810.4	442.3, 668.10
824.43	1143.9, 1386.69
830.1	798.89

Table 4-2. (cont'd.).

Gated γ-Ray (keV)	Coincident γ-Rays (keV)
836.3	668.10
850.5	668.10
906.96	---
916.53	601.7, 1072.2
984.93	271.94, 497.3
1059.3[a]	271.94, 442.3, 668.10
1063.6[b]	271.94, 668.10, 785.56
1072.2	916.53
1143.9	824.43
1151.3	916.53
1272.7	668.10
1386.69	824.43
1404.56	271.94
1808.9	---

[a]There are two separate ≈1059.3-keV γ's.

[b]Perhaps there are also two separate ≈1063.6-keV γ's.

4.1.5. γ-Ray Angular Distributions

The *p*-beam energy for obtaining the γ-ray angular distributions was again 30 MeV. The 10%-efficient Ge(Li) detector was rigidly mounted with its cryostat on the arm of a goniometer with the face of the detector 15 cm from the target. The data were collected at 90°, 100°, 110°, 125°, 140°, and 155° with respect to the beam direction. The angles were taken in random order for the various experiments, and data were typically collected for 2.5-*h* at each angle.

The 271.94- and 117.57-keV isotropic transitions were used as an internal normalization for the spectra taken at different angles. After the normalization of the γ-ray peak areas, least-squares fits to the experimental angular distributions were made, using the computer code GADFIT [GADFIT]. The fits were made to the equation:

$$I = 1 + (A_2/A_0)P_2(\cos\Theta) + (A_4/A_0)P_4(\cos\Theta).$$

The parameters extracted from the fit, A_2/A_0 and A_4/A_0, are included in Table 4-1. Angular distribution coefficients not listed in the tables were for transitions that were very weak or that were parts of multiplets and consequently had very large errors. Where a good fit for A_4/A_0 could not be obtained, the data were refitted with the value for A_4/A_0 set equal to 0.

Some representative angular distributions, together with their calculated fits, are shown in Figure 4.5. The complete set of data with fitted curves is shown in Appendix B.

4.1.6. The ^{143}Eu Level Scheme

Coincidence information, intensity balances, conversion coefficients, and excitation functions for individual γ-rays were the primary factors used to construct a level scheme for ^{143}Eu. Secondary factors were energy

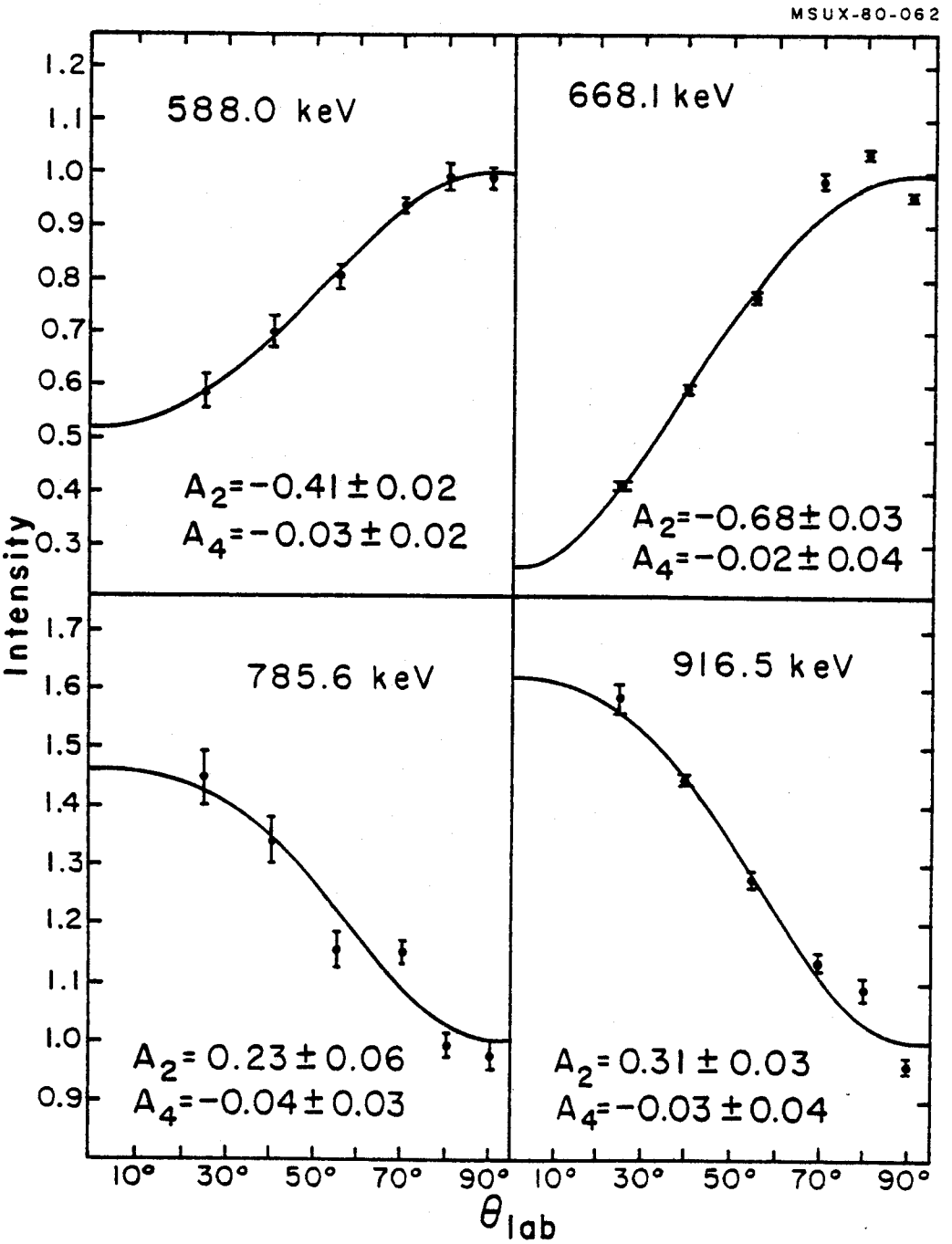

Figure 4-5. Four representative angular distributions of ^{143}Eu γ rays together with their fits calculated by the code GADFIT. The points correspond to 90° and the backward angles, 100°, 110°, 125°, 140°, and 155°.

summing relationships, input from the known $^{143}Gd^{m+g}$ decay scheme [Fi78], and angular distribution data. The spin and parity assignments were made on the basis of angular distribution coefficients, conversion coefficients, and input from the $^{143}Gd^{m+g}$ decay scheme. The resulting level scheme is shown in Figure 4-6. For comparison, the level scheme of ^{143}Eu obtained from the decay of $^{143}Gd^{m+g}$ is shown in Figure 4-7. Specific details of the construction of the level scheme and J^{π} assignments are discussed next.

Ground, 271.94-, and 389.47-keV States

The most intense γ transition in the in-beam, as well as the off-line, experiments is the 271.94-keV transition, which is in coincidence with the 117.57-keV transition (and with six others - cf. Table 4-2). On the other hand, no other γ rays appear to be in coincidence with the 117.57-keV transition. This leads to the adoption of a cascade, with the 117.57-keV transition on top of the 271.94-keV transition, and places states at 271.94 and 389.51 keV. The upper state is also depopulated directly by the 389.47-keV transition, and this energy is adopted for the state.

The ground state has been reported to have $J^{\pi} = 5/2^{+}$ [Ec72], and the 271.94- and 389.47-keV states have been assigned $7/2^{+}$ and $11/2^{-}$, respectively, on the basis of the multipolarities of the three above γ transitions and the log*ft* values for $^{143}Gd^{m}$ β-decay. Also, in the $^{143}Gd^{m}$ decay studies, the 389.47-keV state was measured to have a half-life of 50.0±0.5 μsec. In this present work it has been found that the 117.57- and 271.94-keV transitions are definitely isotropic and the weaker 389.47-keV transition probably isotropic. Although this information does not allow one to comment further on the J^{π} assignments, it is consistent with the long

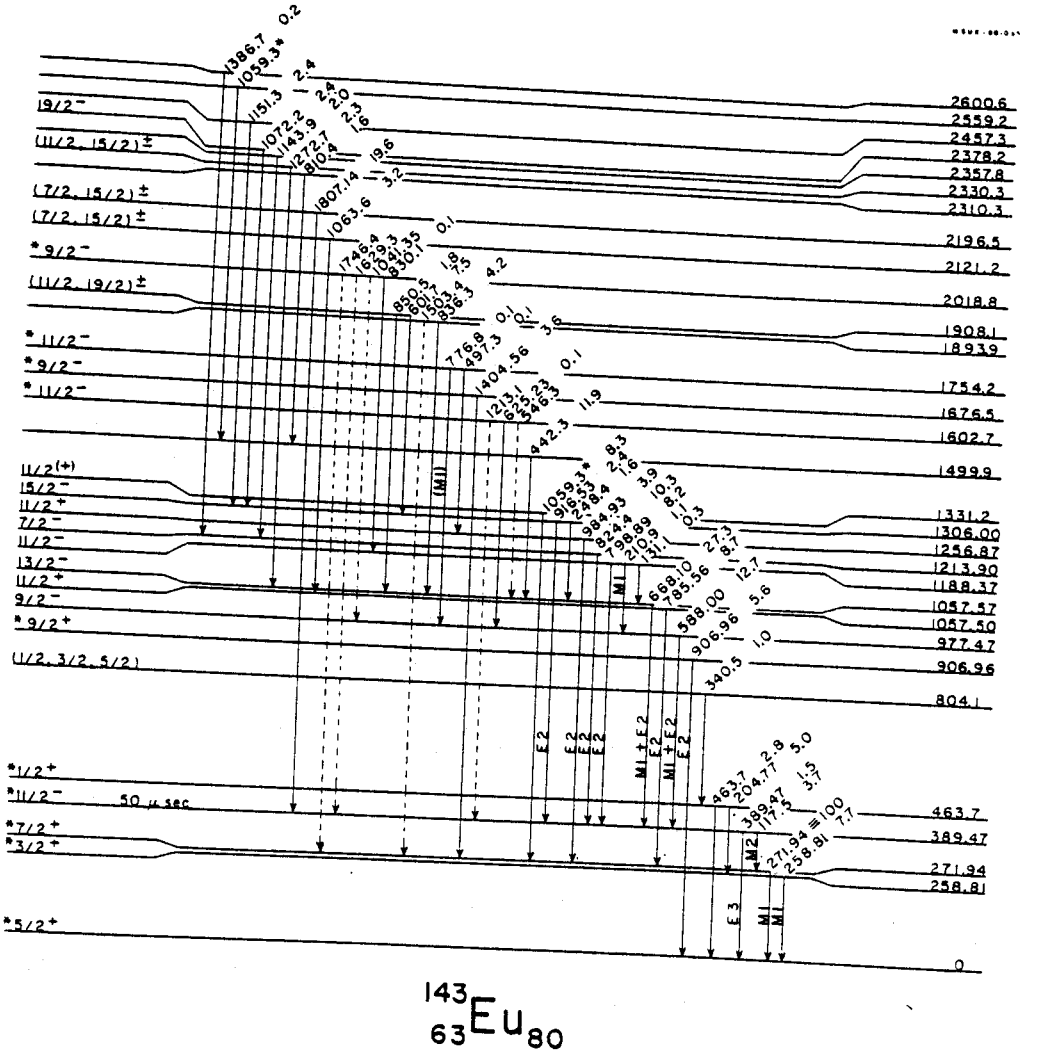

Figure 4-6. ^{143}Eu level scheme as determined by the ^{144}Sm$(p,2n\gamma)^{143}$Eu reaction. The asterisks before J^{π} assignments indicate that we relied heavily on the ^{143}Gd^{m+g} β^+/ε decay [Fi78] for these assignments. Also, the dashed γ transitions are weak transitions seen in ^{143}Gd^{m+g} decay but not seen in our in-beam studies; however, they originate from levels seen in the in-beam studies. It should be noted that there are two 1059.3-keV transitions in this level scheme.

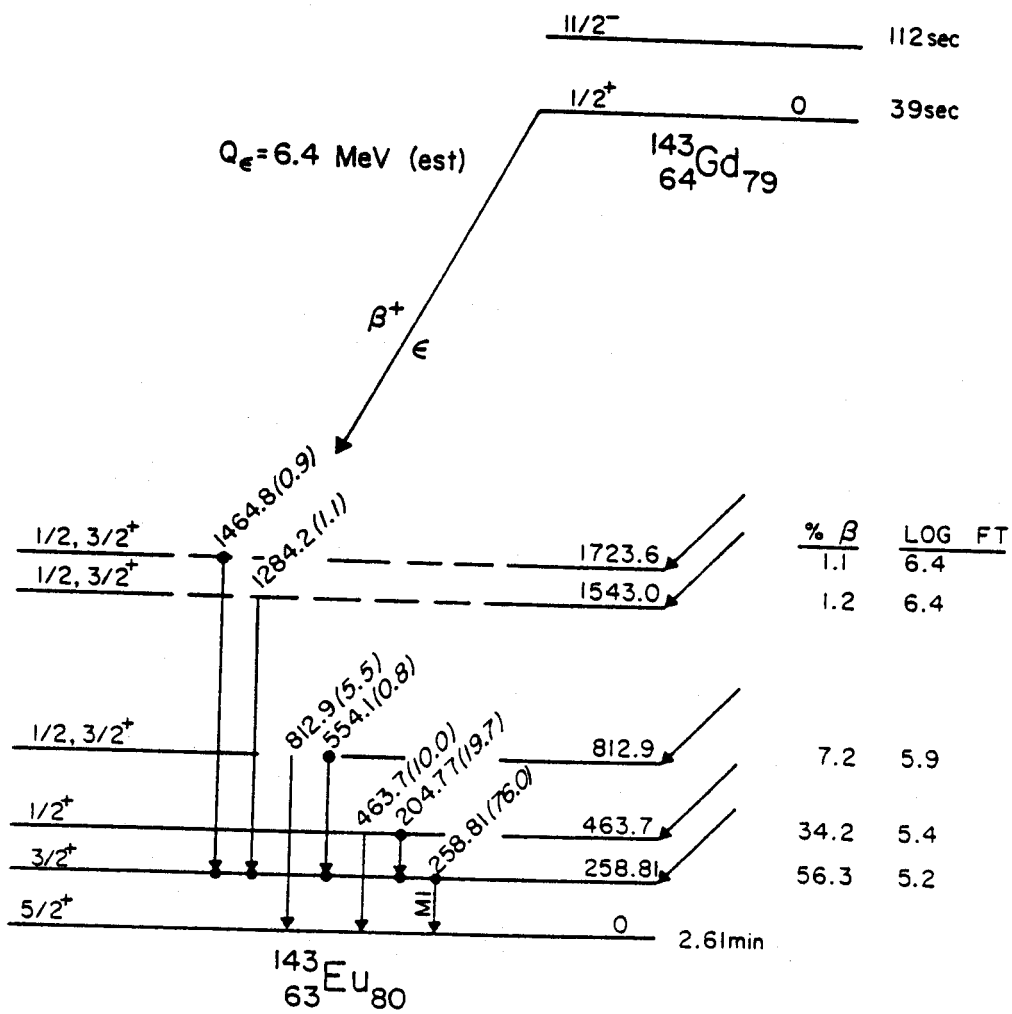

Figure 4-7. Decay schemes of $^{143}Gd^{g}$ and $^{143}Gd^{m}$ from Ref. [Fi78] for comparison with our in-beam studies.

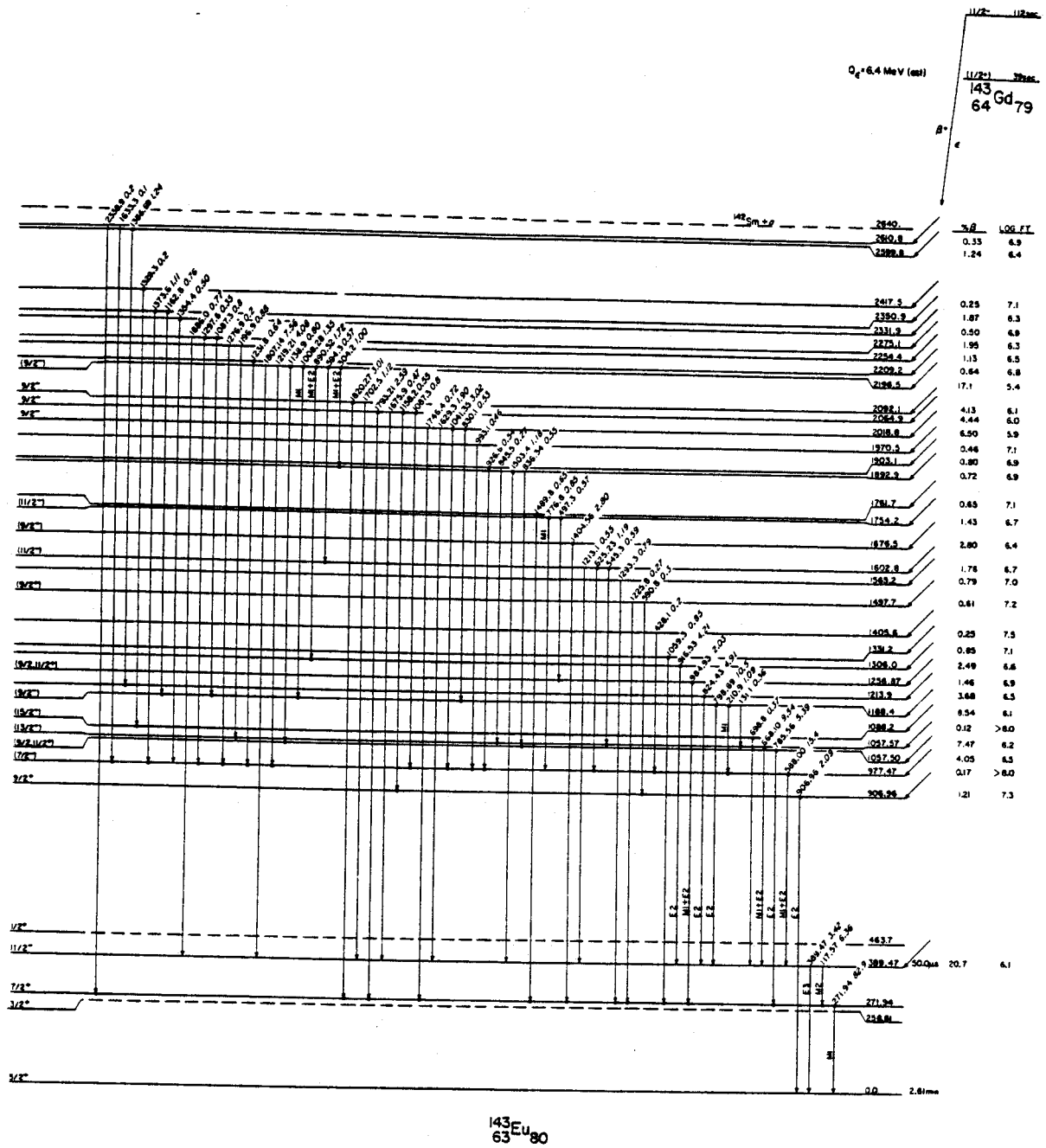

Figure 4-7. (cont'd.).

half-life of the 389.47-keV state (plus the complex feeding into the 271.94-keV state).

258.81-, 463.7-, and 804.1-keV States

The other set of low-lying states, presumably of lower spin, has the interconnecting transitions of 204.77, 258.81, 340.5, and 463.7 keV. Coincidence relations among them and the intensity balances lead to the placement of levels at 258.81, 463.7, and 804.1 keV. The first two were observed in $^{143}Gd^{g}$ decay [Fi78]; the 804.1-keV state has not been previously observed.

Spin assignments for these states were not possible from angular distribution coefficients because all the γ transitions were very weak and had large errors on the values for the transition intensities. However, the 258.81- and 463.7-keV states were assigned $3/2^+$ and $1/2^+$, respectively, from $^{143}Gd^{g}$ decay; presumably their major components are the $\pi d_{3/2}$ and $\pi s_{1/2}$ single-particle states.

Not much can be said about the 804.1-keV state. Its being connected to the 463.7-keV state indicates more that it is related to the $s_{1/2}$ state than what its spin is; for example, it might be $[2^+ \times s_{1/2}]_{1/2^+, 3/2^+, 5/2^+}$ -- any one of these would selectively deexcite to the 463.7-keV state. On the other hand, one might anticipate some feeding from the many higher-lying 9/2 states (cf. below) to a 5/2 state, making $1/2^+$ or $3/2^+$ the preferred assignment. Arguments based on missing transitions are rather weak, however, so one is more safely left with the possibilities, 1/2, 3/2, or 5/2.

977.47-keV State

This state feeds into the $11/2^-$ 389.47-keV state by the 588.00-keV transition. Although the 50.0-μsec $t_{1/2}$ of the 389.47-keV state makes

this impossible to confirm by a direct coincidence measurement, the other coincidence relations with the 588.00-keV γ confirm this placement, as did the extensive coincidence relations from $^{143}Gd^{m}$ decay. From $^{143}Gd^{m}$ decay the 977.47-keV state was tentatively assinged $7/2^{-}$. However, if the 588.00-keV transition is a mixed *M1/E2* transition, the J^{π} assignment is restricted to $9/2^{-}$. $11/2^{-}$, or $13/2^{-}$. The $11/2^{-}$ value is ruled out because of the large negative value of A_2 and the small positive value of A_4. The fact that this state is not fed by γ rays from high-spin states indicates that it most likely is not in the *yrast* sequence, eliminating $J^{\pi} = 13/2^{-}$. Below we shall show that the 1057.57-keV state has $J^{\pi} = 13/2^{-}$ and receives feeding from the high-spin states. It thus appears to be the $13/2^{-}$ *yrast* state, making the possibility of a lower-lying $13/2^{-}$ state unlikely. This state can therefore be assigned $9/2^{-}$.

1057.50-keV State

The coincidence information between the 785.56- and 271.94-keV γ's places this state. It was also seen in $^{143}Gd^{m}$ decay, where it was tentatively assigned $9/2^{+}$ or $11/2^{+}$. The *E2* multipolarity of the 785.56-keV transition allows J^{π} values from $3/2^{+}$ to $11/2^{+}$. The angular distribution data for this transition, however, can be fitted by only two values, $3/2^{+}$ or $11/2^{+}$. The positive value of A_2 and small but negative value of A_4 indicates the transition is a stretched *E2*, eliminating an otherwise possible $7/2^{+}$. From $^{143}Gd^{m}$ decay $3/2^{+}$ can clearly be ruled out, leaving $J^{\pi} = 11/2^{+}$ for this state.

1057.57-keV State

Again, the 50-μsec $t_{1/2}$ of the 389.47-keV state prevents a direct coincidence measurement to place the 1057.57-keV level feeding into it,

but the eight other transitions seen in coincidence with the 688.10-keV transition place the 1057.57-keV level quite securely. This type of argument will not be belabored henceforth but applies equally well to many of the states discussed below. This level was also placed in $^{143}Gd^{m}$ decay and tentatively assigned $13/2^{-}$. The *M1+E2* mixed multipolarity of the 668.10-keV transition limits its J^{π} to $9/2^{-}$, $11/2^{-}$ or $13/2^{-}$. The large negative A_2 and small A_4 rule out $11/2^{-}$. Since the 668.10-keV γ is seen so intensely in the in-beam experiments, *yrast* arguments lead to a preference for the higher spin, i.e., $13/2^{-}$, for this state.

1188.36-keV State

This state, placed by coincidence information from its deexciting 131.1- and 210.9-keV transitions, was confirmed by the strong 798.89-keV transition feeding the $11/2^{-}$ 389.47-keV state. The pure *E2* multipolarity of the latter transition could indicate a stretched quadrupole transition, but the negative A_2 and A_4 values establish it to be a $J \rightarrow J$ pure quadrupole transition. Its J^{π} would thus be $11/2^{-}$. The tentative $9/2^{-}$ assignment reached from $^{143}Gd^{m}$ decay data is believed to be incorrect because the negative A_4 value also rules out a mixed *M1/E2* multipolarity for the 798.89-keV transition.

1213.90-keV State

The 824.43-keV transition that deexcites this state to the $11/2^{-}$ 389.47-keV state is an *E2*, which limits its J^{π} to $7/2^{-}$ through $15/2^{-}$. The angular distribution coefficients limit this further to $7/2^{-}$. (The value of A_2 is too small for a $15/2^{-} \rightarrow 11/2^{-}$ transition; cf. the 785.56-keV transition from the 1057.50-keV state.) This state was left unassigned in the $^{143}Gd^{m}$ decay studies: $J^{\pi} = 7/2^{-}$ should not be allowed with a

log*ft* value of 6.5. However, if it is assumed that much of the intensity of the 824.43-keV transition in $^{143}Gd^{m}$ decay results from missing undetected transitions from higher-lying states [Fi79], then a considerably higher log*ft* value, consistent with the $7/2^-$ assignment, is expected.

1256.87-keV State

For the 984.93-keV transition that deexcites this state to the $7/2^+$ 271.94-keV state, Wisshak et al. assigned *M2+E3* mixed multipolarity. According to the argument in Ref. [Fi78], this assignment was wrong because of the use of an incorrect α_K value -- the latter calculation indicated *M1+E2* multipolarity. The in-beam angular distribution results of the experiment are consistent with a (stretched) quadrupole transition Since the experimental α_K is $(6.9 \pm 1.4) \times 10^{-3}$, and the calculated α_K is 1.6×10^{-2} [Ha68] for an *M2* and 3.4×10^{-3} for an *E2* transition, the *M2* can be excluded. Thus, the 1256.87-keV state has $J^\pi = 11/2^+$.

1306.00-keV State

The 916.53-keV transition (although it has a fairly large error in intensity) deexciting this state appears to be a pure stretched *E2*. Its angular distribution pattern restricts the J^π value of the state to $7/2^-$ or $15/2^-$. *Yrast* considerations suggest a preference for the larger value of $15/2^-$. (Also, the A_2 is uncomfortably large for a $J \rightarrow J + 2$ transition.)

1331.2-keV State

The J^π of ths state is restricted to $3/2^\pm$ or $11/2^\pm$ because of the angular distribution coefficients of the 1059.3-keV transition (whose multipolarity has not been determined). The $3/2^\pm$ value can be ruled out because the $(p,2n\gamma)$ reaction is not likely to populate low-spin states at

higher excitation energies. (Also, again the A_2 appears to be too large for a $J \rightarrow J + 2$ transition.) From the $^{143}Gd^m$ decay data $3/2^{\pm}$ can also be excluded. An $11/2^-$ assignment would require the 1059.3-keV transition to be *M2*, and, although this cannot be definitely ruled out, we prefer the $11/2^+$ assignment. (Also, see the remarks below about a second, weaker 1059.3-keV transition.)

2378.2-keV State

This state, the last one for which it was possible to make a unique J^π assignment from the in-beam data, has its J^π restricted to $11/2^-$ or $19/2^-$ because of the large A_2 value. Its decay solely to the $15/2^-$ state and its large population in the $(p,2n\gamma)$ reaction would lead to a preference for $19/2^-$.

Other States

The remaining states in the level scheme in Figure 4-6 were placed on the basis of coincidence data, corroborated by β-decay data and energy sums. Their J^π values could not be determined uniquely from the present experimental data; however, some J^π values could be excluded on the basis of the angular distributions. Also, some of these states observed in the in-beam work had their assignments made from $^{143}Gd^m$ decay -- these are indicated by asterisks on the level scheme. And five transitions have been included (dashed lines) that were seen in $^{143}Gd^m$ decay but not in the in-beam experiments. It is worth mentioning that there are two 1059.3-keV transitions: in addition to the one deexciting the 1331.2-keV state (cf. above), coincidence data indicate another, weaker one deexciting a state at 2559.4 keV.

4.2. Triaxial Calculations and Discussion

A total of 31 states in $^{143}_{63}Eu_{80}$, many of which had not been populated by ^{143}Gd β decay, was deduced from our in-beam γ-ray experiments. For the purposes of discussion these states can be classified in three categories: 1) single-quasiparticle states, 2) negative-parity collective states, and 3) positive-parity collective states.

4.2.1. Single-Particle States

The four states at 0-, 271.94-, 389.47-, and 463.7-keV can, as expected, be described as consisting primarily of the $\pi d_{5/2}$, $\pi g_{7/2}{}^{-1}$, $\pi h_{11/2}$, $\pi s_{1/2}$ single-quasiparticle states, respectively -- four of the five possible single-proton states between Z = 50 and Z = 82. These states have not been confirmed as single-particle states by direct transfer reactions (no target exists for a straightforward reaction), but similar states have been populated with large spectroscopic factors at comparable positions in N = 82 nuclei [Ne70]. These four states in the N = 82 isotones have also been successfully analyzed by de Takacsy and Das Gupta [Ta76] as single-quasiparticle states.

It is important here to mention that the $3/2^+$ state at 258.81-keV probably does not consist primarily of the $\pi d_{3/2}$ single-quasiparticle state. The major component of the $\pi d_{3/2}$ state, which is more fractionated than the other four single-proton states, lies above 400-keV in the other N = 80 odd-mass isotones [Le78]. Thus, it is unlikely that it should lie at such a low energy in ^{143}Eu. (A state observed at 819.9-keV from ^{143}Gd^g decay may very well contain a major portion of the $\pi d_{3/2}$ wave function.) Also, the calculations (discussed below) show the 258.81-keV state to consist primarily of the $\pi d_{5/2}$ state coupled to the 2^+ ^{142}Sm core.

4.2.2. Negative-Parity Collective States

There are a number of hopefully equivalent ways to describe and interpret the more complex, higher-lying states for odd-mass nuclei in this general region: From the standpoint of β decay alone, a three-quasiparticle (or multi-quasiparticle) approach has worked quite well [Ep71], and it has the advantage of simplicity, almost an exaggerated simplicity. The other extreme of this picture is to use a weak coupling (decoupling) model in which the single-quasiparticle states are coupled to simple phonon excitations of the ^{142}Sm core. A rather qualitative version of this, using the five single-proton states coupled to the 2_1^+, 0_1^+, 2_2^+, 4_1^+, and 3_1^- vibrational states, was discussed in ref. [Fi78]. The two most noteworthy recent quantitative approaches are the triaxial weak-coupling model described by Meyer-ter-Vehn [Me75] and the interacting boson-fermion model of collective states developed and described by Iachello and Scholten [Ia79]. These calculations have been performed using a computer code modified from that of Meyer-ter-Vehn; unfortunately, the only extant calculations of Iachello and Scholten relate to the odd-mass Eu isotopes *above* $N = 82$. Thus, the discussion will be limited here to the triaxial weak-coupling model and it is hoped that in the near future the interacting boson-fermion calculations can be extended to ^{143}Eu and its neighbors.

The negative-parity collective states in ^{143}Eu are expected to consist primarily of the $\pi h_{11/2}$ state coupled to a triaxial core. The lowest excited states of the adjacent even-even nucleus [Le78], ^{142}Sm, were used in order to determine the deformation parameter β and the asymmetry parameter γ. Since the triaxial model applied to the even-even neighbor(s) does not distinguish between prolate ($0° \leqslant \gamma \leqslant 30°$) and oblate ($30° \leqslant \gamma \leqslant 60°$)

deformations, the calculations were performed for both types. The results are shown in Figure 4-8.

For a prolate shape (γ = 23.5°) the agreement with experiments is not good, either in the energy separations or even in the ordering of the levels. The calculated energies of the second $11/2^-$ state (1897.0 keV), the first $9/2^-$ state (1186.0 keV), and the first $13/2^-$ state (1508.0 keV) are considerably greater than the experimental values. Also the prolate calculation places the first $7/2^-$ state at 979.0 keV; if it were to lie this low, it should have been seen experimentally. These contradictions place doubt on ^{143}Eu being prolate. Actually, a prolate-oblate shape transition between N = 77 and N = 79 in the $_{60}$Nd isotopes has been reported by Gizon et al. [Gi78], so ^{143}Eu might be expected to be oblate.

Calculations were made for oblate shapes at both γ = 36.5° (60°-23.5°) and γ = 60°. The agreement with experiments is much improved, both in the level ordering itself and in the energy separations of the lower states, with the exception of the first $15/2^-$ state. The calculated energies of the first $9/2^-$ (900.0-keV), first $13/2^-$ (1058.0), first $15/2^-$ (1365.0), second $11/2^-$ (1386.0), first $7/2^-$, (1472.0), and first $19/2^-$ (2655.0) states at γ = 36.5° confirm the oblate shape for ^{143}Eu. Additional evidence for triaxiality includes the second and third $11/2^-$ (1386.0- and 2295.0-keV) states, as well as the second and third (2220.0- and 2506.0-keV) $9/2^-$ states, in decent agreement with their experimental counterparts. Thus, the higher-lying states appear to favor a triaxial description in preference to a pure oblate shape.

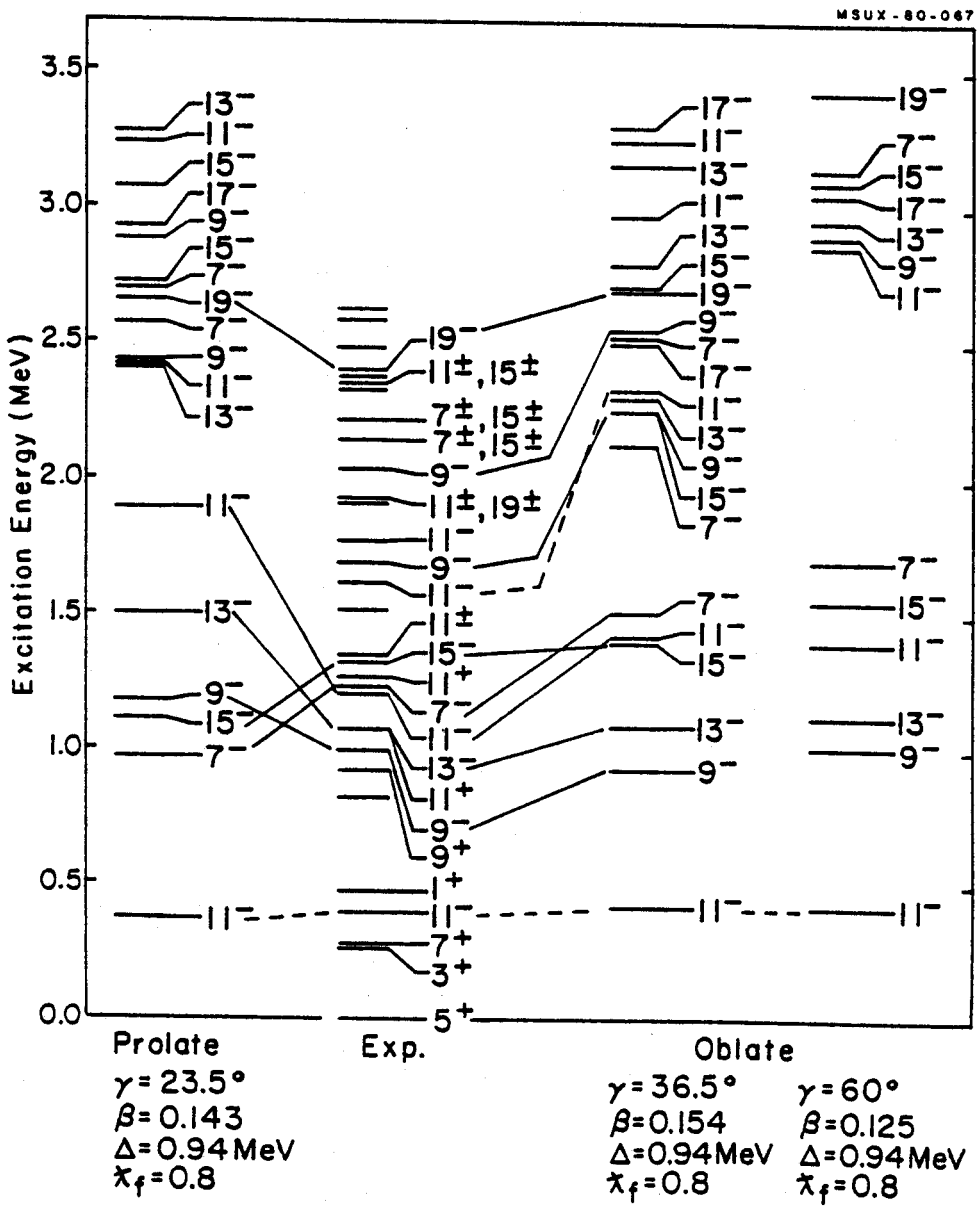

Figure 4-8. Energies of calculated excited negative-parity states in ^{143}Eu compared with our experimental findings. We calculated these energies using a triaxial weak-coupling model, coupling the $\pi h_{11/2}$ state to a deformed core. Results for both prolate and two different oblate deformations are shown; a slight oblate deformation seems indicated. Spins are shown in $2J$.

4.2.3. Positive-Parity Collective States

The positive-parity states can be generated by coupling the $\pi d_{5/2}$ and $\pi g_{7/2}{}^{-1}$ states to the triaxial core. Here the results are considerably poorer because of the ease of mixing with close-lying states having the same positive parity. In Figure 4-9 the results of the calculations using the oblate shape γ of 36.5° are shown for coupling "pure" $\pi d_{5/2}$ and $\pi g_{7/2}{}^{-1}$ to the ^{142}Sm core.

The $\pi d_{3/2}$ coupling leads to the $3/2^+$ state 258.81-keV. This indicates that the 258.81-keV state is primarily a collective state and not the $\pi d_{3/2}$ single-quasiparticle state. In fact, the $\pi d_{3/2}$ state has been observed at 405.0 and 403.9 keV, respectively, in $^{139}_{59}$Pr and $^{141}_{61}$Pm, and lies even higher in the other N = 80 odd-mass isotones.

The calculated $1/2^+$ state from the $\pi d_{5/2}$ coupling lies at 789.0 keV and could correspond to either the 804.1-keV state observed in our experiments or the 812.9-keV state observed in ^{143}Gd^g decay. The second $3/2^+$ and second $1/2^+$ state from this coupling are predicted to lie at 1546.0 and 1929.0 keV, respectively. No such low-spin states were excited near these energies in the in-beam experiments, but the two $1/2^+$ or $3/2^+$ states found at 1543.0 and 1723.6 keV from ^{143}Gd^g decay might have a loose correspondence to them.

The $\pi g_{7/2}{}^{-1}$ coupling predicts the first $11/2^+$ state to lie at 1061.0 keV. This corresponds to the experimental state found at 1057.50 keV.

Finally, the $\pi d_{5/2}$ coupling predicts a $9/2^+$ state lying at 732.0 keV, and the $\pi g_{7/2}{}^{-1}$ coupling, one at 950 keV. The experimentally observed $9/2^+$ state at 906.96 keV deexcites directly to the ground state and not through the 271.94 keV state. This would indicate that it consists primarily of the $\pi d_{5/2}$ coupling.

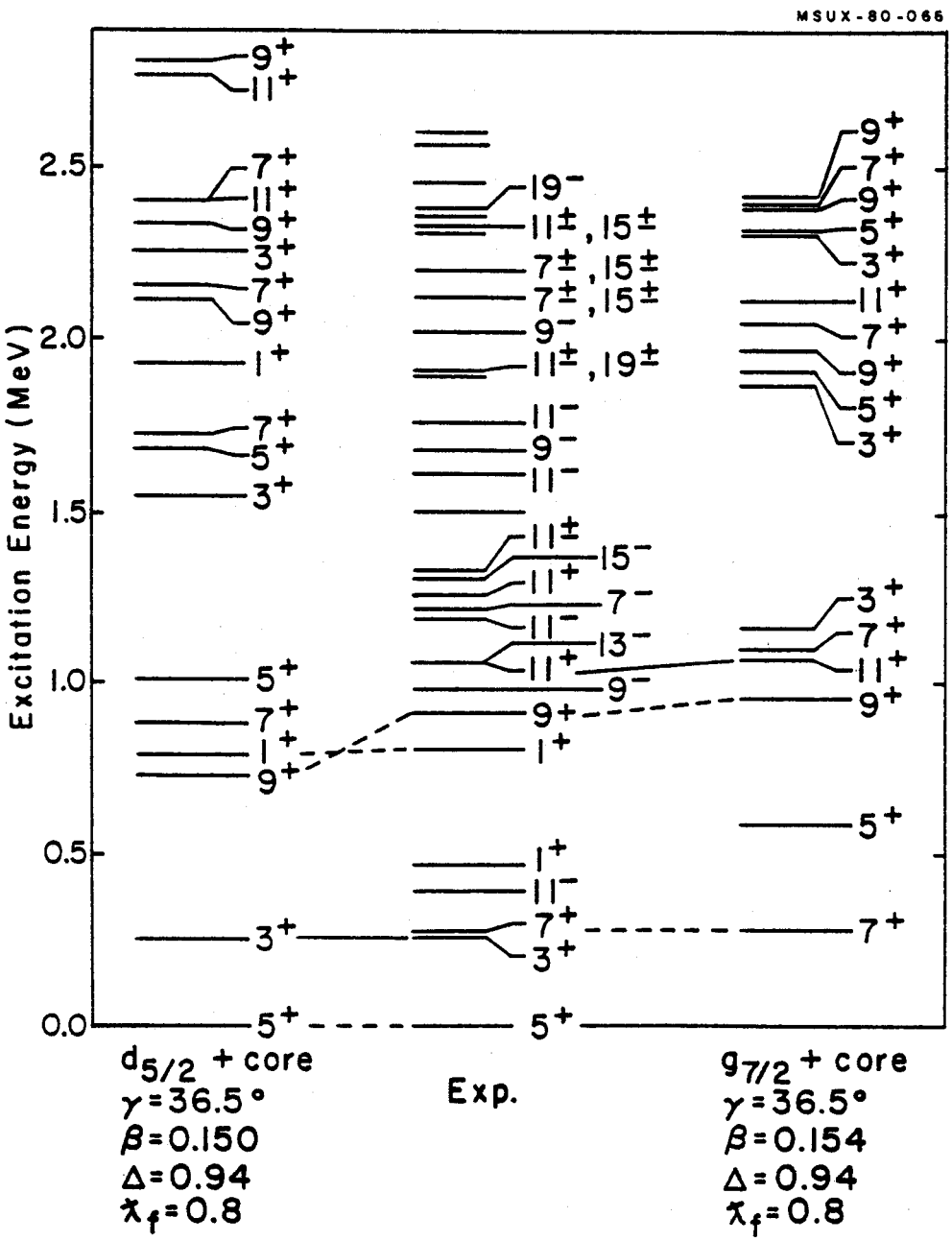

Figure 4-9. Energies of calculated excited positive-parity states in ^{143}Eu compared with our experimental findings. We calculated these energies using a triaxial weak-coupling model, coupling both the $\pi d_{5/2}$ and $\pi g_{7/2}^{-1}$ states to an oblately deformed core. Spins are shown in $2J$.

Little can be said about the higher-lying positive-parity states: first, because of the lack of information that can tie down specific spin assignments, and, second, because of the strong mixing of these positive-parity states with one another.

The triaxial weak-coupling model seems to do an unexpectedly good job of describing the level structure in ^{143}Eu. The calculations for negative-parity states indicate an oblate shape, and those for positive-parity states gave at least a germinal fit.

CHAPTER V

^{141}Pm EXPERIMENTAL RESULTS AND DISCUSSION

The previous investigations of the low-lying excited states of ^{141}Pm have been studied by β-decay of ^{141}Sm^{g} [Ke77] and ^{141}Sm^{m} [Ep72]. These studies, which included measurements of the ^{141}Sm^{g} and ^{141}Sm^{m} half-lives, the γ-ray spectrum, γ-γ coincidences, the internal-conversion electron spectrum, and half-life measurement of the 628.6-keV isomeric state in ^{141}Pm, produced valuable information. However, only selected states below 3 MeV could be populated and unambiguous spin assignments for these states could be made.

The ^{142}Nd(p,2nγ)^{141}Pm and ^{141}Pr(α,4nγ)^{141}Pm reactions were chosen for this study in order to get more information about low spin states as well as high spin states. These experiments corroborated and complemented the previous ^{141}Sm β-decay works and were able to resolve several discrepancies encountered in the β-decay work. Several γ-rays that were not observed by the previous investigators were found.

5.1. Experimental Details and Results for the (p,2nγ) Reaction

5.1.1. Target and Reaction

The excited states in ^{141}Pm were populated via the ^{142}Nd(p,2nγ)^{141}Pm reaction. A target was prepared by drying a thin slurry of 99.9% enriched $^{142}Nd_2O_3$ onto a thin formvar backing. This target was bombarded with a 25-MeV p beam from the MSU (50-MeV) sector-focused cyclotron.

The reaction cross section for (p,xn) reaction as a function of proton particle energy were calculated using the code CS8N [CS8N]. From

these calculations the primary contaminant directly by the 25-MeV p beam is ^{142}Pm. The EC/β^+ decay half-lives of ^{141}Pm and ^{142}Pm are 20.9 min and 40.5 sec, respectively. Their decays also produced identifiable γ-rays from states in ^{141}Nd and ^{142}Nd.

5.1.2. γ-Ray Singles Spectra

The γ-rays from the ^{142}Nd$(p,2n\gamma)^{141}$Pm reaction were detected with a 17%-efficient Ge(Li) detector (with a resolution of 1.9 keV FWHM) at approximately 125° with respect to the beam direction, and the counting period was typically about 2.5-h at counting rates of ~6000-8000 cps. A copper-cadmium absorber was used to shield the detector from x-rays which would otherwise dominate the spectrum. A singles γ-ray spectrum is shown in Figure 5-1. All of the data analysis was accomplished by use of SAMPO, described in Section 3.1. The energy calibrations were performed using ^{60}Co, ^{152}Eu and ^{226}Ra radioactive sources. Transition intensities were determined by correcting net peak areas by use of the detector efficiency curves shown in Figure 5-2.

A total of 40 γ-rays were assigned to ^{141}Pm from $(p,2n\gamma)$ reaction on the basis of singles spectra and coincidence experiments discussed below. These are listed in Table 5-1 together with their relative intensities. The relative intensities of those transitions which were part of doublets and were not able to be resolved are indicated by question marks. Also, this table includes angular distribution coefficients and transition multipolarity assignments which will be discussed later.

5.1.3. Coincidence Spectra

The γ-γ coincidence spectra were obtained with a 25-MeV p beam. In this experiment two detectors, a 10%-efficient Ge(Li) detector and a

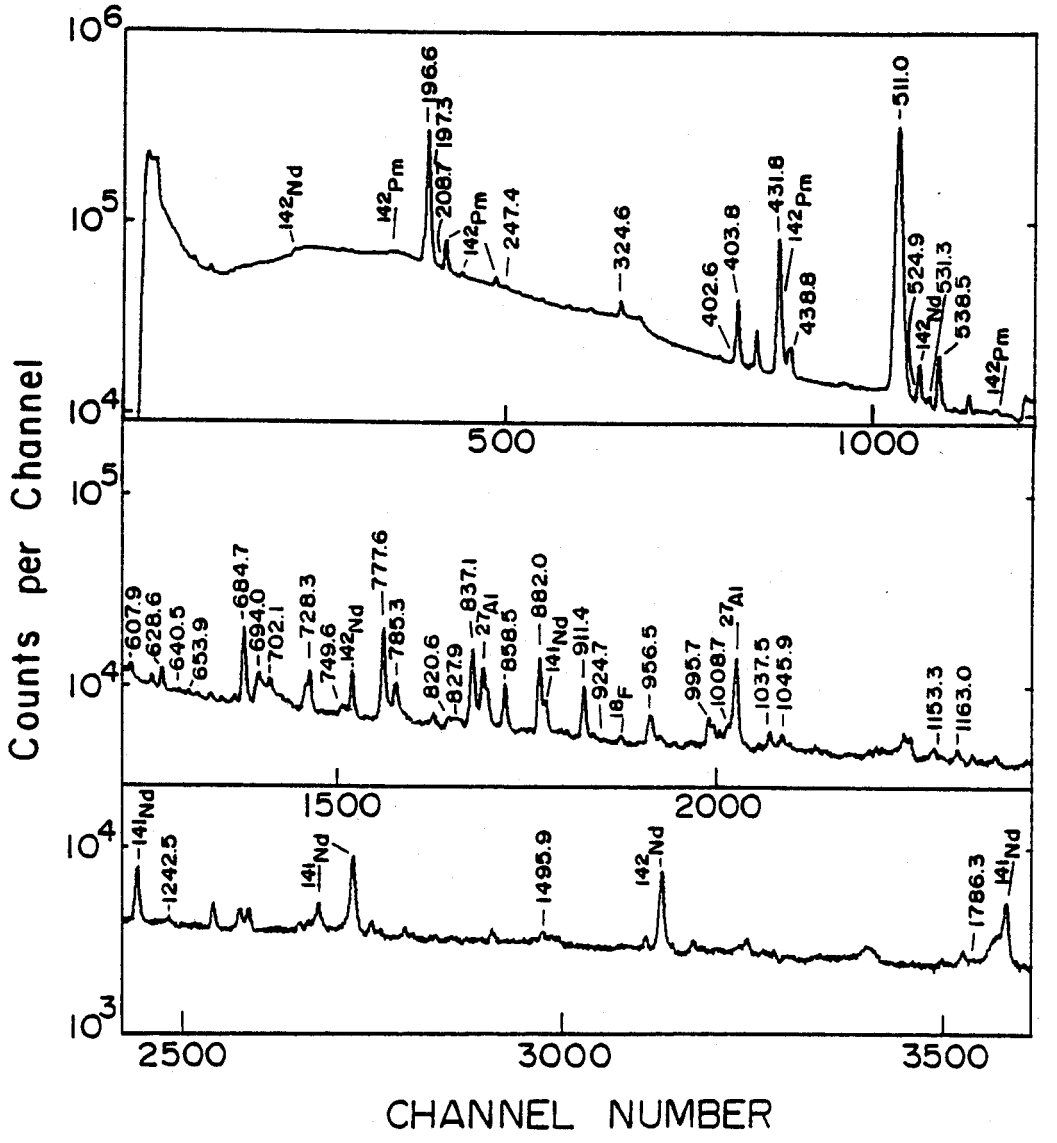

Figure 5-1. γ-ray singles spectrum of $^{142}Nd(p,2n\gamma)^{141}Pm$ taken with the 17%-efficient Ge(Li) detector placed at 125°.

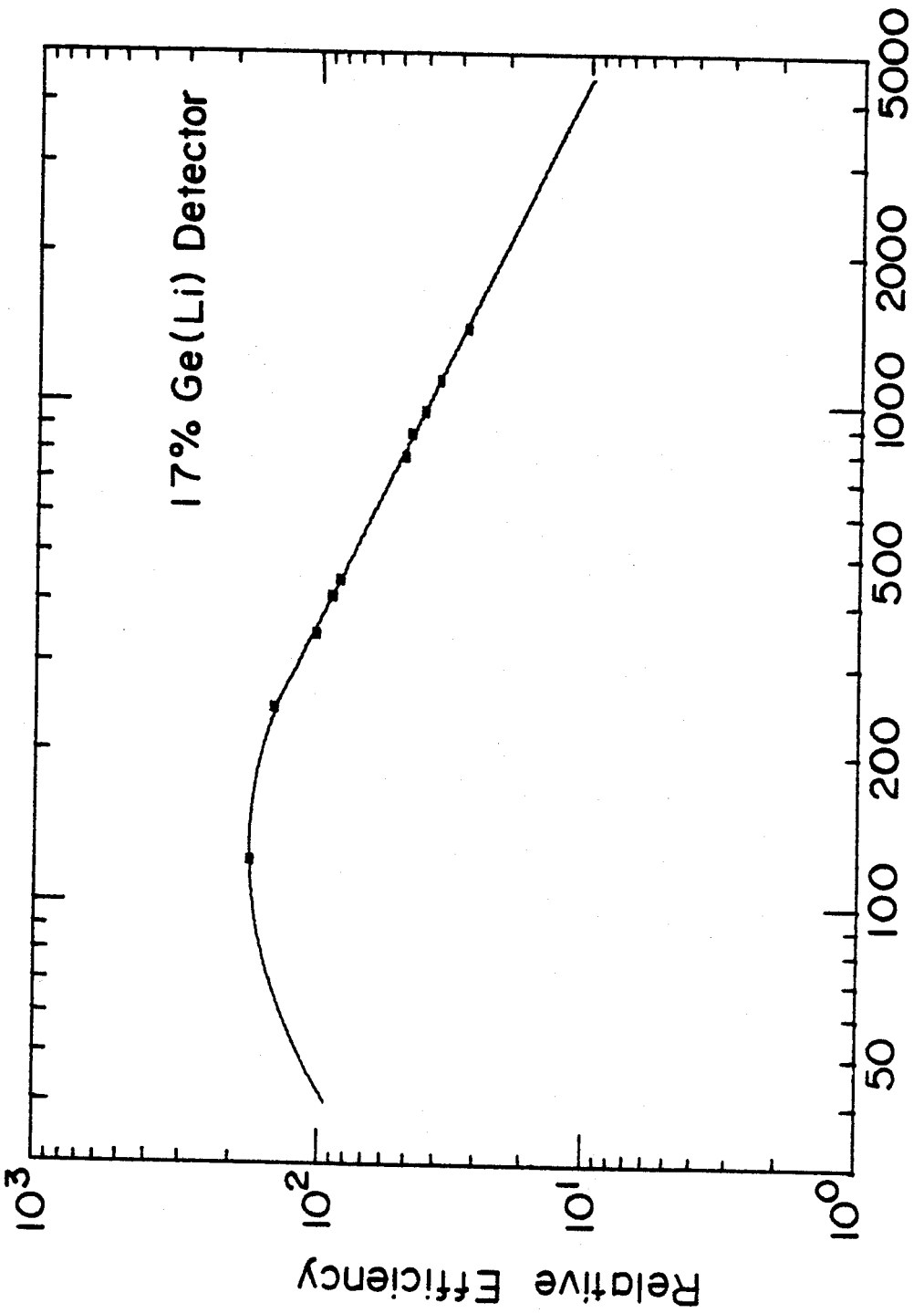

Figure 5-2. A detector efficiency curve for a 17%-efficient Ge(Li) detector with a source detector distance of 20 cm.

Table 5-1. Energies, relative intensities, angular distribution coefficients, and multipolarities for γ transitions in ^{141}Pm from $(p,2n\gamma)$ reactions.

Energy E_γ (keV)	Relative Intensity I_γ	Angular Distribution Coefficients A_2/A_0	A_4/A_0	Multipolarity[a]
196.6±0.1[b]	185.7±11.2[c]	-0.02±0.01	-0.02±0.01	M1
197.3±0.2[b]	?	---	---	---
208.7±0.1[b]	weak	---	---	---
247.4±0.2	1.5±0.2	-0.25±0.12	-0.03±0.19	---
324.6±0.1[b]	6.8±0.5	-0.08±0.02	0.05±0.03	M1
402.6±0.2	?	---	---	---
403.8±0.1[b]	31.3±1.9	-0.10±0.02	0.04±0.02	M1+E2
431.8±0.1[b]	≡100	isotropic	---	M2
438.8±0.1	12.7±1.2	-0.28±0.22	0.25±0.25	E2
524.9±0.2	weak	---	---	---
531.3±0.2	3.2±0.3	0.15±0.08	0.19±0.11	---
538.5±0.2	18.9±1.2	-0.34±0.02	0.02±0.02	M1
607.9±0.2	3.6±0.5	-0.06±0.06	-0.06±0.10	---
628.6±0.1[b]	7.1±0.5	0.01±0.02	0.01±0.04	---
640.5±0.2	weak	---	---	---
653.9±0.2[b]	1.2±0.1	---	---	---
684.7±0.2[b]	28.9±1.8	-0.77±0.01	0.06±0.02	M1+E2
694.0±0.2	8.4±0.8	-0.11±0.04	0.09±0.06	---
702.1±0.1[b]	5.4±0.6	-0.90±0.03	-0.15±0.06	---
728.3±0.1[b]	12.8±0.8	-0.05±0.03	-0.60±0.11	---
749.6±0.1	3.4±0.4	---	---	---

Table 5-1. (cont'd.).

Energy E_γ (keV)	Relative Intensity I_γ	Angular Distribution Coefficients A_2/A_0	A_4/A_0	Multipolarity[a]
777.6±0.1[b]	35.8±2.1	0.27±0.01	-0.05±0.01	E2
785.3±0.2[b]	10.6±0.8	-0.34±0.04	0.04±0.06	E2
820.6±0.2	1.9±0.6	---	---	---
827.9±0.3	1.4±0.5	---	---	---
837.1±0.1[b]	29.9±1.9	0.20±0.03	-0.06±0.04	---
858.5±0.3	14.1±0.8	0.26±0.01	-0.02±0.01	---
882.0±0.1[b]	29.5±1.8	0.26±0.02	-0.11±0.04	---
911.4±0.2[b]	16.1±1.0	0.04±0.02	0.12±0.02	E2
924.7±0.3	weak	---	---	---
956.5±0.3	9.8±0.7	-0.30±0.07	-0.03±0.12	---
995.7±0.2[b]	6.6±0.5	0.44±0.06	0.06±0.09	---
1008.7±0.3	5.0±0.4	-0.43±0.04	-0.10±0.06	---
1037.5±0.3	4.1±0.3	0.35±0.09	-0.03±0.16	---
1045.9±0.4	3.5±0.3	0.14±0.01	-0.13±0.02	---
1153.3±0.3	1.0±0.2	-0.49±0.05	-0.14±0.11	---
1163.0±0.3[b]	3.4±0.3	0.29±0.03	-0.11±0.06	---
1242.5±0.4	1.7±0.2	-0.15±0.06	-0.05±0.09	---
1495.9±0.4	1.9±0.2	---	---	---
1786.3±0.4	0.6±0.2	---	---	---

[a]Transition multipolarity assignments taken from conversion electrons, ref. [Ke77].

[b]These γ-rays were also seen in (α,4nγ) reaction. Therefore, the γ-ray energies are the average of (p,2nγ) and (α,4nγ) reactions.

[c]Part of this intensity belongs to 197.3-keV transition.

16%-efficient Ge(Li) detector (energy resolution 2.6 keV FWHM), were used. More detail on the electronic set-up is discussed in section 3.2. A resolving time of $2\tau \approx 100$ nsec was also used.

In Appendix C, important coincidence gates which were used to make the level assignments are shown.

The coincidence information was used to construct a tentative level scheme. The data from the angular distribution and singles spectra were then used to lend support to the level scheme. Construction of the level scheme and spin assignments will be discussed in section 5-3. A summary of the coincidence data is given in Table 5-2.

5.1.4. γ-Ray Angular Distributions

The *p* beam energy of 25 MeV was obtained for the γ-ray angular distribution experiment. The detector used was a 17%-efficient Ge(Li) detector. The detector was positioned as discussed in section 3.3. The set of angular distribution data for ^{141}Pm consists of spectra taken at 90°, 100°, 110°, 125°, 140°, and 155°. The angles were taken in random order for the various experiments and data were typically collected for 2.5 *h* at each angle.

The 431.8-keV isotropic transition is used as an internal normalization for the spectra taken at different angles. Peak intensities were derived from the peak fitting program SAMPO [Ro69], and fitted to the equation

$$I = 1 + (A_2/A_0)P_2(\cos\Theta) + (A_4/A_0)P_4(\cos\Theta)$$

using the least squares fitting computer code GADFIT [GADFIT]. The parameters extracted from the fit, A_2/A_0 and A_4/A_0 are included in Table 5-1. The A_2 and A_4 values for 196.6- and 628.6-keV transitions turned out to be close to zero, as we expected them to be isotropic due to deexcitation

Table 5-2. Summary of coincidence results for the ^{142}Nd $(p,2n\gamma)$ ^{141}Pm reaction.

Gated γ-Ray (keV)	Coincident γ-Rays (keV)
196.6	197.3, 431.8, 531.3, 607.9, 640.5, 653.9, 684.7, 694.0, 777.6, 820.6, 911.4, 956.5, 995.7, 1045.9, 1163.0, 1495.9, 1786.3
208.7	196.6, 431.8, 1037.5
247.4	538.5
324.6	403.7
(402.6 + 403.8)	196.6, 324.6, 728.3, 749.6, 911.4
431.8	196.6, 208.7
438.8	---
531.3	196.6
538.5	247.4, 924.7
607.9	196.6
628.6	---
640.5	196.6, 1037.5
653.9	196.6, 777.6
684.7	197.3, 702.1, 785.3, 858.5
694.0	196.6, 911.4
702.1	684.7
728.3[a]	402.6, 882.0
749.6	403.8
777.6	196.6, 653.9, 820.6, 995.7, 1008.7
785.3[a]	684.7
820.6	196.6, 777.6
827.9	196.6, 777.6

Table 5-2. (cont'd.).

Gated γ-Ray (keV)	Coincident γ-Rays (keV)
837.1	1037.5
858.5	684.7
882.0	728.3
911.4	196.6, 402.6, 694.0
924.7	538.5
956.5	196.6
995.7	196.6, 777.6
1008.7	196.6, 777.6
1037.5	196.6, 208.7, 640.5, 837.1
1045.9	196.6
1163.0	196.6
1495.9	196.6
1786.3	196.6

[a]There are two transitions with this energy in the level scheme.

from the 628.6-keV isomeric state. The values of A_2/A_0 were, in general, more reliable than the values of A_4/A_0 and could be used to estimate the mixing ratios for the more intense transitions. The data with the fitted curves for some of the γ-rays are shown in Appendix D.

5.2. Experimental Details and Results for the (α,4nγ) Reaction

5.2.1. Target and Reaction

By using an α beam, the high spin excited states in ^{141}Pm were populated via the ^{141}Pr(α,4nγ)^{141}Pm reaction. A target was prepared by drying a thin slurry of 99.9% enriched $^{141}Pr_2O_3$ onto a thin formvar backing.

The α-beam particle beam was produced in the MSU sector-focused isochronous cyclotron. The beam current required for these experiments was about 10 na for most experiments and was readily obtainable for the runs. The reaction cross section for (α,*xn*) reactions as a function of alpha particle energy was calculated using the code CS8N [CS8N] which is shown in Figure 5-3. The maximum cross section for (α,2*n*) through (α,4*n*) reactions are spaced about 10-MeV apart. According to Figure 5-3, the best alpha particle energy for (α,4nγ) reaction in order to minimize the production of contaminant γ-rays would be 54 MeV. At this energy, the amount of contaminant production (α,3*n*) and (α,5*n*) is about 4% of the total cross section.

The highest energy alpha beam, 47 MeV, which could be obtained by the cyclotron was used for the ^{141}Pr(α,4nγ)^{141}Pm experiments. By using a 47-MeV alpha particle, the amount of the main contaminant ^{142}Pm is going to be about 34% of the total cross section. The other contaminants produced directly to a lesser extent would be ^{143}Pm and ^{143}Nd. The EC/β^+ decay of ^{141}Pm and ^{142}Pm also produce identifiable γ-rays from states in

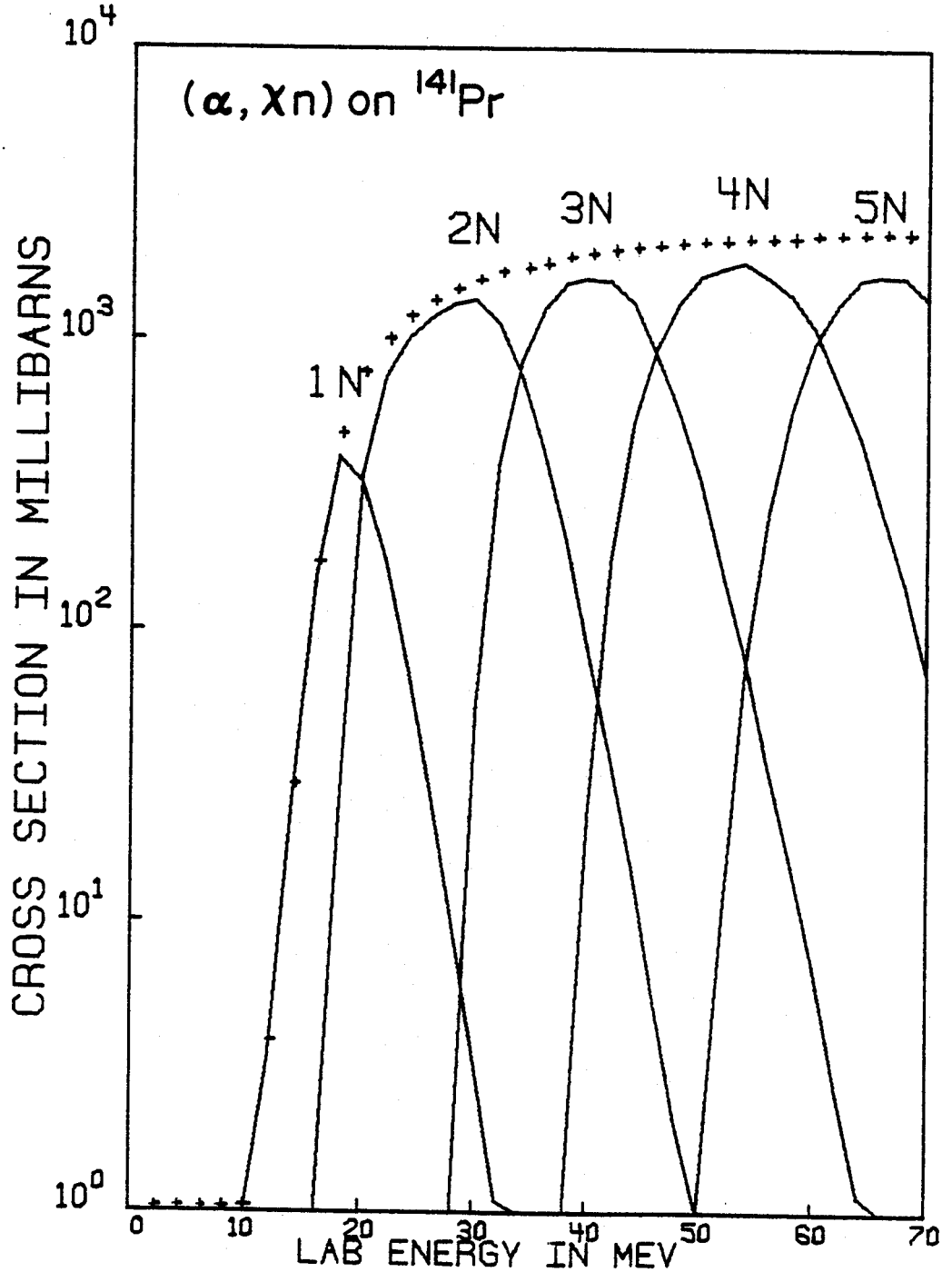

Figure 5-3. Excitation functions for $^{141}Pr(\alpha,xn)$ reactions calculated using the code CS8N.

^{141}Nd and ^{142}Nd respectively. These predictions were observed in the experiments. Some other impurities came from the reaction of alpha particles with oxygen in the target.

5.2.2. γ-Ray Singles Spectra

The detector which was chosen for the singles experiments was a 7.7%-efficient Ge(Li) detector (with a resolution of 1.9 keV FWHM). This detector was placed at 125° with respect to the beam direction and the counting period was typically about 2.5 *h* at counting rates of ≈6000-8000 cps. A copper-cadmium absorber was used to shield the detector from x-rays which would otherwise dominate the spectrum. In Figure 5-4, a singles γ-ray spectrum is shown. The general experimental techniques and data analysis used were the same as discussed in section 3.1. Several radioactive sources, such as ^{60}Co, ^{152}Eu and ^{226}Ra, were used to perform energy calibrations. An efficiency curve for the detector was obtained (Figure 5-5) and relative intensities for the transitions were determined.

A total of 33 γ-rays were assigned to ^{141}Pm from (α,4*n*γ) reaction on the basis of singles spectra and coincidence experiments discussed below. Energies and intensities of peaks that are believed to belong to ^{141}Pm are listed in Table 5-3. The relative intensities of those transitions which were part of doublets and were not able to be resolved are indicated by question marks. In general, γ-rays are not listed in this table unless coincidence information demands that they should be. Since most of the contaminants are known to be ^{142}Pm, ^{142}Nd, and ^{141}Nd, the energies of these γ-rays are not included. Also, this table includes angular distribution coefficients and transition multipolarity assignments which will be discussed later.

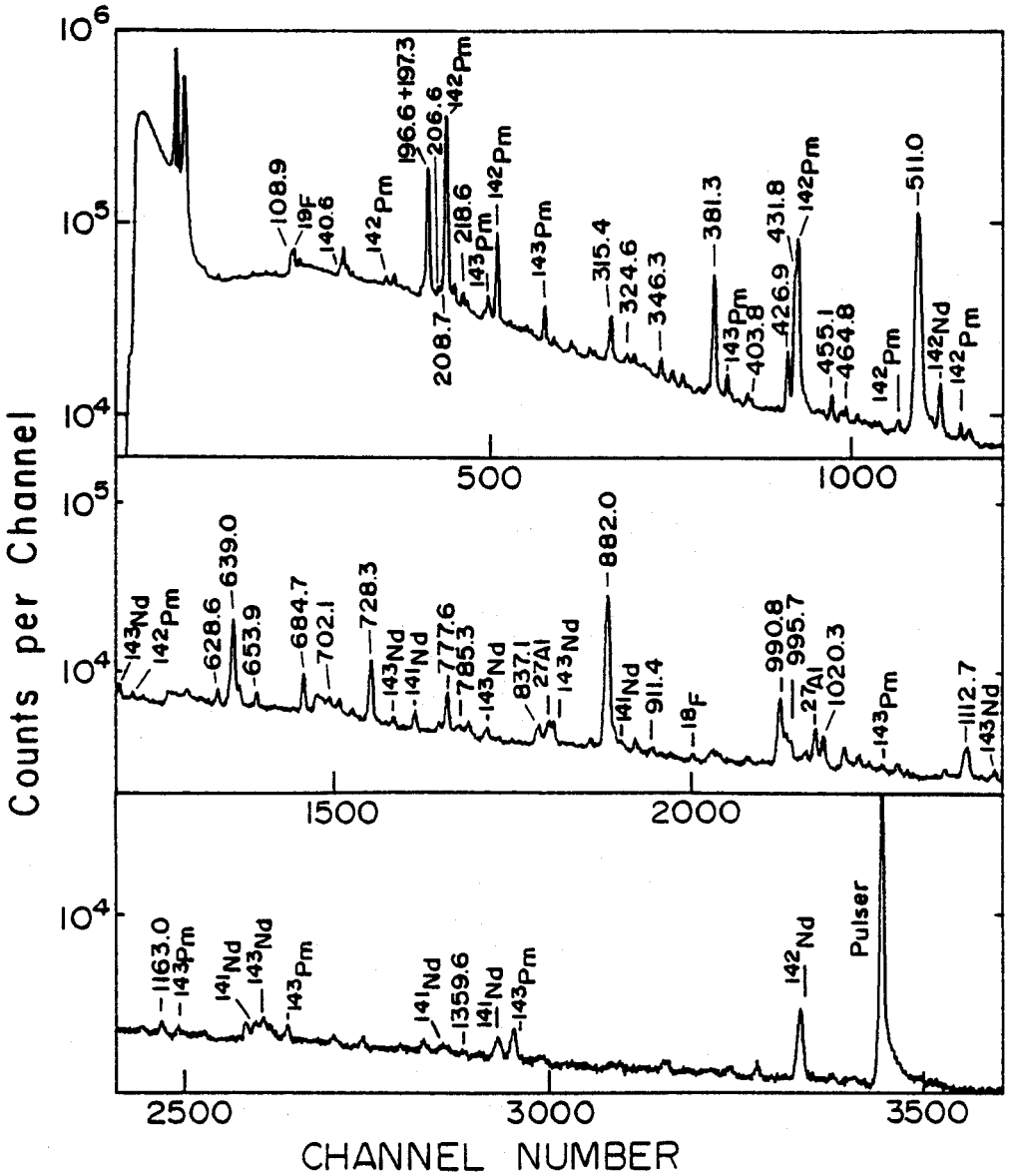

Figure 5-4. γ-ray singles spectrum of $^{141}Pr(\alpha,4n\gamma)^{141}Pm$ taken with a 7.7%-efficient Ge(Li) detector placed at 125°.

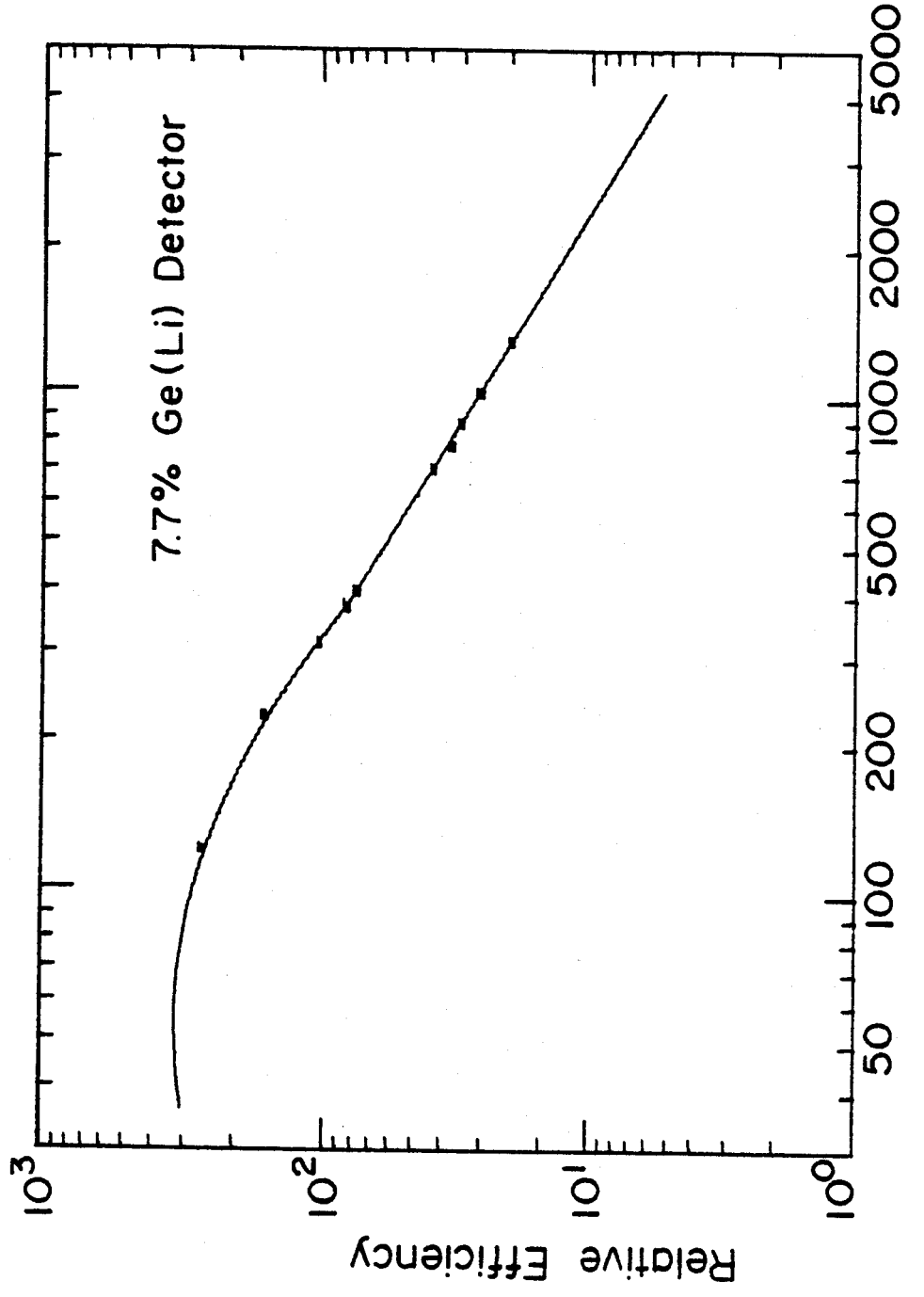

Figure 5-5. A detector efficiency curve for a 7.7%-efficient Ge(Li) detector with a source-detector distance of 20 cm.

Table 5-3. Energies, relative intensities, angular distribution coefficients, and multipolarities for γ transitions in ^{141}Pm from (α,4nγ) reactions.

Energy E_γ (keV)	Relative Intensity I_γ	Angular Distribution Coefficients A_2/A_0	A_4/A_0	Multipolarity[a]
108.9±0.2	?	---	---	---
140.6±0.2	10.3±1.2	-0.13±0.07	-0.03±0.10	---
196.6±0.1[b]	338.1±8.6[c]	-0.06±0.06	-0.02±0.07	M1
197.3±0.2[b]	?	---	---	---
206.6±0.2	weak	---	---	---
208.7±0.1[b]	?	---	---	---
218.6±0.2	3.1±0.2	---	---	---
315.4±0.1	33.8±0.8	-0.18±0.05	0.02±0.07	---
324.6±0.1[b]	5.7±0.3	-0.26±0.07	0.02±0.09	M1
346.3±0.2	10.9±0.4	-0.44±0.03	-0.01±0.04	---
381.3±0.1	106.6±2.5	-0.11±0.03	0.02±0.05	---
403.8±0.1	2.7±0.4	---	---	M1+E2
426.9±0.1	21.2±0.9	-0.39±0.04	0.03±0.05	---
431.8±0.1[b]	≡100	0.02±0.02	0.04±0.04	M2
455.1±0.2	7.8±0.7	0.30±0.06	0.04±0.08	---
464.8±0.2	5.1±0.5	-0.22±0.05	0.12±0.07	---
628.6±0.1[b]	6.1±0.4	0.07±0.03	0.04±0.04	---
639.0±0.1	43.9±1.1	-0.02±0.03	0.02±0.04	---
653.9±0.2[b]	4.2±0.5	-0.50±0.07	0.08±0.10	---
684.7±0.2[b]	11.2±0.4	-0.89±0.02	0.08±0.03	M1+E2

Table 5-3. (cont'd.).

Energy E_γ (keV)	Relative Intensity I_γ	Angular Distribution Coefficients A_2/A_0	A_4/A_0	Multipolarity[a]
702.1±0.1[b]	3.5±0.3	-0.59±0.02	0.01±0.03	---
728.3±0.1[b]	22.3±0.5	0.28±0.03	-0.02±0.05	---
777.6±0.1[b]	10.3±0.2	0.32±0.04	0.01±0.06	E2
785.3±0.2[b]	1.3±0.2	-0.93±0.09	0.27±0.12	E2
837.1±0.1[b]	3.1±0.2	0.22±0.08	-0.06±0.12	---
882.0±0.1[b]	85.1±2.1	0.06±0.02	-0.02±0.04	---
911.4±0.2[b]	1.4±0.2	---	---	E2
990.8±0.2	16.0±0.4	-0.22±0.02	0.02±0.03	---
995.7±0.2[b]	4.8±0.2	0.41±0.03	0.03±0.04	---
1020.3±0.3	5.1±0.2	-0.03±0.03	-0.04±0.04	---
1112.7±0.2	4.1±0.2	-0.15±0.04	0.18±0.05	---
1163.0±0.3[b]	1.5±0.1	0.15±0.06	0.02±0.09	---
1359.6±0.4	weak	---	---	---

[a]Transition multipolarity assignments taken from conversion electrons, ref. [Ke77].

[b]These γ-rays were also seen in (p,2nγ) reaction; therefore, the γ-ray energies are the average of (p,2nγ) and (α,4nγ) reactions.

[c]Part of this intensity belongs to 197.3-keV transition.

5.2.3. Coincidence Spectra

Using the same geometry and electronic set-up described in section 3.2, three-parameter coincidence events were recorded on five magnetic tapes, each containing 3×10^6 events. The detectors used were both of large volume (7.7% and 16%-efficient) and the TAC resolving time was about $2\tau \approx 4$ μsec.

The coincidence gates for most of the transitions which have been placed are shown in Appendix E.

The coincidence information was used to construct a tentative level scheme. The data from the angular distribution and singles spectra were then used to lend support to the level scheme. Construction of the level scheme and spin assignments will be discussed in section 5-3. The results of the coincidence measurements are summarized in Table 5-4.

5.2.4. γ-Rays Angular Distributions

A 47-MeV α-beam produced by the MSU cyclotron was used for γ-ray angular distribution experiments. The 7.7%-efficient Ge(Li) detector was mounted on the arm of the goniometer apparatus as described in section 3.3. The data were collected at 90°, 110°, 125°, 140°, 150°, and 160° with respect to the beam direction. The angles were taken in random order for the various experiments, and data were typically collected for 2.5 *h* at each angle.

A normalization was provided by using a stationary 16%-efficient Ge(Li) detector. The resulting distributions were fitted to an expansion of Legendre Polynomials to give the experimental A_2/A_0 and A_4/A_0 coefficients. These are listed in Table 5-3. The A_2 and A_4 values for 196.6-, 431.8- and 628.6-keV transitions turned out to be close to zero; we

Table 5-4. Summary of coincidence results for the ^{141}Pr (α,4nγ) ^{141}Pm reaction.

Gated γ-Ray (keV)	Coincident γ-Rays (keV)
108.9	324.6, 403.8, 728.3
196.6	197.3, 346.3, 426.9, 431.8, 455.1, 464.8, 653.9, 684.7, 777.6, 882.0, 911.4, 995.7, 1112.7, 1163.0
208.7	196.6, 431.8, 728.3
315.4	728.3, 882.0
324.6	108.9, 403.8
346.3	197.3, 381.3, 822.0
381.3	206.6, 426.9, 455.1, 639.0, 882.0, 1112.7
403.8	108.9, 324.6, 728.3
426.9	206.6, 381.3, 455.1, 639.0, 1020.3, 1112.7
431.8	196.6, 346.3, 381.3, 426.9 684.7, 882.0
455.1	381.1, 426.9, 639.0, 728.3
464.8	197.3, 728.3, 882.0
628.6	---
639.0	197.3, 381.3, 455.1, 882.0
653.9	196.6, 777.6
684.7	197.3, 381.3, 639.0, 702.1, 785.3
702.1	684.7
728.3[a]	108.9, 197.3, 315.4, 464.8, 882.0
777.6	196.6, 653.9, 995.7
785.3	684.7
882.0	196.6, 315.4, 381.3, 431.8, 464.8 639.0, 728.3, 1020.3, 1112.7

Table 5-4. (cont'd.).

Gated γ-Ray (keV)	Coincident γ-Rays (keV)
911.4	196.6, 990.8
990.8	196.6, 911.4
1020.3	882.0
1112.7	197.3, 381.3, 882.0
1163.0	196.6

[a]There are two transitions with this energy in the level scheme.

expected them to be isotropic due to deexcitation from the 628.6-keV isomeric state. The angular distribution coefficients not listed in the table were either part of unresolvable multiplets or too weak for accurate peak fitting. These coefficients were then compared to theoretical values [Ya67] to aid in assigning spins. The values of A_2/A_0 were, in general, more reliable than the values of A_4/A_0 and could be used to estimate the mixing ratios for the more intense transitions. The data with the fitted curves for some of the γ-rays are shown in Appendix F.

5.3. Construct of the ^{141}Pm Level Scheme and Comparison

The proposed level schemes for ^{141}Pm, both from $(p,2n\gamma)$ and $(\alpha,4n\gamma)$ reactions, were constructed based primarily on the coincidence information, intensity balances, conversion coefficients and delayed-coincidence spectra [in the case of $(\alpha,4n\gamma)$ reaction]. Secondary factors were energy summing relationships, input from the known $^{141}Sm^{m+g}$ decay scheme [Ep72, Ke77], and angular distribution data from this study. The spin and parity assignments were made on the basis of angular distribution coefficients, conversion coefficients, and input from the $^{141}Sm^{m+g}$ decay scheme.

This section will be broken into three parts: 1) level scheme and spin-parity assignments from $(p,2n\gamma)$ reaction, 2) level scheme and spin-parity assignments from $(\alpha,4n\gamma)$ reaction, and 3) comparison between these two reactions and with other experimental results.

5.3.1. Level Scheme and Spin-Parity Assignments from $(p,2n\gamma)$ Reaction

The resulting level scheme from $(p,2n\gamma)$ reaction is shown in Figure 5-6. Specific details of construction of the level scheme and J^π assignments are discussed next.

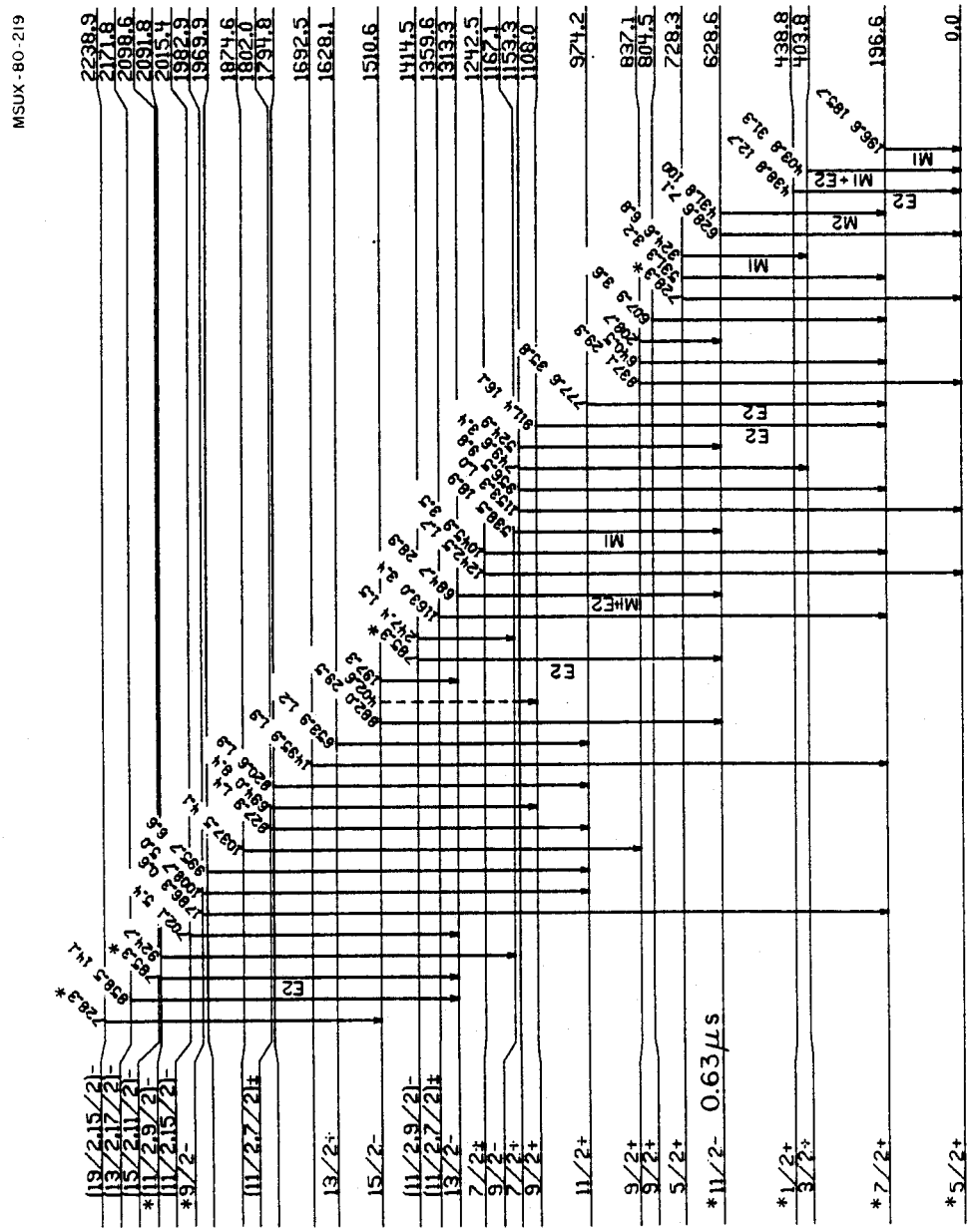

Figure 5-6. Level scheme of ^{141}Pm obtained from (p,2nγ) reaction.

Ground, 196.6-, and 628.6-keV States

The most intense γ transition in the in-beam as well as the off-line experiments is 196.6-keV transition, which is in coincidence with the 431.8-keV transition (and with others -cf. Table 5-2). On the other hand, no other γ-rays appear to be in coincidence with the 431.8-keV (except 208.7-keV transition which is visibly weak - see 431.8-keV gates in Appendix C). This leads to the adoption of a first excited state at 196.6-keV. This is completely consistent with the systematics of this region, and placement of the 628.6-keV state which decays to the 196.6-keV level via the 431.8-keV transition and to the ground state via the 628.6-keV transition also results.

The J^{π} of the ground state of ^{141}Pm is known to be $5/2^{+}$ [Ya75 and Ec72], and the 196.6- and 628.6-keV states have been assigned $7/2^{+}$ and $11/2^{-}$, respectively, on the basis of the multipolarities of the 196.6- and 431.8-keV transitions and logft values for ^{141}Sm^{m} β-decay. The half-life of 628.6-keV state was measured by several people. The latest measurement was 0.59 μsec [Ke77]. In this work, the half-life of this isomeric state has been measured from $(\alpha,4n\gamma)$ reaction to be 0.63 μsec - cf. section 5.3.2.

Because of the isomeric nature of the 628.6-keV state, one expects the 196.6-, 431.8-, and 628.6-keV transitions to be definitely isotropic. In fact, this was proven from both $(p,2n\gamma)$ and $(\alpha,4n\gamma)$ to be true (e.g. see the values of A_2 and A_4 for the 196.6- and 628.6-keV transitions in Table 5-1). Although this information does not allow us to comment further on the J^{π} assignments, it is conceivable to believe J^{π} assignments from ^{141}Sm^{m} β-decay both by the systematics of the region and by the fact of the long half-life of the 628.6-keV state are reasonable.

403.8-, 438.8-, and 728.3-keV States

These states are the other low-lying and presumably lower spin states. The fact that 438.8-keV transition is not in coincidence with any transition leads to the placement of a level at 438.8 keV. This level has been reported to have $J^{\pi} = 1/2^{+}$ with some feeding from the many higher-lying, lower-spin states [Ke77]. Therefore, it is not unusual not to see these low-spin states at such a high excitation energy in $(p,2n\gamma)$ reaction. Spin assignment for 438.8-keV state was not possible from angular distribution coefficients because of their large errors. However, $J^{\pi} = 1/2^{+}$ assignment, on the basis of the multipolarity and the logft value for $^{141}Sm^{g}$ β-decay, seems to be appropriate considering both the shell model and nuclear systematics. Also, absence of any transitions in coincidence with 438.8-keV transition in $(p,2n\gamma)$ reaction is another evidence for this spin assignment.

From the 403.8-keV gated spectrum (which includes 402.6-keV gate as well) shown in Appendix C, one can see evidence for coincidences with the 324.4- and 749.6-keV transitions (the rest of the γ-rays are in coincidence with 402.6-keV transition). The intensity balances suggest levels at 403.8 , 728.3 , and 1153.3 keV.

The 403.8-keV transition is a mixed *M1/E2* transition; therefore the J^{π} assignment is restricted to $3/2^{+}$, $5/2^{+}$, or $7/2^{+}$. The $5/2^{+}$ value is ruled out because of the large negative value of A_2 and the small positive value of A_4. The logft of 5.8 for this level from $^{141}Sm^{g}$ decay and the missing transition from this level to the $7/2^{+}$ level at 196.6 keV, rule out $J^{\pi} = 7/2^{+}$. Thus, 403.8-keV state has $J^{\pi} = 3/2^{+}$.

The 728.3-keV state feeds into the $5/2^{+}$ ground, $7/2^{+}$ 196.6-, and $3/2^{+}$ 403.8-keV states by the 728.3-, 531.3- and 324.6-keV transitions,

respectively. From $^{141}Sm^{g}$ decay, *M1* or *E2* multipolarity was assigned for the 324.6-keV transition. Our data is consistent with almost pure *M1* multipolarity which limits J^{π} for 728.3-keV state to $1/2^{+}$, $3/2^{+}$, or $5/2^{+}$. The $3/2^{+}$ value is ruled out because of the negative value of A_2 and the small positive value of A_4. On the other hand, the lack of a long half-life for this state rules out the possibility of *M3* multipolarity for 531.3-keV transition and therefore $J^{\pi} = 1/2^{+}$ can be ruled out. The angular distribution coefficients for this transition give more support to eliminate $1/2^{+}$ assignment (any transitions deexcite from $1/2^{+}$ should be isotropic), and to accept $5/2^{+}$. Also, log*ft* of 6.8 for 728.3-keV state from $^{141}Sm^{g}$ decay is consistent with $5/2^{+}$ assignment.

804.5-keV State

The coincidence information between 607.9- and 196.6-keV γ's places this state. It was also seen in $^{141}Sm^{m}$ decay, where it was tentatively assigned $9/2^{+}$ or $11/2^{+}$. With the $11/2^{+}$ assignment, the 607.9-keV transition would be pure *E2* and with the $9/2^{+}$ assignment it would be mixed *M1/E2*. The angular distribution coefficients, even with such large errors, prefer $9/2^{+}$.

837.1-keV State

This state was placed by coincidence information from its deexciting 208.7- and 640.5-keV transition as well as by its energy sum relationships. The angular distribution coefficients of 837.1-keV transition that deexcites this state to the $5/2^{+}$ ground state limits its J^{π} to $1/2^{+}$ or $9/2^{+}$. From the $^{141}Sm^{m}$ decay data, $1/2^{+}$ can be excluded. Also, the deexcitations of 640.5- and 208.7-keV transitions into 196.6- and 628.6-keV states do not confirm a $1/2^{+}$ assignment. Thus, the 837.1-keV state has $J^{\pi} = 9/2^{+}$.

974.2-keV State

The coincidence information between the 196.6- and 777.6-keV [second strongest transition in $(p,2n\gamma)$ reaction] γ's places this state. The 777.6-keV transition was reported to have *E1* or *E2* multipolarity. The angular distribution coefficients are consistent with a stretched *E2* transition which limits its J^{π} to $3/2^{+}$ or $11/2^{+}$. From $^{141}Sm^{m}$ decay, spin $3/2^{+}$ can clearly be ruled out, leaving $J^{\pi} = 11/2^{+}$ for this state. It is not hard to believe the tentative $9/2^{+}$ assignments reached from $^{141}Sm^{m}$ decay data to be incorrect because the negative A_4 value rules out a mixed *M1/E2* multipolarity for the 777.6-keV transition. Also, Eppley's et al. argument about 974.2-keV transition to ground state (this transition has not been seen in in-beam) in order to eliminate $11/2^{+}$ assignment, is a very poor argument.

1108.0-keV State

Again, coincidence relationships between 196.6- and 911.4-keV transitions places this state at 1108.0 keV. The small positive value A_2 and the large positive value of A_4 for 911.4-keV transition, are consistent with $J + 1$ to J pure *E2* transition which restricted the J^{π} assignment to $5/2^{+}$ or $9/2^{+}$. The $5/2^{+}$ value can be ruled out because the $(p,2n\gamma)$ reaction is not likely to populate low-spin states at higher excitation energies. From the $^{141}Sm^{m}$ decay data we can also exclude $5/2^{+}$. Therefore, J^{π} for the 1108.0-keV state would be $7/2^{+}$

1153.3-keV State

This state has been placed on the basis of coincidence information and energy sums of 524.9-, 749.6-, 956.5-, and 1153.3-keV transitions (not seen in $^{141}Sm^{g+m}$ decay). These deexcitations restricted the J^{π}

of this state to $7/2^+$ which is also consistent with angular distribution coefficients of 956.5- and 1153.3-keV transitions.

1167.1-keV State

This state feeds into the $11/2^-$ 628.6-keV state by the 538.5-keV transition (although the long half-life of the 628.6-keV state makes this impossible to confirm by a direct coincidence measurement, the other coincidence relations with the 538.5-keV confirm this placement as did the extensive coincidence relations from $^{141}Sm^m$ β-decay). If the 538.5-keV transition is a *M1* transition (Table 5-1), the J^π assignment is restricted to $9/2^-$, $11/2^-$, or $13/2^-$. The $11/2^-$ value is ruled out because of the large negative value of A_2 and the small positive value of A_4. The fact that this state is not fed by γ-rays from a high-spin state indicates that it most likely is not in the *yrast* sequence, eliminating $J^\pi = 13/2^-$ (below we shall show that the 1313.3-keV state has $J^\pi = 13/2^-$ and receives feeding from the high-spin states). Thus, the 1167.1-keV state has $J^\pi = 9/2^-$.

1242.5-keV State

The coincidence relationships between 196.6- and 1045.9-keV transitions and also the 1242.5-keV cross-over transition place this level at 1242.5-keV (not seen in $^{141}Sm^{g+m}$ decay). The J^π of this state is restricted to $3/2^\pm$, $7/2^\pm$, or $11/2^\pm$ because of the angular distribution of the 1045.9- and 1242.5-keV transitions (whose multipolarities have not been determined). The $3/2^\pm$ value can be ruled out because the $(p,2n\gamma)$ reaction is not likely to populate low-spin states at higher excitation energies. The fact that this state has not been observed in the $(\alpha,4n\gamma)$ reaction and has a large negative value of A_4 for the 1045.9-keV transition,

rule out $J^{\pi} = 11/2^{\pm}$, leaving $J^{\pi} = 7/2^{\pm}$ for this state. A $7/2^{-}$ assignment would require the 1045.9- and 1242.5-keV transitions to be a mixed *E1/M2*, and although this cannot be definitely ruled out, the $7/2^{+}$ assignment is most likely preferable.

1313.3-keV State

Again, the long half-life of the 628.6-keV state prevents a direct coincidence measurement to place the 1313.3-keV level feeding into it, but the five other transitions seen in coincidence with the 684.7-keV transition place the 1313.3-keV level quite securely. The 684.7-keV transition is reported to have *M1* or *E2* multipolarity [Ke77]. The angular distribution coefficients are consistent with a mixed *M1/E2* transition. A large negative value of A_2 and small positive value of A_4 restrict the J^{π} to $9/2^{-}$ or $13/2^{-}$. Since the 684.7-keV transition is seen so intensely in both $(p,2n\gamma)$ and $(\alpha,4n\gamma)$ reactions, *yrast* arguments lead us to prefer the higher spin, i.e., $13/2^{-}$ for this state.

1359.6-keV State

This state has not been seen in β-decay. The angular distribution coefficients for the 1163.0-keV transition restricted its J^{π} to $7/2^{\pm}$ or $11/2^{\pm}$. The small positive A_2 and the large negative A_4 are more likely consistent with $J + 2$ to J stretched *E2* transition. An $11/2^{-}$ assignment would require the 1163.0-keV transition to be *M2*, and, although this cannot be definitely ruled out, one would prefer the $11/2^{+}$ assignment.

1414.5-keV State

The coincidence relationships between 538.5- and 247.4-keV transition and 785.3-keV energy sum places this level at 1414.5-keV. The J^{π} of this state is restricted to $11/2^{-}$ or $9/2^{-}$ because of the angular distribution

coefficients of the transitions deexciting from this level.

1510.6-keV State

This state has been observed both by (p,2$n\gamma$) and (α,4$n\gamma$) reactions (not seen in β-decay). The angular distribution pattern of 882.0-keV transition, deexciting from this state, is consistent with a stretched *E2* and restricts the J^{π} value of the state to $7/2^-$ or $15/2^-$. *Yrast* considerations lead us to prefer the larger value of $15/2^-$.

Other States

The remaining states in the level scheme in Fig. 5-6 were placed on the basis of coincidence data, corroborated by β-decay data. Their J^{π} values could not be determined uniquely from our present experimental data; however, some J^{π} values could be excluded on the basis of angular distribution coefficients and the first spin assignments are more probable. Also, some of these states observed in (p,2$n\gamma$) reaction had their assignments made from $^{141}Sm^{m+g}$ decay — these are indicated by asterisks on the level scheme. It is worth mentioning that there are two 728.3-keV and two 785.3-keV transitions in the level scheme.

5.3.2. Level Scheme and Spin-Parity Assignments from (α,4$n\gamma$) Reaction

The proposed level scheme from (α,4$n\gamma$) reaction is shown in Figure 5-7. The intensities are normalized to 100 for the 431.8-keV transition strength. It should be mentioned here that this transition is part of a doublet (there is a 433.7-keV transition coming from ^{142}Pm). In the level scheme there are also more γ-ray intensities going into the 628.6-keV state than coming out (about 11% more).

Finally, the placement of those states (12 states) that depopulate directly or indirectly into the 628.6-keV isomeric state is based on the

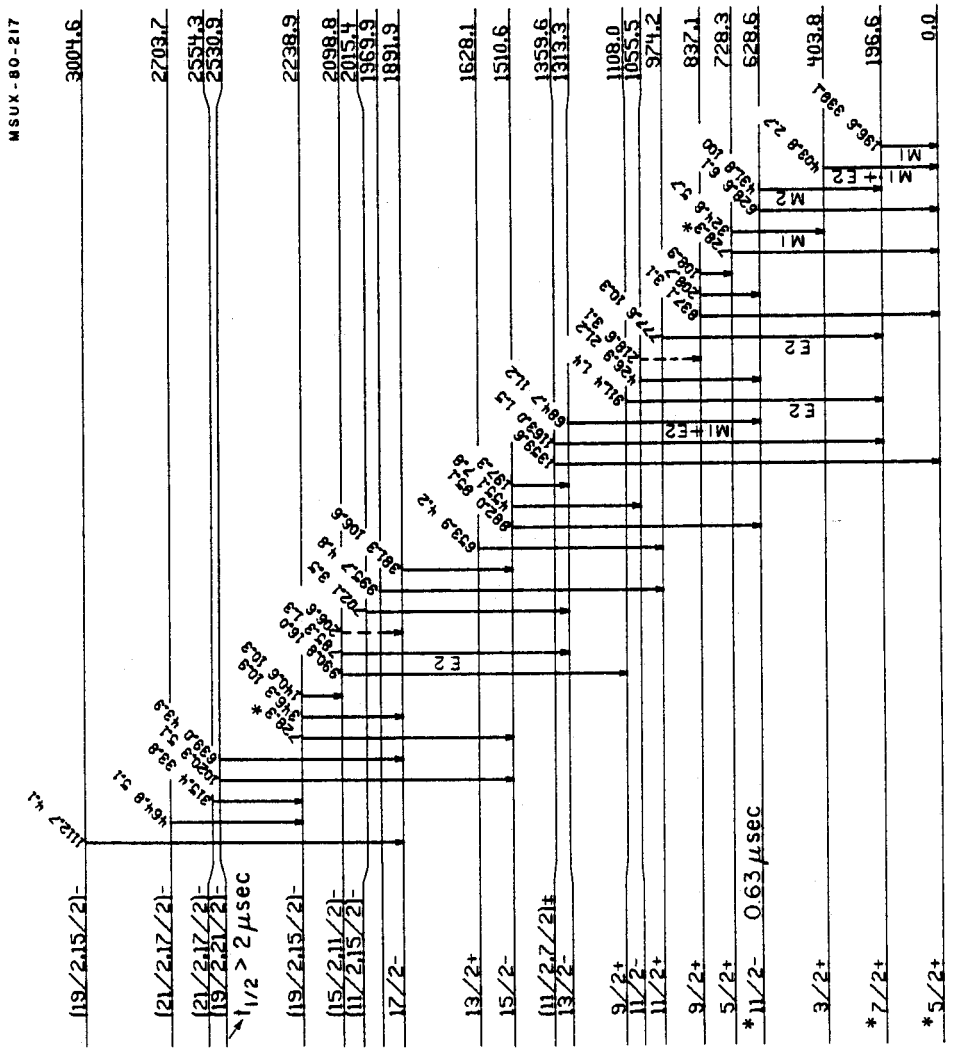

Figure 5-7. Level scheme of ^{141}Pm obtained from (α,4nγ) reaction.

delayed coincidence spectrum as well as prompt coincidence spectra. The 431.8-keV delayed gate (shown in Figure 5-8) enhances those transitions that feed into the 628.6-keV state ($t_{1/2}$ = 0.63 μsec) in ^{141}Pm. To obtain this spectrum, the X-axis was gated on the 431.8-keV transition and time-axis was gated on the proper side of the TAC spectrum.

Specific details of construction of the level scheme and J^{π} assignments are discussed below.

Ground, 196.6-, and 628.6-keV States

Again, the most intense γ transition in (α,4nγ) reaction as well as the (p,2nγ) reaction and off-line experiments is 196.6-keV transition. Its coincidence relationship with 431.8-keV and energy sums place the first excited state at 196.6-keV and the isomeric state at 628.6 keV. The latter decays to the 196.6-keV via the 431.8-keV transition and to the ground state via the 628.6-keV transition.

The half-life of this state was measured to be 0.22±0.01 μsec by Arl't et al. [Ar70], 0.7±0.02 μsec by Warner et al. [Wa71], and 0.59±0.02 μsec by Kennedy et al. [Ke77]. From the coincidence experiment for the (α,4nγ) reaction, the half-life of this state could be measured. A FAST-SLOW coincidence system with two Ge(Li) detectors and a Time-To-Amplitude Converter (TAC), were used (c.f. section 5.2.3.). The TAC resolving time was about 2τ ~ 4 μsec. The X-axis was gated on the 431.8-keV transition and the Y-axis was gated on the entire spectrum above 450-keV. The time spectrum after background subtractions is shown in Figure 5-9. A prompt peak in the time spectrum is due to prompt-coincidences of 433.7-keV γ-ray with other transitions in ^{142}Pm. Using the computer code KINFIT [Dy71], the half-life for the 628.6-keV state turned out to be 0.63±0.02 μsec.

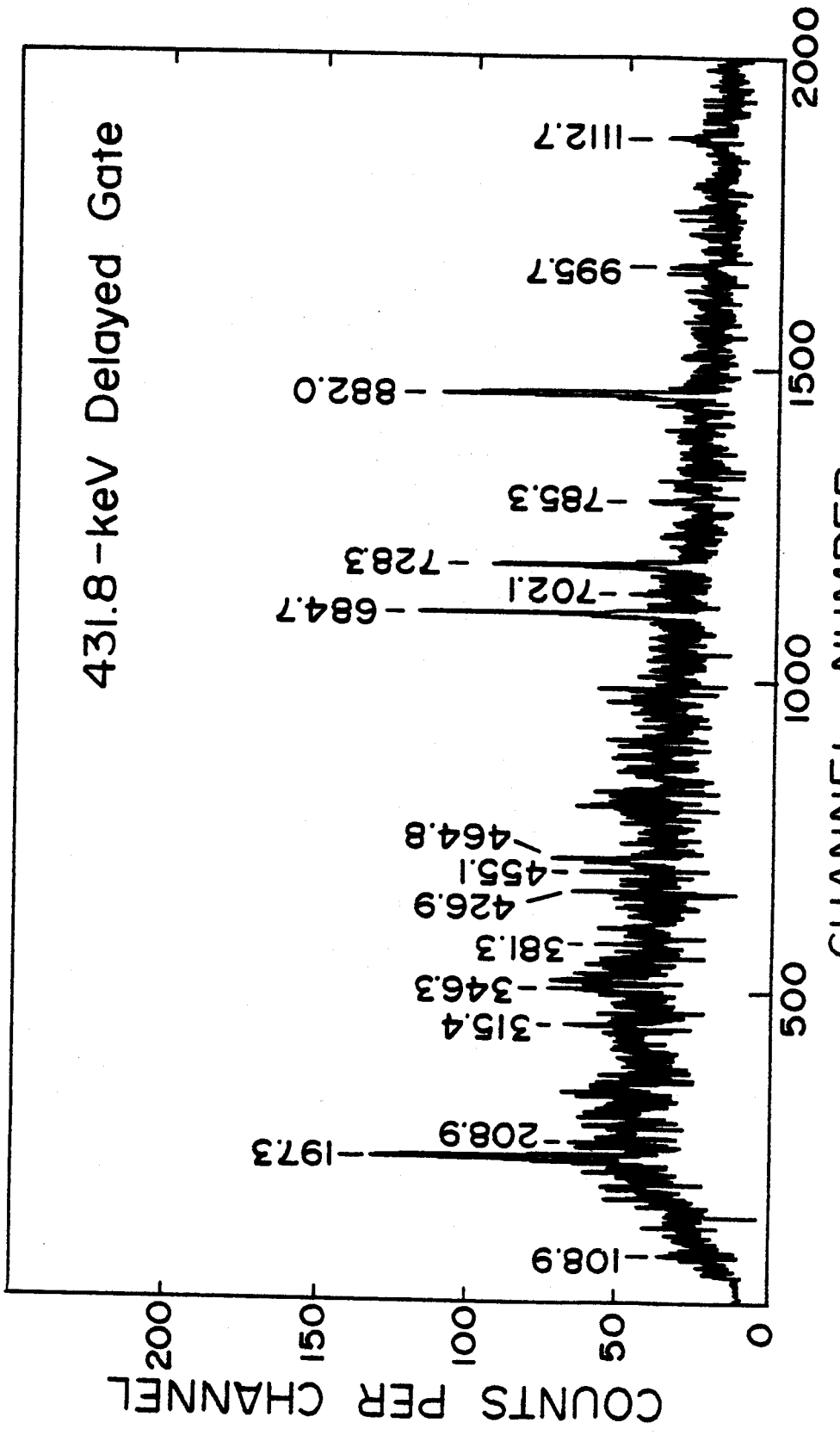

Figure 5-8. Delayed coincidence spectrum. This spectrum enhances those transitions that feed directly or indirectly into the 628.6-keV state ($\tau_{1/2}$ = 0.63 μsec) in ^{141}Pm.

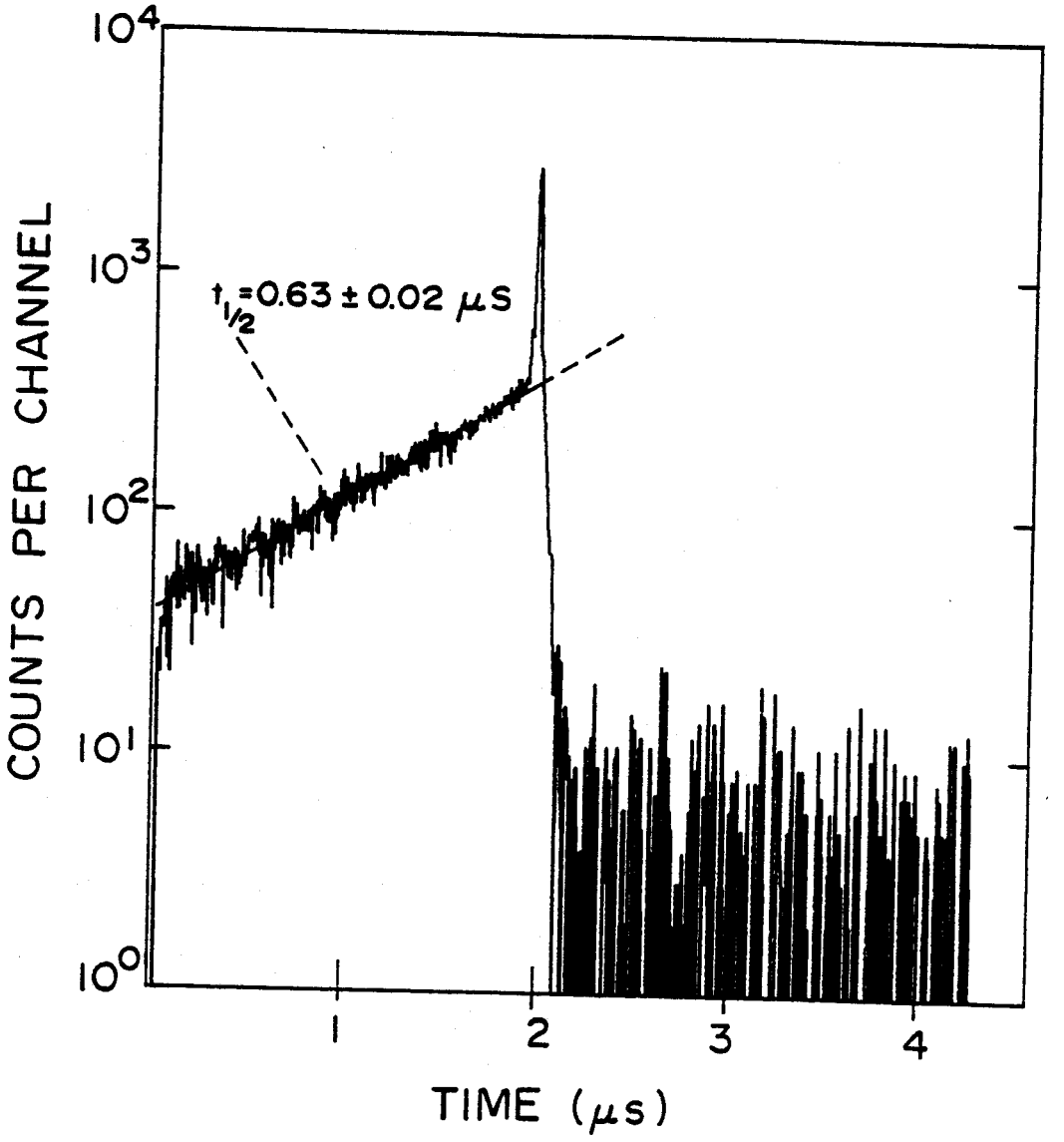

Figure 5-9. Time axis projection on a semi-logarithmic plot illustrating the half-life of 628.6-keV state in ^{141}Pm.

As mentioned in section 5.3.1., because of the isomeric nature of the 628.6-keV state, the 196.6-, 431.8-, and 628.6-keV transitions are isotropic. In fact, this was proven from $(\alpha,4n\gamma)$ reaction to be true (e.g. see the values of A_2 and A_4 for these transitions in Table 5-3). Therefore, J^π assignments for 196.6- and 628.6-keV states are not possible. From $^{141}Sm^m$ β-decay, the J^π for the ground-, 196.6-, and 628.6-keV states were assigned to be $5/2^+$, $7/2^+$ and $11/2^-$, respectively. It is conceivable to believe these J^π assignments, both by the systematics of the region and by the fact of the long half-life of the 628.6-keV state, are reasonable.

403.8- and 728.3-keV States

The other set of low-lying states has the interconnecting transitions of 324.6-, 403.8-, and 728.3-keV. Coincidence relations between 324.6- and 403.8-keV transition, and 728.3-keV energy sum lead to the placement of levels at 403.8 and 728.3 keV.

Because the 403.8-keV transition was seen as weak in $(\alpha,4n\gamma)$ reaction, the angular distribution coefficients could not be measured for this transition. Therefore, the $J^\pi = 3/2^+$ assignment from $(p,2n\gamma)$ reaction (discussed in section 5.3.1.) was adopted for 403.8-keV state.

The 324.6-keV transition deexciting from 728.3-keV state is reported [Ke77] to have *M1* or *E2* multipolarity. Our data is consistent with an almost pure *M1* which limits J^π for 728.3-keV state to $1/2^+$, $3/2^+$, or $5/2^+$. By using the same arguments as the $(p,2n\gamma)$ reaction, the $1/2^+$ and $3/2^+$ assignments can be ruled out, leaving $J^\pi = 5/2^+$ for this state.

837.1-keV State

This state has been seen in the $(p,2n\gamma)$ reaction, but 108.9-keV transition from this state into 728.3-keV state is missing in the $(p,2n\gamma)$

reaction. Instead, the 640.5-keV transition from this state into the 196.6-keV state has been observed in the $(p,2n\gamma)$ reaction and not seen in the $(\alpha,4n\gamma)$ reaction.

The angular distribution coefficients are consistent with the $J^{\pi} = 9/2^{+}$ assignment discussed in section 5.3.1.

974.2-, 1108.0-, 1313.3-, 1359.6-, 1510.6-, 1628.1- 1969.9-, 2015.4-, 2098.8, and 2238.9-keV States

These are other states which have also been observed in the $(p,2n\gamma)$ reaction. Generally, the placement of these states are based on the coincidence information, delayed-coincidence spectrum, intensity balances, and energy summing relationships supported by both $(p,2n\gamma)$ and $(\alpha,4n\gamma)$ reactions.

The J^{π} assignments for these states were made on the basis of angular distribution coefficients and transition multipolarities. Where there was a large error in the A_2 or A_4 values in one case, the values from the other case were chosen.

Some other states which have not been seen in the $(p,2n\gamma)$ reaction will be discussed next.

1055.5-keV State

The coincidence relationships between 426.9- and 455.1-keV transitions, intensity balance, and the 882.0-keV energy sum lead us to place a level at 1055.5-keV.

The angular distribution coefficients for 426.9- and 455.1-keV γ's restricted the J^{π} of this state to $11/2^{-}$ or $13/2^{-}$. The fact that this state is not fed by γ-rays from high-spin state indicates that it most likely is not in the *yrast* sequence, eliminating $J^{\pi} = 13/2^{-}$ (as discussed in section 5.3.1. The 1313.3-keV state has J^{π} $13/2^{-}$ and receives feeding

from the high-spin states). Thus, the 1055.5-keV state has $J^{\pi} = 11/2^{-}$.

1891.9-, 2530.9-, 2554.3-, 2703.7-, and 3004.6-keV States

These states are the high-lying and higher spin states which are seen only in the $(\alpha,4n\gamma)$ reaction.

The tentative J^{π} assignments made for these states are based on the A_2 and A_4 values of transitions deexciting from them. Except for 1891.9-keV state, no unique J^{π} assignment was possible.

The 2530.9-keV state has a specific significance. The fact that the 639.0- and 1020.3-keV transitions deexciting from this level have an isotropic nature (see Table 5-3 for their A_2 and A_4 values) and no γ-rays seen feeding to this level, would lead us to believe that this is most likely an isomeric state. The half-life measurement for this state was not possible from the $(\alpha,4n\gamma)$ coincidence data, but estimated to be more than 2 μsec.

5.3.3. Comparison Between the $(p,2n\gamma)$ and $(\alpha,4n\gamma)$ Reaction and with other Experimental Results

States in ^{141}Pm deduced from the present work are compared with the $^{141}Sm^{m+g}$ β^{+}/EC decay [Ep72, K277] in Figure 5-10. Levels in columns 1 and 2 are based on the $(p,2n\gamma)$ and $(\alpha,4n\gamma)$ reactions reported here while levels in column 3 are from β-decay. The state at 1055.5-keV as seen in the $(\alpha,4n\gamma)$ reaction by no means is identical with the 1046.4-keV state observed in β-decay. Many high-spin states have been observed from the $(\alpha,4n\gamma)$ reaction not seen in β-decay or the $(p,2n\gamma)$ reaction as one expects due to higher angular momentum transfer by alpha particles. Also, a number of levels exist which were populated in one or two of the three types of experiments.

Figure 5-10. Energy levels of ^{141}Pm. Levels in columns 1 and 2 are from present work while levels in column 3 are from β-decay. Spins are shown in $2J$.

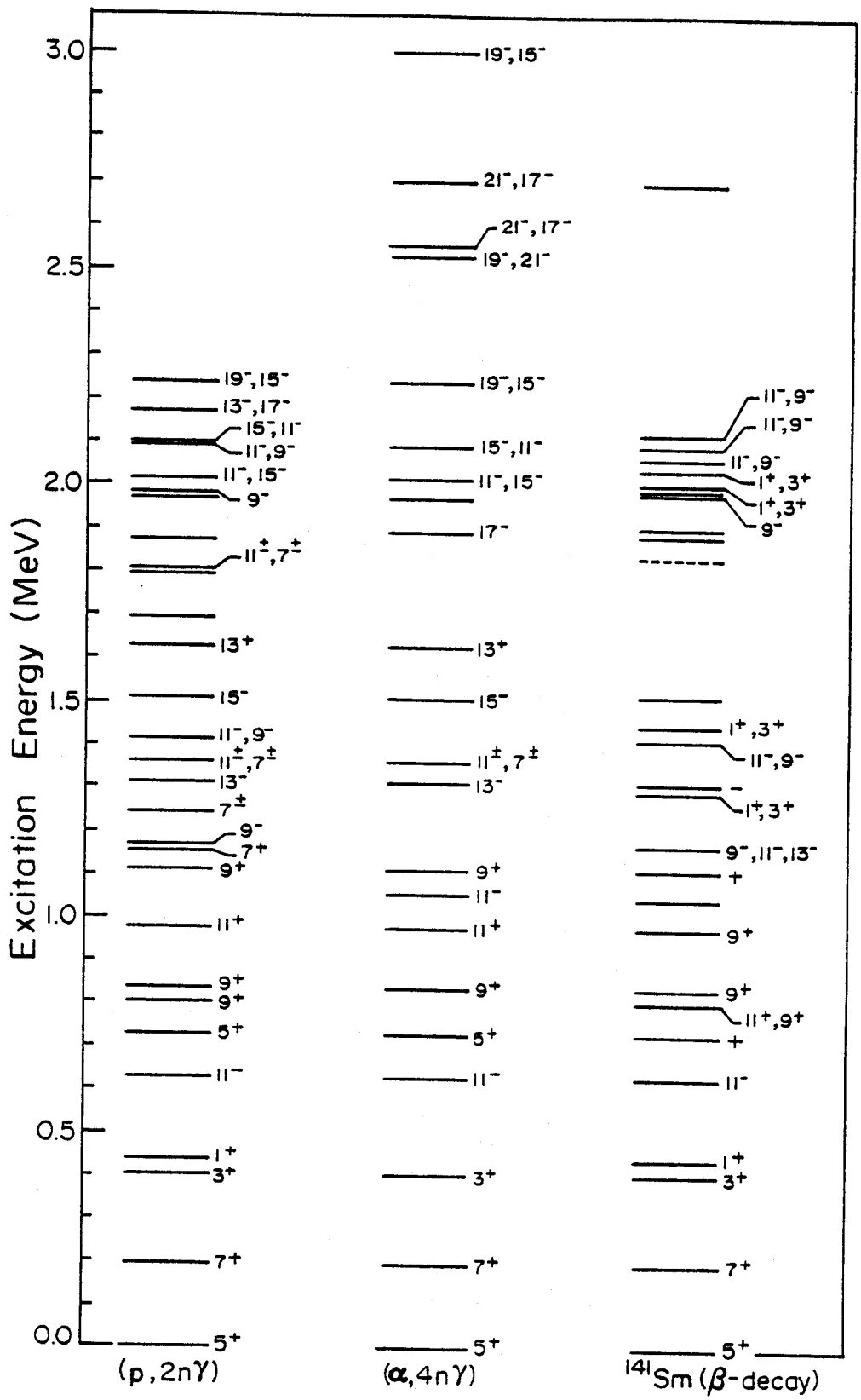
Excitation Energy (MeV)
3.0
2.5
2.0
1.5
1.0
0.5
0.0
(p, 2nγ)
(α, 4nγ)
141Sm (β-decay)

Spins of excited states of ^{141}Pm are almost well established in this work by incorporating the results of the β-decay study.

5.4. Discussion of Level Configurations

For convenience of discussion, the states in ^{141}Pm can be divided into three classes: 1) single-quasiparticle states, 2) negative-parity collective states, and 3) positive-parity collective states.

5.4.1. Single-Quasiparticle States

The five lowest-lying states in ^{141}Pm all seen in the $(p,2n\gamma)$ reaction as well as β-decay are presumed to be described best as the single-quasiparticle shell-model states. They lie at $0(\pi d_{5/2})$, $196.6(\pi g^{-1}_{7/2})$, $403.8(\pi d_{3/2})$, $438.8(\pi s_{1/2})$, and 628.6 keV$(\pi h_{11/2})$. In the case of the N=82 isotones, these five states have been analyzed by de Takacsy et al. [Ta76] as single-quasiparticle states. Also, extrapolations of the calculations of Kisslinger et al. [Ki60] confirm the arguments about these states.

5.4.2. Negative-Parity Collective States

From the β-decay standpoint, a three-quasiparticle approach was used to describe some of the negative-parity states [Ep72]. The triaxial weak-coupling model will be used here in order to explain the other negative-parity collective states.

The negative-parity collective states in ^{141}Pm are expected to consist primarily of the $\pi h_{11/2}$ state coupled to a ^{140}Nd triaxial core. There is evidence that the 2^+ one-phonon quadrupole vibrational state lies at ≈770 keV in ^{140}Nd [Re63].

The 1167.1-keV state ($9/2^-$) is presumably a coupling of the $\pi h_{11/2}$ single-particle state to a 2^+ ^{140}Nd core. It lies at approximately the expected energy and it contains considerable mixing with a three-quasiparticle state [Mu71]. Systematically, this level has been seen at 977.47-keV in ^{143}Eu (cf. section 4.2.2.).

The 1414.5-keV state feeds the 1167.1-keV state preferring the $(\pi h_{11/2} \times 2_1^+)_{11/2^-}$ assignment and leaving the $(\pi h_{11/2} \times 2_1^+)_{13/2^-}$ configuration for the 1313.3-keV state.

The state at 1510.6 keV is observed to deexcite through the $\pi h_{11/2}$ state. This state is tentatively assigned as the $(\pi h_{11/2} \times 2_1^+)_{15/2^-}$ configuration.

A triaxial calculation needs to be done in order to find the configuration of the other negative-parity collective states. These calculations should involve the five single-proton states coupled to the 2_1^+, 0_2^+, 2_2^+, 4_1^+, and 3_1^-, and other higher-spin vibrational states in ^{140}Nd.

5.4.3. Positive-Parity Collective States

As one might expect, the weak-coupling triaxial model delivers poorer results for these states because of the ease of mixing with nearby states having the same positive parity. No specific calculations have been performed for these states; therefore the assignments of the positive-parity collective states will be made primarily on the basis of the excitation energy and the decay systematics of these states.

The states at 728.3 ($5/2^+$), 837.1 ($9/2^+$) and 1153.3 keV($7/2^+$) are most likely a coupling of a $\pi d_{5/2}$ single particle state with the 2^+ core. The first two states deexcite strongly to the $\pi d_{5/2}$ ground state presumably with *E2(+M1)* multipolarities.

The 804.5-$(9/2^+)$, 974.2-$(11/2^+)$, 1108.0-$(9/2^+)$, and 1692.5-keV states, presumably consist of the $\pi g_{7/2}^{-1}$ single-particle states coupled to a core because of the strong depopulation through the $\pi g_{7/2}$ single-particle state.

Little can be said about the higher-lying positive-parity states; first of all because of the lack of specific spin assignments, and secondly, because of strong mixing with nearby positive-parity states.

CHAPTER VI

^{139}Pr EXPERIMENTAL RESULTS AND DISCUSSION

The γ-ray decays of the excited states of ^{139}Pr below 3 MeV of excitation have been previously studied via the electron-capture decay of the ground and meta-stable states of ^{139}Nd [Be69, Bu71] and the ^{141}Pr$(p,t)^{139}$Pr scattering reaction [Go72]. These studies include the γ-ray spectrum, γ-γ coincidences, the internal-conversion electron spectrum, and half-life measurement of the 822.0-keV isomeric state in ^{139}Pr.

In-beam spectroscopic methods have been used in this study to establish the level schemes of the ^{139}Pr nucleus. The single γ-rays, γ-γ coincidences, and angular distribution functions were studied in the reactions $(p,2n\gamma)$ and $(\alpha,4n\gamma)$ on suitable targets.

6.1. Experimental Details and Results for the $(p,2n\gamma)$ Reactions

6.1.1. Target and Reaction

A target was prepared by drying a thin slurry of 99.9% enriched $^{140}CeO_2$ onto a thin formvar backing. This target was bombarded with a 25-MeV proton beam from the MSU cyclotron.

The primary contaminants encountered in this study were ^{138}Pr, ^{138}Ce, and ^{140}Ce. In addition, ^{19}F and ^{27}Al lines were present in all spectra. A coincidence experiment was employed to delineate the transitions of interest further.

6.1.2. γ-Ray Singles Spectra

^{139}Pr singles spectra were taken with a 17%-efficient Ge(Li) detector (with a resolution of 1.9 keV FWHM) at approximately 125° with respect to the beam direction. The counting period was typically about 2.5 *h* at counting rates of 6000-8000 cps. A copper-cadmium absorber was used to shield the detector from x-rays which would otherwise dominate the spectrums. A singles γ-ray spectrum collected in this manner is shown in Figure 6.1. The energy calibrations of the γ-ray transitions were performed using well-known radioactivities, e.g. ^{60}Co, ^{152}Eu, and ^{226}Ra. Transition intensities were determined by correcting net peak areas by use of detector efficiency curves shown before in Figure 5-2.

A total of 44 γ-rays deexciting from 25 levels were assigned to ^{139}Pr from the $(p,2n\gamma)$ reaction on the basis of singles spectra and coincidence experiments discussed below. These are listed in Table 6-1, together with their relative intensities. The relative intensities of those transitions which were part of doublets and were not able to be resolved are indicated by question marks. Also, this table includes angular distribution coefficients and transition multipolarity assignments which will be discussed later.

6.1.3 Coincidence Spectra

Using two Ge(Li) detectors as described in section 5.1.3., extensive prompt γ-γ coincidence measurements were performed with a 25-MeV proton beam. A resolving time of $2\tau \approx 100$ nsec was used.

In Appendix G, important coincidence gates which were used to construct the level scheme are shown.

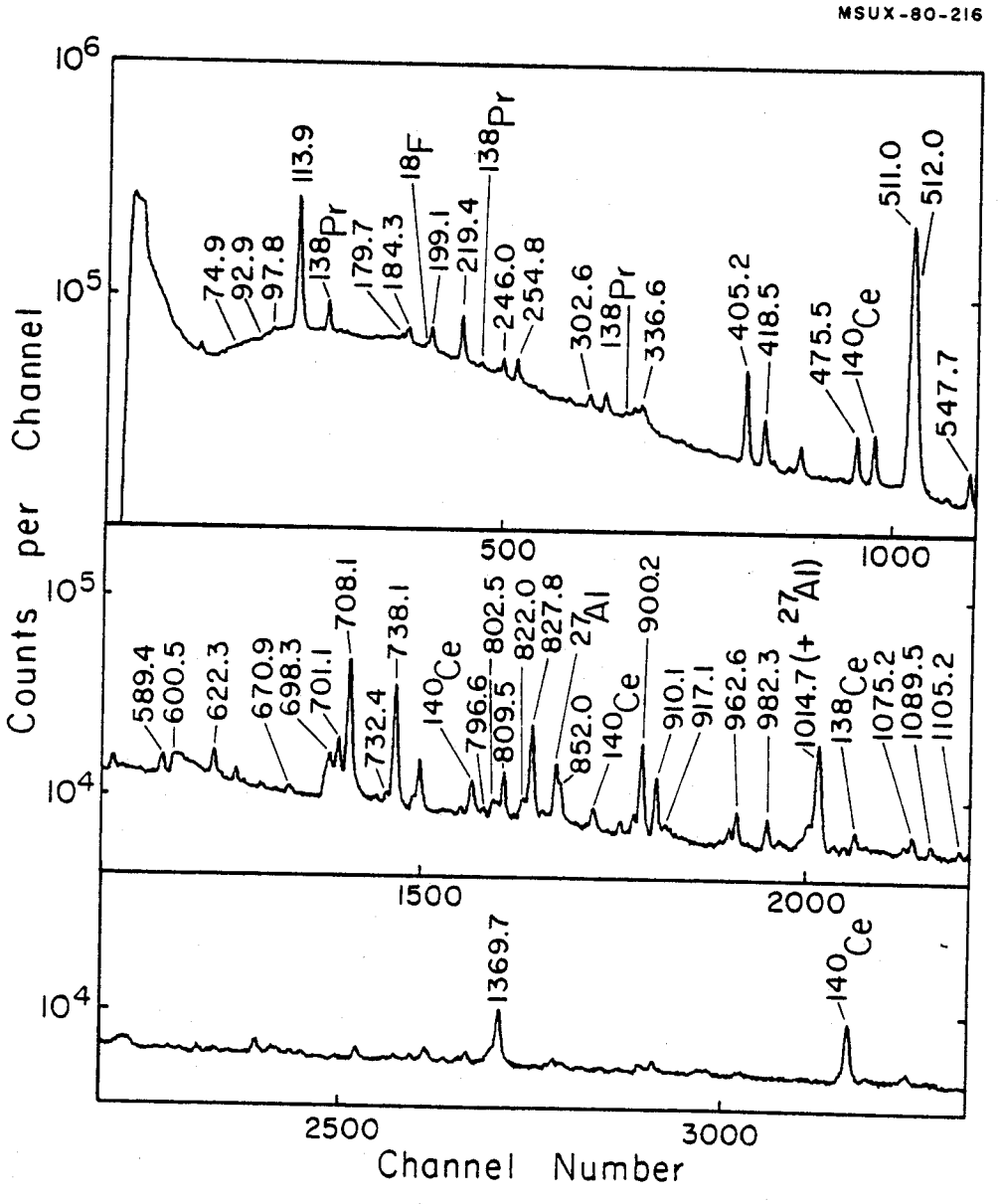

Figure 6-1. γ-ray singles spectrum of $^{140}Ce(p,2n\gamma)^{141}Pm$ taken with the 17%-efficient Ge(Li) detector placed at 125°.

Table 6-1. Energies, relative intensities, angular distribution coefficients, and multipolarities for γ transitions in ^{139}Pr from $(p,2n\gamma)$ reactions.

Energy E_γ (keV)	Relative Intensity I_γ	Angular Distribution Coefficients A_2/A_0	A_4/A_0	Multipolarity[a]
74.9±0.1[b]	weak	---	---	---
92.9±0.3	weak	---	---	M1,E2
97.8±0.1	1.8±0.2	---	---	---
113.9±0.1[b]	≡100	-0.03±0.03	-0.03±0.05	M1+E2
179.7±0.2[b]	2.0±0.3	---	---	---
184.3±0.1	6.7±0.4	-0.14±0.05	-0.06±0.08	M1
199.1±0.1[b]	9.7±0.6	-0.32±0.11	-0.09±0.12	---
219.4±0.1[b]	19.1±1.2	-0.25±0.03	0.03±0.03	---
246.0±0.1[b]	6.8±0.4	-0.38±0.08	-0.03±0.12	---
254.8±0.1	8.0±0.5	-0.08±0.02	-0.05±0.02	M1,E2
302.6±0.2	?	---	---	---
336.6±0.1[b]	4.3±0.3	-0.35±0.03	-0.05±0.04	---
405.2±0.1	33.1±2.0	-0.11±0.02	0.03±0.03	M1+E2
418.5±0.1[b]	13.7±0.9	---	---	---
475.5±0.1	12.7±0.8	0.01±0.01	0.01±0.02	---
512.0±0.2	?	---	---	---
547.7±0.1	9.4±0.6	-0.35±0.01	0.07±0.03	M1
589.4±0.1	6.0±0.4	-0.13±0.03	0.09±0.04	---
600.5±0.2	?	---	---	---
622.3±0.1	7.8±0.5	-0.05±0.04	0.01±0.06	---
670.9±0.2	2.3±0.1	-0.19±0.15	0.08±0.19	---

Table 6-1. (cont'd.).

Energy E_γ (keV)	Relative Intensity I_γ	Angular Distribution Coefficients A_2/A_0	A_4/A_0	Multipolarity[a]
698.3±0.2	11.3±0.9	---	---	---
701.1±0.1[b]	15.9±1.2	-0.87±0.13	0.10±0.20	M1+E2
708.1±0.1[b]	75.3±4.6	isotropic	---	M2
732.4±0.2	3.2±0.6	---	---	---
738.1±0.1[b]	59.1±3.6	0.18±0.02	-0.04±0.03	E2
796.6±0.3	1.9±0.4	---	---	E1
802.5±0.2	5.1±0.4	-0.20±0.07	-0.02±0.13	E2
809.5±0.1	12.7±0.8	0.13±0.04	0.09±0.06	E1
822.0±0.2[b]	5.7±0.5	-0.03±0.01	-0.03±0.02	E3
827.8±0.1[b]	37.2±2.3	0.11±0.02	-0.01±0.03	E2
852.0±0.3	?	---	---	---
900.2±0.1[b]	34.2±2.1	0.20±0.01	-0.08±0.01	---
910.1±0.2[b]	17.6±1.1	-0.21±0.01	0.10±0.01	E2+M1
917.1±0.3	2.4±0.2	-0.19±0.04	0.15±0.06	---
962.6±0.3	?	---	---	---
982.3±0.2	7.2±0.4	0.14±0.08	0.08±0.11	E1
1014.7±0.3[b]	?	-0.38±0.04	0.07±0.04	---
1075.2±0.2	4.7±0.3	-0.15±0.05	-0.05±0.07	E1
1089.5±0.3	2.7±0.2	---	---	---
1105.2±0.3	2.2±0.2	-0.59±0.10	0.18±0.12	---
1369.7±0.2	4.8±0.4	-0.68±0.07	0.09±0.10	---

Table 6-1. (cont'd.).

[a]Transition multipolarity assignments taken from conversion electrons, ref. [Bu71].

[b]These γ-rays were also seen in (α,4nγ) reactions. Therefore, the γ-ray energies are the average of (*p*,2nγ) and (α,4nγ) reactions.

The placement of those states that depopulate directly or indirectly into the 822.0-keV isomeric state is based on the delayed coincidence spectrum as well as prompt coincidence spectra. The 113.9-keV delayed gate (shown in Figure 6-2) enhances those transitions that feed into the 822.0-keV state ($\tau_{1/2}$ = 36 nsec) and the 113.9-keV state ($\tau_{1/2}$ = 2.6 nsec) in ^{139}Pr. To obtain this spectrum, the X-axis was gated on the 113.9-keV transition and the time-axis was gated on the proper side of the TAC spectrum.

A summary of the coincidence data is given in Table 6-2.

6.1.4. γ-Ray Angular Distributions

Although in the (p,2nγ) reaction the alignment of the final nucleus is less than in the (α,4nγ) reactions, the angular distribution measurements of the γ-rays can give valuable information for spin assignments and checking the proposed level scheme. For these purposes, single γ-ray spectra in the reaction ^{140}Ce(p,2nγ)^{139}Pr at angles 90°, 110°, 125°, 140°, and 155° with respect to the beam axis have been measured using a 17%-efficient Ge(Li) detector. The angles were taken in random order for the various experiments and data were typically collected for 2.5 h at each angle.

The 708.1-keV isomeric transition assumed to have an isotropic distribution were fitted to an expansion of Legendre Polynomials to give the experimental A_2/A_0 and A_4/A_0 coefficients. These are listed in Table 6-1. The A_2 and A_4 values for the 113.9- and 822.0-keV transitions turned out to be close to zero, as one expected them to be isotropic due to deexcitation from the 822.0-keV isomeric state.

The data with the fitted curves for some of the γ-rays are shown in Appendix H.

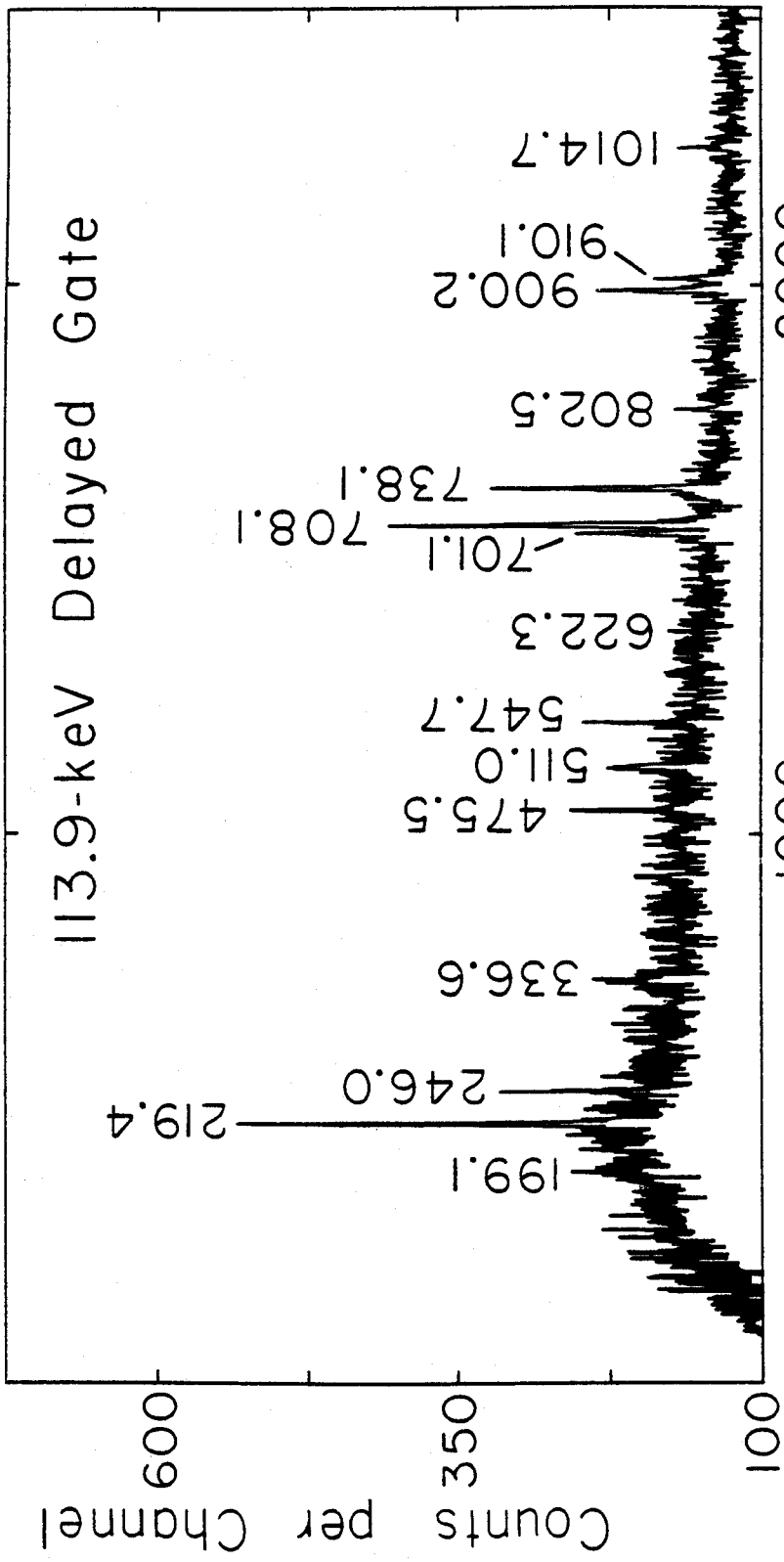

Figure 6-2. Delayed coincidence spectrum. This spectrum enhances those transitions that feed into the 822.0-keV state ($\tau_{1/2}$ = 36 nsec) and the 113.9-keV state ($\tau_{1/2}$ = 2.6 nsec) in ^{139}Pr from $(p,2n\gamma)$ reaction.

Table 6-2. Summary of coincidence results for the $^{140}Ce(p,2n\gamma)^{139}Pr$ reaction.

Gated γ-Ray (keV)	Coincident γ-Rays (keV)
92.9	113.9, 738.1, 982.3
113.9	219.4, 246.0, 336.6, 475.5, 698.3 701.1, 708.1, 732.4, 738.1, 900.2, 910.1, 982.3, 1014.7, 1075.2, 1089.5
179.7	219.4, 246.0, 900.2
184.3	405.2, 512.0
199.1	219.4, 701.1
219.4	113.9, 179.7, 199.1, 246.0, 336.6, 701.1, 708.1, 822.0, 900.2
246.0	113.9, 179.7, 219.4, 708.1, 900.2
254.8	219.4, 547.7
302.6	113.9, 600.5, 802.5, 910.1
336.6	219.4, 900.2
405.2[a]	184.3, 512.0, 670.9, 802.5
418.5	113.9, 701.1, 708.1
475.5	113.9
547.7	113.9, 254.8, 302.6, 708.1
589.4	---
600.5	113.9, 405.2, 910.1
622.3	113.9, 809.5, 910.1
670.9	405.2, 802.5
698.3	113.9, 219.4, 910.1
701.1	113.9, 199.1, 219.4, 246.0, 708.1
708.1	113.9, 219.4, 246.0, 254.8, 336.6, 547.7, 701.1, 802.5, 900.2, 1105.2

Table 6-2. (cont'd.).

Gated γ-Ray (keV)	Coincident γ-Rays (keV)
732.4	113.9, 738.1
738.1	113.9, 732.4, 982.3, 1014.7, 1075.2, 1089.5
796.6	827.8
802.5	113.9, 302.6, 405.2, 708.1
809.5	113.9, 622.3, 910.1
822.0	---
827.8	796.6, 962.6
900.2	113.9, 179.7, 219.4, 246.0, 336.6, 708.1
910.1	113.9, 219.4, 600.5, 622.3 698.3, 809.5
962.6	827.8
982.3	113.9, 738.1
1014.7	113.9, 738.1
1075.2	113.9, 738.1
1089.5	113.9, 738.1
1105.2	113.9, 708.1
1369.7	---

[a]There are two transitions with this energy in the level scheme.

6.2. Experimental Details and Results for (α,4nγ) Reaction

6.2.1. Target and Reaction

The states in ^{139}Pr were excited by the ^{139}La(α,4nγ)^{139}Pr reaction. A target was prepared by drying a thin slurry of 99.9% enriched $^{139}La_2O_3$ onto a thin formvar backing.

The reaction cross sections for (α,*xn*) reactions as a function of alpha particle energy were calculated using the code CS8N [CS8N]. The optimum alpha particle energy for the (α,4nγ) reaction in order to minimize the production of the γ-rays is 50 MeV. At this energy, the amount of contaminant production (α,3*n*) and (α, 5 *n*) is about 4% of the total cross section.

The highest energy alpha beam, 47 MeV, which could be obtained by the MSU cyclotron was used for the ^{139}Pr experiments. The amount of the main contaminant ^{140}Pr at this energy is going to be about 14% of the total cross section.

The contaminants encountered in this study were ^{141}Pr, ^{140}Pr, ^{140}Ce, ^{139}Ce, ^{138}Ce, and ^{139}La. In addition, ^{18}F and ^{29}P lines coming from oxide in the target and also ^{27}Al lines were present in all spectra.

6.2.2. γ-Ray Singles Spectra

The ^{139}Pr singles γ-ray spectra taken with a 7.7%-efficient Ge(Li) detector had a resolution of 1.9 keV FWHM. This detector was placed at 125° with respect to the beam direction. Typically, a beam current of $\approx$10 *na* was used and the detector was placed 20 cm from the target, resulting in a counting rate of $\approx$6000-8000 cps. A singles γ-ray spectrum taken over a 2.5-*h* period is shown in Figure 6-3. The energy calibrations of the γ-ray transitions were performed using well-known radioactivities, e.g. ^{60}Co, ^{152}Eu, and ^{226}Ra. Transition intensities were determined by

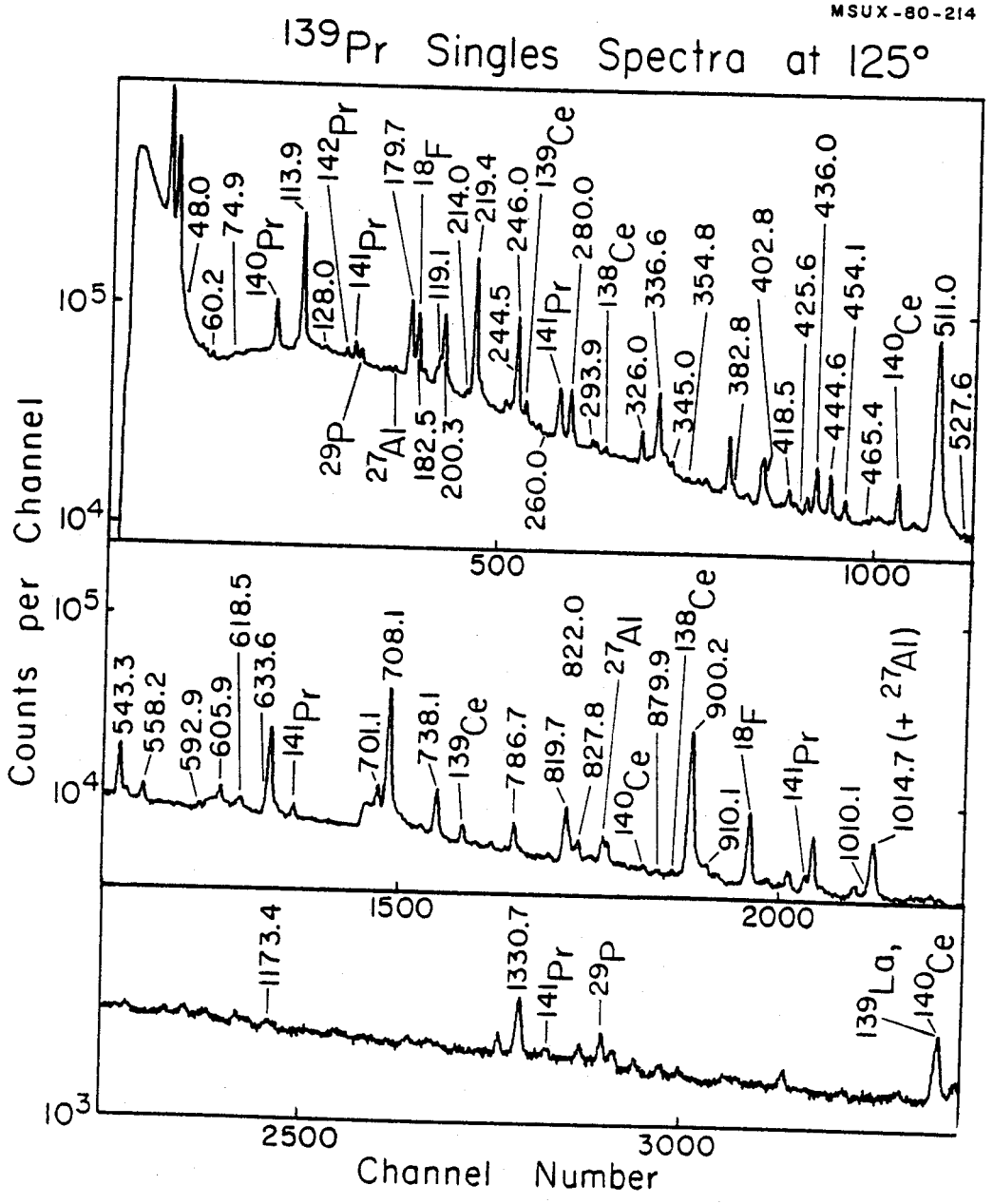

Figure 6-3. γ-ray singles spectrum of $^{139}La(\alpha,4n\gamma)^{139}Pr$ taken with a 7.7%-efficient Ge(Li) detector placed at 125°.

correcting net peak areas by use of detector efficiency curves shown before in Figure 5-5.

A total of 49 γ-rays deexciting from 33 levels were assigned to ^{139}Pr from the (α,4nγ) reaction, on the basis of singles spectra and coincidence experiments discussed below. These are listed in Table 6-3, together with their relative intensities. The relative intensities of those transitions which were part of doublets and were not able to be resolved are indicated by question marks. In general, γ-rays are not listed in this table unless coincidence information demands that they should be. Also, this table includes angular distribution coefficients and transition multipolarity assignments which will be discussed later.

Because of a heavy population of γ-rays below 500 keV, the singles spectrum was also taken with a LEPS (Low Energy Photon Spectrometer) at 90° with respect to the beam direction for better resolving of the doublet transitions. This detector is a small volume (2.5 cm^3) planar Ge(Li) crystal having a 0.7 keV resolution at 122 keV. This singles γ-ray spectrum taken over a 2.5-*h* period is shown in Figure 6-4.

6.2.3. Coincidence Spectra

Using the same geometry and electronic set-up described in section 3.2, three-parameter coincidence events were recorded on ten magnetic tapes, each containing 3 x 10^6 events. The detectors used had small volume (2.5 cm^3 planar) and large volume (10%-efficient). The TAC resolving time was about 2τ ≈ 2 μsec.

The coincidence gates for most of the transitions which have been placed are shown in Appendix I. The gates have been arranged according to increasing energy. Samples of both X-gates (identifying high energy

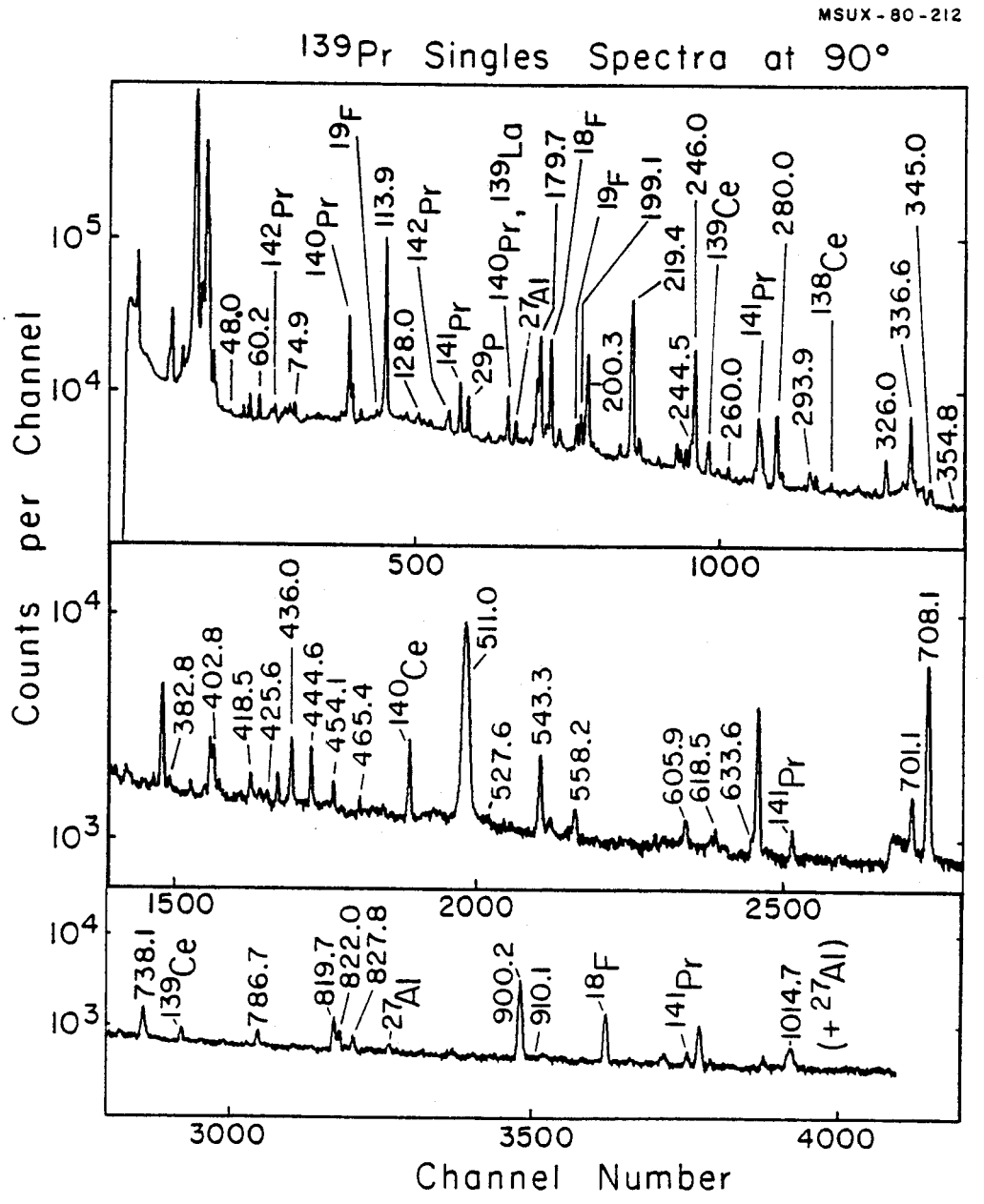

Figure 6-4. Low energy γ-ray singles spectrum of $^{139}La(\alpha,4n\gamma)^{139}Pr$ taken with a small volume planar Ge(Li) detector placed at 90°.

Table 6-3. Energies, relative intensities, angular distribution coefficients, and multipolarities for γ transitions in ^{139}Pr from $(\alpha,4n\gamma)$ reactions.

Energy E_γ (keV)	Relative Intensity I_γ	Angular Distribution Coefficients A_2/A_0	A_4/A_0	Multipolarity[a]
48.0±0.1	weak	---	---	---
60.2±0.1	1.8±0.1	-0.03±0.09	-0.05±0.14	---
74.9±0.1[b]	weak	---	---	---
113.9±0.1[b]	≡100	-0.05±0.03	0.02±0.03	M1+E2
128.0±0.1	1.5±0.2	-0.29±0.08	0.09±0.14	---
179.7±0.1[b]	45.7±3.4	-0.34±0.03	0.02±0.04	---
182.5±0.1	?	---	---	---
199.1±0.1[b]	13.7±4.0	-0.28±0.06	0.15±0.07	---
200.3±0.1	34.4±4.8	-0.26±0.12	-0.19±0.14	---
214.0±0.1	weak	---	---	---
219.4±0.1[b]	116.6±7.4	-0.28±0.03	0.03±0.04	---
244.5±0.1	?	---	---	---
246.0±0.1[b]	59.4±4.0	-0.44±0.04	0.03±0.04	---
260.0±0.1	weak	---	---	---
280.0±0.1	20.1±1.6	-0.23±0.02	0.04±0.03	---
293.9±0.1	3.4±0.2	-0.35±0.07	-0.03±0.07	---
326.0±0.1	12.3±0.8	-0.31±0.03	-0.01±0.04	---
336.6±0.1[b]	34.9±2.4	-0.41±0.03	0.01±0.04	---
345.0±0.1	3.6±0.3	-0.49±0.07	0.07±0.09	---
354.8±0.1	1.5±0.1	-0.29±0.09	0.31±0.11	---
382.8±0.1	1.3±0.1	---	---	---

Table 6-3. (cont'd.).

Energy E_γ (keV)	Relative Intensity I_γ	Angular Distribution Coefficients A_2/A_0	A_4/A_0	Multipolarity[a]
402.8±0.1	13.9±1.4	0.28±0.07	-0.08±0.08	---
418.5±0.1[b]	6.4±0.5	---	---	---
425.6±0.1	weak	---	---	---
436.0±0.1	19.0±1.2	-0.46±0.03	0.04±0.04	---
444.6±0.1	16.6±1.1	0.23±0.03	-0.05±0.04	---
454.1±0.1	7.1±0.1	0.20±0.02	0.01±0.03	---
465.4±0.1	weak	---	---	---
527.6±0.1	weak	---	---	---
543.3±0.1	30.2±2.0	-0.34±0.03	0.04±0.04	---
558.2±0.1	8.7±0.6	-0.61±0.04	0.06±0.05	---
592.9±0.1	weak	---	---	---
605.9±0.1	6.4±0.5	-0.68±0.09	0.05±0.13	---
618.5±0.1	4.8±0.4	0.23±0.09	0.05±0.12	---
633.6±0.1	?	---	---	---
701.1±0.1[b]	10.4±1.4	-0.91±0.08	0.11±0.1	M1+E2
708.1±0.1[b]	163.9±10.1	-0.03±0.03	0.03±0.04	M2
738.1±0.1[b]	28.1±1.8	0.15±0.04	-0.02±0.05	E2
786.7±0.1	13.5±0.9	-0.26±0.05	-0.10±0.05	---
819.7±0.1	25.3±1.6	-0.26±0.06	0.01±0.07	---
822.0±0.1[b]	6.7±0.6	-0.03±0.05	0.04±0.06	E3
827.8±0.1[b]	6.8±0.5	0.04±0.07	0.07±0.08	E2

Table 6-3. (cont'd.).

Energy E_γ (keV)	Relative Intensity I_γ	Angular Distribution Coefficients A_2/A_0	A_4/A_0	Multipolarity[a]
879.9±0.1	weak	---	---	---
900.2±0.1[b]	160.8±10.0	0.23±0.03	-0.07±0.04	---
910.1±0.1[b]	1.8±1.2	---	---	E2+M1
1010.1±0.1	?	---	---	---
1014.7±0.1[b]	?	---	---	---
1173.4±0.1	weak	---	---	---
1330.7±0.1	23.2±1.5	0.19±0.03	-0.03±0.04	---

[a]Transition multipolarity assignments taken from conversion electrons, ref. [Bu71].

[b]These γ-rays were also seen in $(p,4n\gamma)$ reactions. Therefore, the γ-ray energies are the averages of $(p,2n\gamma)$ and $(\alpha,4n\gamma)$ reactions.

coincidences) and Y-gates (identifying low energy coincidences) are shown. The coincidence information was used to construct the level scheme.

The placement of those states that depopulate directly into the 822.0-keV isomeric state is based on the delayed coincidence spectrum as well as prompt coincidence spectra. The 708.1-keV delayed gate (shown in Figure 6-5) enhances those transitions that feed into the 822.0-keV state ($t_{1/2}$ = 36 nsec) in ^{139}Pr.

A summary of the coincidence data is given in Table 6-4.

6.2.4. γ-Rays Angular Distributions

The set of angular distrubition data for ^{139}Pr consists of spectra taken at 90°, 110°, 125°, 140°, and 160° with a 7.7%-efficient Ge(Li) detector mounted on the arm of the goniometer apparatus as described in section 3.3. The angles were taken in random order for the various experiments, and data was typically collected for 2.5 *h* at each angle.

Normalization was provided by using a stationary 16%-efficient Ge(Li) detector. The resulting distributions were fitted to an expansion of Legendre Polynomials to determine the experimental A_2/A_0 and A_4/A_0 coefficients. These are listed in Table 6-3. The A_2 and A_4 values for the 113.9-, 708.1-, and 822.0-keV transitions turned out to be close to zero, expected them to be isotropic due to deexcitation from the 822.0-keV isomeric state.

Of course, the detector resolution which is worse for the 7.7% detector than for the LEPS also affects the results by making the doublet peaks more difficult to analyze reliably. Also, the angular distrubition coefficients not listed in the table were either part of unresolvable or too weak for accurate peak fitting. The data which were fitted for some of the γ-rays are shown in Appendix J.

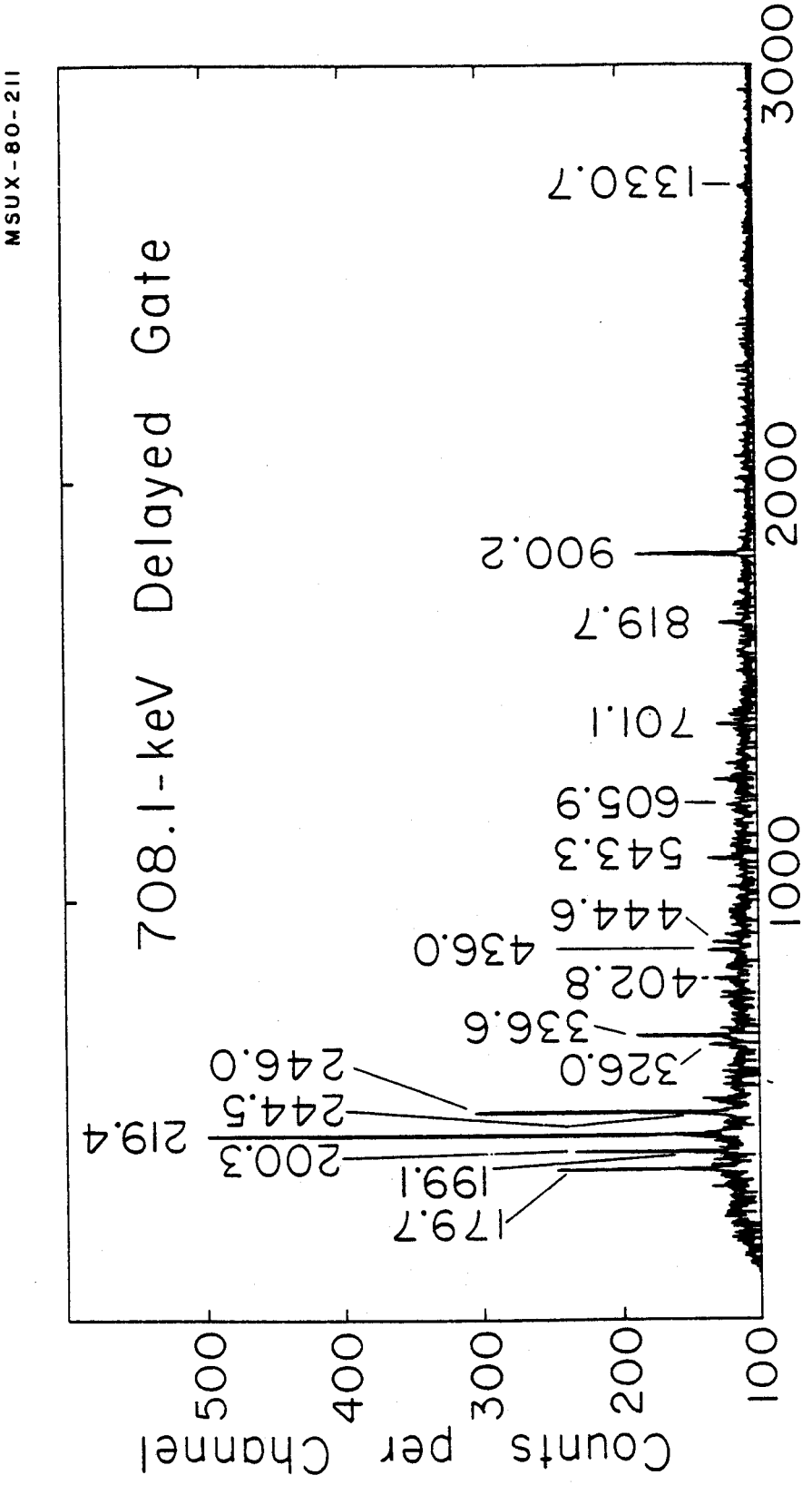

Figure 6-5. Delayed coincidence spectrum. This spectrum enhances those transitions that feed into the 822.0-keV state ($\tau_{1/2}$ = 36 nsec) in ^{139}Pr from the (α,4nγ) reaction.

Table 6-4. Summary of coincidence results for the $^{139}La(\alpha,4n\gamma)^{139}Pr$ reaction.

Gated γ-Ray (keV)	Coincident γ-Rays (keV)
60.2	200.3, 219.4, 244.5, 444.6, 819.7, 900.2
113.9	179.7, 199.1, 200.3, 214.0, 219.4, 244.5, 246.0, 260.0, 326.0, 336.6, 402.8, 418.5, 436.0, 444.6, 454.1, 543.3, 558.2, 633.6, 701.1, 708.1, 738.1, 819.7, 900.2, 910.1, 1014.7, 1330.7
128.0	200.3, 219.4, 244.5, 326.0, 336.6, 345.0, 436.0, 543.3, 605.9, 900.2
179.7	113.9, 199.1, 200.3, 219.4, 244.5, 246.0, 280.0, 326.0, 336.6, 354.8, 382.8, 402.8, 418.5, 436.0, 444.6, 451.1, 465.3, 558.2, 618.5, 701.1, 708.1, 738.1, 900.2, 1330.7
182.5	179.7, 200.3, 219.4, 246.0, 280.0, 336.6, 454.1, 543.3, 708.1, 822.0, 900.2, 1173.4
(199.1+200.3)	60.2, 113.9, 128.0, 199.1, 200.3, 214.0, 244.5, 246.0, 280.0, 326.0, 336.6, 345.0, 382.8, 436.0, 454.1, 543.3, 558.2, 609.5, 701.1, 708.1, 738.1, 786.7, 819.7, 900.2
214.0	182.5, 200.3, 219.4, 246.0, 280.0, 336.6, 543.3, 819.7, 900.2
219.4	60.2, 113.9, 179.7, 182.5, 199.1, 200.3, 214.0, 244.5, 246.0, 260.0, 280.0, 293.9, 326.0, 336.6, 345.0, 354.8, 402.8, 436.0, 444.6, 454.1, 543.3, 558.2, 605.9, 618.5, 633.6, 701.1, 708.1, 786.7, 819.7, 900.2, 1330.7
244.5	179.7, 200.3, 219.4, 246.0, 326.0, 336.6, 436.0, 543.3, 708.1, 786.7, 819.7, 900.2
246.0	113.9, 179.7, 182.5, 199.1, 200.3, 214.0, 219.4, 244.5, 260.0, 280.0, 293.9, 326.0, 336.6, 402.8, 418.5, 436.0, 444.6, 454.1, 543.3, 618.5, 633.6, 701.1, 708.1, 786.7, 900.2, 1330.7
260.0	113.9, 179.7, 219.4, 293.9, 708.1

Table 6-4. (cont'd.).

Gated γ-Ray (keV)	Coincident γ-Rays (keV)
280.0	182.5, 200.3, 214.0, 219.0, 336.6, 543.3
293.9	113.9, 219.4, 246.0, 260.0, 708.1, 786.7, 900.2
326.0	48.0, 113.9, 128.0, 179.7, 200.3, 219.4, 246.0, 336.6, 402.8, 436.0, 444.6, 543.3, 708.1, 786.7, 900.2, 1330.7
336.6	113.9, 128.0, 179.7, 182.5, 199.1, 200.3, 214.0, 219.4, 244.5, 246.0, 280.0, 326.0, 436.0, 444.6, 543.3, 701.1, 708.1, 738.1, 786.7, 900.2
345.0	200.3, 219.4, 336.6, 543.3, 605.9, 900.2
354.8	113.9, 179.7, 219.4, 246.0, 708.1, 900.2 1330.7
402.8	113.9, 179.7, 219.4, 246.0, 326.0, 436.0, 708.1, 900.2, 1330.7
418.5	113.9, 200.3, 246.0, 336.6, 444.6, 543.3, 701.1, 708.1
425.6	113.9, 199.1, 219.4, 701.1, 708.1, 900.2
436.0	48.0, 60.2, 113.9, 128.0, 179.7, 200.3, 219.4, 244.5, 246.0, 326.0, 336.6, 402.8, 418.5, 444.6, 543.3, 701.1, 708.1, 786.7, 900.2, 1330.7
444.6	60.2, 113.9, 219.4, 336.6, 543.3, 708.1, 786.7, 900.2
454.1	113.9, 179.7, 182.5, 200.3, 219.4, 246.0, 708.1, 900.2
527.6	179.7, 246.0, 336.6
543.3	113.9, 128.0, 182.5, 200.3, 219.4, 244.5, 280.0, 326.0, 336.6, 418.5, 436.0, 444.6, 558.2, 605.9, 708.1, 786.7, 900.2
558.2	60.2, 113.9, 179.7, 200.3, 219.4, 246.0, 336.6, 543.3, 708.1, 819.7, 900.2

Table 6-4. (cont'd.).

Gated γ-Ray (keV)	Coincident γ-Rays (keV)
592.9	113.9, 179.7, 246.0, 336.6, 708.1
605.9	60.2, 113.9, 128.0, 200.3, 219.4, 336.6, 345.0, 543.3, 708.1, 900.2
618.5	179.7, 219.4, 246.0, 900.2
633.6	113.9, 200.3, 219.4, 246.0, 708.1, 900.2
701.1	113.9, 179.7, 199.1, 219.4, 246.0, 336.6, 418.5, 708.1
708.1	113.9, 179.7, 219.4, 246.0, 326.0, 336.6, 402.8, 418.5, 436.0, 543.3, 701.1, 819.7, 900.2, 1330.7
738.1	113.9, 336.6, 1014.7
786.7	48.0, 113.9, 200.3, 219.4, 244.5, 246.0, 326.0, 336.6, 436.0, 444.6, 543.3, 708.1, 819.7, 900.2
819.7	60.2, 113.9, 182.5, 200.3, 219.4, 244.5, 444.6, 708.1, 900.2
822.0	---
827.8	---
900.2	48.0, 60.2, 113.9, 128.0, 179.7, 200.3, 219.4, 244.5, 246.0, 260.0, 293.9, 326.0, 336.6, 345.0, 402.8, 436.0, 444.6, 543.3, 708.1, 786.7, 819.7, 1330.7
910.1	113.9
1010.1	113.9
1014.7	74.9, 113.9, 738.1
1173.4	113.9, 179.7, 182.5, 200.3, 219.4, 246.0 336.6, 543.3, 708.1, 900.2
1330.7	113.9, 179.7, 219.4, 246.0, 326.0, 402.8, 436.0, 708.1, 900.2

6.3. Construct of the ^{139}Pr Level Scheme and Comparison

The proposed level schemes for ^{139}Pr, both from $(p,2n\gamma)$ and $(\alpha,4n\gamma)$ reactions, are supported primarily by coincidence information, intensity balances, and delayed-coincidence spectra; and secondly by angular distribution data, energy summing relationships and from known $^{139}Nd^{m+g}$ decay scheme [Be69, Bu71]. The spin values and parities given in both level schemes were derived from the angular distribution coefficients, conversion coefficients, ratios of γ-ray intensities in the proton and alpha induced reactions, and input from the $^{139}Nd^{m+g}$ decay scheme.

This section will be broken into three parts: 1) level scheme and spin-parity assignments from the $(p,2n\gamma)$ reaction, 2) level scheme and spin-parity assignments from the $(\alpha,4n\gamma)$ reaction, and 3) comparison between these two reactions and with other experimental results.

6.3.1. Level Scheme and Spin-Parity Assignments from $(p,2n\gamma)$ Reaction

In Figure 6-6, the level scheme of ^{139}Pr obtained from the $(p,2n\gamma)$ reaction is given. Specific details of the construction of the level scheme and J^{π} assignments are discussed next.

Ground, 113.9-, and 822.0-keV States

The large relative intensity of the 113.9-keV transition combined with its coincidence behavior leads to a placement of a first excited state at 113.9 keV.

The isomeric state at 822.0 keV was first placed on the basis of prompt-coincidence spectra. It was then confirmed by the delayed-coincidence spectrum shown in Figure 6-2. This isomeric state decays to the 113.9-keV level via the 708.1-keV transition and to the ground state via the 822.0-keV transition.

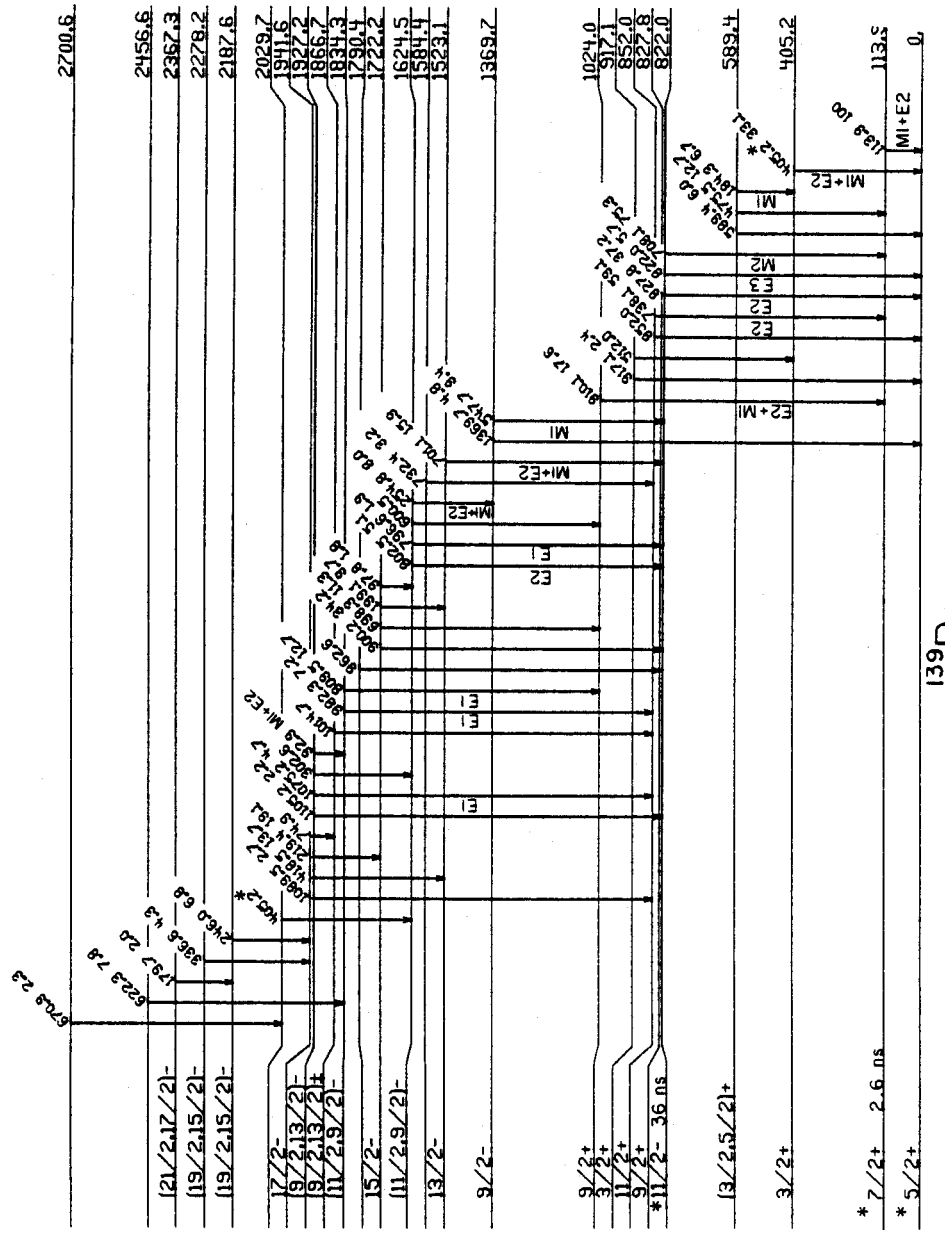

Figure 6-6. Level scheme of ^{139}Pr obtained from the $(p,2n\gamma)$ reaction.

The ground state has been reported to have $J^{\pi} = 5/2^{+}$ [Ep72], and the 113.9- and 822.0-keV states have been assigned $7/2^{+}$ and $11/2^{-}$ [Be69, Bu71], respectively on the basis of multipolarities of the three above γ transitions and the log*ft* values for $^{139}Nd^{m}$ β-decay. Also, in the $^{139}Nd^{m}$ decay studies, the 113.9- and 822.0-keV states were measured to have half-lives of 2.6 and 36 nsec, respectively.

In this study, 113.9-, 708.1-, and 822.0-keV transitions were found to be definitely isotropic (e.g. see the values of A_2 and A_4 for 113.9- and 822.0-keV transitions in Table 6-1.) Although this information does not allow us to comment further on the J^{π} assignments, it is consistent with the half-life of the 822.0-keV state.

405.2-, 589.4-, and 917.1-keV States

The other set of low-lying states, presumably of lower spin, has the interconnecting transitions of 184.3, 405.2, 475.5, and 512.0 keV. Coincidence relations among them and the intensity balances lead to the placement of levels at 405.2, 589.4, and 917.1 keV. These states were also observed in $^{139}Nd^{g}$ decay.

The 405.2-keV transition is a mixed *M*1/*E*2 transition; therefore, the J^{π} assignment is restricted to $3/2^{+}$, $5/2^{+}$, or $7/2^{+}$. The $5/2^{+}$ value is ruled out because of the large negative value of A_2 and the small positive value of A_4. The log*ft* of 6.4 for this level from $^{139}Nd^{g}$ decay and the missing transition from this state to the $7/2^{+}$ level at 113.9 keV, rules out $J^{\pi} = 7/2^{+}$. Thus, the 405.2-keV state has $J^{\pi} = 3/2^{+}$.

The 589.4-keV state feeds into the $5/2^{+}$, $7/2^{+}$ 113.9-keV, and $3/2^{+}$ 405.2-keV states by the 589.4-, 475.5-, and 184.3-keV transitions, respectively. From $^{139}Nd^{g}$ decay, *M*1 or *E*2 multipolarity was assigned for the 184.3-keV transition. The A_2 and A_4 values for this transition

are consistent with the *M*1 multipolarity. The angular distribution coefficients of transitions deexciting from this level limit its J^{π} to $3/2^{+}$ or $5/2^{+}$.

The 917.1-keV state feeds into the $5/2^{+}$ ground state by the 917.1-keV transition and most probably into the $3/2^{+}$ 405.2-keV state by the 512.0-keV transition. The angular distribution coefficients for the 917.1-keV transition limit its J^{π} to $3/2^{+}$ or $7/2^{+}$. From ^{139}Nd^{g} decay, $7/2^{+}$ can clearly be ruled out (log*ft* = 6.6), leaving $J^{\pi} = 3/2^{+}$ for this state.

827.8-keV State

The coincidence relationships between 827.8-, 796.6-, and 962.6-keV transitions, and the relative γ-ray intensities, place the levels at 827.8, 1624.5, and 1790.4 keV.

The 827.8-keV transition that deexcites from 827.8-keV state to the $5/2^{+}$ ground state is an *E*2. The angular distribution data for this transition can be fitted with only two values, $1/2^{+}$ or $9/2^{+}$. $J^{\pi} = 1/2^{+}$ can be eliminated from the β-decay work; thus, this level has $J^{\pi} = 9/2^{+}$.

852.0-keV State

The coincidence information between the 113.9- and 738.1-keV [third strongest peak in the $(p,2n\gamma)$ reaction] γ's places this state. The 738.1-keV transition was reported to have *E*2 + *M*1 multipolarity. The angular distribution coefficients are consistent with a stretched *E*2 transition which restricts its J^{π} to $3/2^{+}$ or $11/2^{+}$. Again from ^{139}Nd^{m} decay, spin $3/2^{+}$ can be ruled out, leaving $J^{\pi} = 11/2^{+}$ for this state. The tentative $9/2^{+}$ assignments reached from β-decay data by Beery et al. [Be69] are believed to be incorrect because the negative A_4 value rules out a mixed

*M*1/*E*2 multipolarity for the 738.1-keV transition. Also, their argument regarding the 852.0-keV transition to the ground state is a very poor argument [this transition has not been seen in the (α,4*n*γ) reaction].

1024.0-keV State

This state was placed on the basis of the coincidence relationships between 113.9- and 910.0-keV γ-rays. The 910.1-keV transition that deexcites from this state to the $7/2^+$ 113.9-keV state is an *E*2 or *M*1 [Bu71]. The angular distribution coefficients are consistent with J to $J \pm 1$ *E*2 + *M*1 mixed transition which limits the J^π assignment to $5/2^+$ or $9/2^+$ for this state. The $5/2^+$ value can be ruled out because the (p,2*n*γ) reaction is not likely to populate low-spin states at higher excitation energy. From the $^{139}Nd^m$ decay, $5/2^+$ can also be included; therefore, J^π for 1024.0-keV state would be $9/2^+$.

1369.7-keV State

This state feeds into the $11/2^-$ 822.0-keV state by the 547.7-keV transition. If this transition is an *M*1 transition (Table 6-1), the J^π assignment is restricted to $9/2^-$, $11/2^-$, or $13/2^-$. The $11/2^-$ is ruled out because of the large negative value of A_2 and the small positive value of A_4. The fact that this state is not fed by γ-rays from a high-spin state indicates that it most likely is not in the *yrast* sequence, thus eliminating $J^\pi = 13/2^-$ (below it is shown that the 1523.1-keV state has $J^\pi = 13/2^-$ and receives feeding from the high-spin states). Thus, the 139.7-keV state has $J^\pi = 9/2^-$.

1523.1-keV State

The 701.1-keV γ-ray deexciting from this level to an $11/2^-$ 822.0-keV state is reported to have *M*1 or *E*2 multipolarity [Bu71]. The angular

distribution coefficients are consistent with a mixed $M1/E2$ transition and restrict the J^{π} to $9/2^-$ or $13/2^-$. Since the 701.1-keV γ-ray is seen so intensely in both $(p,2n\gamma)$ and $(\alpha,4n\gamma)$ reactions, *yrast* arguments lead us to prefer the higher spin, i.e., $13/2^-$, for this state.

1722.2-keV State

This state has been observed both by $(p,2n\gamma)$ and $(\alpha,4n\gamma)$ reactions (not seen in β-decay). The angular distribution coefficients of 199.1- and 900.2-keV β-rays decaying from this state limit its J^{π} value to $15/2^-$.

1941.6-keV State

This state is the last state for which unique spin assignments were possible. The angular distribution coefficients of a 219.4-keV transition deexciting from this level to the $15/2^-$ 1722.2-keV state are consistent with stretched $M1$ or $M1/E2$ mixed transitions. The J^{π} assignment is restricted to $13/2^-$ or $17/2^-$ due to the large negative value of A_2 and the small positive value of A_4. Since 219.4-keV γ was seen so intensely in both the $(p,2n\gamma)$ and $(\alpha,4n\gamma)$ reactions, *yrast* arguments lead us to prefer the higher spin, i.e., $17/2^-$, for this state (which also receives feeding from high-spin states).

Other States

The remaining states are not uniquely determined, however some spins could be eliminated on the basis of angular distribution coefficients from the $(p,2n\gamma)$ or $(\alpha,4n\gamma)$ reactions.

All of the spins suggested for 1624.5-, 1834.3-, 1866.7-, and 1927.2-keV states in the present work should thus be considered only tentative (the first J^{π} assignment is preferable). Also, J^{π} assignments for 2187.6-,

2278.2-, and 2367.3-keV states will be discussed in section 6.3.2. It should be mentioned here that there are two 405.2-keV transitions in the level scheme which were indicated by asterisks.

6.3.2. Level Scheme and Spin-Parity Assignment for (α,4nγ) Reaction

The prompt coincidence data as well as the delayed-coincidence spectrum (Figure 6-5) and intensity balances have been primarily used to construct the tentative level scheme. Secondary factors were energy summing relationships and angular distribution coefficients. This level scheme, up to 5 MeV excitation, is shown in Figure 6-7. The use of the LEPS detector as discussed in section 6.2.3. enabled us to identify the low-energy transitions. Many states not seen from the (p,2nγ) reaction have been found due to a higher angular momentum transfer of alpha particle.

The J^{π} assignments for states below 2 MeV as seen from the (p,2nγ) reaction (except for 1124.0- and 1414.9-keV states) are discussed in section 6.3.1. These assignments were made on the basis of angular distribution coefficients, transitions, multipolarities, and input from $^{139}Nd^{g+m}$ data. Where there was a large error in the A_2 or A_4 values in one case, the values from the other case were chosen.

The unique spin assignments for the levels above 2 MeV were not possible. More experiments such as γ-ray excitation functions, electron-conversion, and γ-ray lifetimes need to be done in order to assign unique J^{π} to these levels. From angular distrubition data of the present work, some spins could be excluded, however, the J^{π} assignments should be considered only tentative. Specific details of J^{π} assignment will be discussed next.

The angular distribution coefficients for the 246.0-, 336.6-, and 819.7-keV transitions deexciting from 2187.6-, 2278.2-, and 2761.3-keV

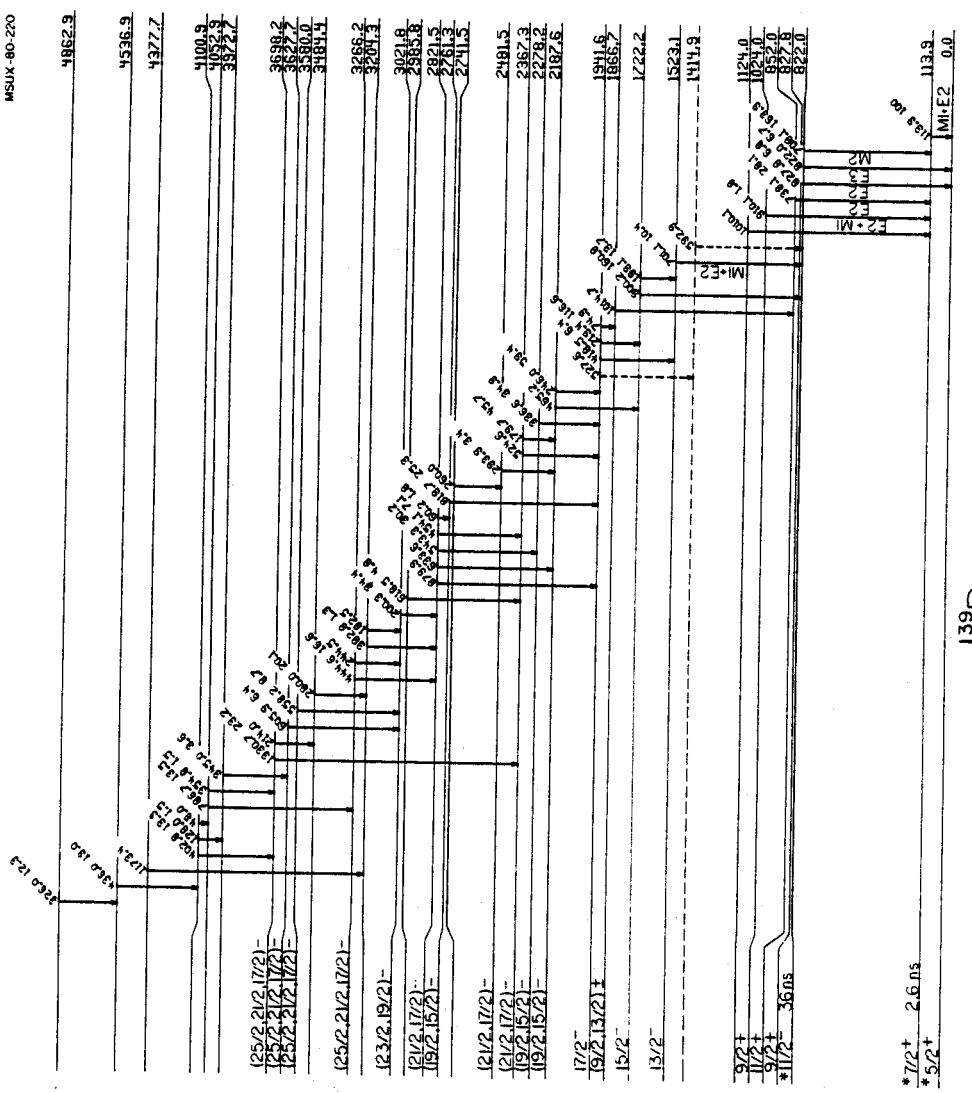

Figure 6-7. Level scheme of ^{139}Pr obtained from (α,4nγ) reaction.

states, respectively, are consistent with stretched *M*1 transitions which restricted their J^{π} to $15/2^-$ or $19/2^-$. The fact that 246.0 keV deexciting from a 2187.6-keV state has been observed so intensely in the $(\alpha,4n\gamma)$ reaction, and that there are many γ-rays feeding to this state from higher-spin states, leads to a preference of $19/2^-$ over $15/2^-$ for this level.

The levels at 2367.3-, 2481.5-, and 2821.5-keV were assigned $21/2^-$ or $17/2^-$ based on the angular distribution data of 179.7-, 293.9-, and 543.3-keV transitions, deexciting from them respectively, and are consistent with a stretched *M*1. Among them, the 2367.3-keV state most likely has $J^{\pi}=21/2^-$ based on the *yrast* argument. Also, the A_2 and A_4 values for the 454.1-keV transition deexciting from the 2821.5-keV state are consistent with $J \rightarrow J$ or $J \rightarrow J \pm 2$ *E*2 transition. This also confirms the J^{π} assignments for this state.

The 200.3-keV transition feeding from the 3021.8-keV state to the 2821.5-keV state has *M*1 or *M*1/*E*2 multipolarity due to angular distribution coefficients. This restricted the J^{π} assignments for the 3021.8-keV state to $23/2^-$ or $19/2^-$. Again, *yrast* consideration would lead to a preference of $23/2^-$.

Finally, the states at 3266.2^-, 3580.0^-, 3627.7^-, and 3698.2-keV could be assigned as $25/2^-$, $21/2^-$, or $17/2^-$ according to the angular distribution coefficients of transitions decaying from these states. It should be mentioned here that there is also a possibility of a $15/2^-$ assignment for these states; however one could eliminate the $15/2^-$ assignment because it is highly unlikely to observe a lower-spin state at such a high excitation energy.

6.3.3. Comparison Between the $(p,2n\gamma)$ and $(\alpha,4n\gamma)$ Reactions and with Other Experimental Results

The two previous major investigations [Be69, Bu71] of the $^{139}Nd^{m+g}$ β-decay have revealed a wealth of information about the ^{139}Pr excited states, their associated transitions, the spins and parities of these excited states, and especially information about the multipolarities of many of the ^{139}Pr transitions by Butsev et al. [Bu71]. Unfortunately, only one scattering reaction producing ^{139}Pr has been reported. Goles et al. [Go72] have investigated the $^{141}Pr(p,t)^{139}Pr$ reaction. In their study, DWBA calculations for two-nucleon pickups were attempted but no spin assignments were made.

Many high-spin, high-lying states not viewed previously have been observed in the present in-beam work. Also, in the case of the $(\alpha,4n\gamma)$ reaction, many higher-spin states were populated due to a higher angular momentum transfer of alpha particles.

Figure 6-8 shows the comparison between this work and other investigations. Levels in columns one and two are based on the $(p,2n\gamma)$ and $(\alpha,4n\gamma)$ reactions reported here, while levels in columns three and four are from β-decay and scattering reaction, respectively.

6.4. Discussion of Level Configurations

The states in ^{139}Pr can be classified into three categories: 1) single quasiparticle states, 2) negative-parity collective states, and 3) positive-parity collective states.

6.4.1. Single-Quasiparticle States

In ^{139}Pr one can expect to see evidence of all the available single-proton states between Z=50 and Z=82. The most clearcut single-quasiparticle

Figure 6-8. Energy levels of ^{139}Pr. Levels in columns 1 and 2 are from present work while levels in column 3 are from β-decay [Be69, Bu71] and levels in column 4 are from scattering reaction [Go72]. Spins are shown in $2J$.

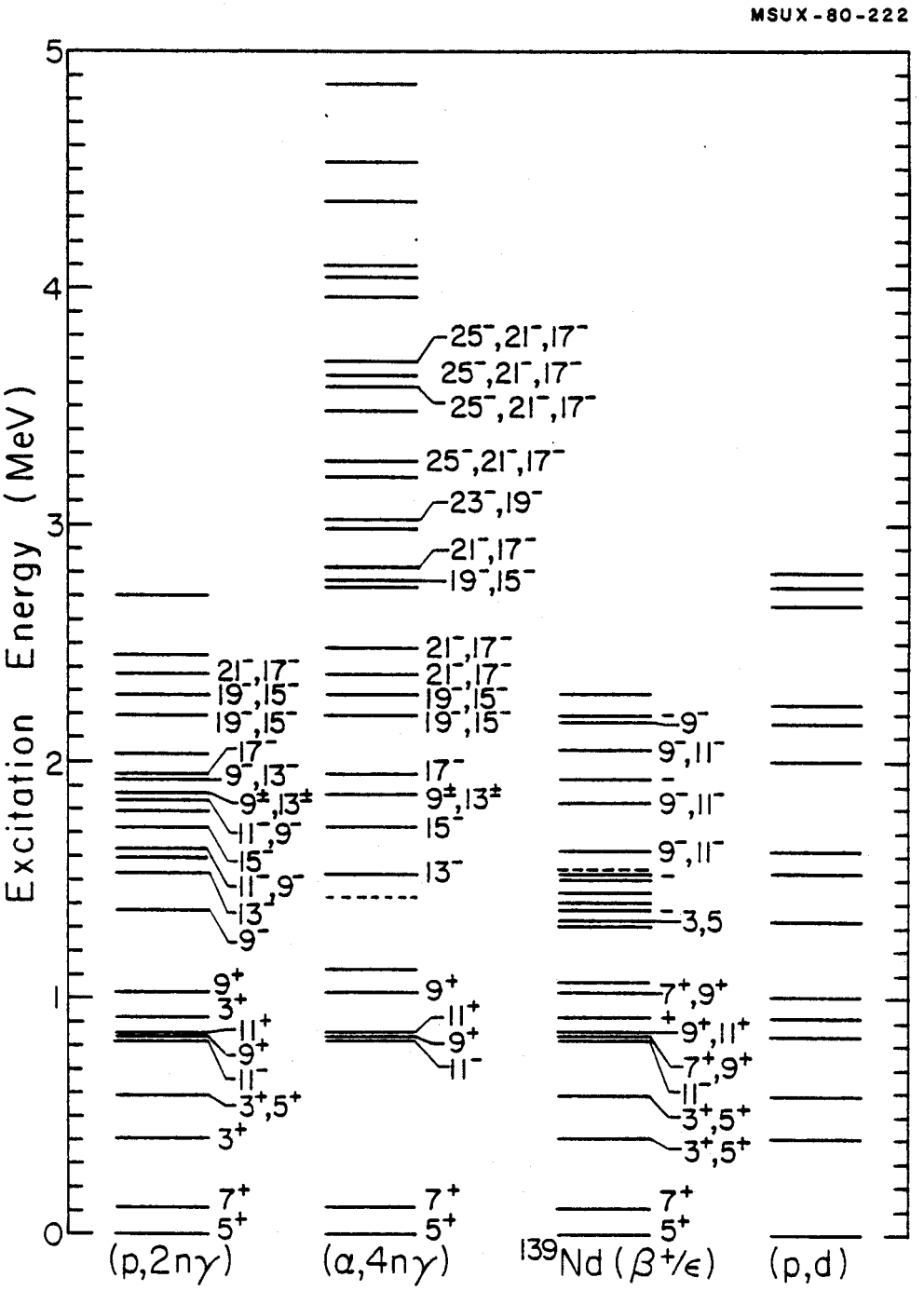
MSUX-80-222
Excitation Energy (MeV)
0
1
2
3
4
5
(p,2nγ)
(α,4nγ)
139Nd (β+/ε)
(p,d)
5+
7+
3+
3+,5+
11-
9+
11+
3
9+
9-,13-
17-
19-,15-
19-,15-
21-,17-
9±,13±
11-,9-
15-
11-,9-
13-
9-
5+
7+
9+
11-
9+
11+
9±,13±
15-
17-
19-,15-
19-,15-
21-,17-
21-,17-
19-,15-
23-,19-
25-,21-,17-
25-,21-,17-
25-,21-,17-
5+
7+
3,5
3+,5+
11-
7+,9+
9+,11+
+
9+
7+,9+
9-,11-
9-,11-
9-,11-
-
9-

states are those at 0, 113.9, 405.2, and 822.0 keV. The ground state undoubtedly consists primarily of a single $d_{5/2}$ proton outside a closed $g_{7/2}$ subshell and the 113.9 keV state simply promotes a $g_{7/2}^{-1}$ proton state. The retarded *M*1 transition between them is characteristic of the ℓ-forbidden *M*1's between the $g_{7/2}$ and $d_{5/2}$ states in a wide variety of nuclei in this region.

The level at 405.2 keV is presumably a single $d_{3/2}$ proton state. Systematically, this level has been seen at 403.8 keV in ^{141}Pm (c.f. section 5.4.1), but not in ^{143}Eu.

The 822.0-keV state shows evidence of being a single $h_{11/2}$ proton outside the closed $g_{7/2}$ subshell. The *M*2 transition from this state to the 113.9 keV state is retarded, while the *E*3 to the ground state is enhanced over single-particle estimates.

The position of the $s_{1/2}$ state is not so clear, but it is probably fragmented and contributes to several states above 1 MeV.

6.4.2. Negative-Parity Collective States

The negative-parity collective states in ^{139}Pr are expected to consist primarily of the $\pi h_{11/2}$ state coupled to a ^{138}Ce triaxial core. The first 2^+ excited state in ^{138}Ce lies at ≈790 keV [Sh77].

The low-lying $(\pi h_{11/2} \times 2_1^+)$ states should be rather pure configurations and should be observed at about 1612 keV in ^{139}Pr. The 1369.7-, 1523.1-, and 1722.2-keV states all deexcite through the $\pi h_{11/2}$ state and may represent three of the states in the $(\pi h_{11/2} \times 2_1^+)$ multiplet.

The $(\pi h_{11/2} \times 2_1^+)_{9/2^-}$ configuration lies at 1369.7 keV. The 1523.1-keV state feeds the 822.0-keV state and presumably has a $(\pi h_{11/2} \times 2_1^+)_{13/2^-}$ configuration. A state at 1722.2 keV is observed to deexcite through the $\pi h_{11/2}$ state. This state is tentatively assigned as the $(\pi h_{11/2} \times 2_1^+)_{15/2^-}$ configuration.

The states corresponding to $(\pi h_{11/2} \times 4_1^+)$ are expected to lie near 2648 keV. The $(\pi h_{11/2} \times 4_1^+)_{17/2^-}$ configuration was observed experimentally at 1941.6 keV and leaving the other components for the 2187.6- and 2278.2-keV states.

Little can be said about the rest of the higher-lying, high-spin states in ^{139}Pr due to the lack of experimental data. On the other hand, triaxial calculations need to be performed in order to assign appropriate configurations to these states. Such calculations should involve the five single-proton states coupled to the 2_1^+, 0_1^+, 2_2^+, 4_1^+, 3_1^-, and other higher spin vibrational states in ^{138}Ce.

It should be mentioned here that states at 1624.5, 1834.3, and 1927.2 keV have been described as three-quasiparticle states by Beery et al. [Be69, Mc69].

Finally, the shell model calculation was performed by Muthukrishnan et al. [Mu71] in order to describe the negative-parity levels in ^{139}Pr. Their calculations are not in sound agreement with the experimental data and that is because the shell model is not an appropriate model for this region.

6.4.3. Positive-Parity Collective States

The positive-parity states can be generated by coupling the $\pi d_{5/2}$ and $\pi g_{7/2}$ to the ^{138}Ce core. These states are all expected to give poorer weak-coupling descriptions due to the ease of mixing with nearby positive-parity states.

The $(\pi d_{5/2} \times 2_1^+)$ states should lie at ≈790 keV in ^{139}Pr. They should deexcite to the $\pi d_{5/2}$ ground state by $E2(+M1)$ transitions. The state at 827.8 keV is presumably the $(\pi d_{5/2} \times 2_1^+)_{9/2^+}$ component and the state at 917.1 keV is probably the $(\pi d_{5/2} \times 2_1^+)_{3/2^+}$ component. No

definite spin assignments were made for the 589.4-keV state, however it is not unlikely to assume this level has a $(\pi d_{5/2} \times 2_1^+)_{5/2^+}$ configuration.

The $(\pi g_{7/2} \times 2_1^+)$ couplings lead to observable $9/2^+$ and $11/2^+$ states in the vicinity of 904 keV which should deexcite through the $\pi g_{7/2}$ single-particle state through strong $E2$ transitions. The most likely candidates lie at 1024.0 and 852.0 keV, respectively.

CHAPTER VII

SYSTEMATICS OF THE ODD-MASS N=80 NUCLEI

The positions of known states in odd-mass N=80 isotones are shown in Figure 7-1. The data for ^{133}I, ^{135}Cs, and ^{137}La are from β-decay or a combination of β-decay and in-beam studies and were taken from Refs. [Pa68, Ho71], [Al68, He75], and [Na73, Hen75], respectively. The ^{139}Pr, ^{141}Pm, and ^{143}Eu data are from the present in-beam work only. Also, in the case of ^{139}Pr, the states above 3 MeV from (α,4$n\gamma$) reaction are not shown in this figure.

Because few reaction studies have been made (no in-beam work in detail) on ^{133}I, ^{135}Cs, and ^{137}La in this region, the levels can be traced for the most part only over three isotones (^{139}Pr, ^{141}Pm, and ^{143}Eu) with any certainty.

The low-lying level spectra in odd-mass N=80 nuclei are expected to be single-quasiparticle states between Z=50 and Z=82 closed shells. Here, the available single-particle orbits are $g_{7/2}$, and $d_{3/2}$, lying relatively close together, and then, after a gap of ≈500-1000 keV, $h_{11/2}$, $s_{1/2}$, and $d_{3/2}$, also relatively close together. These five single-particle states cannot be traced in all of the N=80 isotones (only in the case of ^{141}Pm have all these five states been observed experimentally). The 258.8 keV ($3/2^+$) state in ^{143}Eu is not the $d_{3/2}$ single-particle state as discussed in section 4.2.1. Also, in some of these nuclei the positions of the $d_{3/2}$ and $s_{1/2}$ states are not so clear, but they are probably fragmented and contribute to several states above 1 MeV. In N=80 isotones there is a change of ground-state spin between ^{137}La and ^{139}Pr. The $d_{3/2}$ and $h_{11/2}$ states

Figure 7-1. The position of known states in odd-mass N=80 isotones. The data for ^{133}I, ^{135}Cs, and ^{137}La are from β-decay or a combination of β-decay and in-beam studies. The ^{139}Pr, ^{141}Pm, and ^{143}Eu data are from the present in-beam study. The states in ^{139}Pr above 3 MeV from $(\alpha,4n\gamma)$ reaction are not shown in this figure. Also, spins are shown in $2J$.

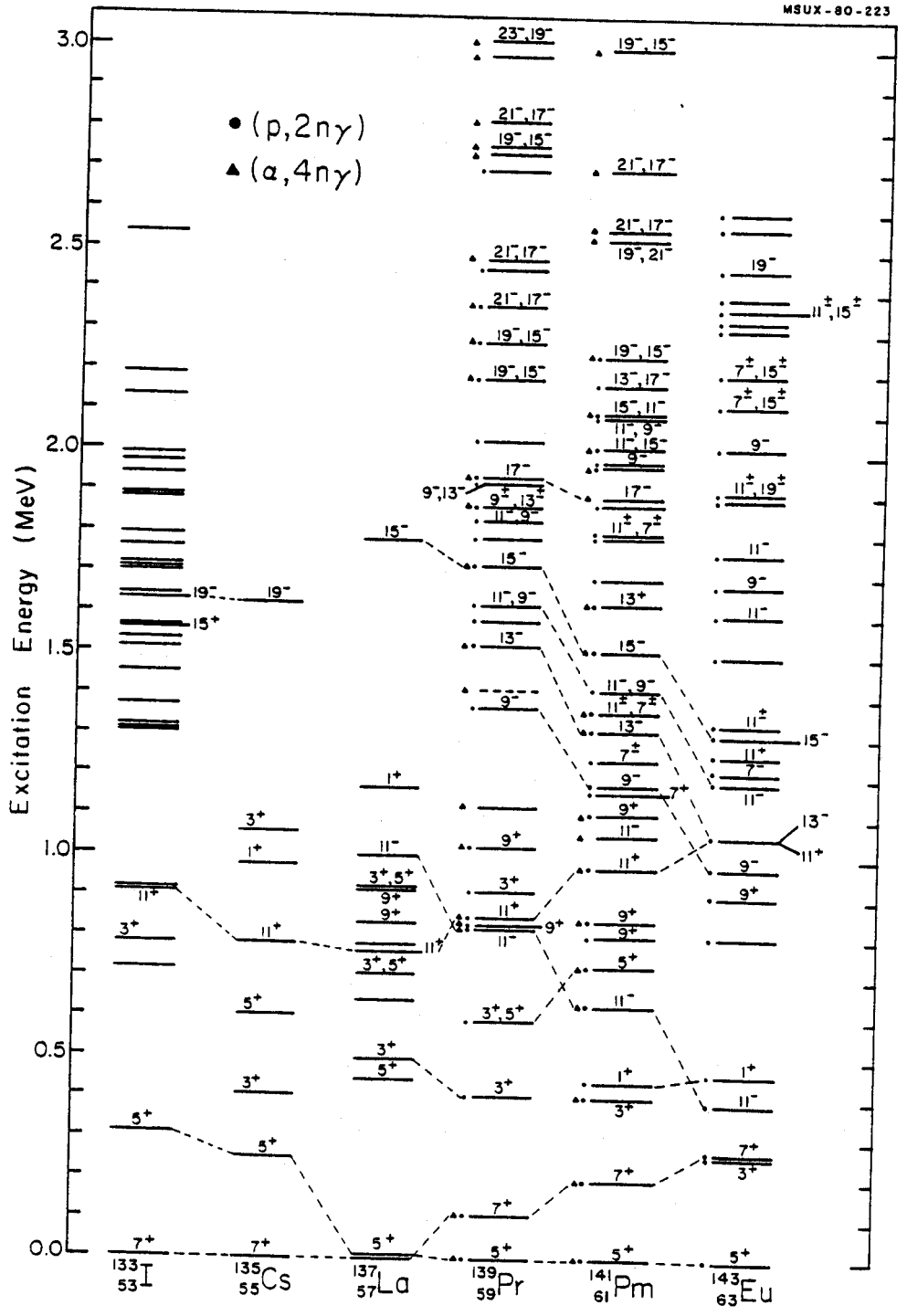
MSUX-80-223
● (p,2nγ)
▲ (α,4nγ)
Excitation Energy (MeV)
3.0
2.5
2.0
1.5
1.0
0.5
0.0
133 53 I
135 55 Cs
137 57 La
139 59 Pr
141 61 Pm
143 63 Eu

decrease in energy with increasing proton number from the ^{137}La through ^{143}Eu. This trend has been observed in odd-mass N=82 isotones experimentally and theoretically [Ta76].

The low-lying negative-parity collective states ($9/2^-$, $13/2^-$, $15/2^-$) in this region are assumed to be odd proton coupled to the first 2^+ state of the even-neighbor cores. These states decrease in energy with an increasing proton number as one goes from ^{137}La through ^{143}Eu. In fact, this has been observed to be true for first 2^+ states in even-even N=80 isotones from the ^{134}Xe through ^{142}Sm cores.

The higher negative-parity states observed in some of the odd-mass N=80 nuclei are believed to result from single proton states coupled to the 0_1^+, 2_2^+, 4_1^+, 3_1^-, and other higher-spin vibrational states in cores. The calculations need to be done in the case of ^{139}Pr and ^{141}Pm before a good understanding of the systematic trends of the negative-parity collective states in this region can be obtained.

The only positive-parity collective state which can be traced systematically is the first $11/2^+$ state. Its energy decreases from ^{133}I to ^{137}La and thereafter increases to ^{143}Eu.

CHAPTER VIII

SUMMARY AND CONCLUSIONS

In-beam γ-ray spectroscopy has been used to investigate the behavior of the excited states in ^{143}Eu, ^{141}Pm, and ^{139}Pr in order to learn more about the systematics in this region. The $(p,2n\gamma)$ reaction was used to populate the states in ^{143}Eu, whereas the states in ^{141}Pm and ^{139}Pr were populated via both the $(p,2n\gamma)$ and the $(\alpha,4n\gamma)$ reaction. The Ge(Li)-Ge(Li) γ-γ-t coincidence technique used was very useful in the placement of γ-rays in the level scheme. Many weak γ-rays were placed in the level scheme with the coincidence information which otherwise might not have been placed. Also, the coincidence information was very useful in the determination of which γ-rays were doublets.

The combined use of γ-ray angular distributions from the present work and previous conversion electron data and log*ft* values made the unique spin-parity assignments possible for many states in these nuclei and limited the J^{π} assignments for some other states.

The weak-coupling triaxial calculations have been shown to give an excellent quantitative as well as qualitative understanding of the low-lying level structure in ^{143}Eu. The calculations for negative-parity states indicate an oblate shape, and those for positive-parity states gave at least a germinal fit. No calculations have been done in the case of ^{141}Pm and ^{139}Pr, but in both cases the level structures were explained quite satisfactorily in terms of a triaxial weak-coupling model.

Although the results reported here produce some new insights into the systematics of the N=80 region, more experimental work (e.g. excitation

functions, conversion electron data) as well as theoretical calculations (for ^{141}Pm and ^{139}Pr) are needed before a good understanding of the behavior of the nuclei in this region can be obtained.

BIBLIOGRAPHY

BIBLIOGRAPHY

A

[ALICE] Written by M. Blann and F. Plasil, adapted for the MSU Heavy-Ion Laboratory Sigma-7 computer by W. H. Bentley.

[Al68] P. Alexander and J. P. Lau, Nucl. Phys. A121, 612(1968).

[Ar70] R. Arl't, G. Beyer, Y. Vanryschuk, V. A. Morosov, T. M. Muminov, V. I. Rason, J. Sazynski, H. Faia, H. Strusny, and E. Herrmann, JINR report No. P6-5517, 1970 (unpublished).

[Au72] IIEVENT, a computer code written by Richard Au, MSU Heavy-Ion Laboratory (unpublished).

B

[Be69] D. B. Beery, W. H. Kelly, and Wm. C. McHarris, Phys. Rev. 188, 1851(1969).

[Bu71] V. S. Butsev, T. Vylov, V. G. Kalinnikov, N. A. Tikhonov, and E. H. Herrmann, Izv. Akad. Nauk SSSR. Ser. Fiz. 35, 1618 (1971); Bull. Acad. Sci. USSR, Phys. Ser. 35, 1474(1972).

D

[Da58] A. S. Davydov and G. F. Filippov, Nucl. Phys. 8, 237(1958).

[Dy71] J. L. Dye and V. A. Nicely, J. Chem. Education, 48, 443(1971).

E

[Ec72] C. Eckstrom, S. Ingelman, M. Olsmats, and B. Wannberg, Phys. Scripta 6, 181(1972).

[Ek72] C. Ekstrom, S. Ingelman, M. Olmats, B. Wannberg, G. Andersson, and A. Rosen, Nucl. Phys. A196, 178(1972).

[Ep71] R. E. Eppley, Wm. C. McHarris, and W. H. Kelly, Phys. Rev. C 3, 282(1971).

[Ep72] R. E. Eppley, R. R. Todd, R. A. Warner, Wm. C. McHarris, and W. H. Kelly, Phys. Rev. C 5, 1084(1972).

F

[Fi78] R. B. Firestone, R. A. Warner, Wm. C. McHarris, and W. H. Kelly, Phys. Rev. C 17, 718(1978).

[Fi79] R. B. Firestone, R. C. Pardo, and Wm. C. McHarris, Phys. Lett. 89B, 36(1979).

G

[GADFIT] GADFIT, computer code written by R. A. Warner, for the MSU Heavy-Ion Laboratory Sigma-7 computer.

[Gi78] J. Gizon, A. Gizon, R. M. Diamond and F. S. Stephen, J. Phys. G(Nucl. Phys.) 4, 1171(1978).

[Go72] R. W. Goles, R. A. Warner, and Wm. C. McHarris, Phys. Rev. C 6, 587(1972).

H

[Ha68] R. S. Hager and E. C. Seltzer, Nucl. Data Tables A4, 1(1968).

[He62] K. Hecht and G. R. Satchler, Nucl. Phys. 32, 286(1962).

[He75] E. A. Henry, Nucl. Data Sheets B14, 191(1975).

[Hen75] E. A. Henry, N. Smith, P. G. Johnson, and R. A. Meyer, Phys. Rev. C 12, 1314(1975).

[Her50] G. Herzberg(1950), "Spectra of Diatomic Molecules", second edition, D. Van Nostrand Co. Inc., Toronto, p. 283.

[Ho71] D. J. Horen, Oak Ridge National Lab. Report No. ORNL-4730, 1971(unpublished).

I

[Ia79] Iachello and O. Scholten, Phys. Rev. Lett. 43, 679(1979).

K

[Ke77] G. G. Kennedy, J. Deslauriers, S. C. Giyrathi, and S. K. Mark, Phys. Rev. C 15, 792(1977).

L

[Le78] C. M. Lederer and V. S. Shirley, Table of Isotopes, 7th Ed., Wiley, N. Y. (1978).

M

[Mc69] Wm. C. McHarris, D. B. Beery, and W. H. Kelly, Phys. Rev. Lett., 22, 1191(1969).

[Me75] J. Meyer-ter-Vehn, Nucl. Phys. A249, 111-165(1975).

[Mu71] R. Muthukrishnan and A. Kromminga, Phys. Rev. C 3, 229(1971).

N

[Na73] K. Nakai, P. Kleinheinz, J. R. Leigh, K. H. Maier, F. S. Stephens, R. M. Diamond, and G. Lovhoiden, Phys. Lett. 44B, 443(1973).

[Ne70] E. Newman, K. S. Toth, R. L. Aulile, R. M. Gaedke, M. F. Roche, and B. H. Wildenthal, Phys. Rev. C 1, 1118(1970).

P

[Pa65] V. V. Pashkevich and R. A. Sardaryan, Nucl. Phys. 65, 401(1965).

[Pa68] B. Parsa, G. E. Gordon, and W. B. Walters, Nucl. Phus. A110, 674(1968).

R

[Re63] V. V. Remaev, Yu. S. Korda, and A. P. Klyucharen. Izv. Akad. Nauk SSSR Ser. Fiz. 27, 125(1963).

[Ro69] J. T. Routti and S. G. Prussin, Nucl. Instr. Meth. 72, 125(1969).

S

[Sh77] J. D. Sherman, D. L. Hendrie, and M. S. Zisman, Phys. Rev. C 15, 903(1977).

T

[Ta76] N. de Takacsy and S. Das Gupta, Phys. Rev. C 13, 399(1976).

V

[Va73] J. Van Klinken, D. Hales, H. Klewe-Nebenius, K. Wisshak, G. Nawicki, J. Buschmann, S. Goring, R. Lohken, H. Rebel, and G. Schatz, Gesellschaft fur Kernforschung mbH KFK 1768(1973).

W

[Wa71] R. A. Warner, R. R. Todd, R. E. Eppley, W. H. Kelly and Wm. C. McHarris, Bull. Am. Phys. Soc. 16, 1161(1971).

[Wi76] K. Wisshak, A. Hanser, H. Klewe-Nebenius, J. Bushmann, H. Rebel, H. Faust, H. Toki, and A. Fassler, Z. Phys. A 277, 129(1976).

Y

[Ya67] T. Yamazaki, Nucl. Data Tables A3, 1(1967).

[Ya75] F. Y. Yap, R. R. Todd, W. H. Kelly, Wm. C. McHarris, and R. A. Warner, Phys. Rev. C 11, 952(1975).

APPENDICES

APPENDIX A

Gated Coincidence Spectra of Transition in ^{143}Eu.

Figure A. Gated spectra of transitions in ^{143}Eu from $(p,2n\gamma)$ reaction. Background subtraction using the adjacent continuum has been included. The spectra are arranged according to increasing energy.

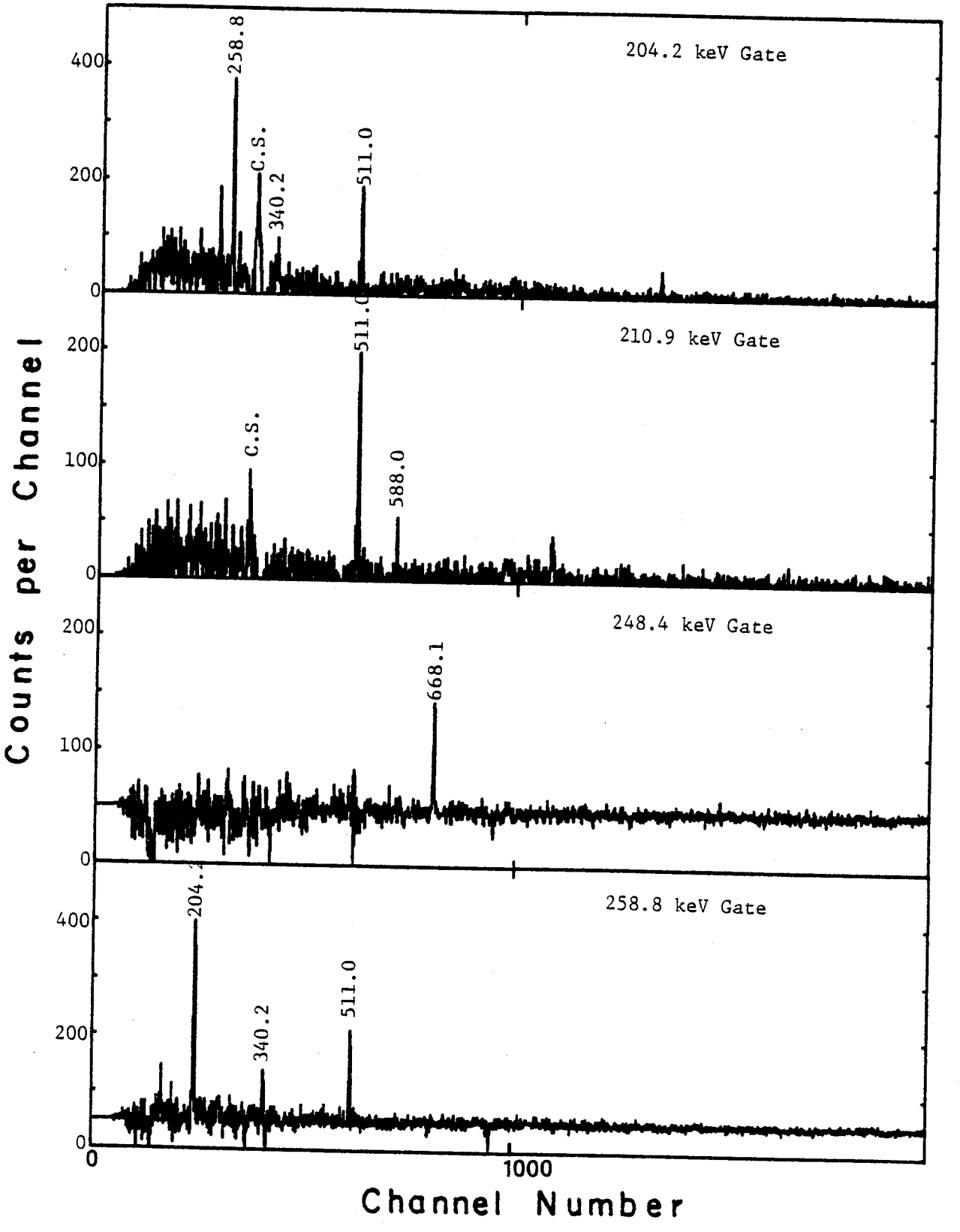
204.2 keV Gate
258.8
C.S.
340.2
511.0
210.9 keV Gate
511.0
C.S.
588.0
248.4 keV Gate
668.1
258.8 keV Gate
204.4
340.2
511.0
Counts per Channel
Channel Number
0
1000
400
200
100

Figure A.

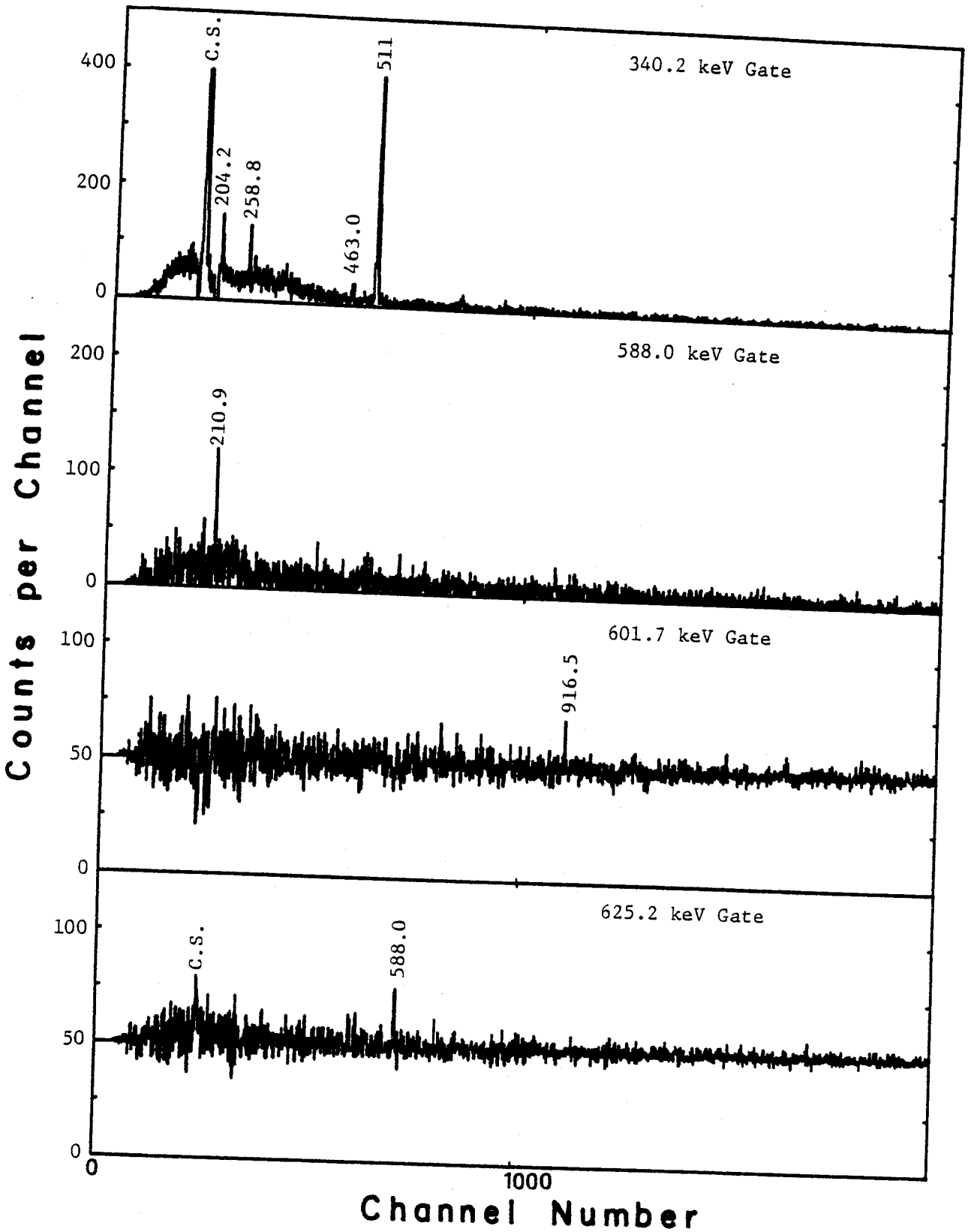

Figure A. (cont'd.).

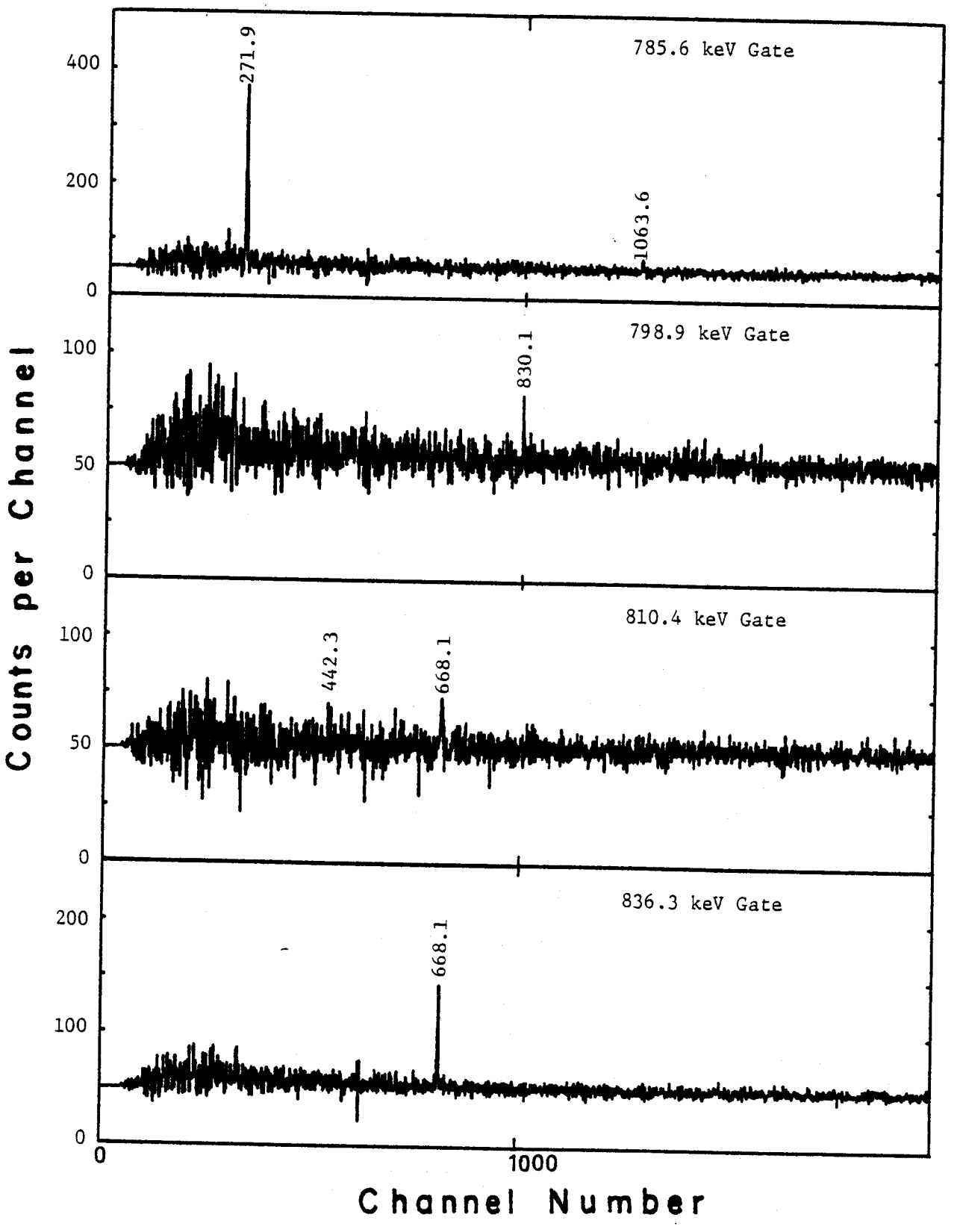

Figure A. (cont'd.).

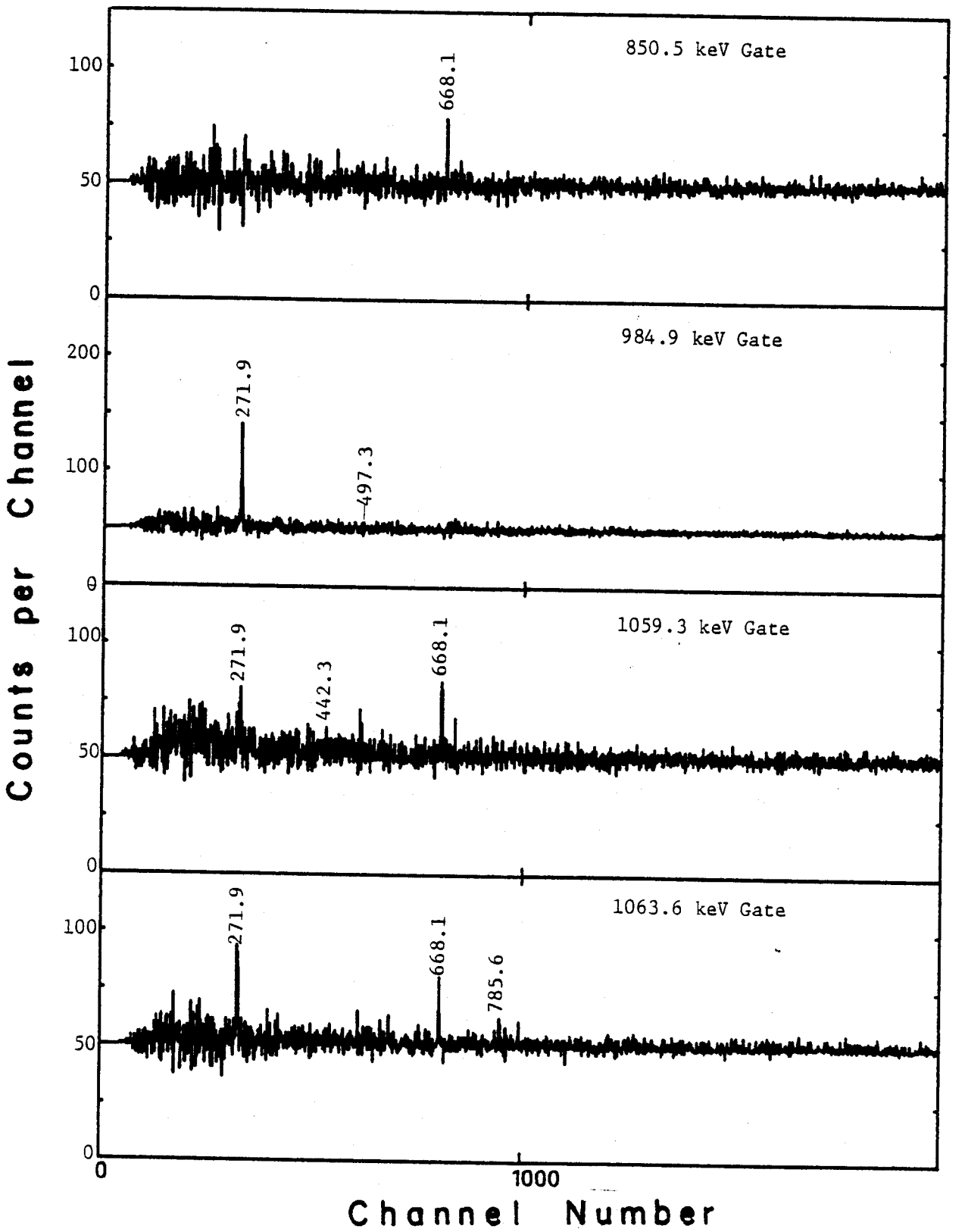

Figure A. (cont'd.).

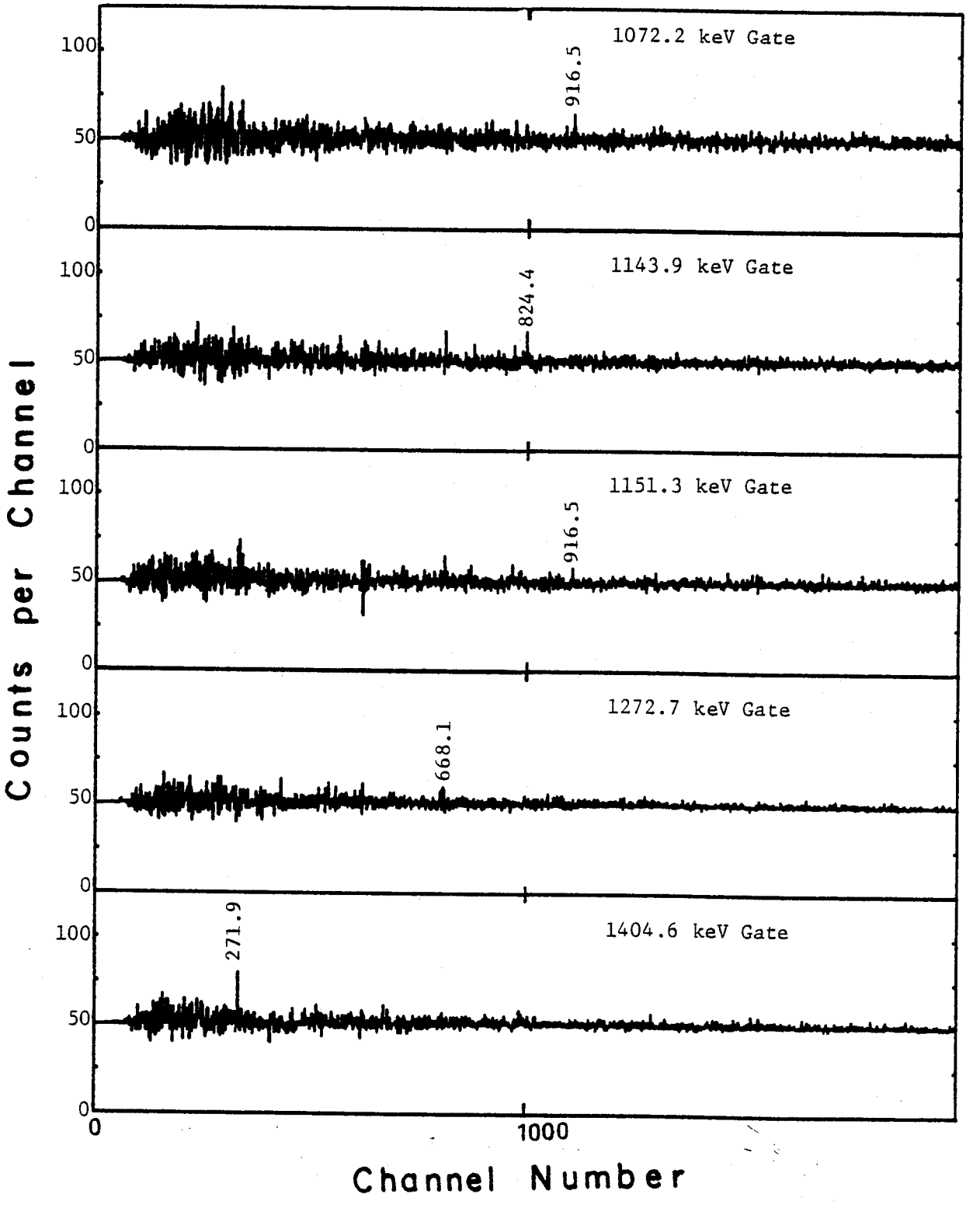

Figure A. (cont'd.).

APPENDIX B

Angular Distribution Plots of ^{143}Eu Transitions.

Figure B. Angular distribution plots of ^{143}Eu transitions obtained from $(p,2n\gamma)$ reaction. The data were taken in the 90-180° quadrant.

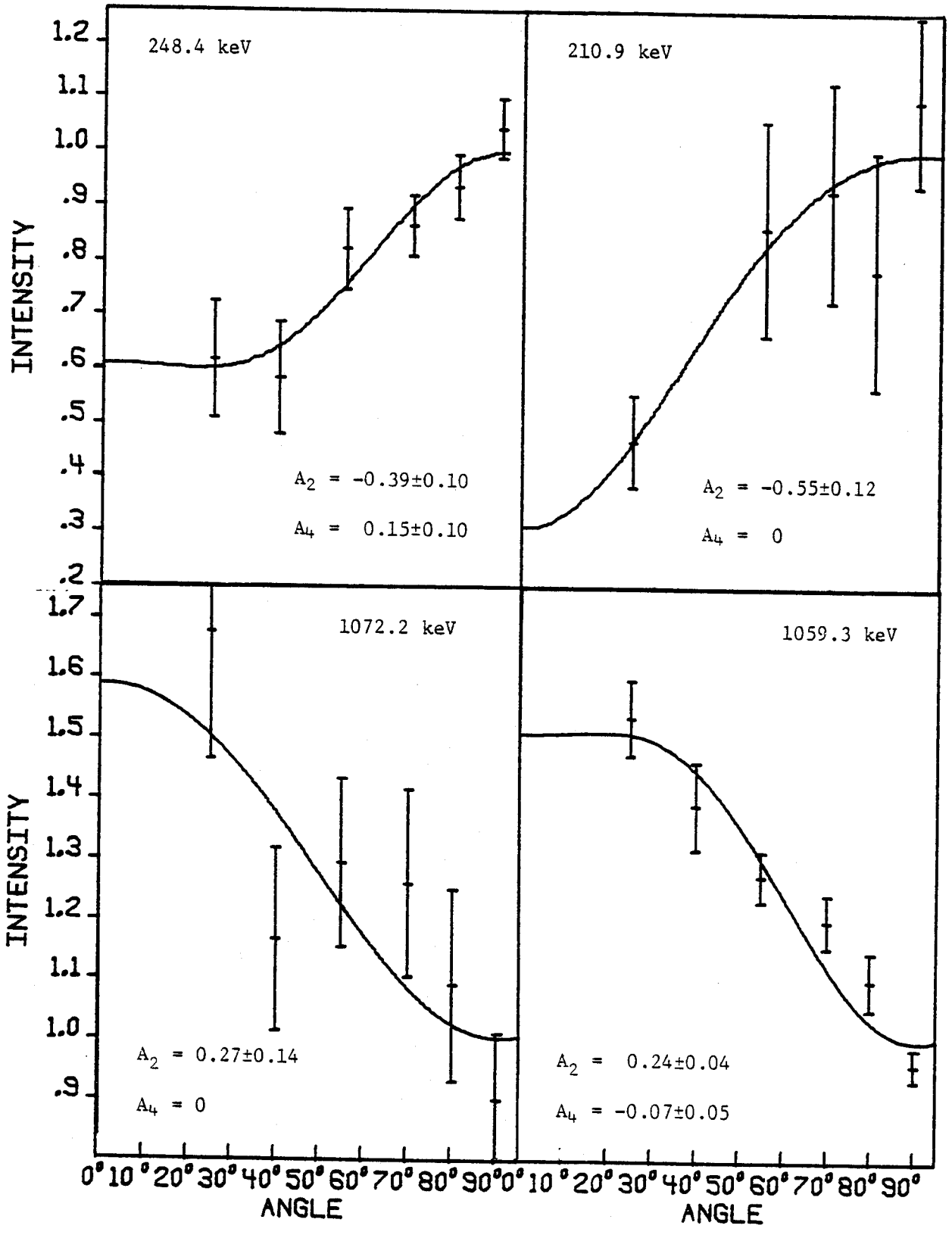
248.4 keV
A_2 = -0.39±0.10
A_4 = 0.15±0.10
210.9 keV
A_2 = -0.55±0.12
A_4 = 0
1072.2 keV
A_2 = 0.27±0.14
A_4 = 0
1059.3 keV
A_2 = 0.24±0.04
A_4 = -0.07±0.05
INTENSITY
INTENSITY
1.2
1.1
1.0
.9
.8
.7
.6
.5
.4
.3
.2
1.7
1.6
1.5
1.4
1.3
1.2
1.1
1.0
.9
0° 10° 20° 30° 40° 50° 60° 70° 80° 90°
0° 10° 20° 30° 40° 50° 60° 70° 80° 90°
ANGLE
ANGLE

Figure B.

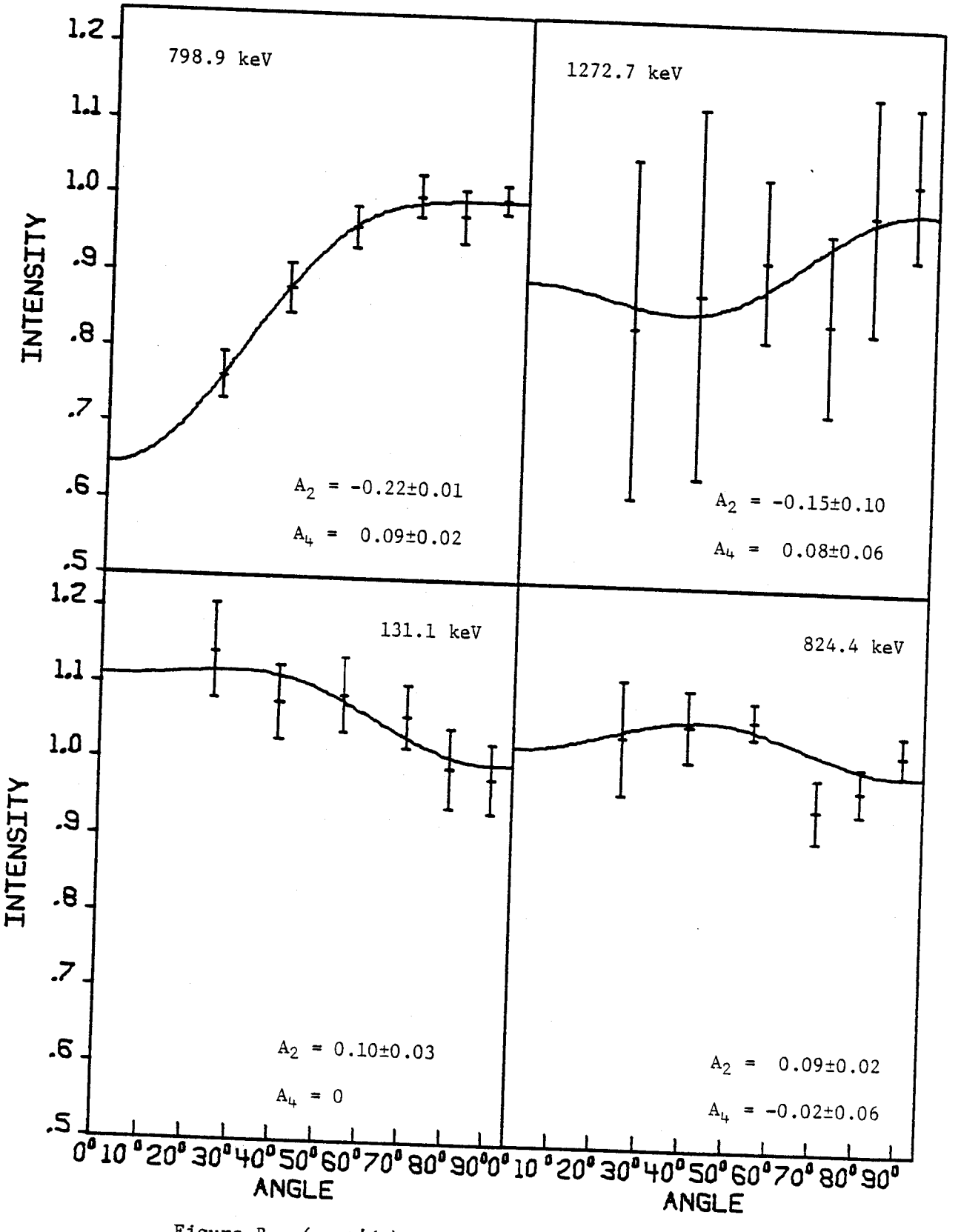

Figure B. (cont'd.).

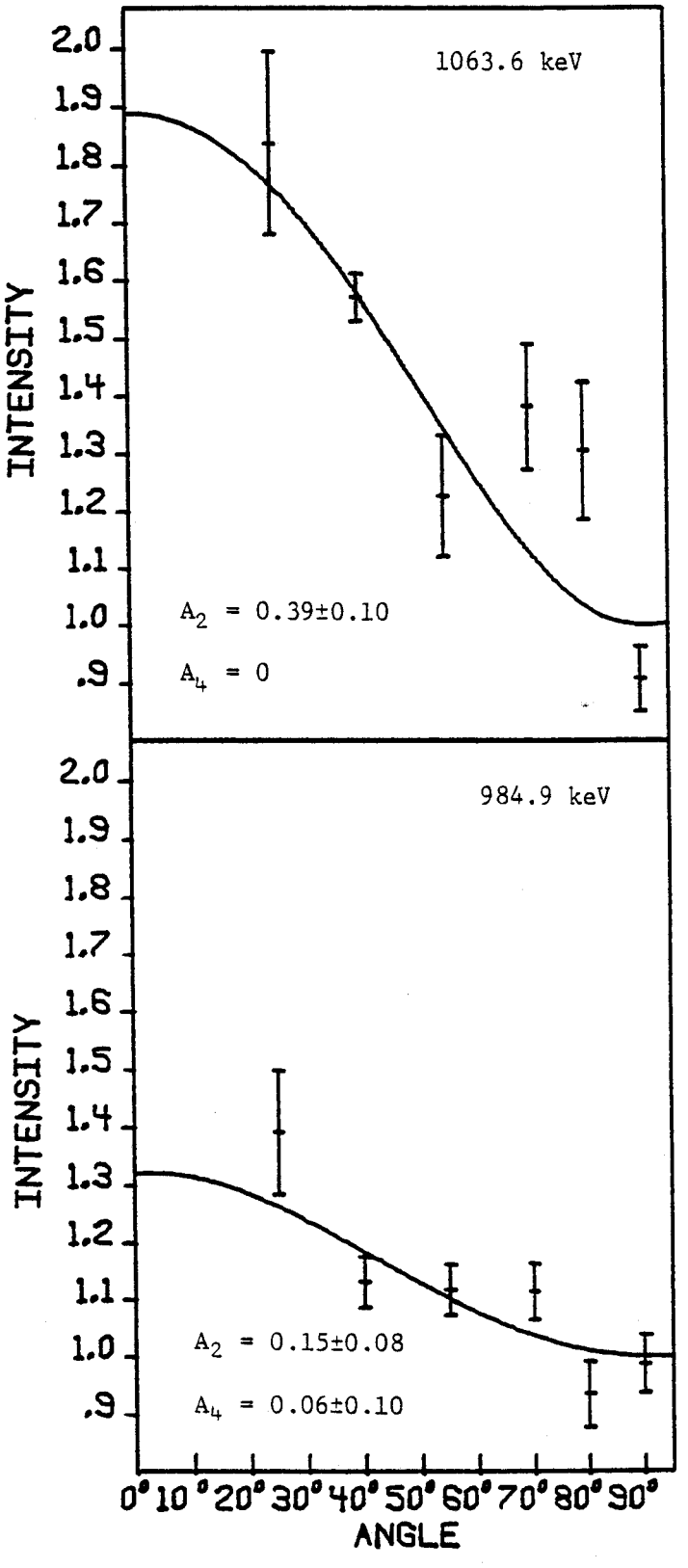

Figure B. (cont'd.).

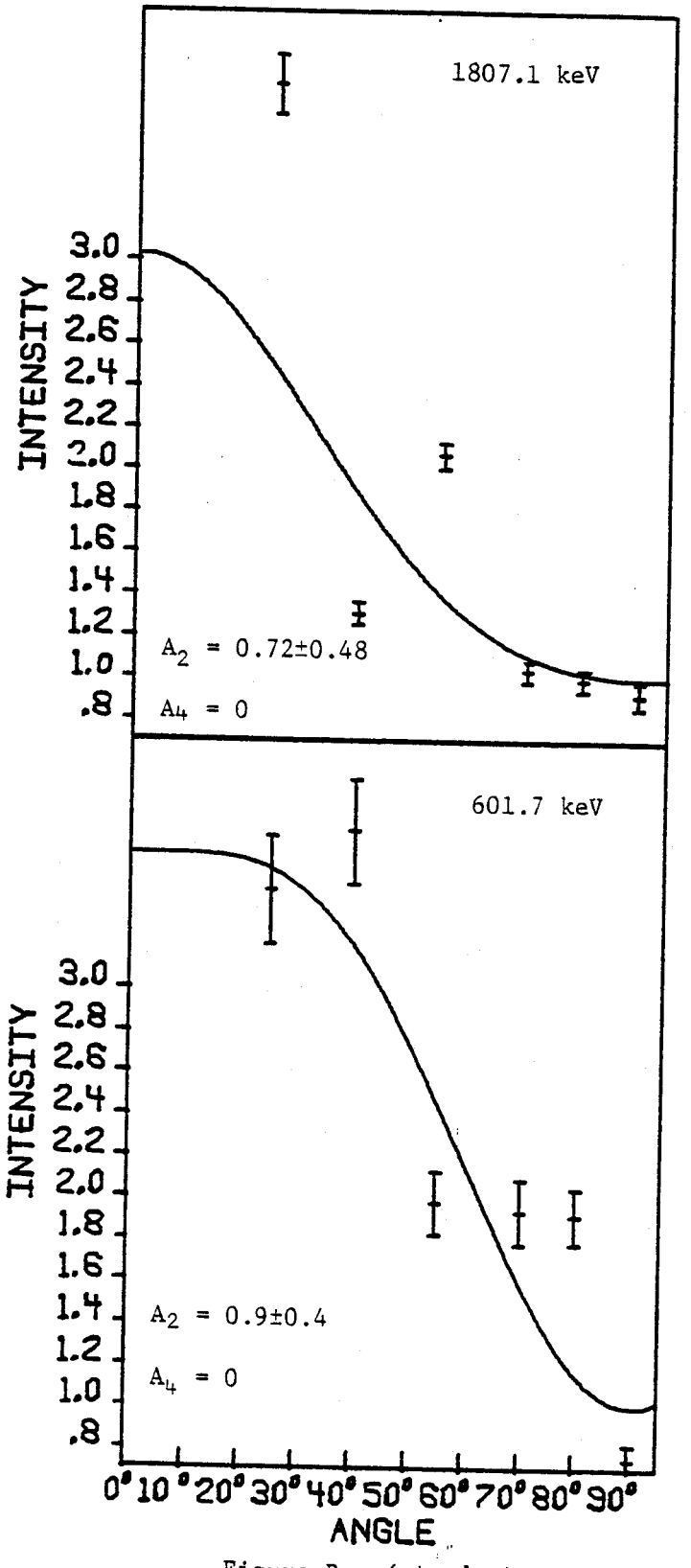

Figure B. (cont'd.).

APPENDIX C

Gated Coincidence Spectra of Transitions in ^{141}Pm from (p,2$n\gamma$) Reaction.

Figure C. Integral coincidence and gated spectra of transitions obtained from (p,2$n\gamma$) reaction. The data were taken in the 90-180° quadrant.

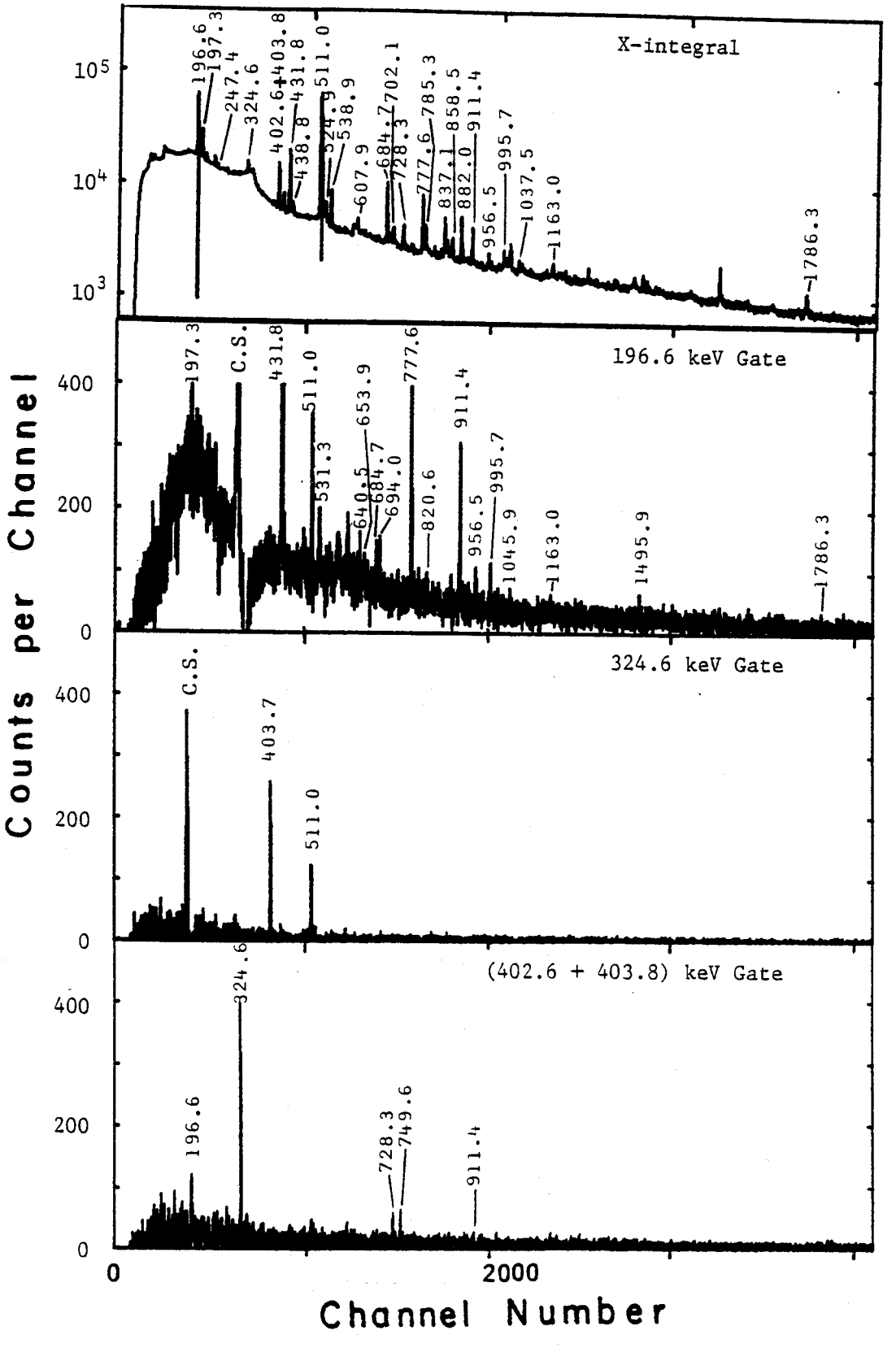
X-integral
196.6
197.3
247.4
324.6
402.6+403.8
431.8
511.0
538.9
607.9
684.7
702.1
728.3
777.6
785.3
837.1
858.5
882.0
911.4
956.5
995.7
1037.5
1163.0
1786.3
196.6 keV Gate
197.3
C.S.
431.8
511.0
531.3
640.5
653.9
684.7
694.0
777.6
820.6
911.4
956.5
995.7
1045.9
1163.0
1495.9
1786.3
324.6 keV Gate
C.S.
403.7
511.0
(402.6 + 403.8) keV Gate
324.6
196.6
728.3
749.6
911.4
Counts per Channel
Channel Number
0
2000
200
400
10^3
10^4
10^5

Figure C.

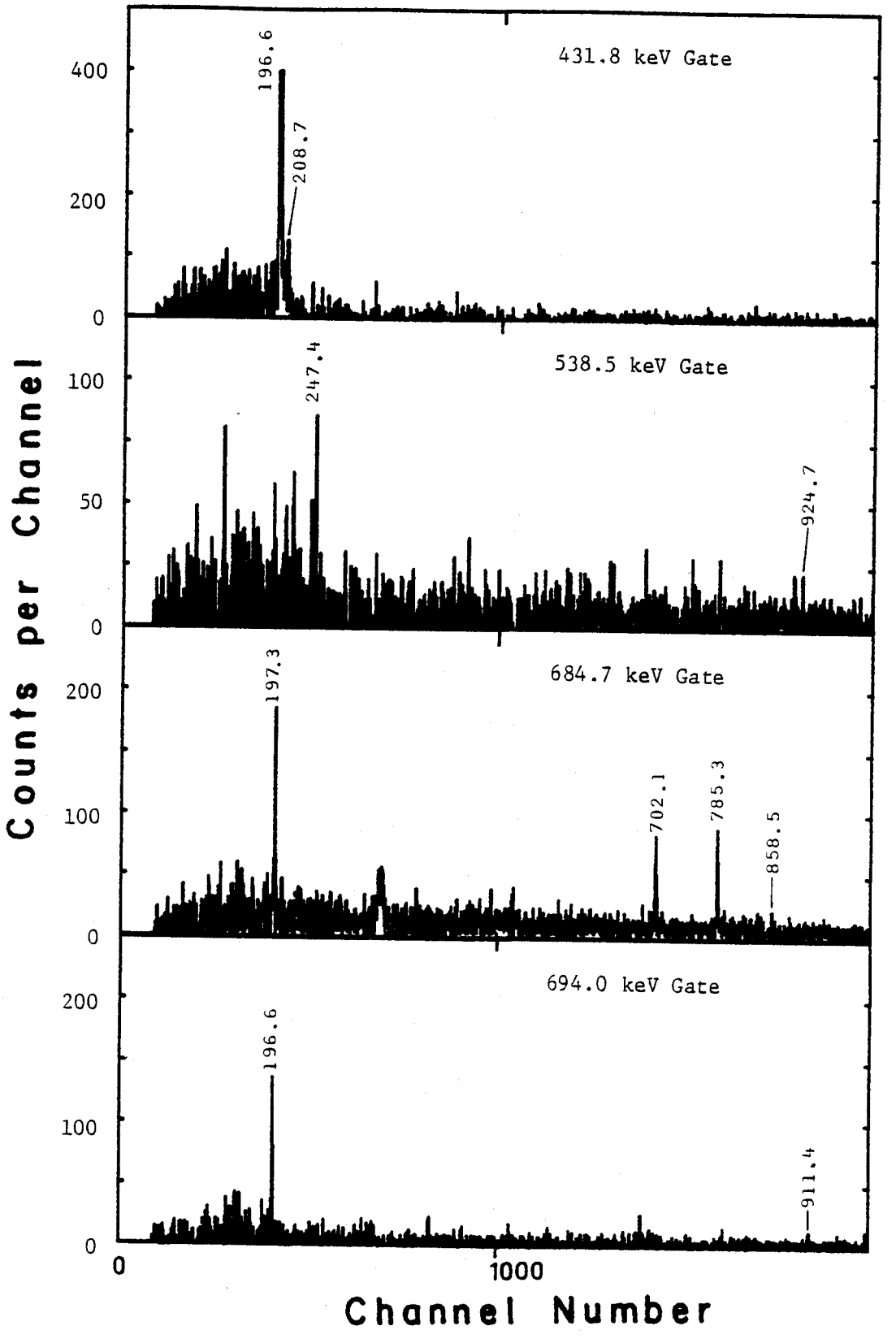

Figure C. (cont'd.).

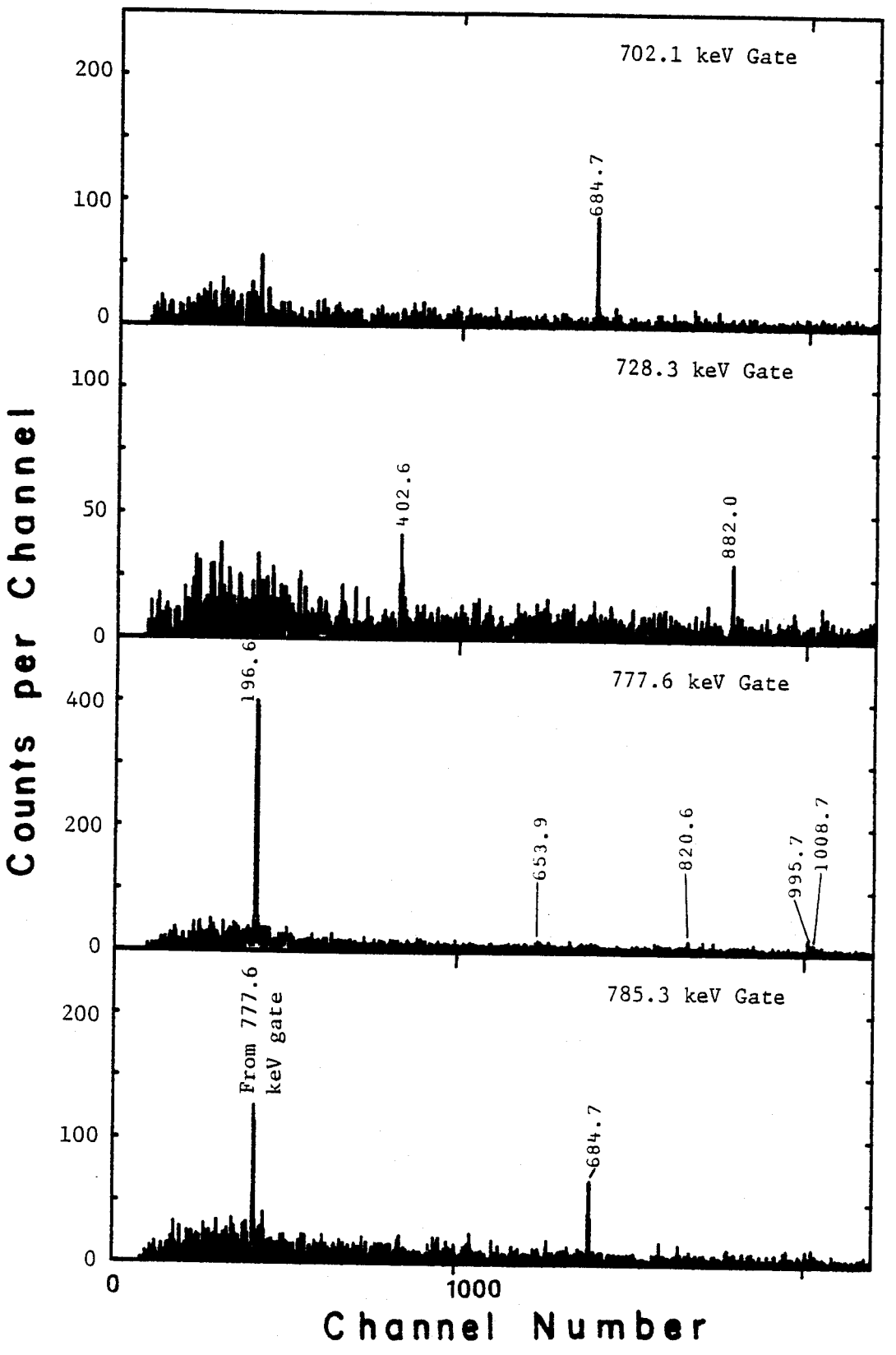

Figure C. (cont'd.).

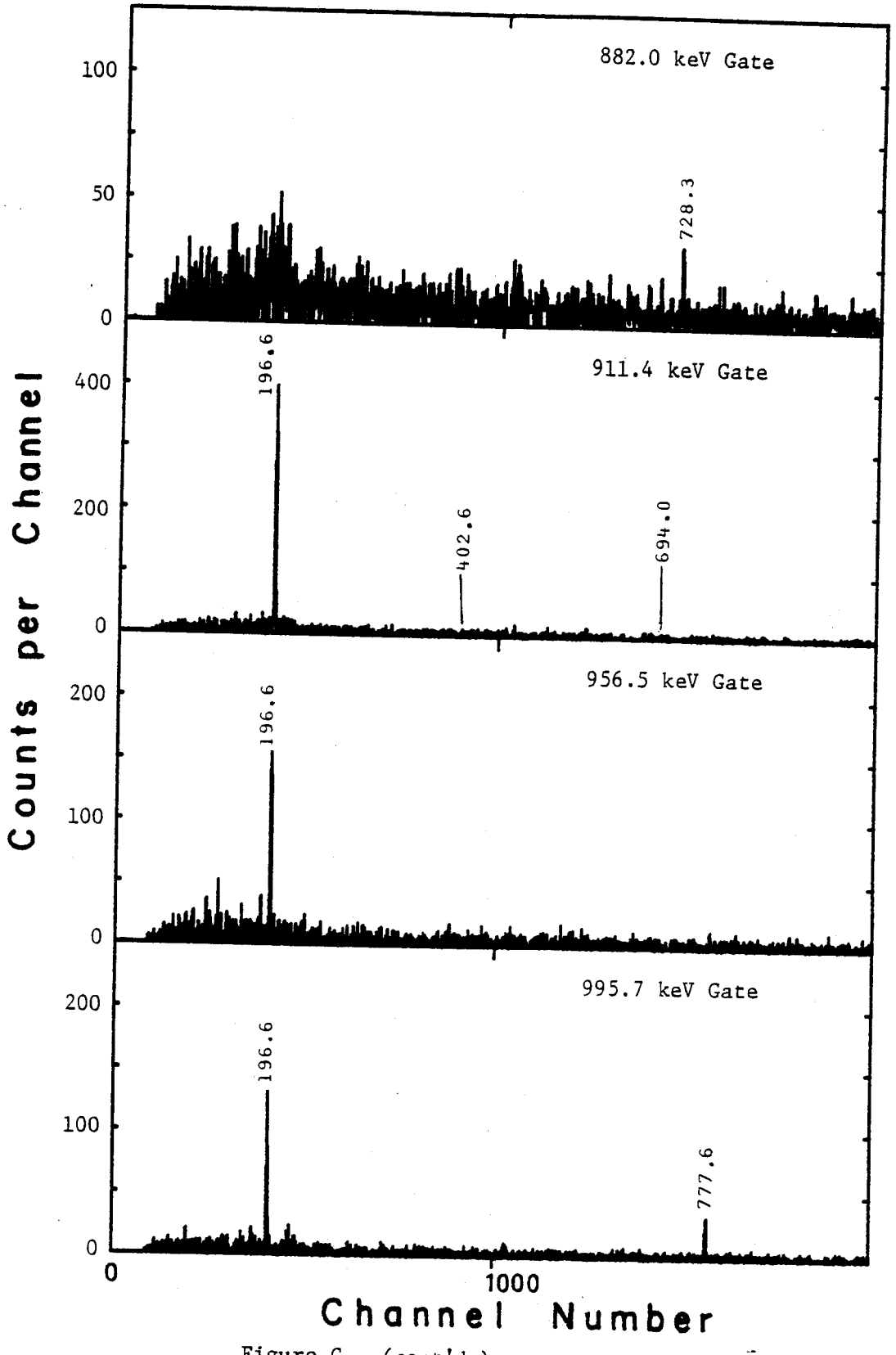

Figure C. (cont'd.).

APPENDIX D

Angular Distribution Plots of ^{141}Pm Transitions from (p,2$n\gamma$) Reaction.

Figure D. Angular distribution plots of ^{141}Pm transitions obtained from (p,2$n\gamma$) reaction. The data were taken in the 90-180° quadrant.

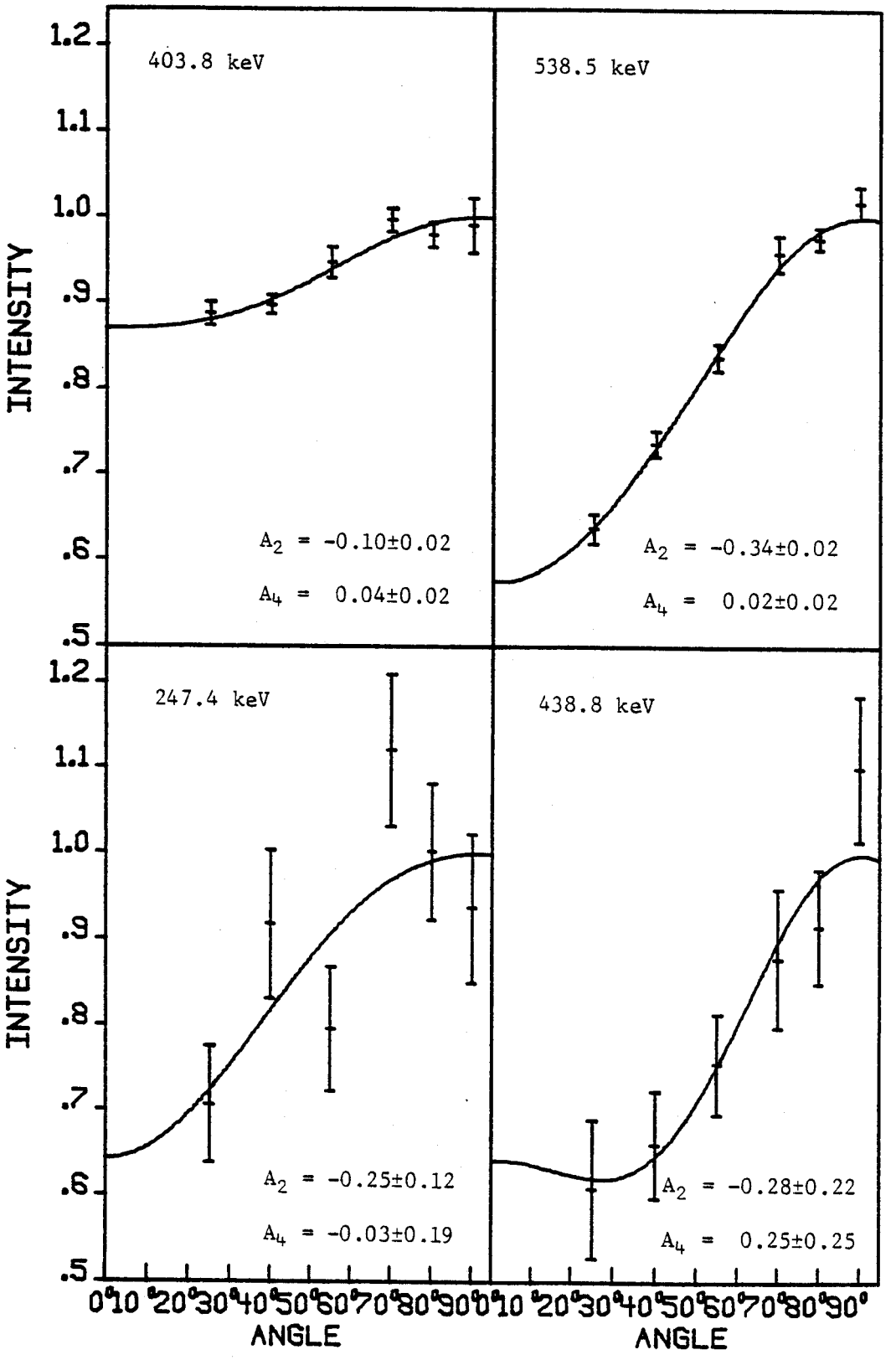
403.8 keV
538.5 keV
247.4 keV
438.8 keV
A2 = -0.10±0.02
A4 = 0.04±0.02
A2 = -0.34±0.02
A4 = 0.02±0.02
A2 = -0.25±0.12
A4 = -0.03±0.19
A2 = -0.28±0.22
A4 = 0.25±0.25
INTENSITY
INTENSITY
1.2
1.1
1.0
.9
.8
.7
.6
.5
0°10°20°30°40°50°60°70°80°90°
0°10°20°30°40°50°60°70°80°90°
ANGLE
ANGLE

Figure D.

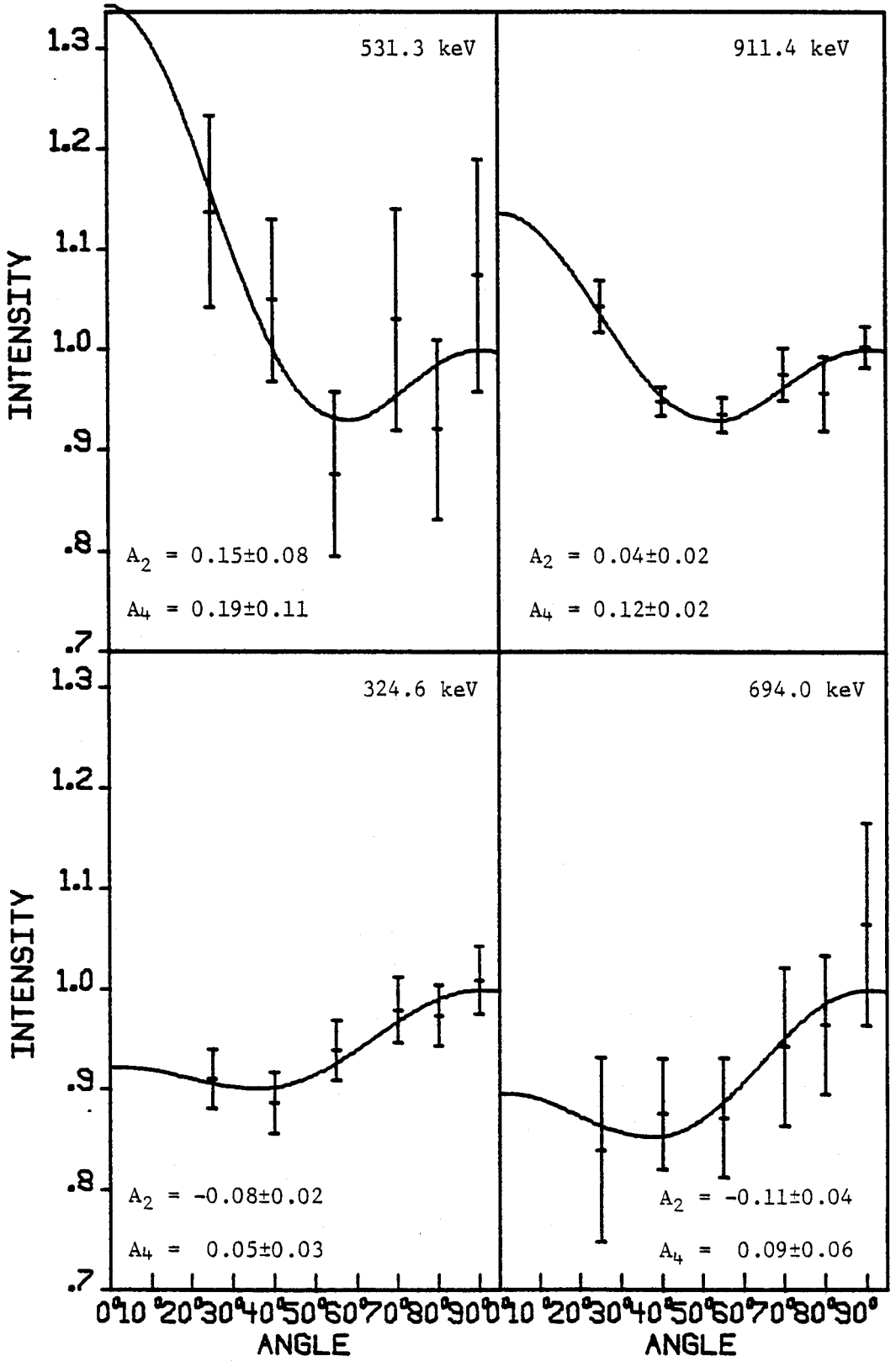

Figure D. (cont'd.).

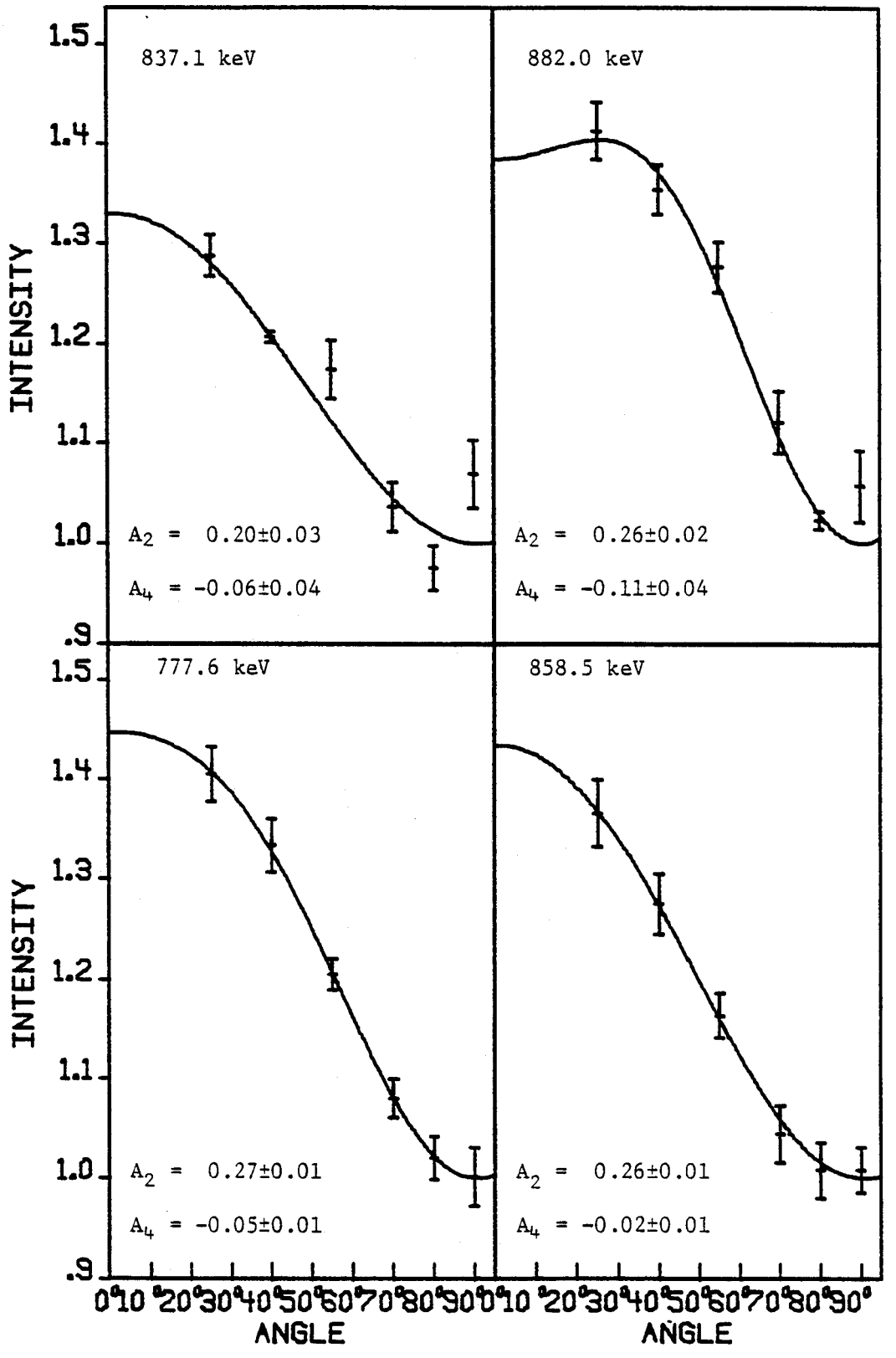

Figure D. (cont'd.).

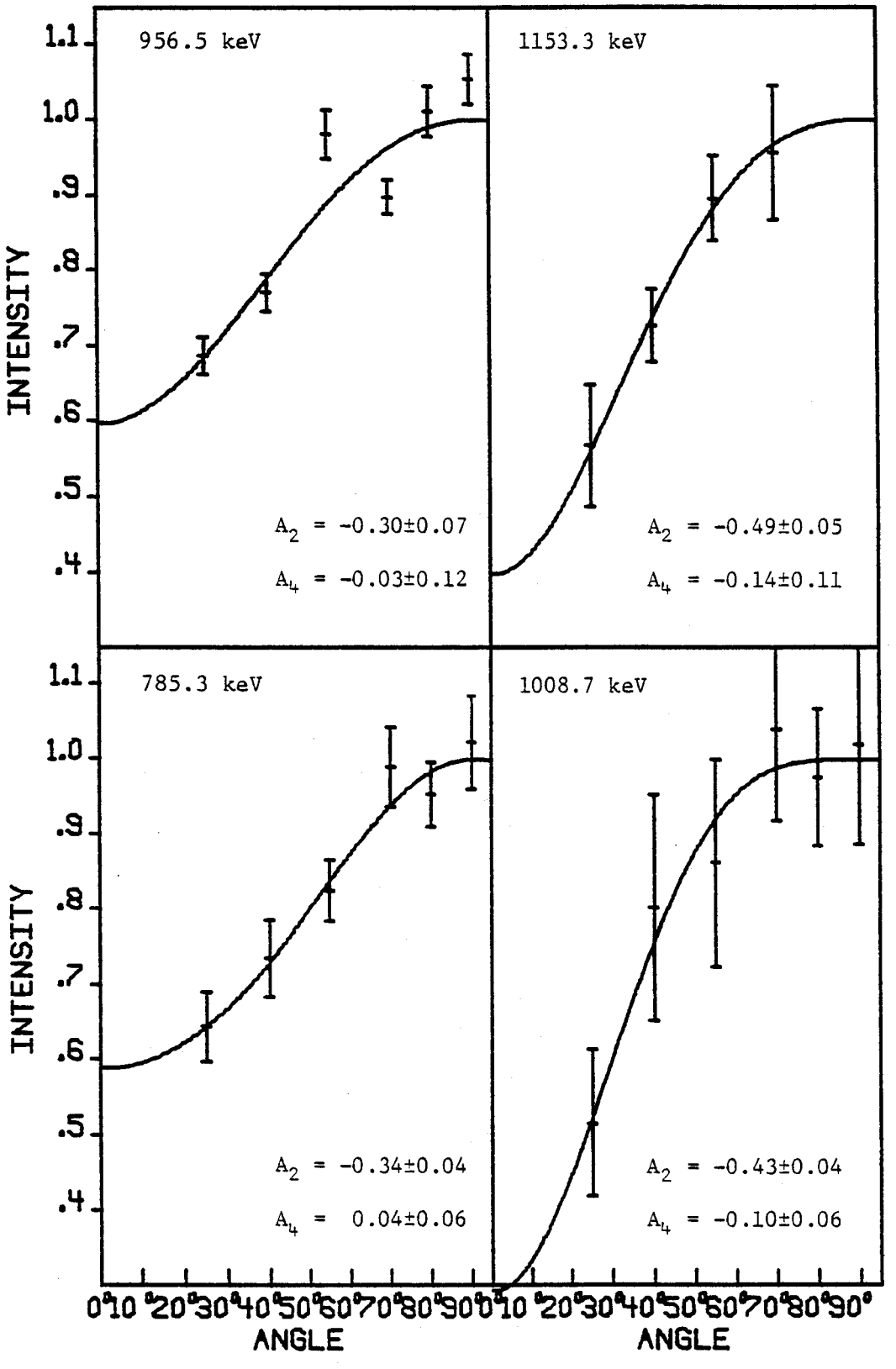

Figure D. (cont'd.).

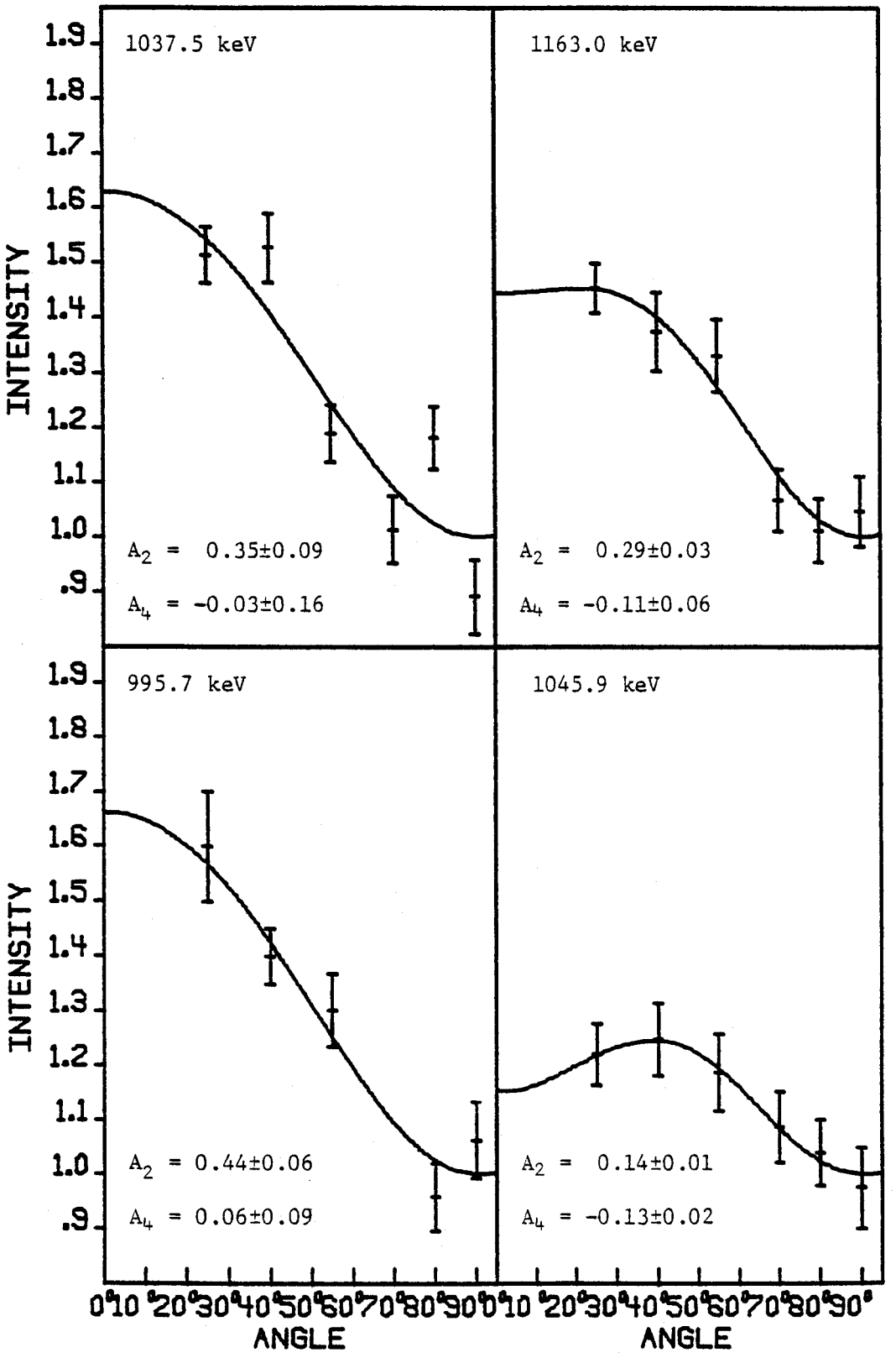

Figure D. (cont'd.).

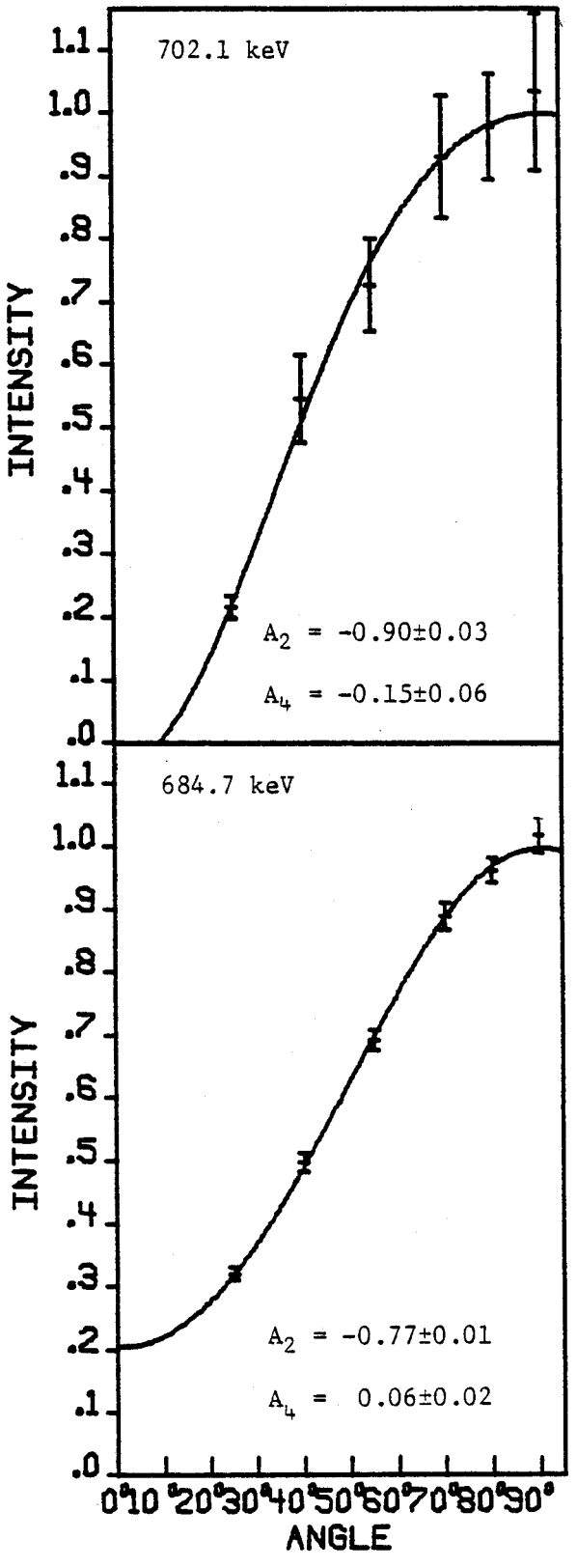

Figure D. (cont'd.).

APPENDIX E

Gated Coincidence Spectra of Transitions in ^{141}Pm from (α,4nγ) Reaction.

Figure E. Integral coincidence and gated spectra of transitions in ^{141}Pm from (α,4nγ) reaction. Background subtraction using the adjacent continuum has been included. The spectra are arranged according to increasing energy.

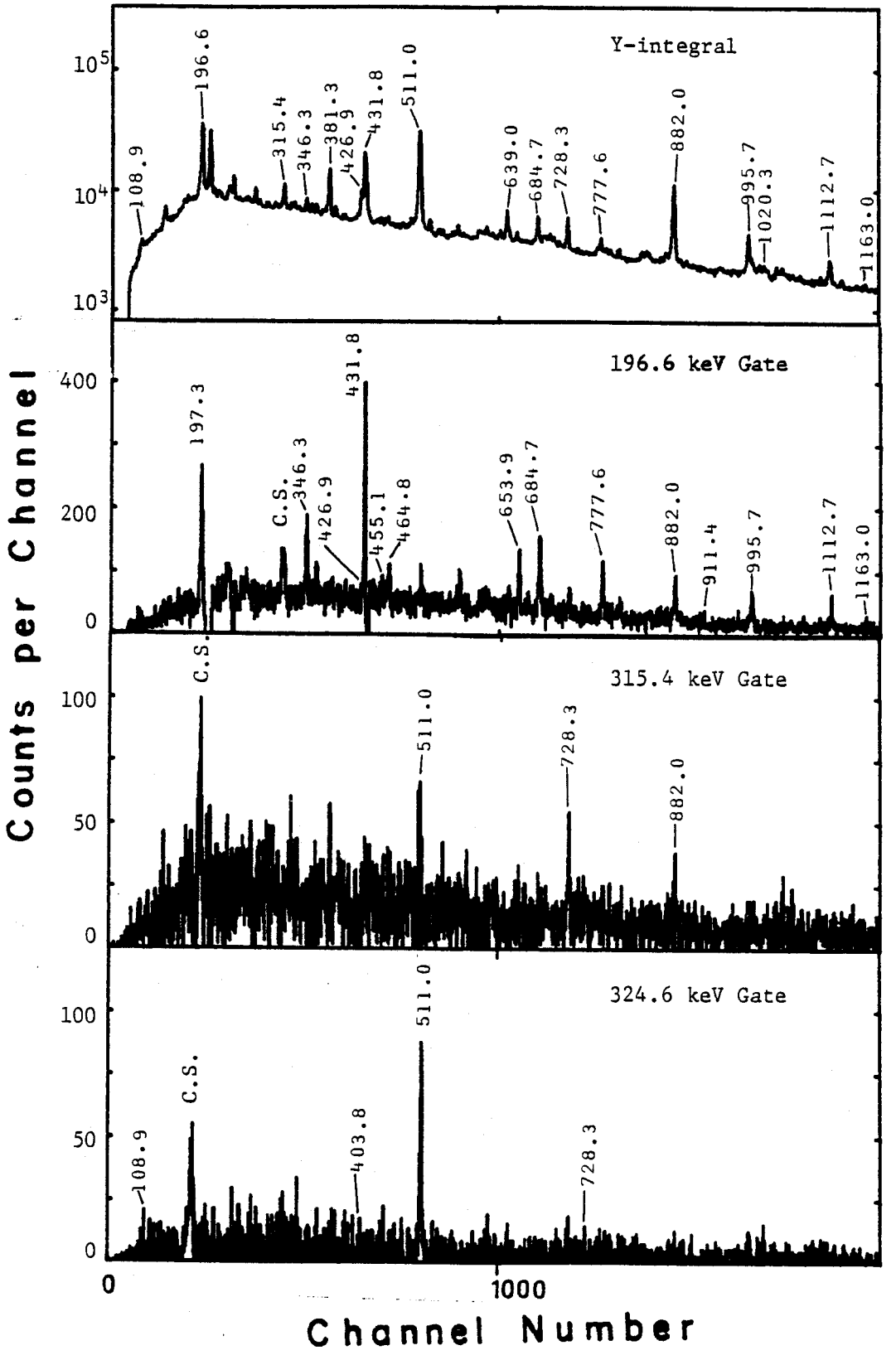
Y-integral
196.6 keV Gate
315.4 keV Gate
324.6 keV Gate
Counts per Channel
Channel Number
C.S.
108.9
196.6
315.4
346.3
381.3
426.9
431.8
511.0
639.0
684.7
728.3
777.6
882.0
995.7
1020.3
1112.7
1163.0
197.3
455.1
464.8
653.9
911.4
403.8

Figure E.

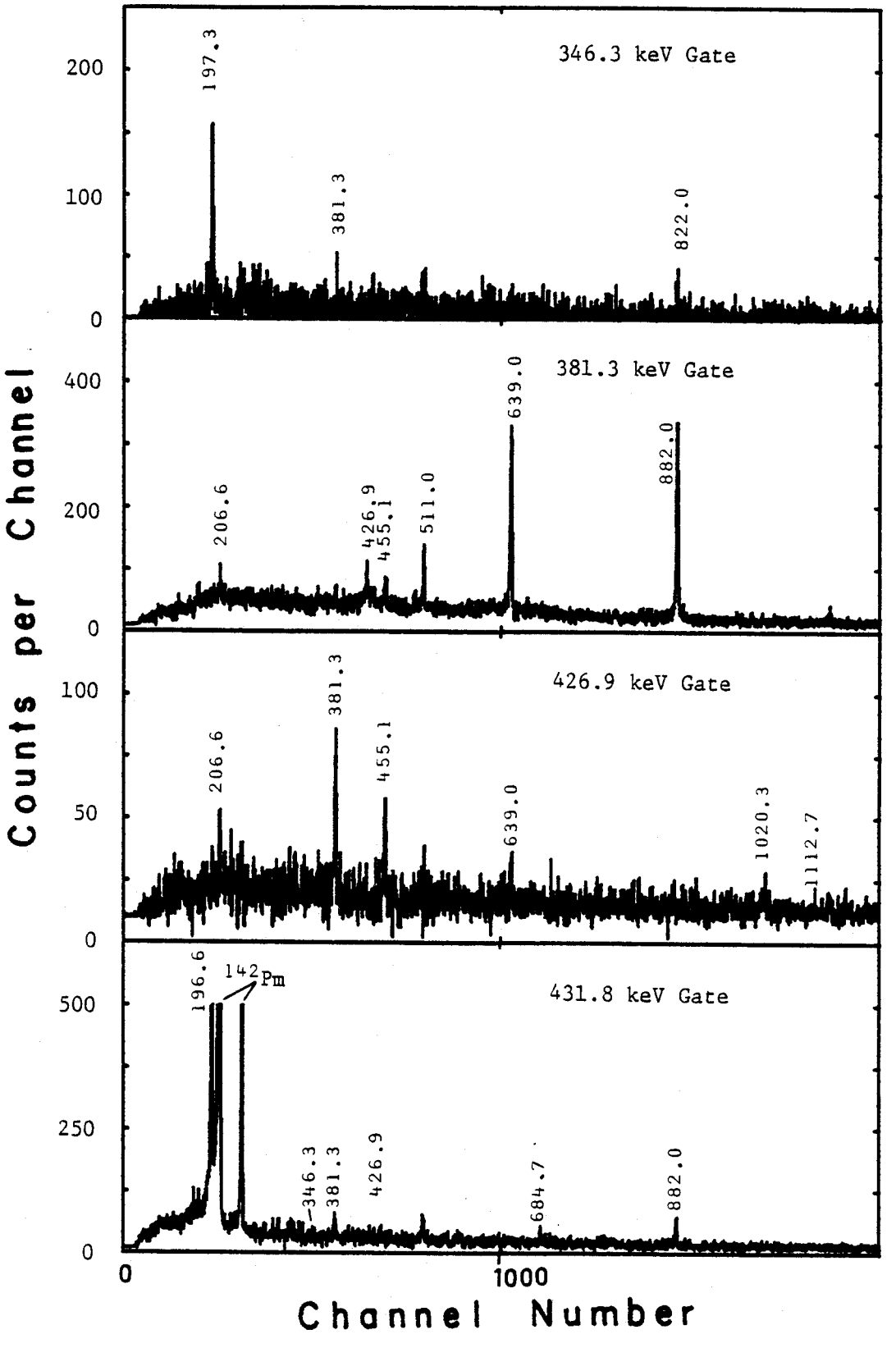

Figure E. (cont'd.).

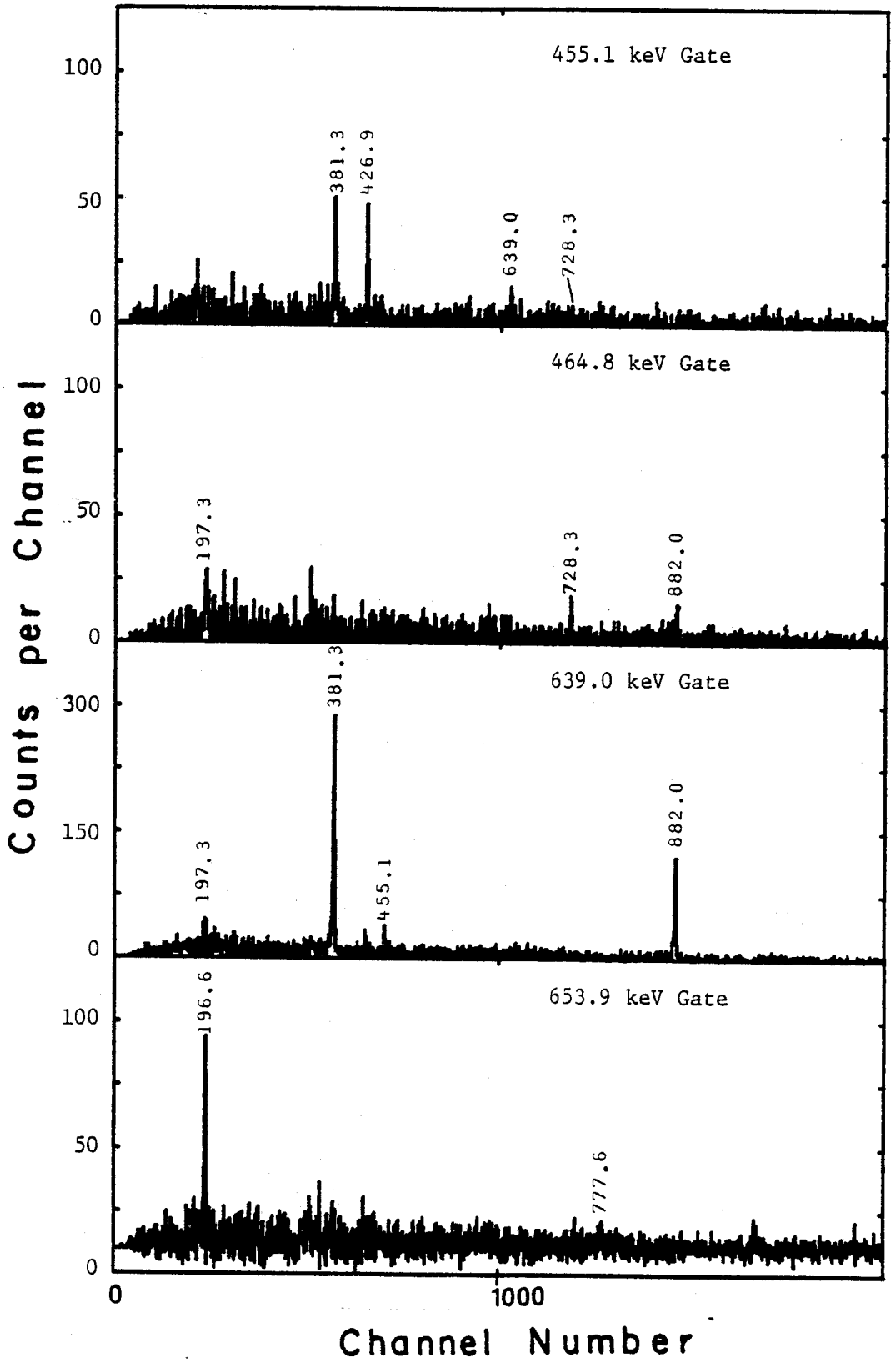

Figure E. (cont'd.).

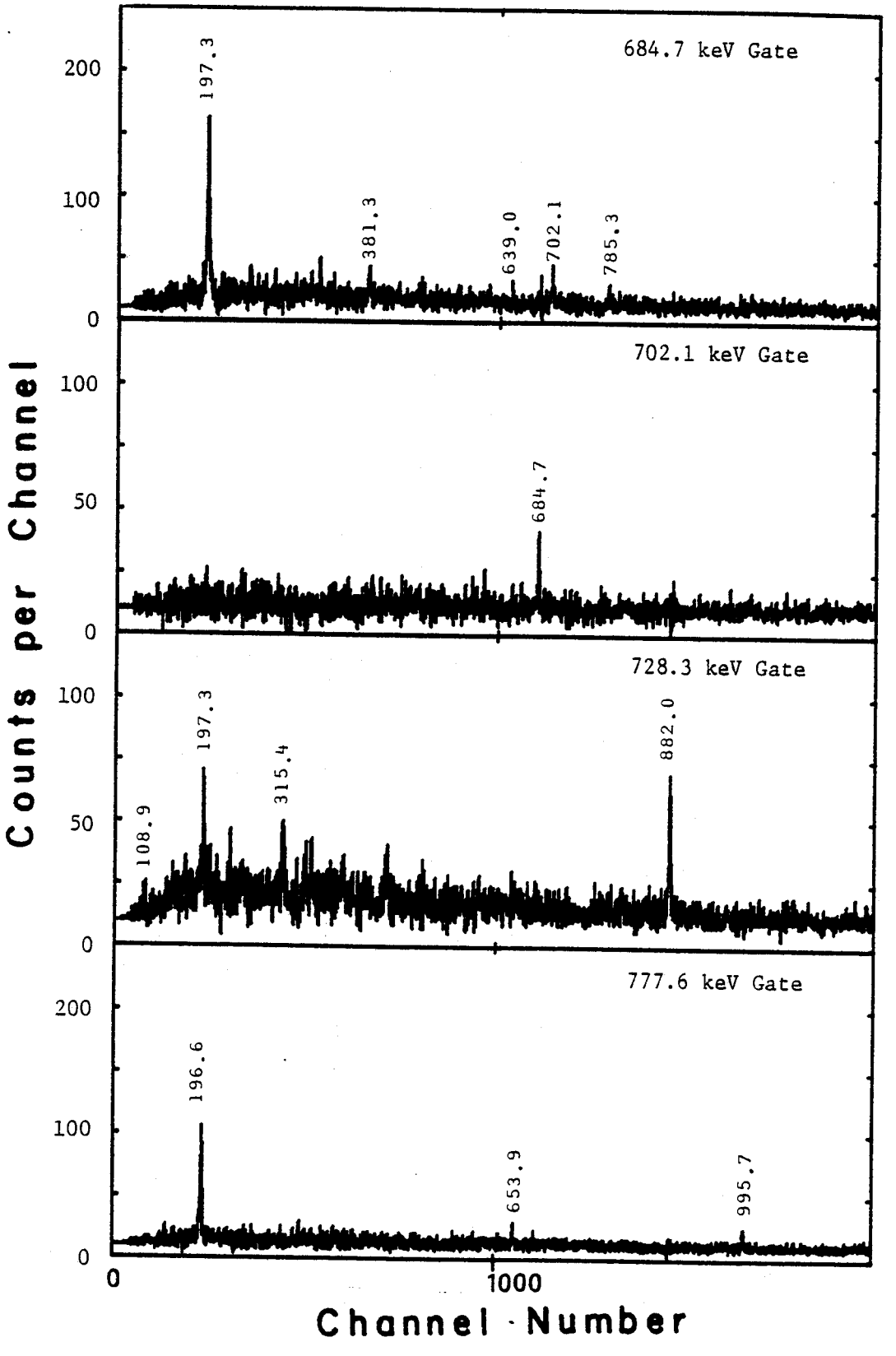

Figure E. (cont'd.).

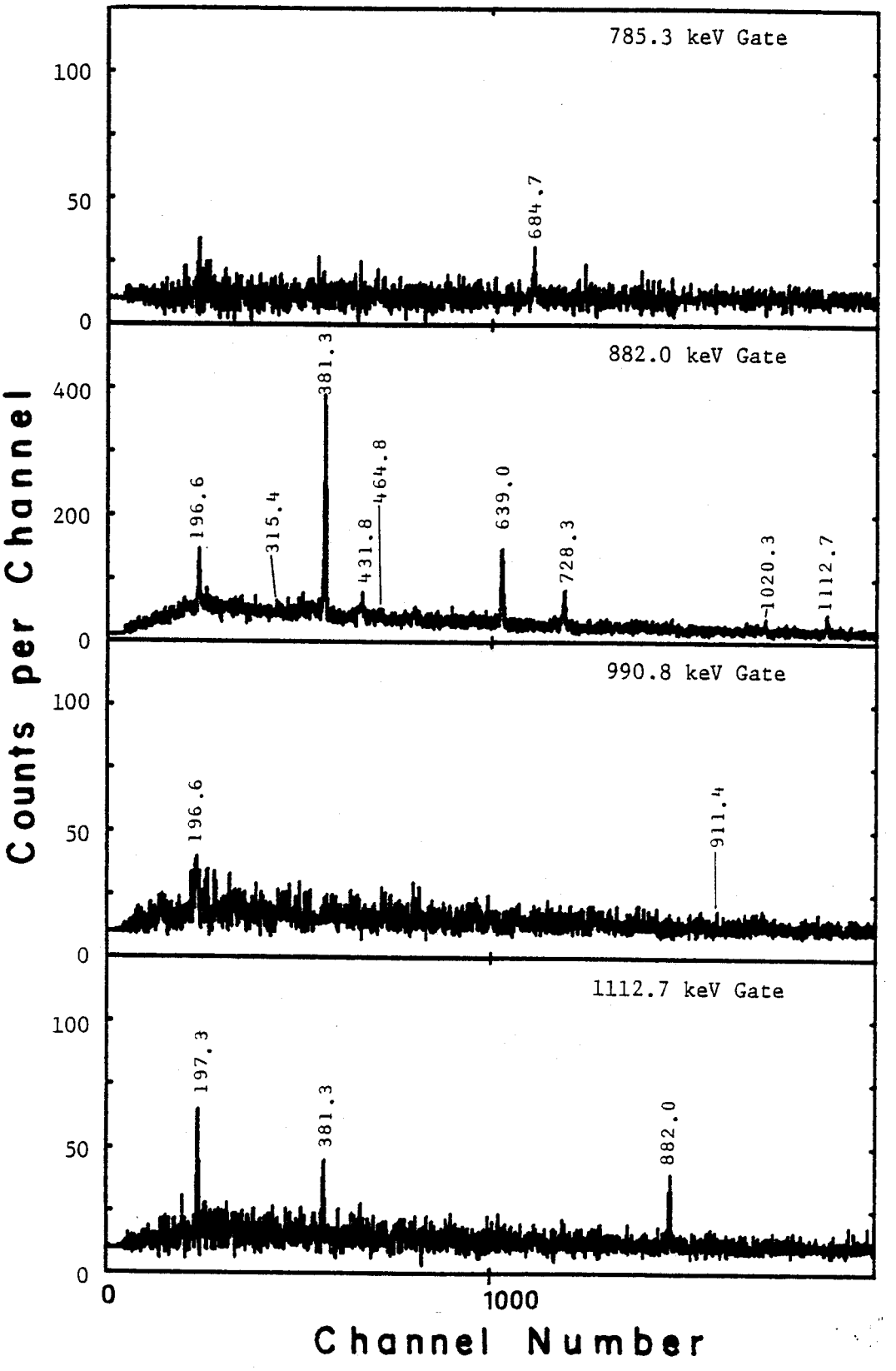

Figure E. (cont'd.).

APPENDIX F

Angular Distribution Plots of ^{141}Pm Transitions from (α,4nγ) Reaction.

Figure F. Angular distribution plots of ^{141}Pm transitions obtained from (α,4nγ) reaction. The data were taken in the 90-180° quadrant.

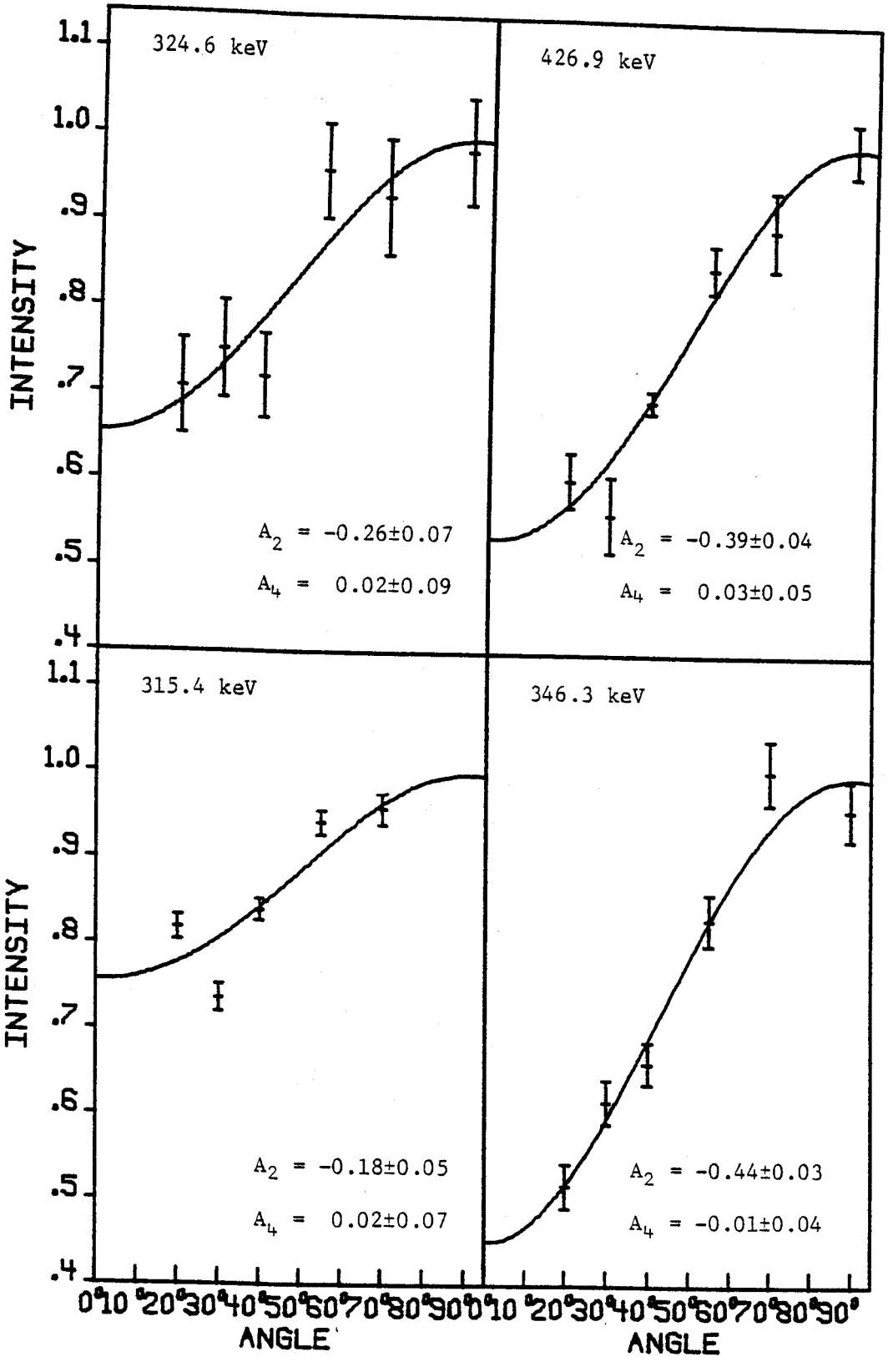
324.6 keV
426.9 keV
315.4 keV
346.3 keV
INTENSITY
INTENSITY
1.1
1.0
.9
.8
.7
.6
.5
.4
A_2 = -0.26±0.07
A_4 = 0.02±0.09
A_2 = -0.39±0.04
A_4 = 0.03±0.05
A_2 = -0.18±0.05
A_4 = 0.02±0.07
A_2 = -0.44±0.03
A_4 = -0.01±0.04
0°10°20°30°40°50°60°70°80°90°
0°10°20°30°40°50°60°70°80°90°
ANGLE
ANGLE

Figure F.

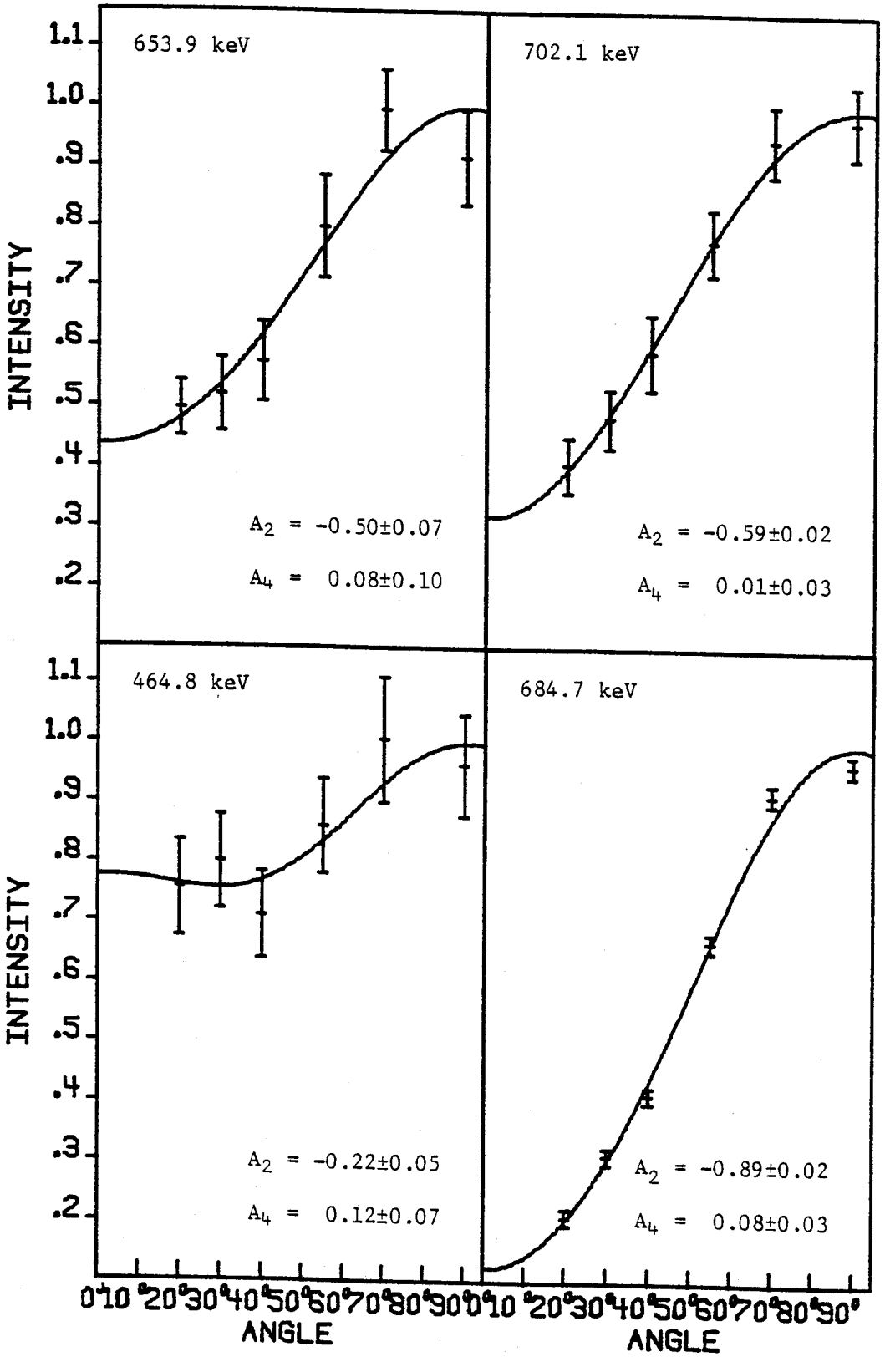

Figure F. (cont'd.).

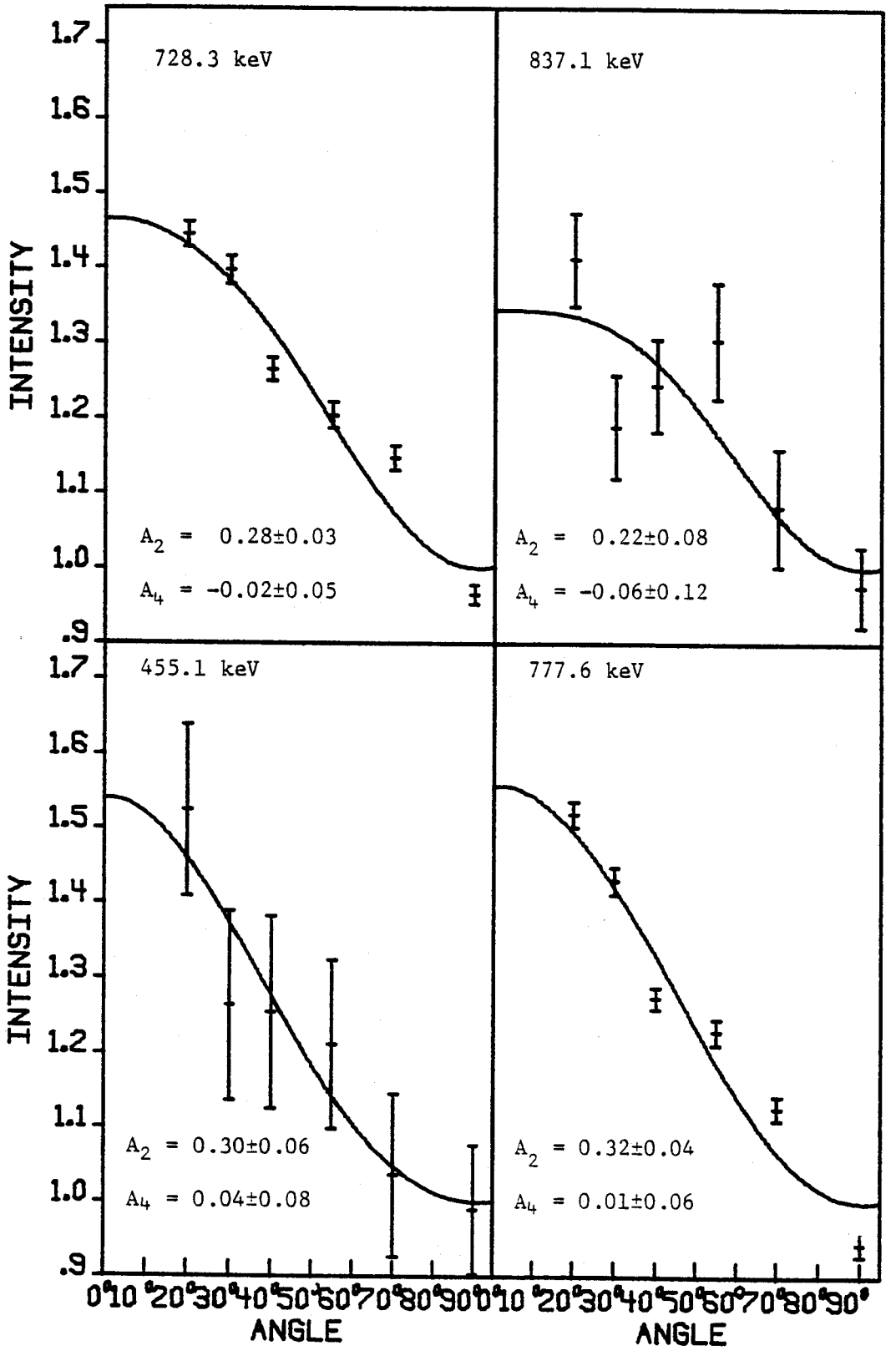

Figure F. (cont'd.).

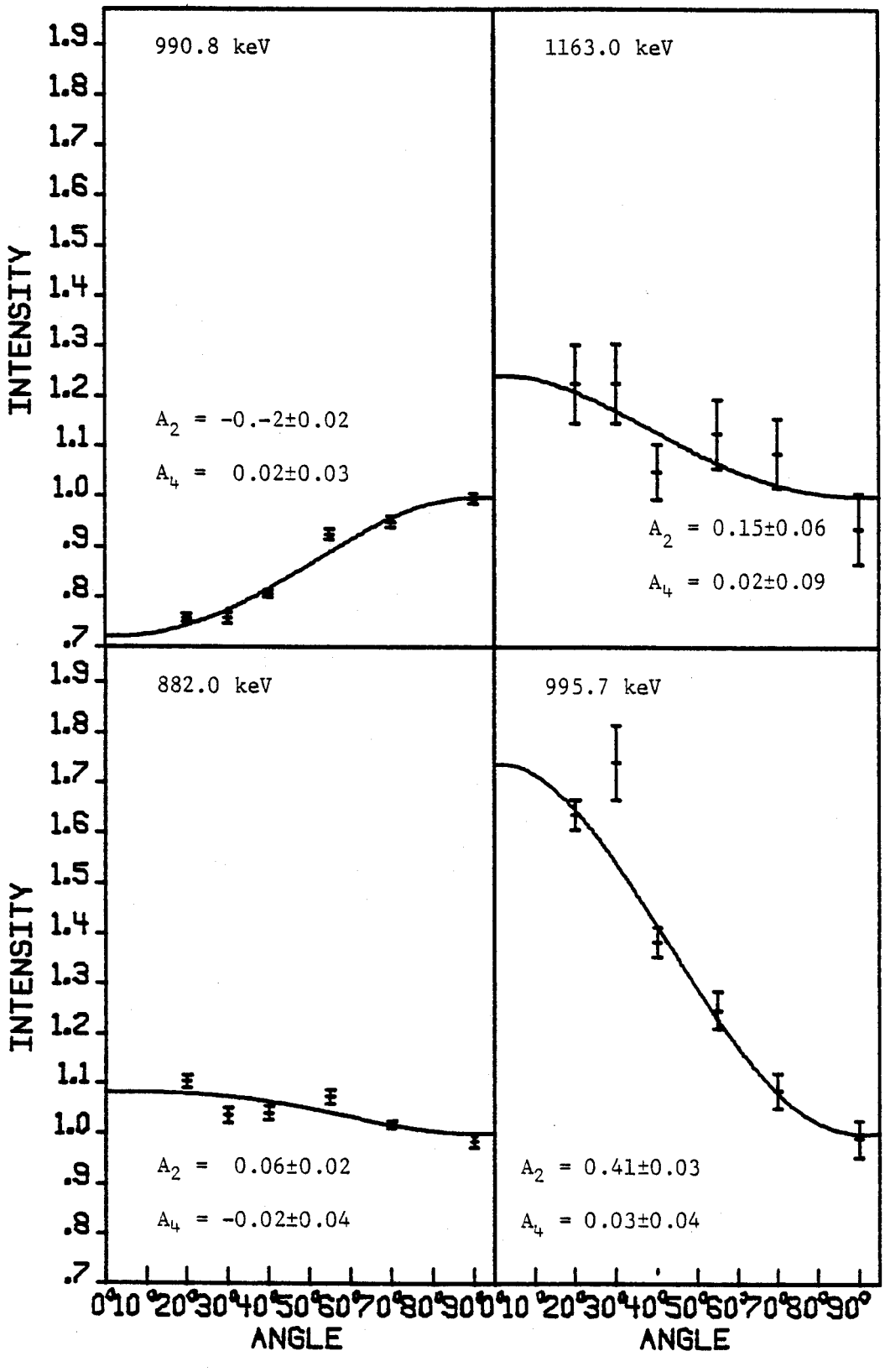

Figure F. (cont'd.).

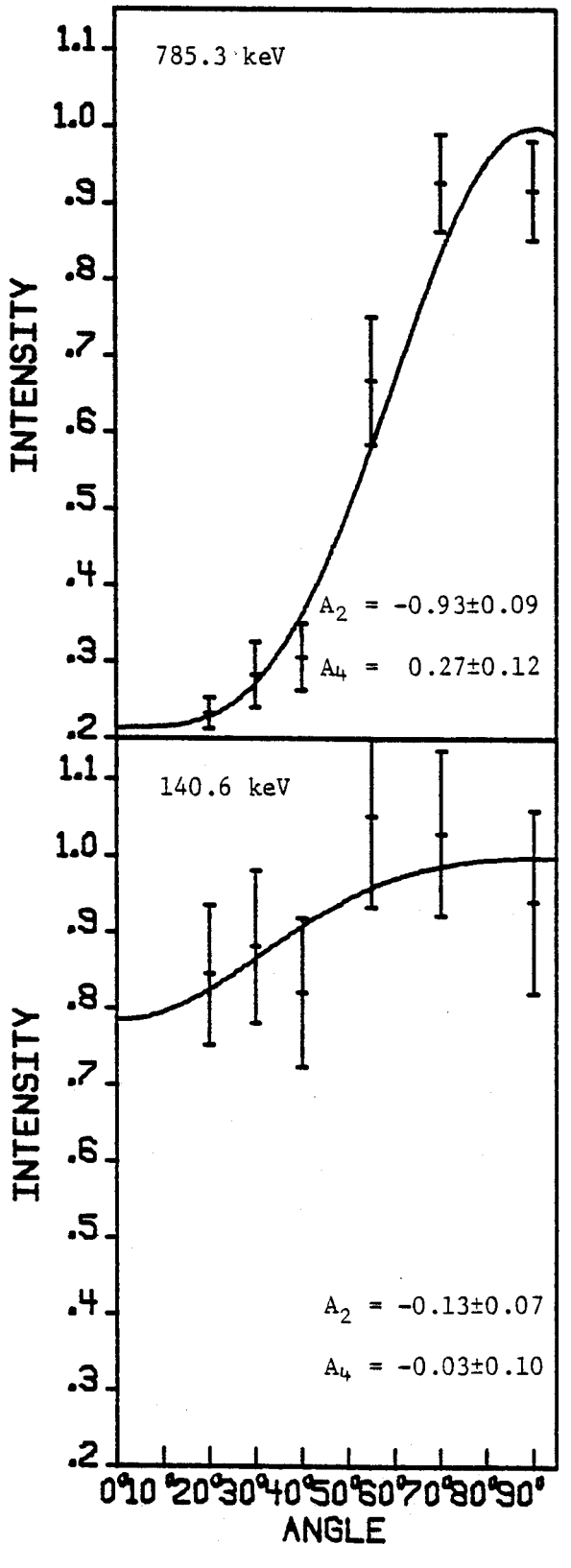

Figure F. (cont'd.).

APPENDIX G

Gated Coincidence Spectra of Transitions in ^{139}Pr from $(p,2n\gamma)$ Reaction.

Figure G. Integral coincidence and gated spectra of transitions in ^{139}Pr from $(p,2n\gamma)$ reaction. Background subtraction using the adjacent continuum has been included. The spectra are arranged according to increasing energy.

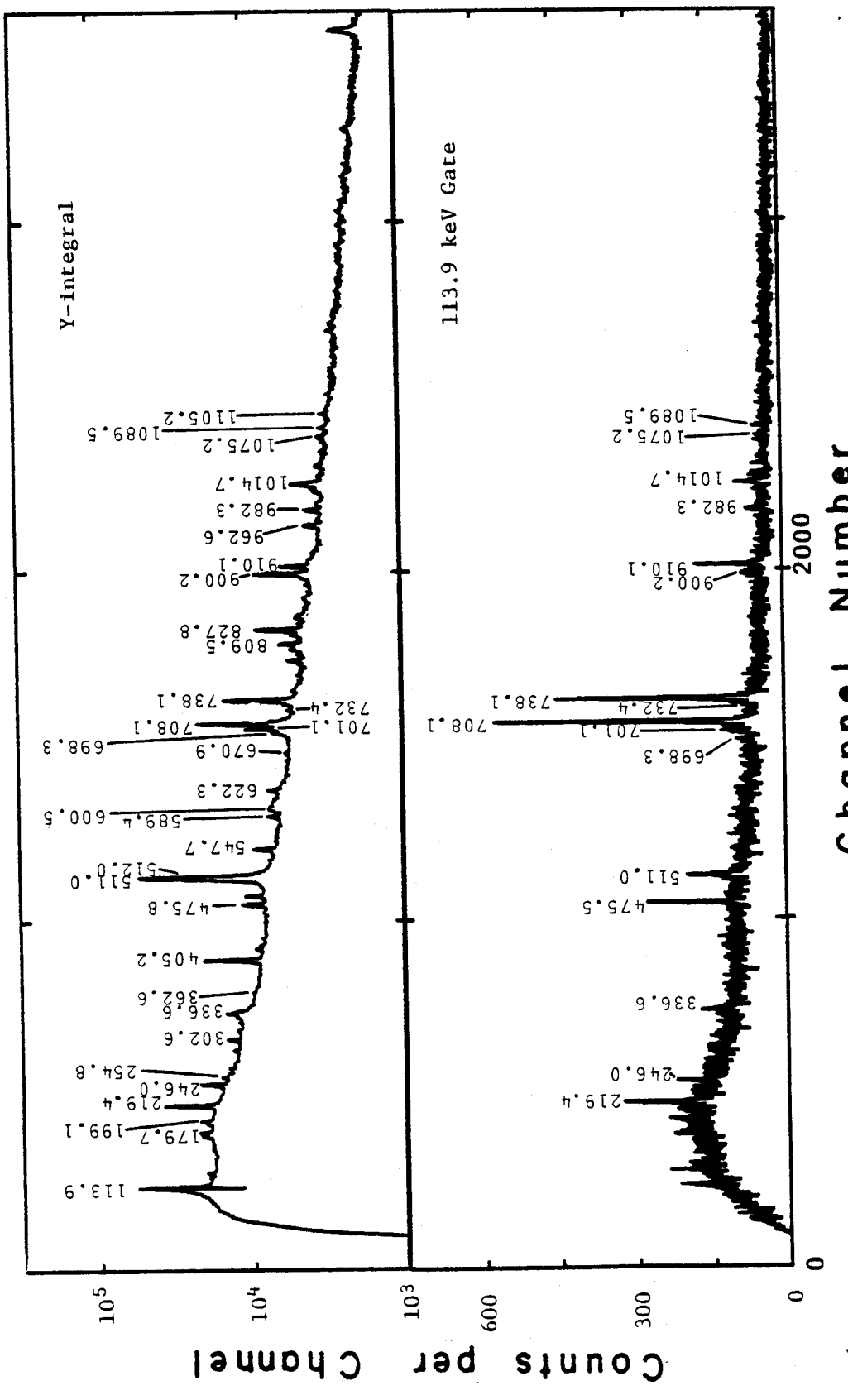
Y-integral
113.9 keV Gate
Counts per Channel
Channel Number
10^5
10^4
10^3
600
300
0
2000
113.9
179.7
199.1
219.4
246.0
254.8
302.6
336.6
362.6
405.2
475.8
511.0
512.0
547.7
589.4
600.5
622.3
670.9
698.3
701.1
708.1
732.4
738.1
809.5
827.8
900.2
910.1
962.6
982.3
1014.7
1075.2
1089.5
1105.2

Figure G.

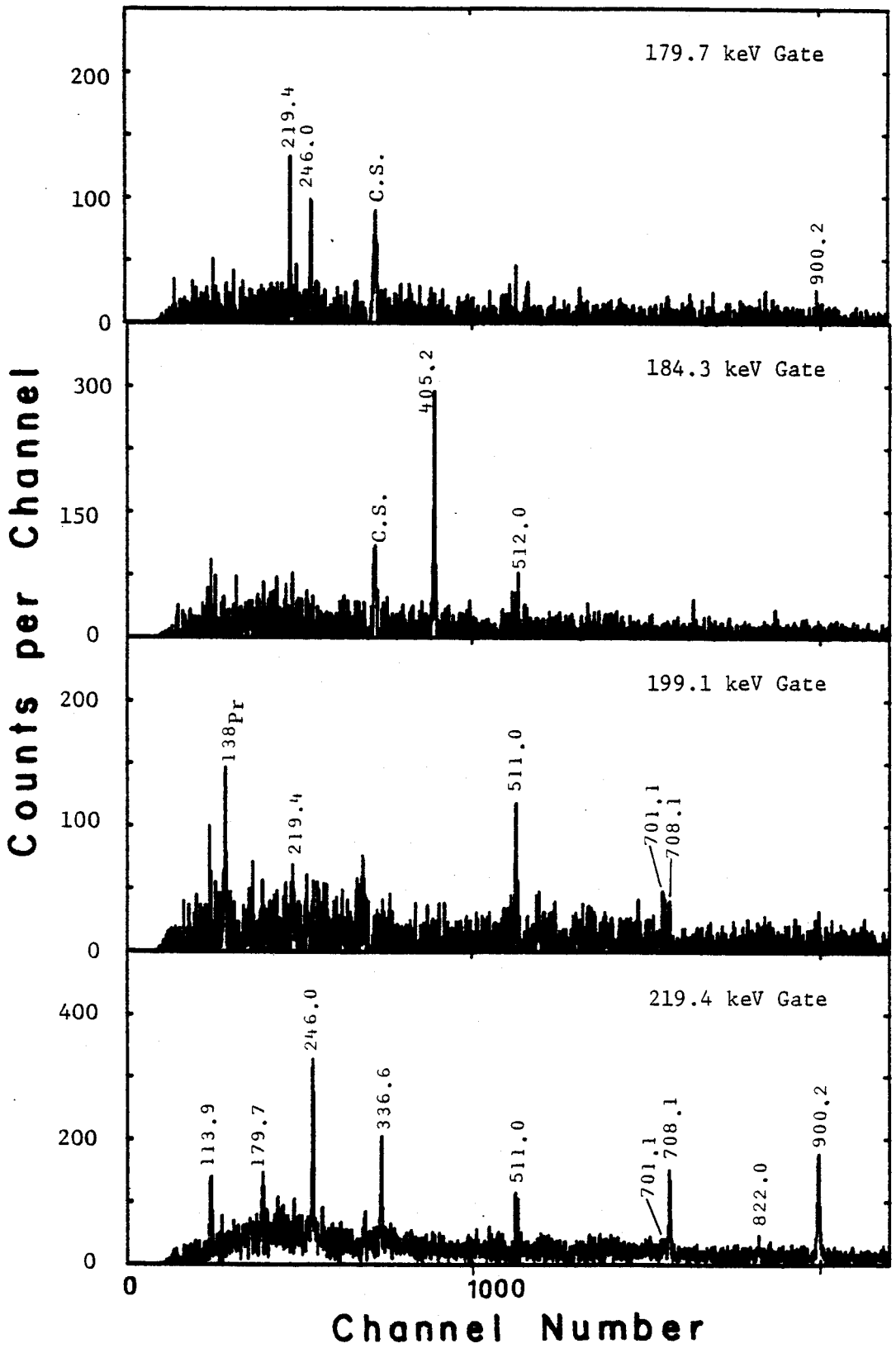

Figure G. (cont'd.).

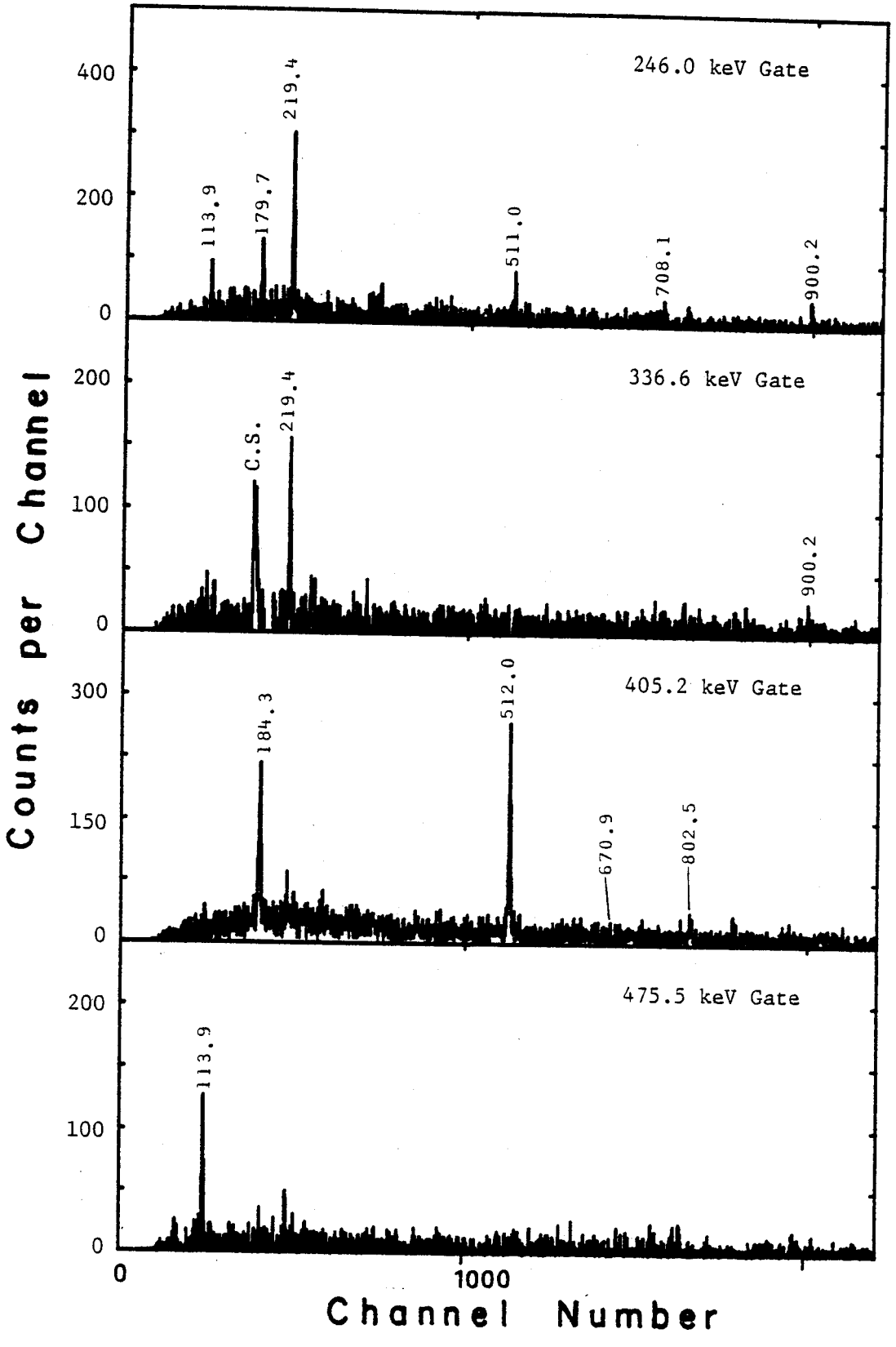

Figure G. (cont'd.).

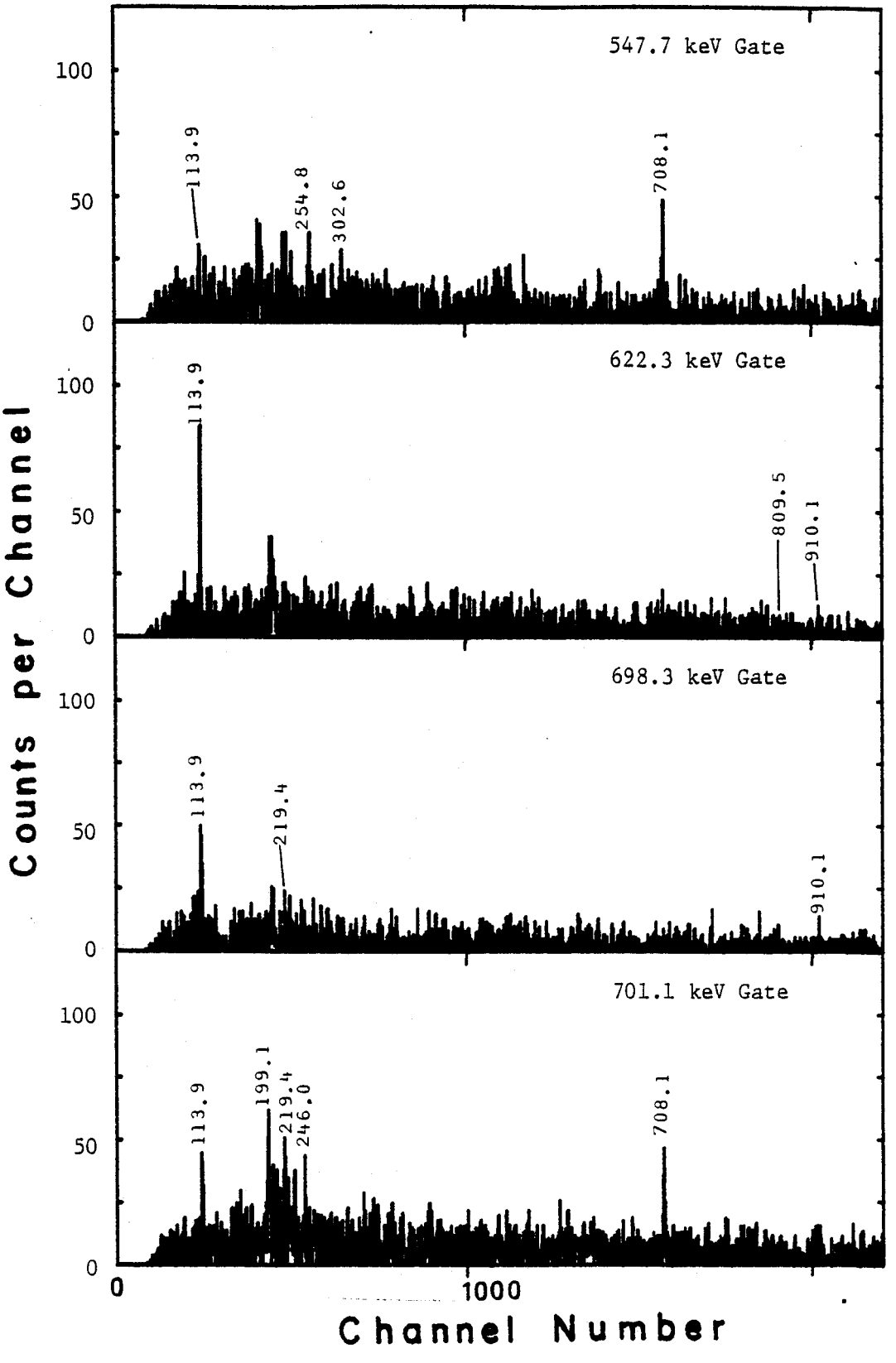

Figure G. (cont'd.).

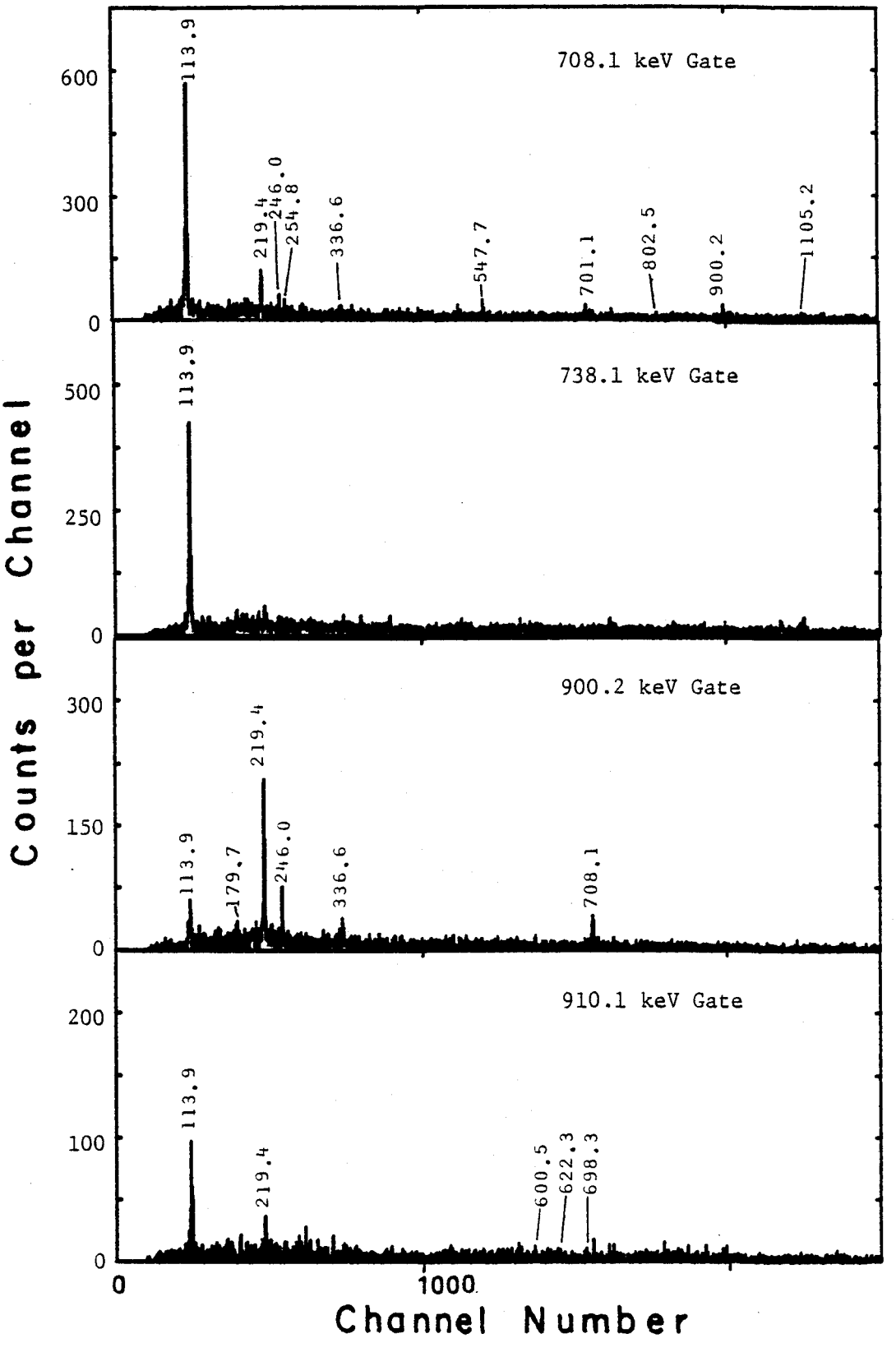

Figure G. (cont'd.).

APPENDIX H

Angular Distribution Plots of ^{139}Pr Transitions from $(p,2n\gamma)$ Reaction.

Figure H. Angular distribution plots of ^{139}Pr transitions obtained from $(p,2n\gamma)$ reaction. The data were taken in the 90-180° quadrant.

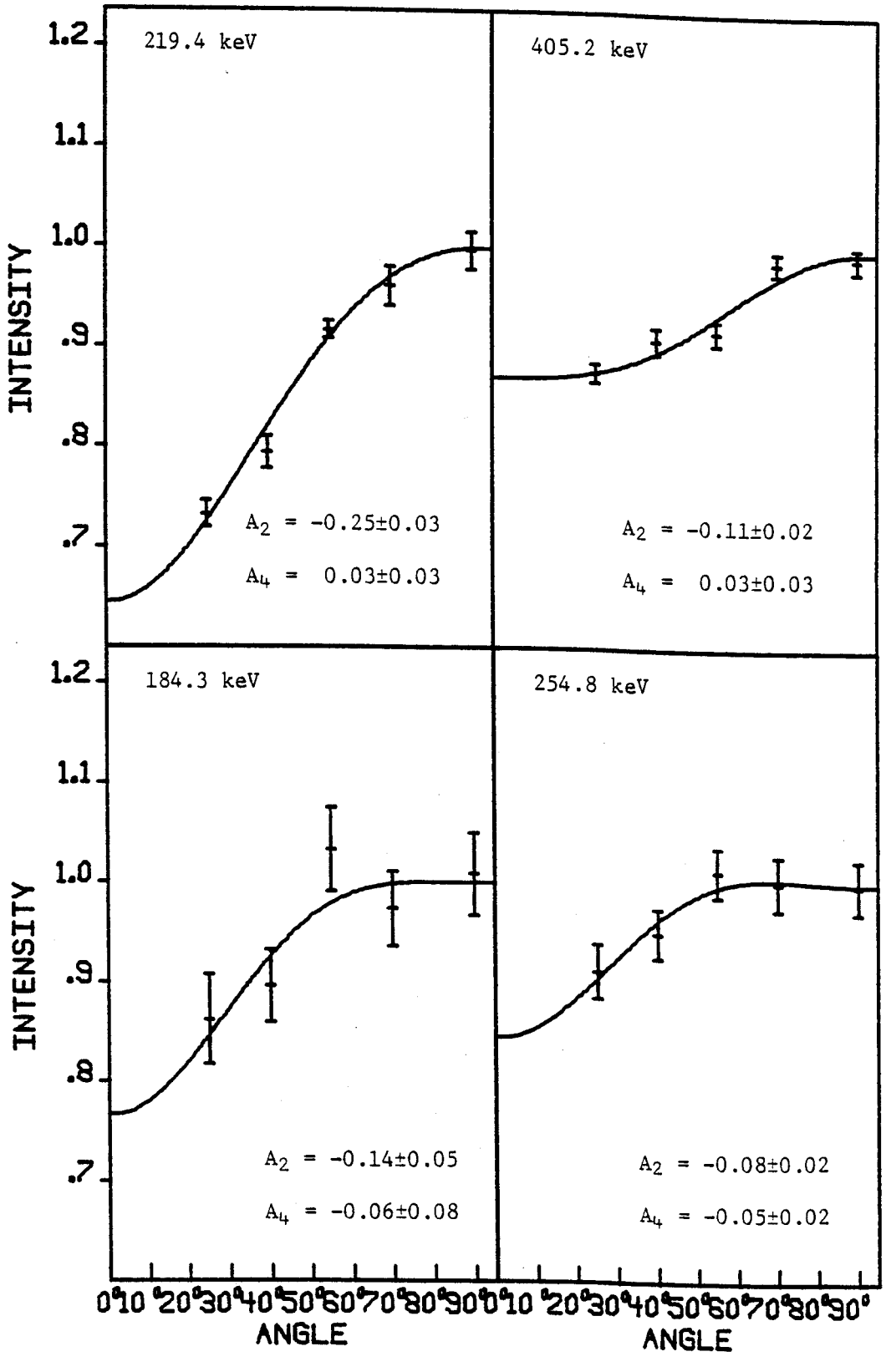
219.4 keV
405.2 keV
184.3 keV
254.8 keV
A2 = -0.25±0.03
A4 = 0.03±0.03
A2 = -0.11±0.02
A4 = 0.03±0.03
A2 = -0.14±0.05
A4 = -0.06±0.08
A2 = -0.08±0.02
A4 = -0.05±0.02
INTENSITY
INTENSITY
1.2
1.1
1.0
.9
.8
.7
0°10°20°30°40°50°60°70°80°90°
ANGLE
ANGLE

Figure H.

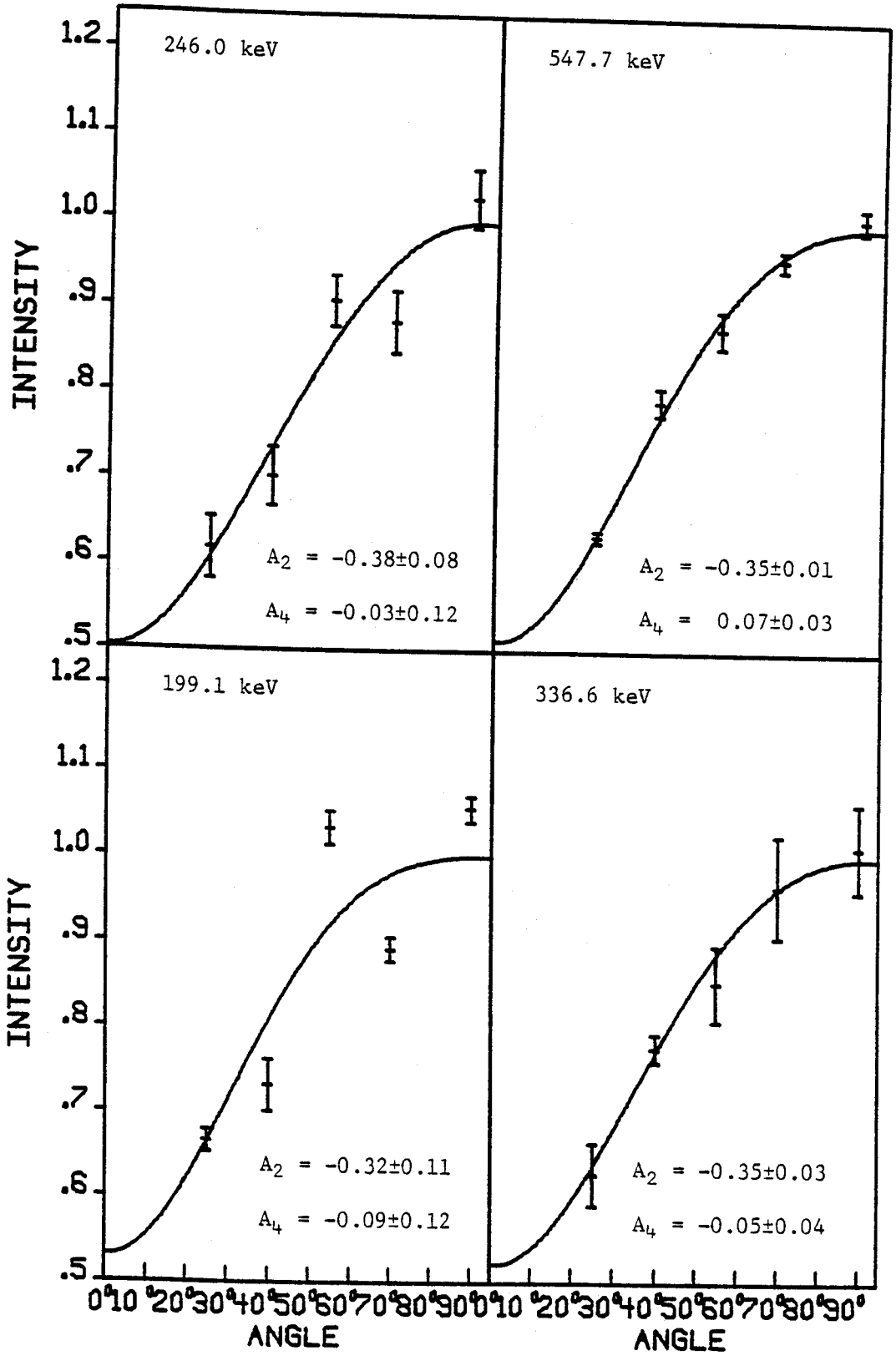

Figure H. (cont'd.).

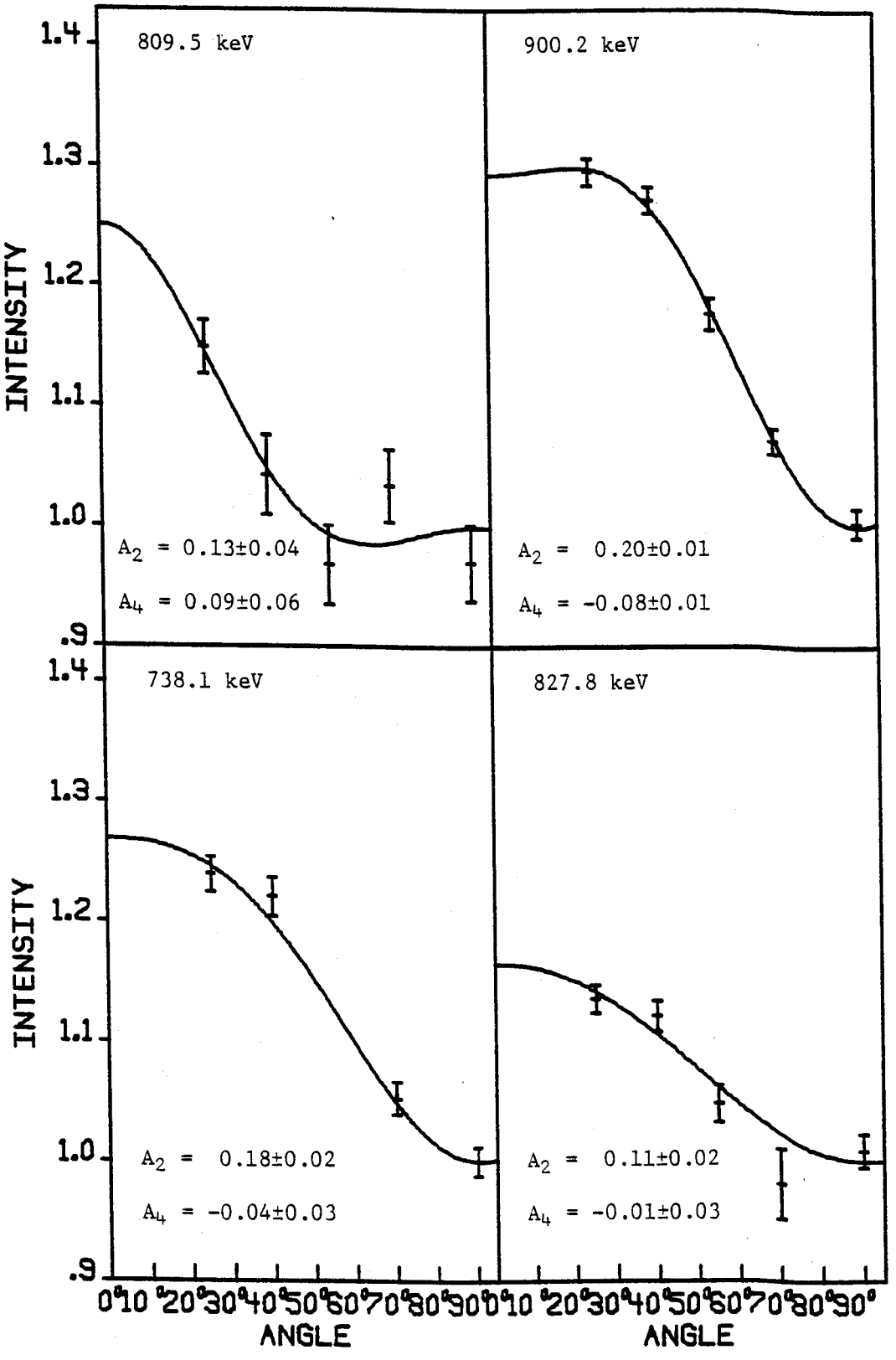

Figure H. (cont'd.).

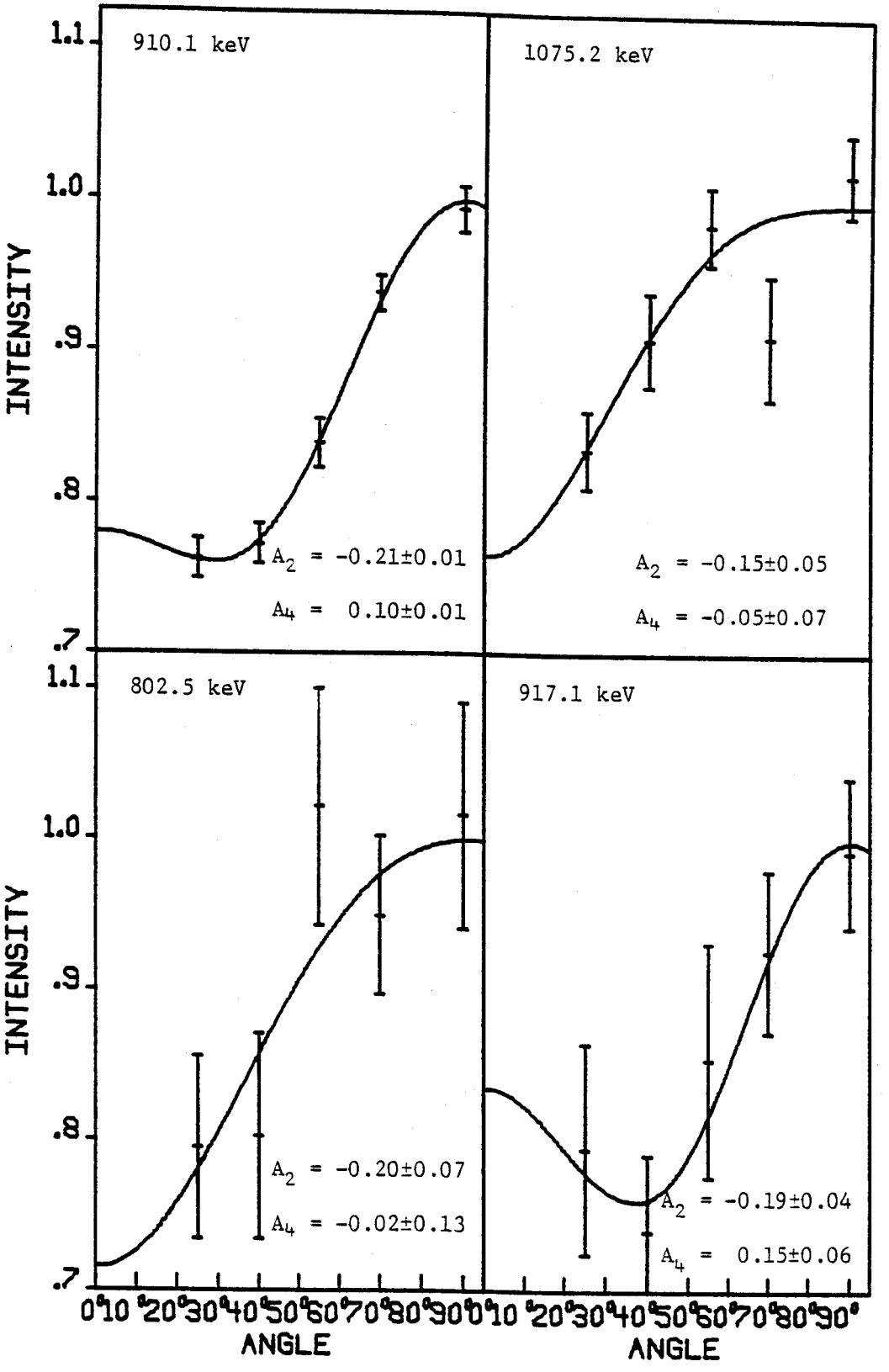

Figure H. (cont'd.).

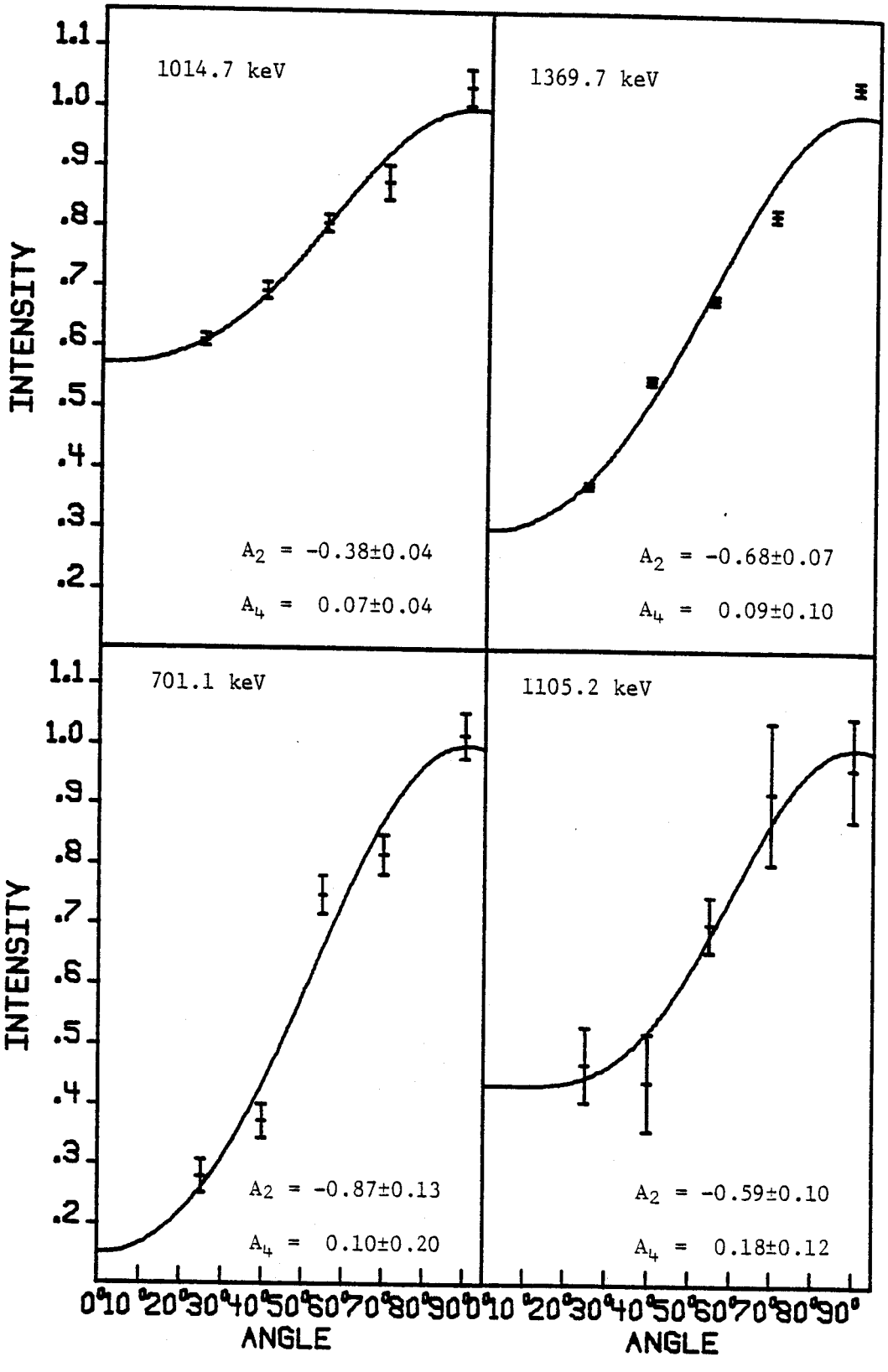

Figure H. (cont'd.).

APPENDIX I

Gated Coincidence Spectra of Transitions in ^{139}Pr from (α,4nγ) Reaction.

Figure I-1. Y-integral coincidence and Y-gated spectra (identifying high energy coincidences) of transitions in ^{139}Pr from (α,4nγ) reaction. Background subtraction using the adjacent continuum has been included. The spectra are arranged according to increasing energy.

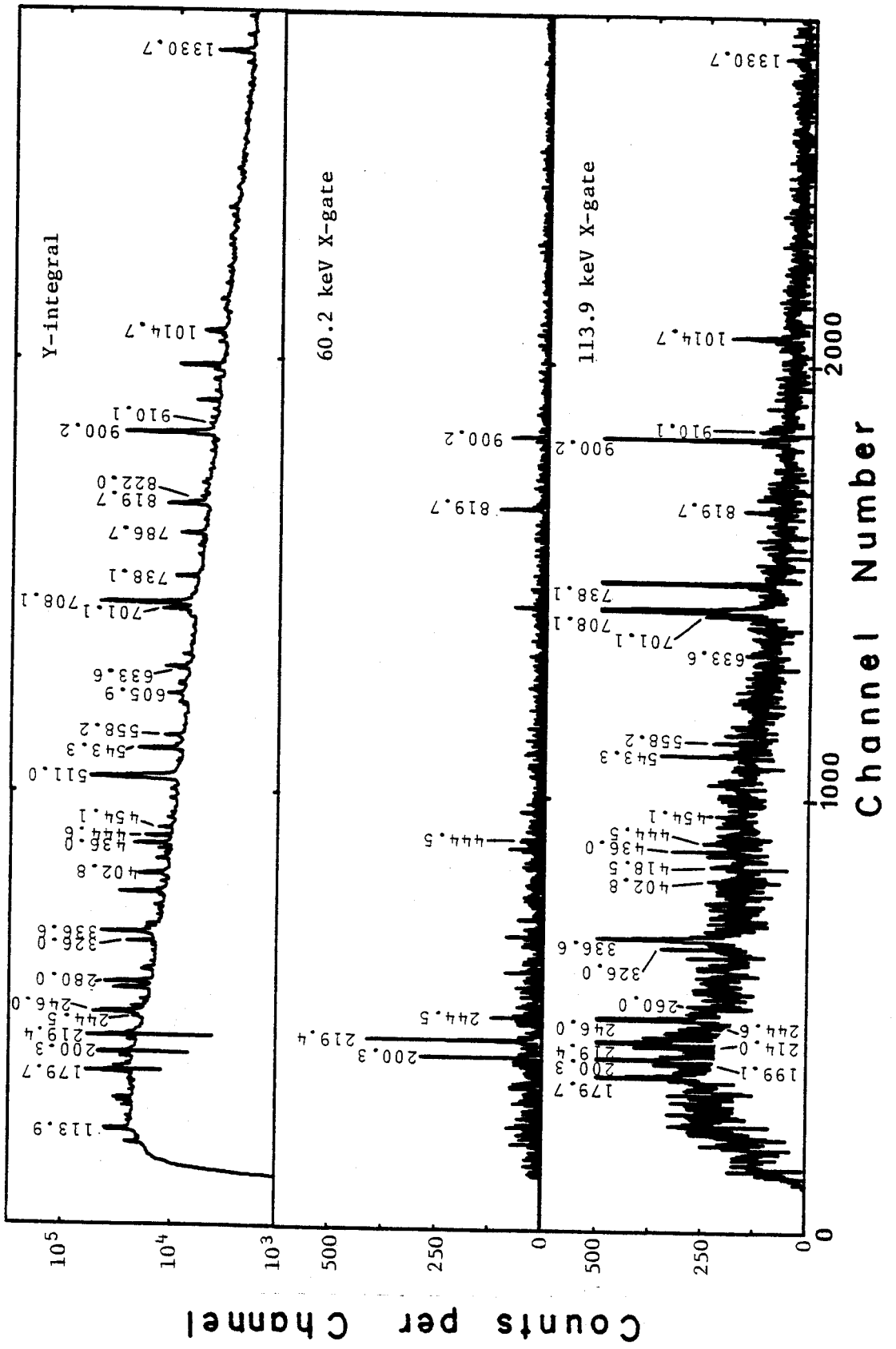
Counts per Channel
Channel Number
Y-integral
60.2 keV X-gate
113.9 keV X-gate
113.9
179.7
200.3
219.4
244.5
246.0
280.0
326.0
336.6
402.8
435.6
444.5
454.1
511.0
543.3
558.2
605.9
633.6
701.1
708.1
738.1
786.7
819.7
822.0
900.2
910.1
1014.7
1330.7
199.1
213.0
260.0
502.8
518.5
536.0
544.5

Figure I-1.

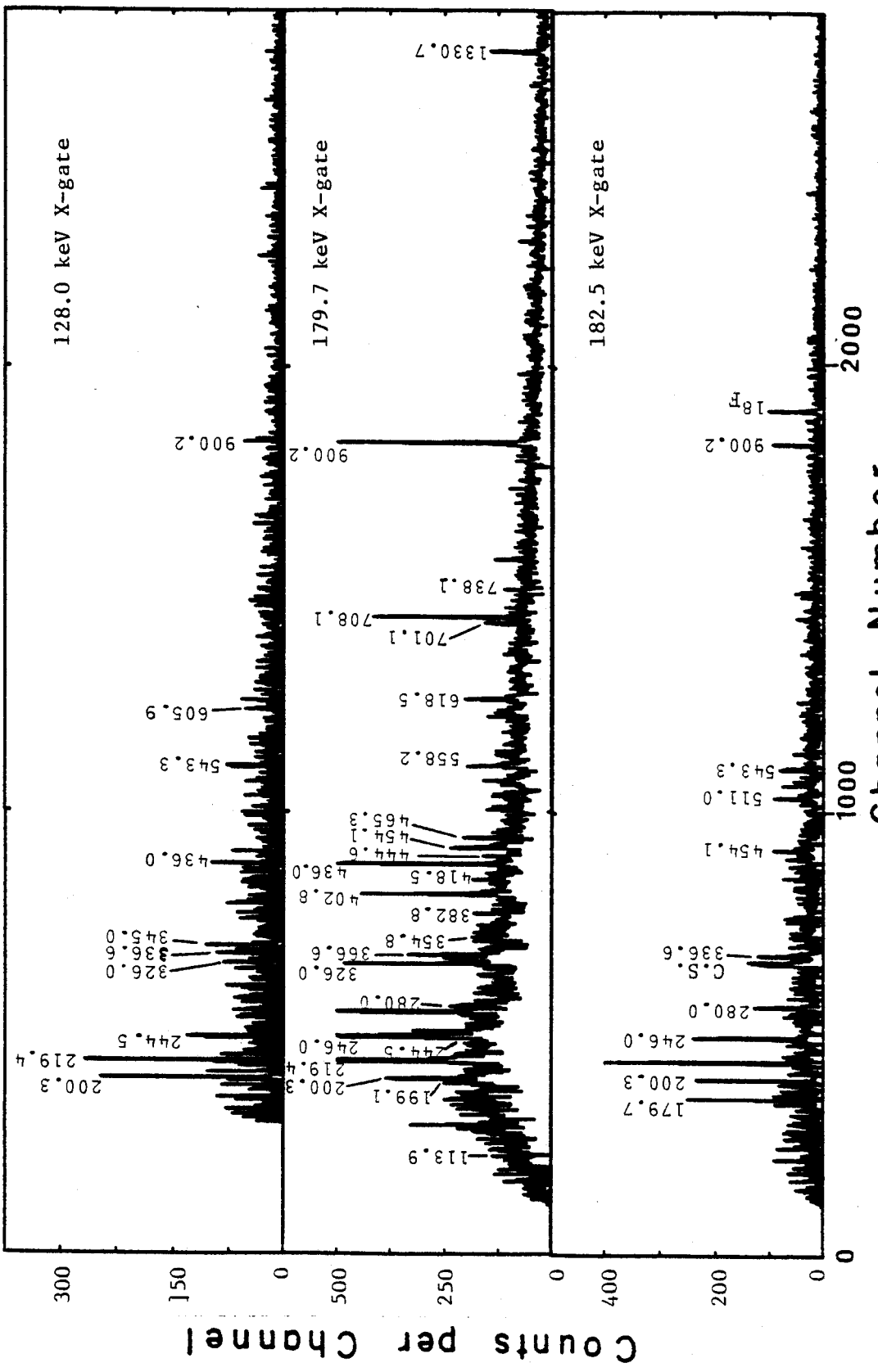

Figure I-1. (cont'd.).

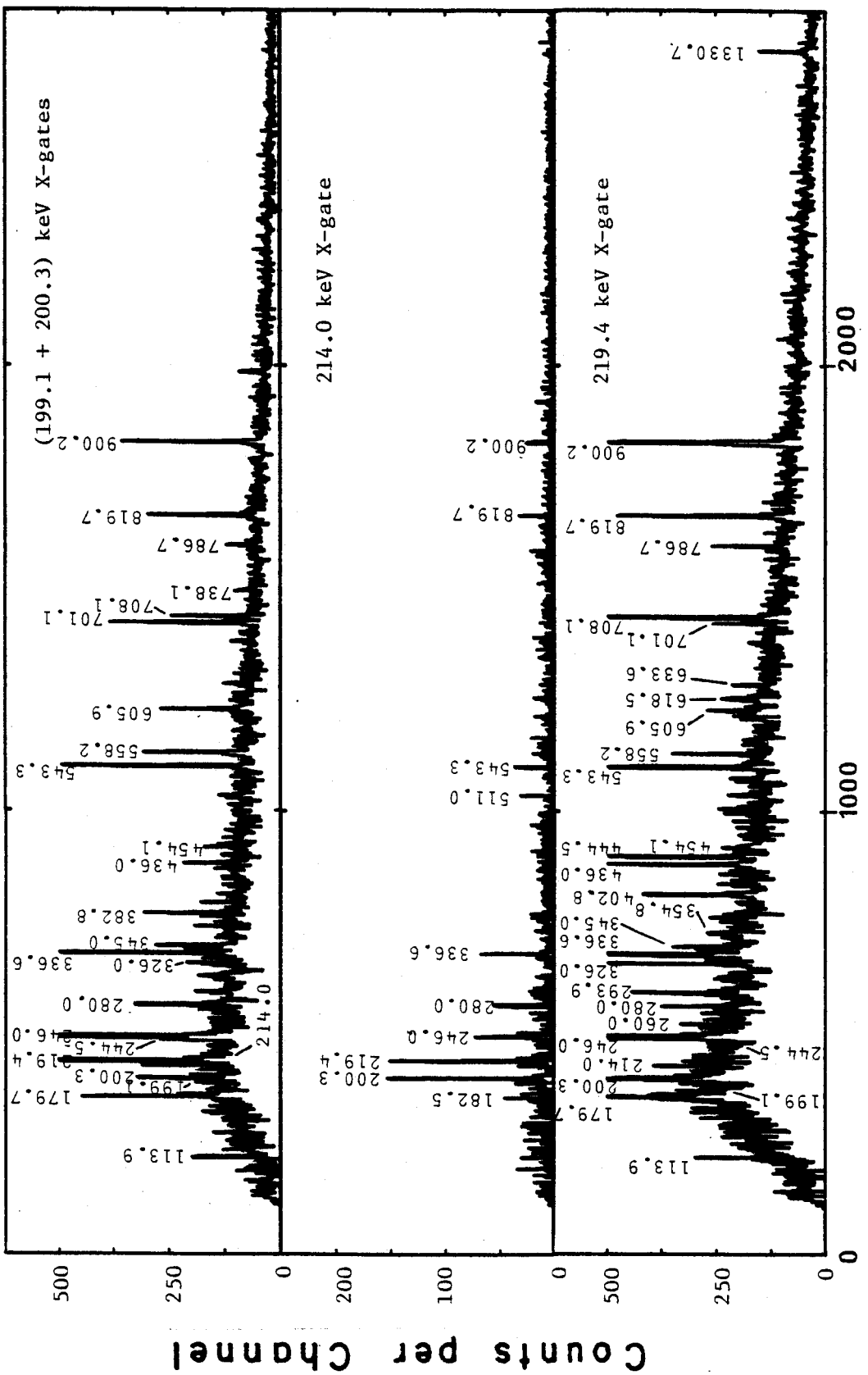

Figure I-1. (cont'd.).

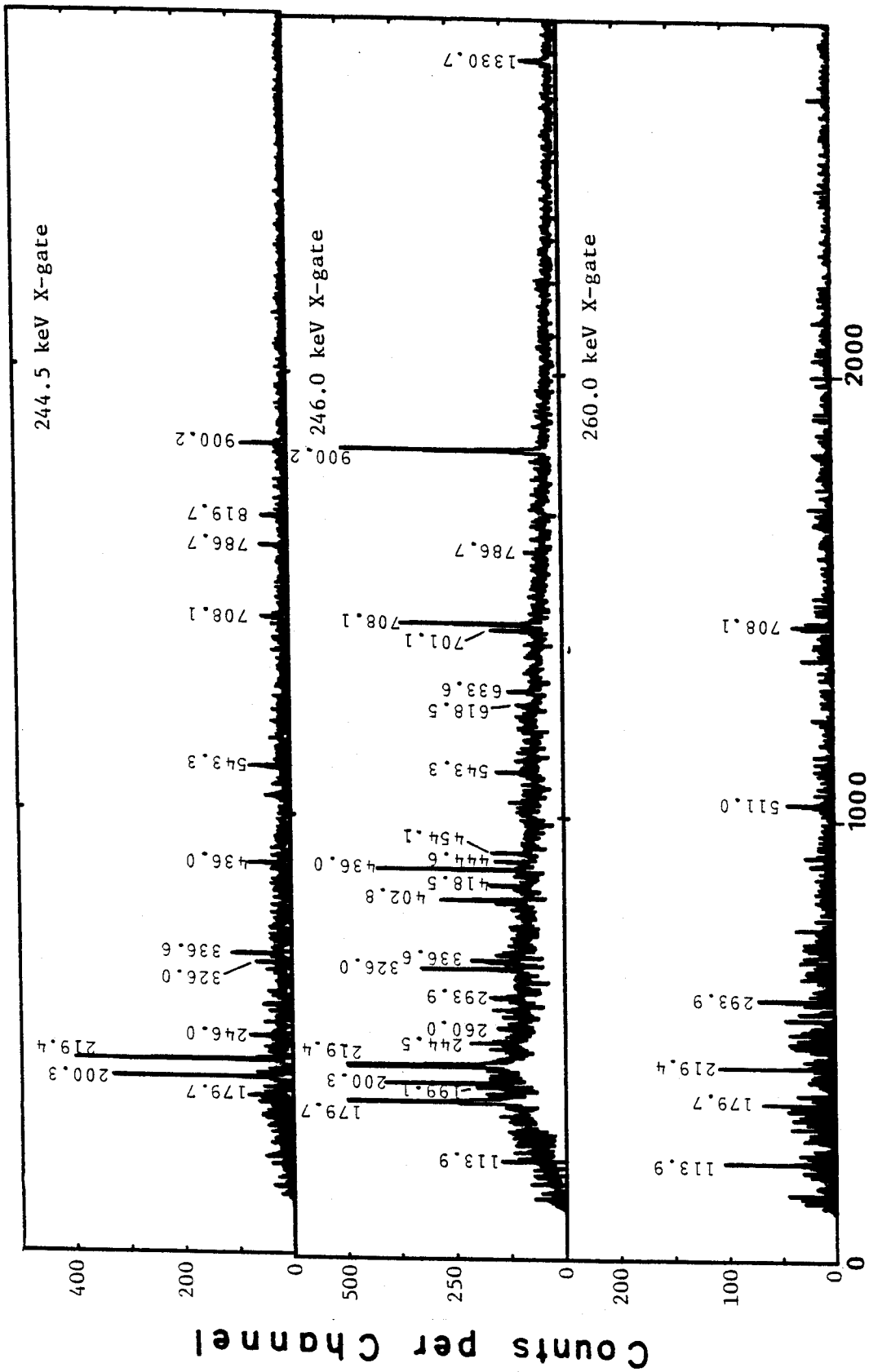

Figure I-1. (cont'd.).

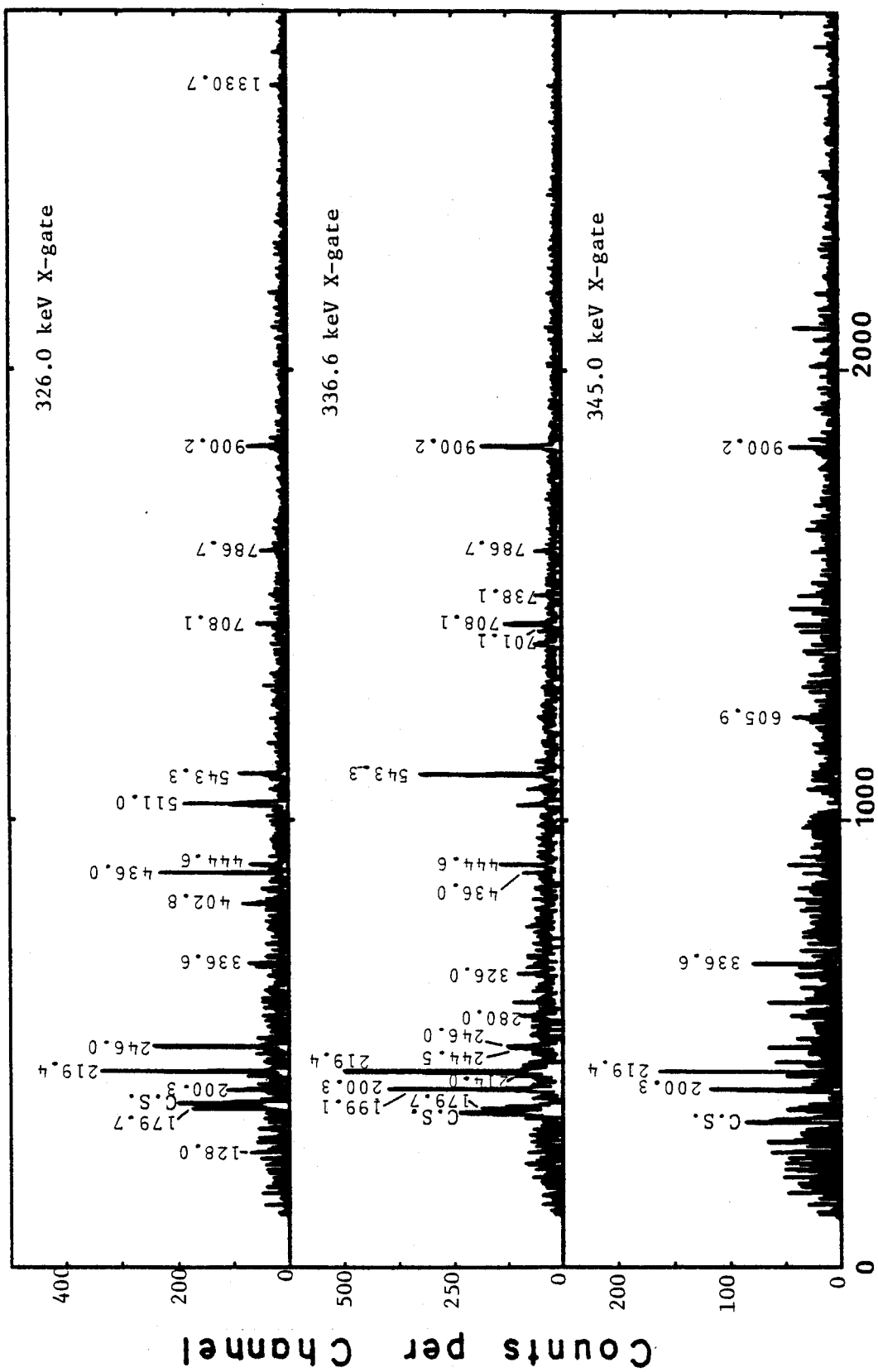

Figure I-1. (cont'd.).

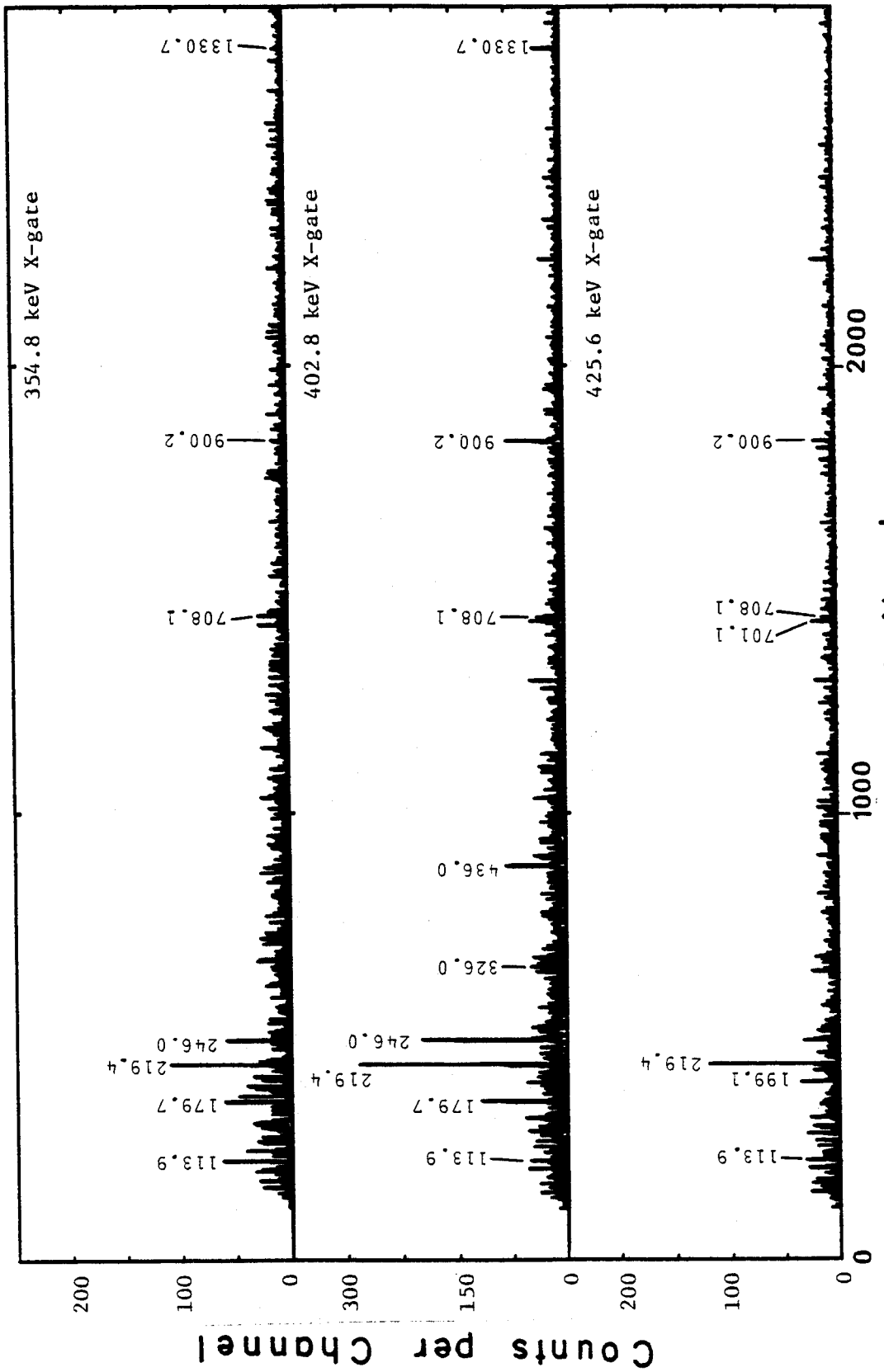

Figure I-1. (cont'd.).

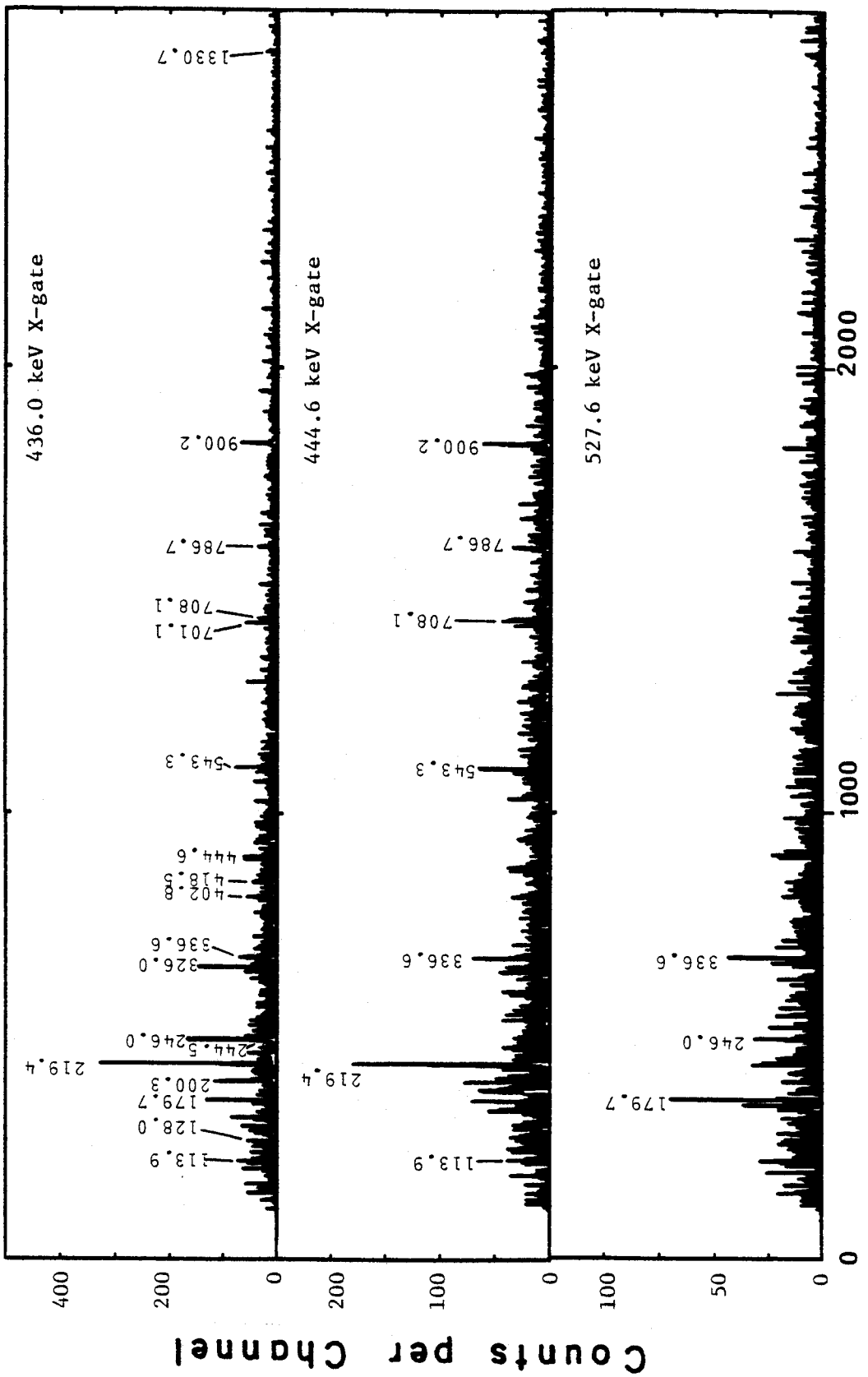

Figure I-1. (cont'd.).

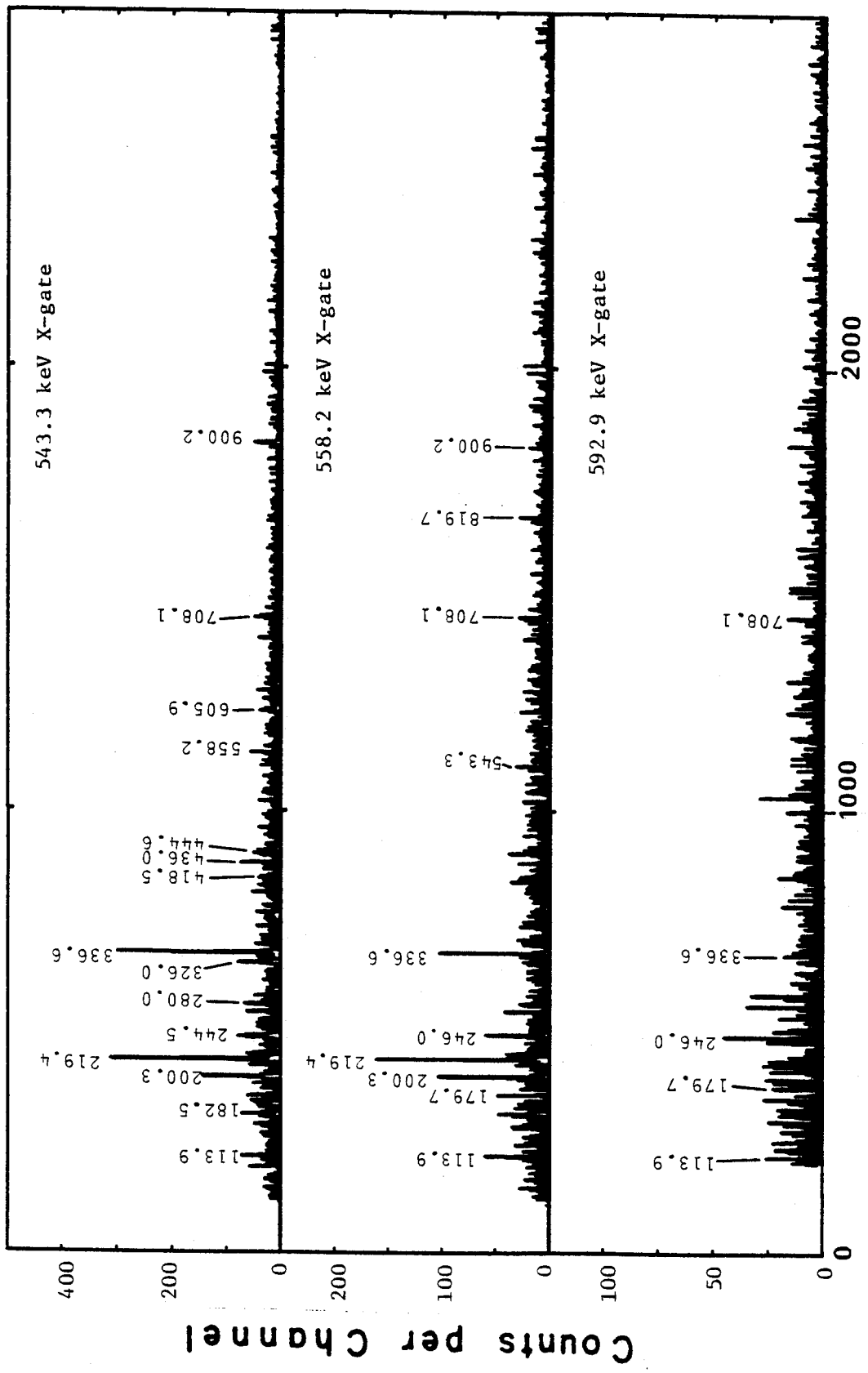

Figure I-1. (cont'd.).

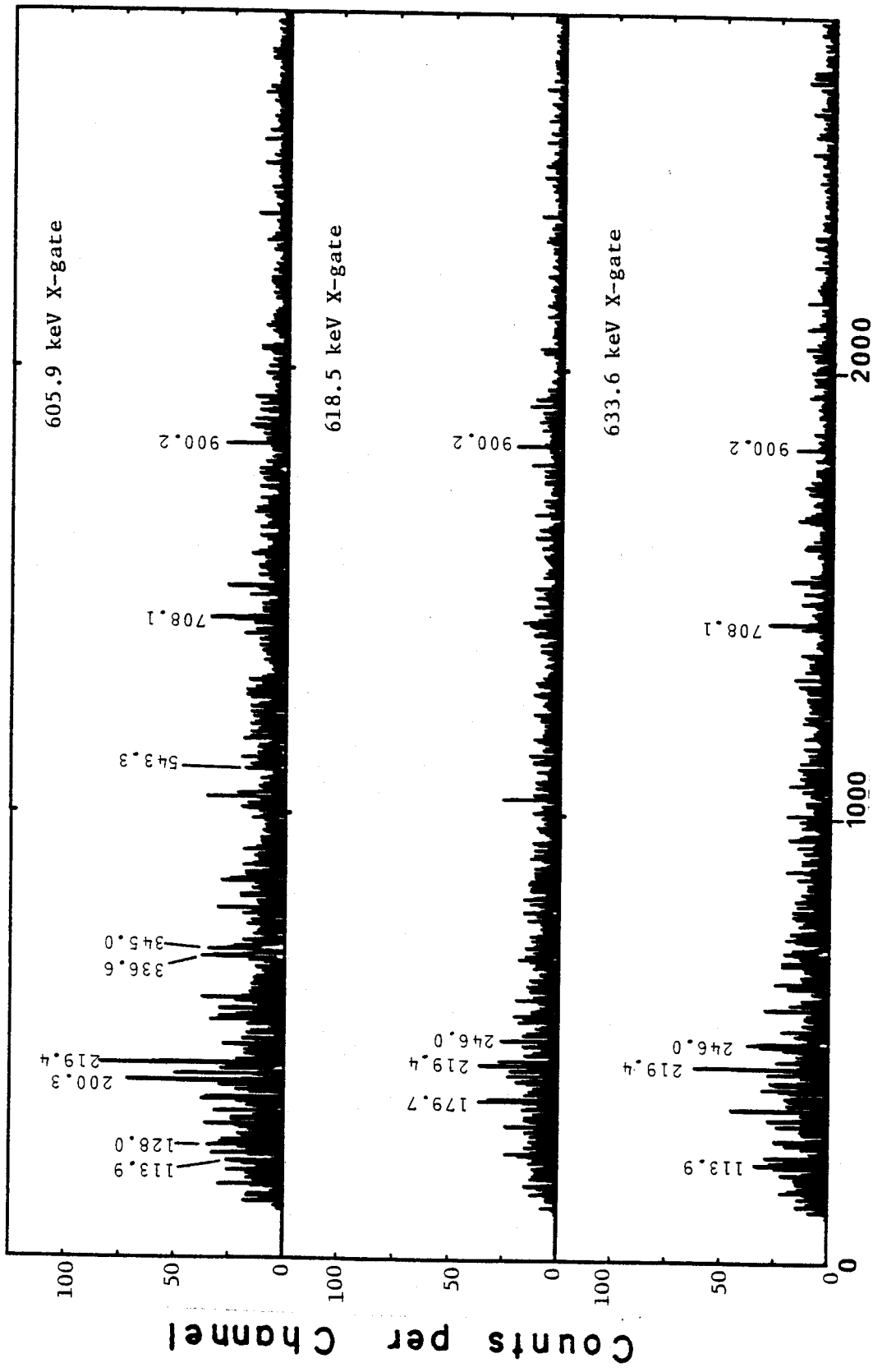

Figure I-1. (cont'd.).

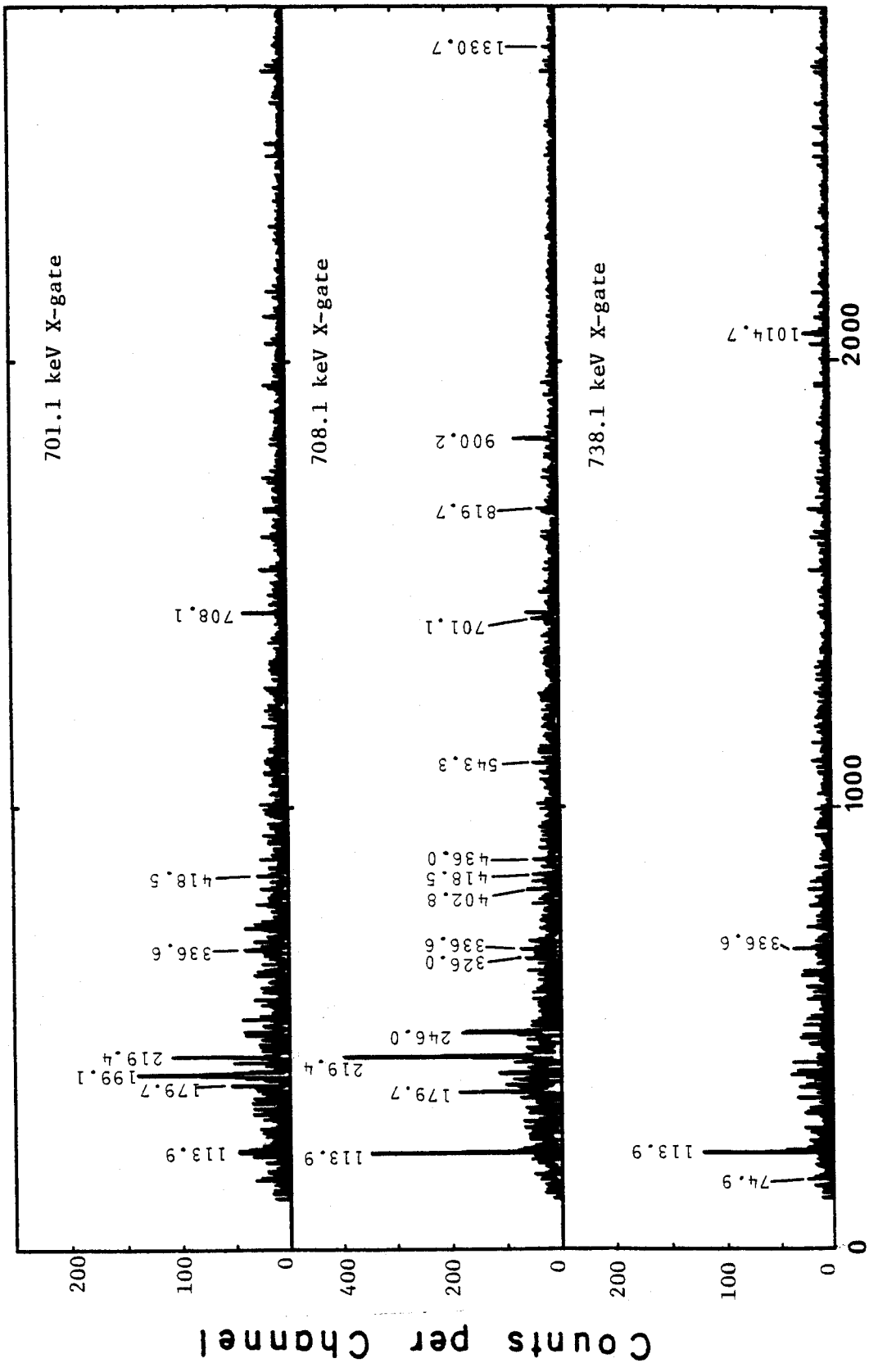

Figure I-1. (cont'd.).

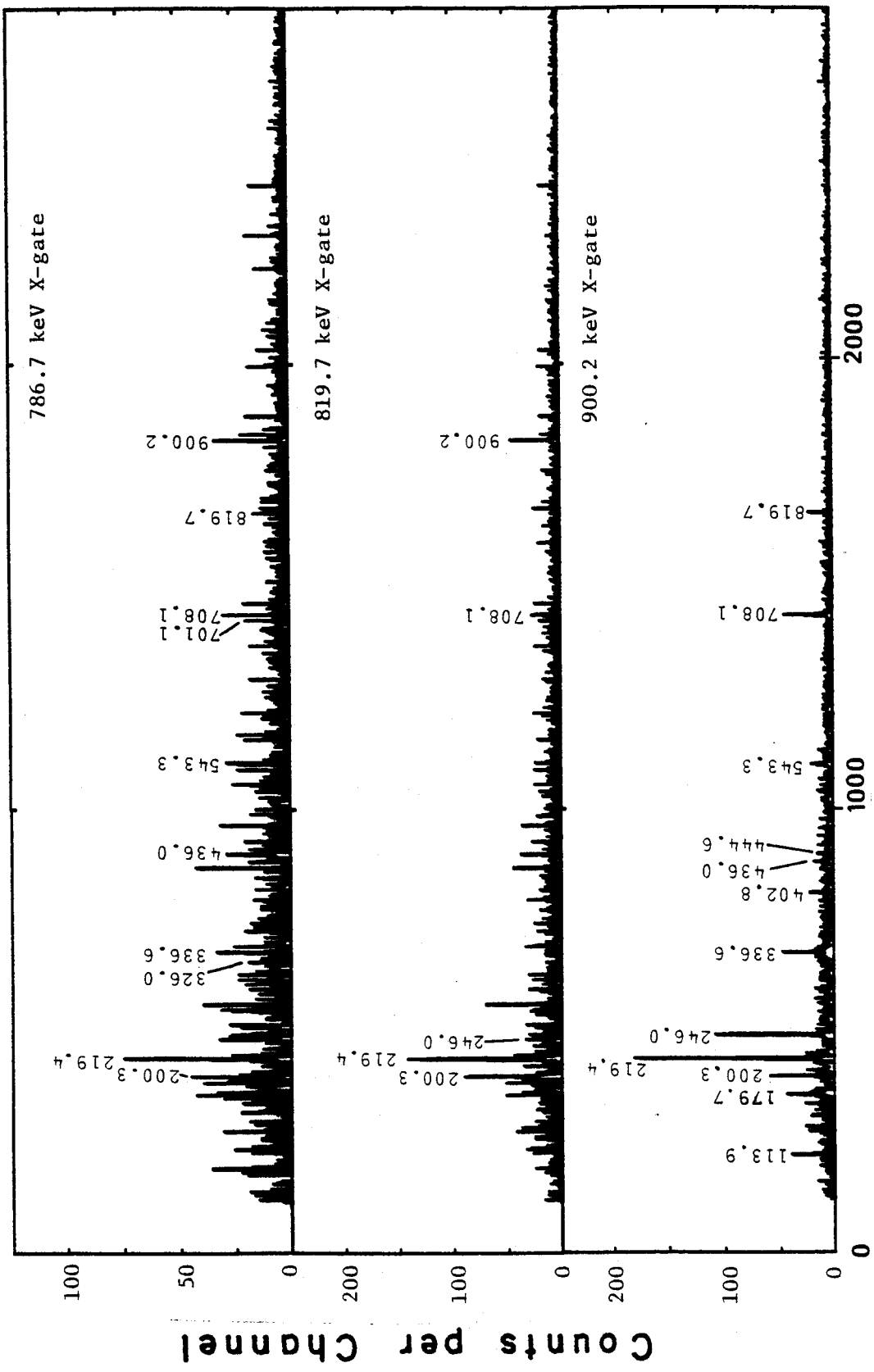

Figure I-1. (cont'd.).

Figure I-2. X-integral coincidence and X-gated spectra (identifying low energy coincidences) of transitions in ^{139}Pr from (α,4nγ) reaction. Background subtraction using the adjacent continuum has been included. The spectra are arranged according to increasing energy.

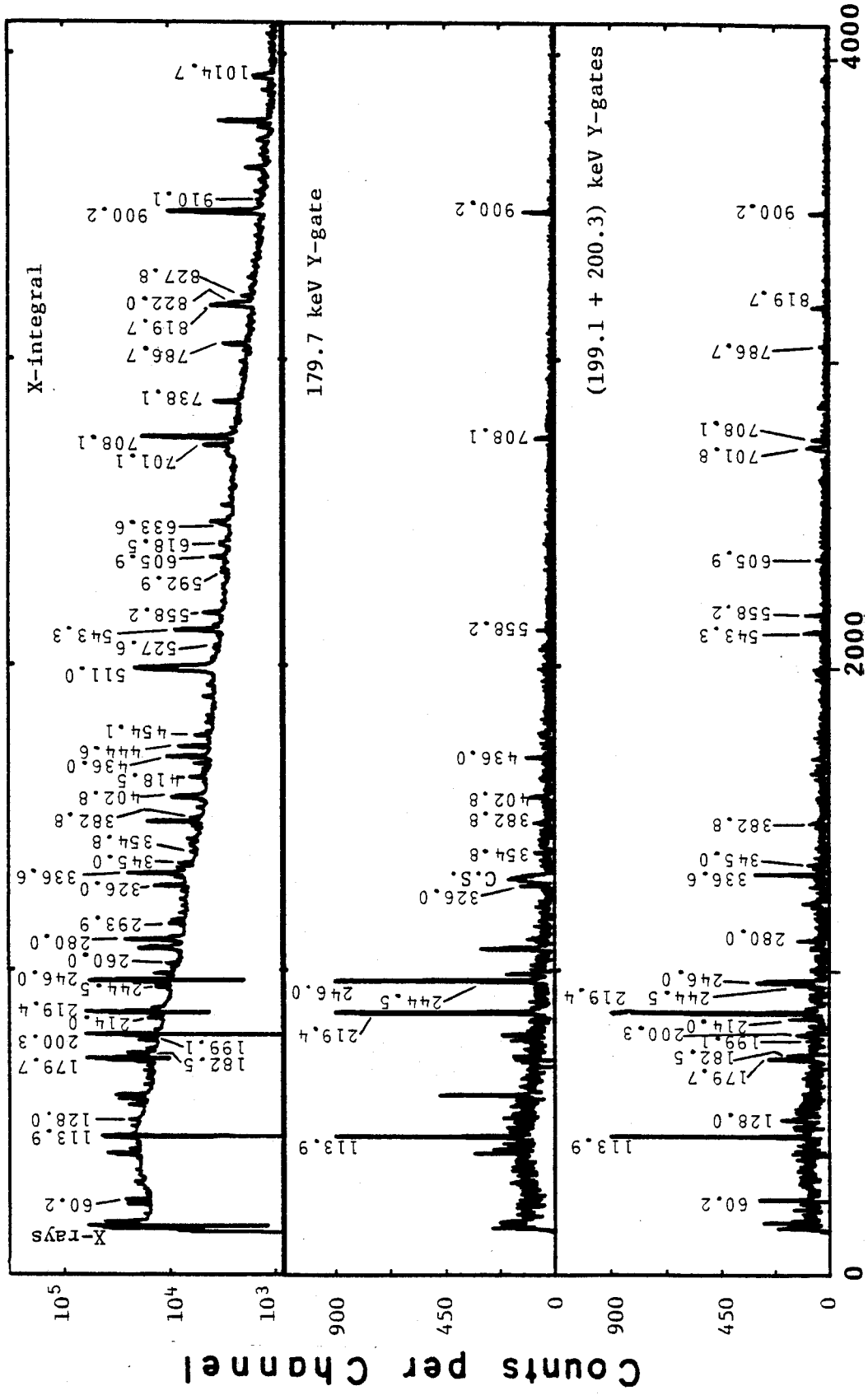
X-integral
X-rays
60.2
113.9
128.0
179.7
182.5
199.1
200.3
219.4
244.5
246.0
260.0
280.0
293.9
326.0
336.6
345.0
354.8
382.8
402.8
418.5
436.0
444.6
454.1
511.0
527.6
543.3
558.2
592.9
605.9
618.5
633.6
701.1
708.1
738.1
786.7
819.7
822.0
827.8
900.2
910.1
1014.7
179.7 keV Y-gate
113.9
219.4
244.5
246.0
326.0
C.S.
354.8
382.8
402.8
436.0
558.2
708.1
900.2
(199.1 + 200.3) keV Y-gates
60.2
113.9
128.0
179.7
182.5
199.1
200.3
214.0
219.4
244.5
246.0
280.0
336.6
345.0
382.8
543.3
558.2
605.9
701.8
708.1
786.7
819.7
900.2
Counts per Channel
10^5
10^4
10^3
900
450
0
900
450
0
0
2000
4000
Channel Number

Figure I-2.

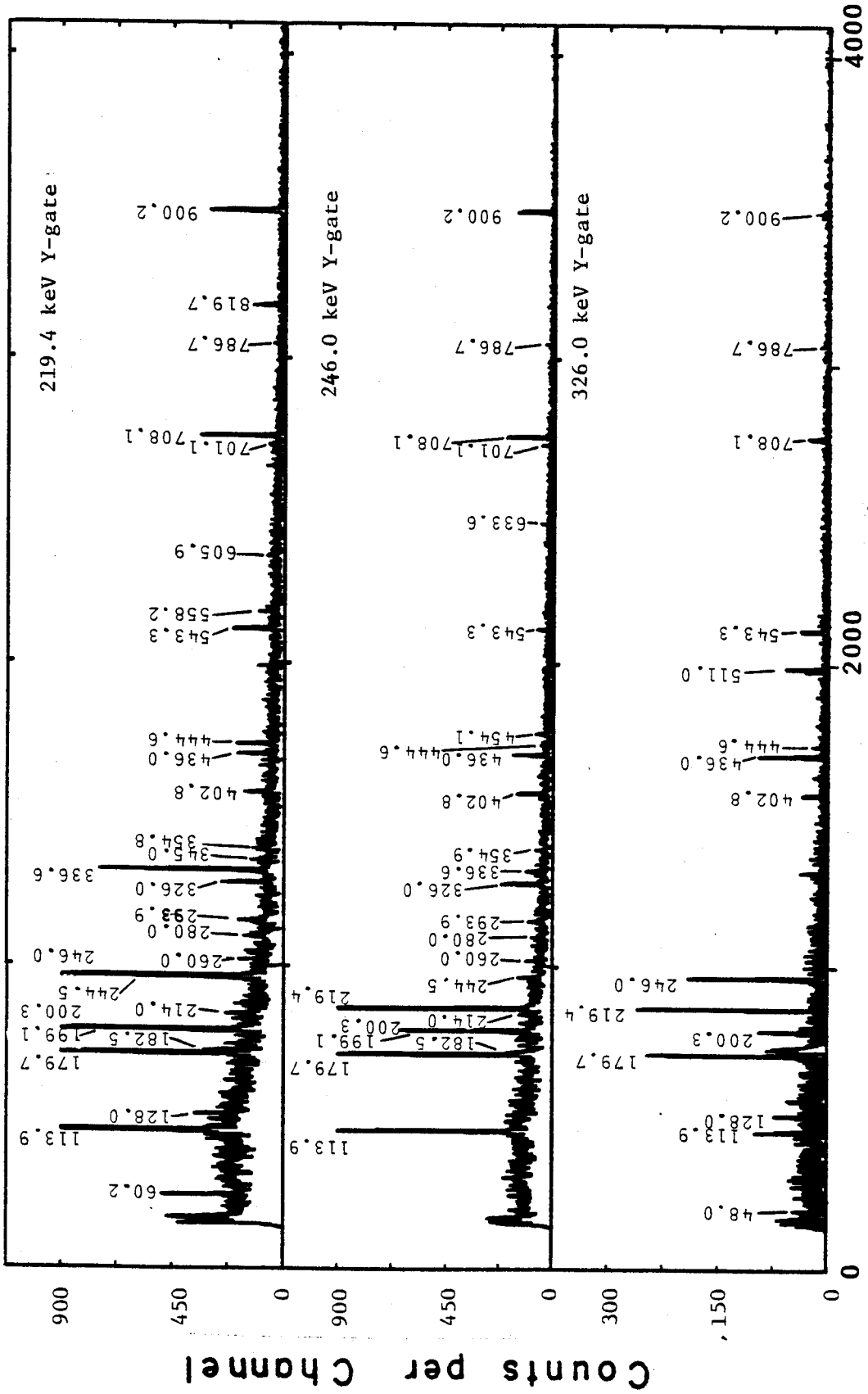

Figure I-2. (cont'd.).

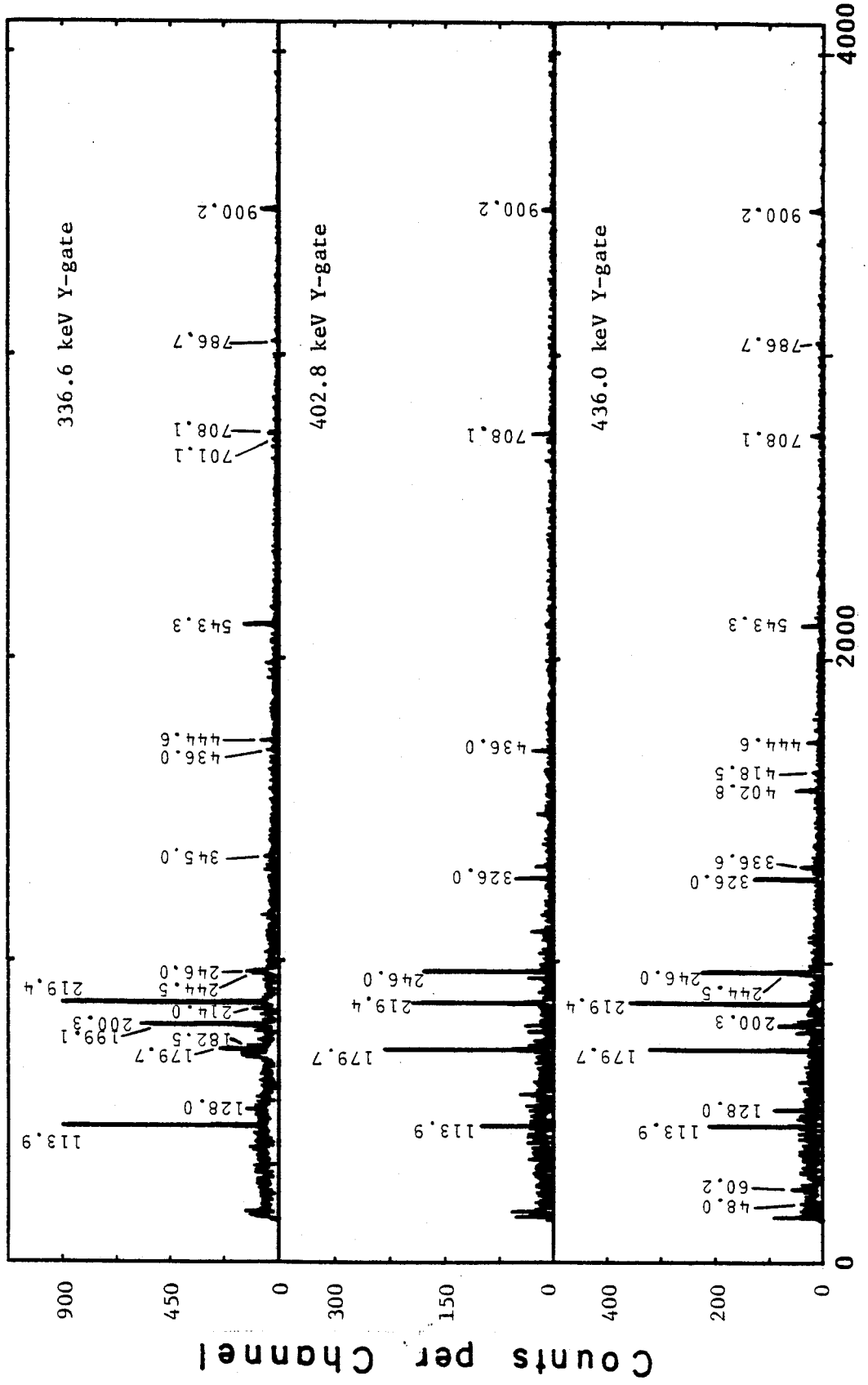

Figure I-2. (cont'd.).

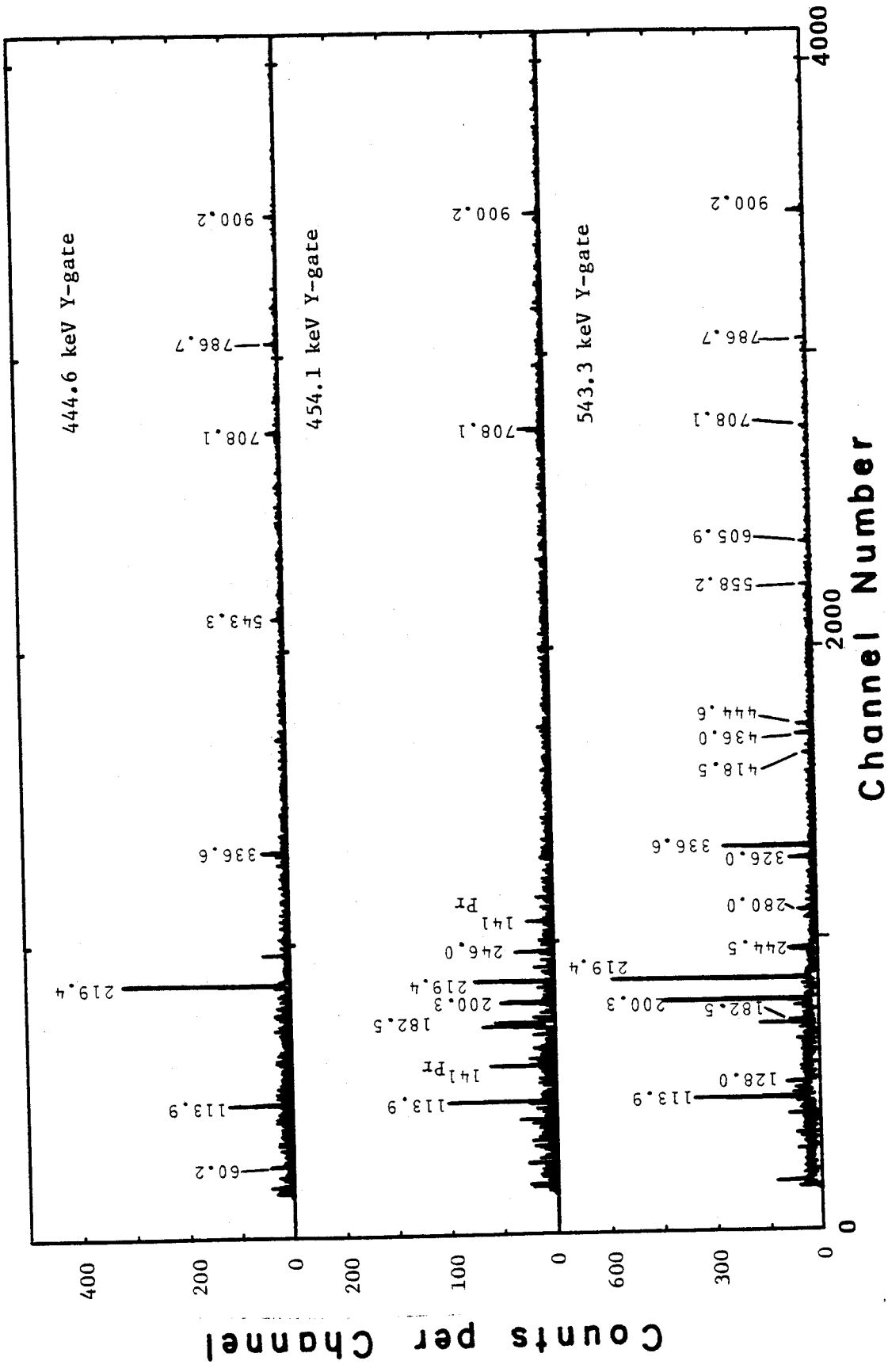

Figure I-2. (cont'd.).

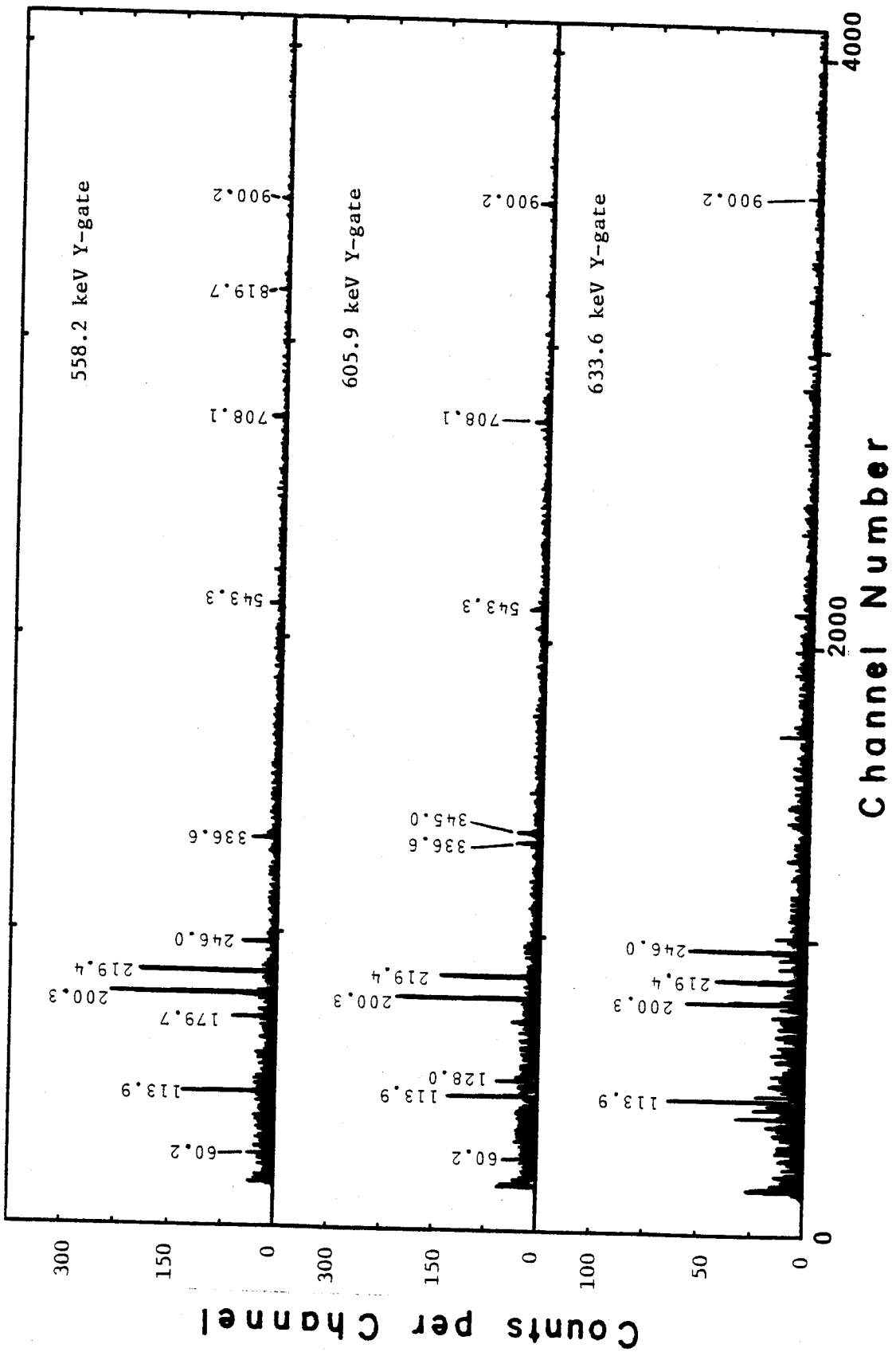

Figure I-2. (cont'd.).

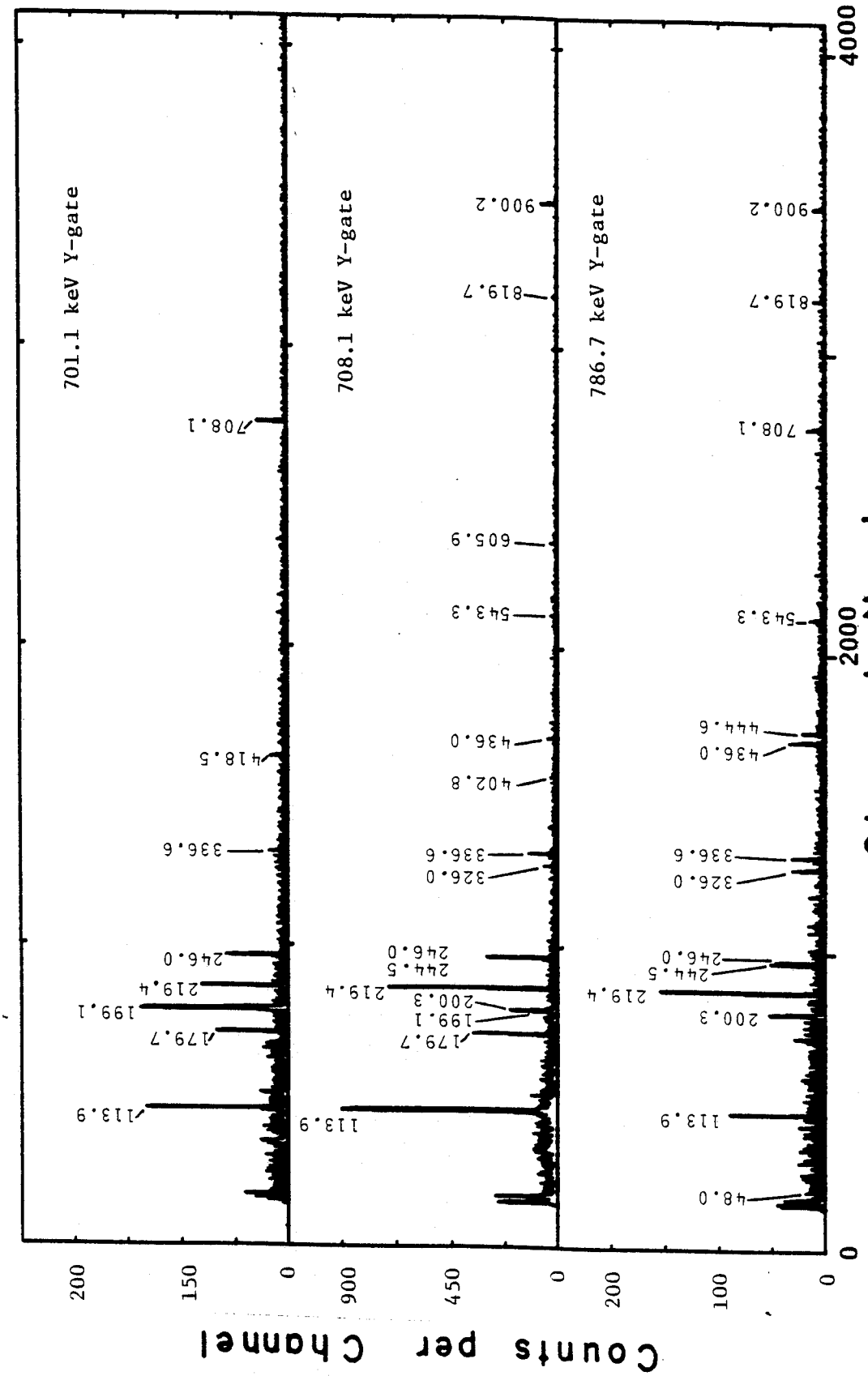

Figure I-2. (cont'd.).

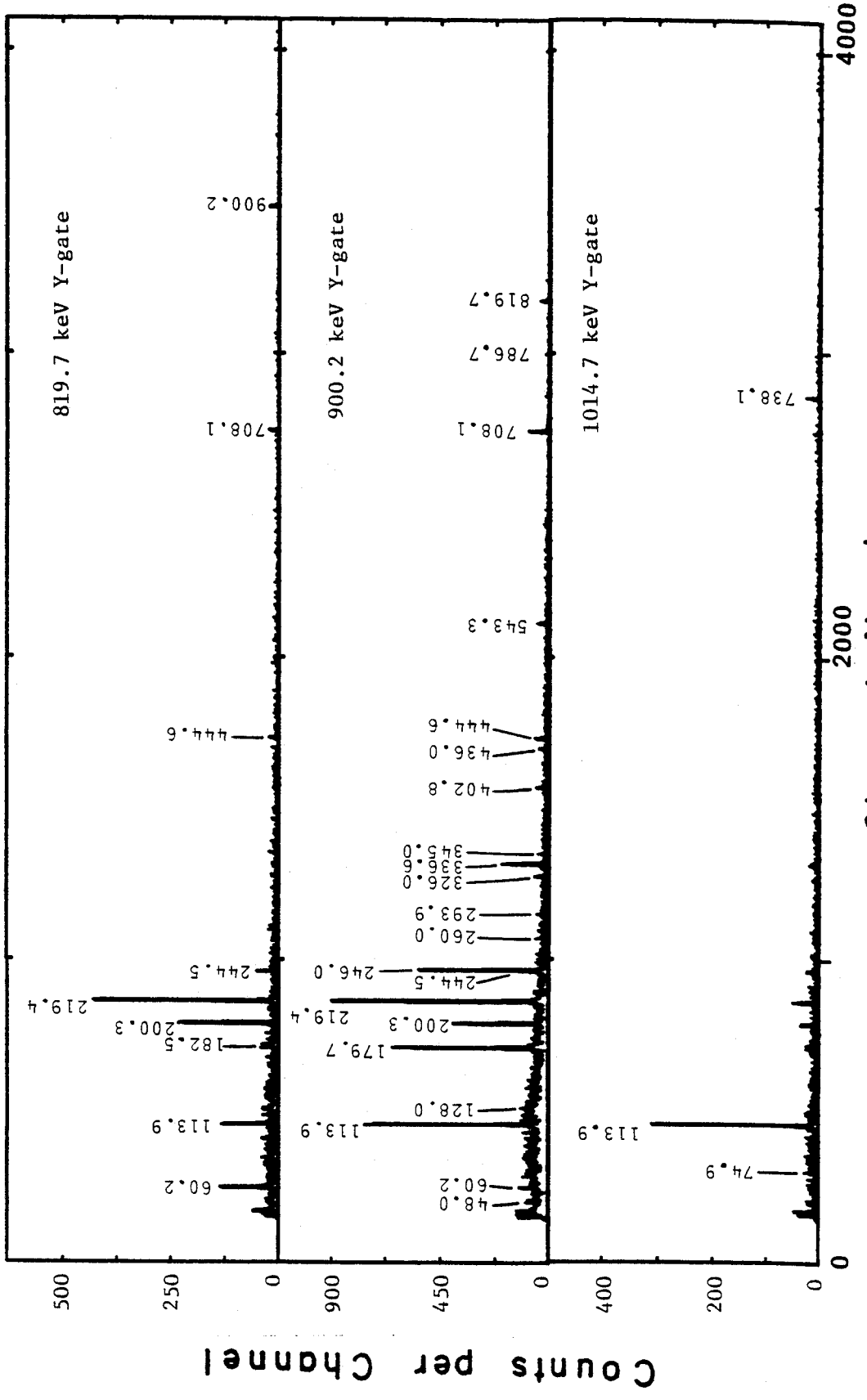

Figure I-2. (cont'd.).

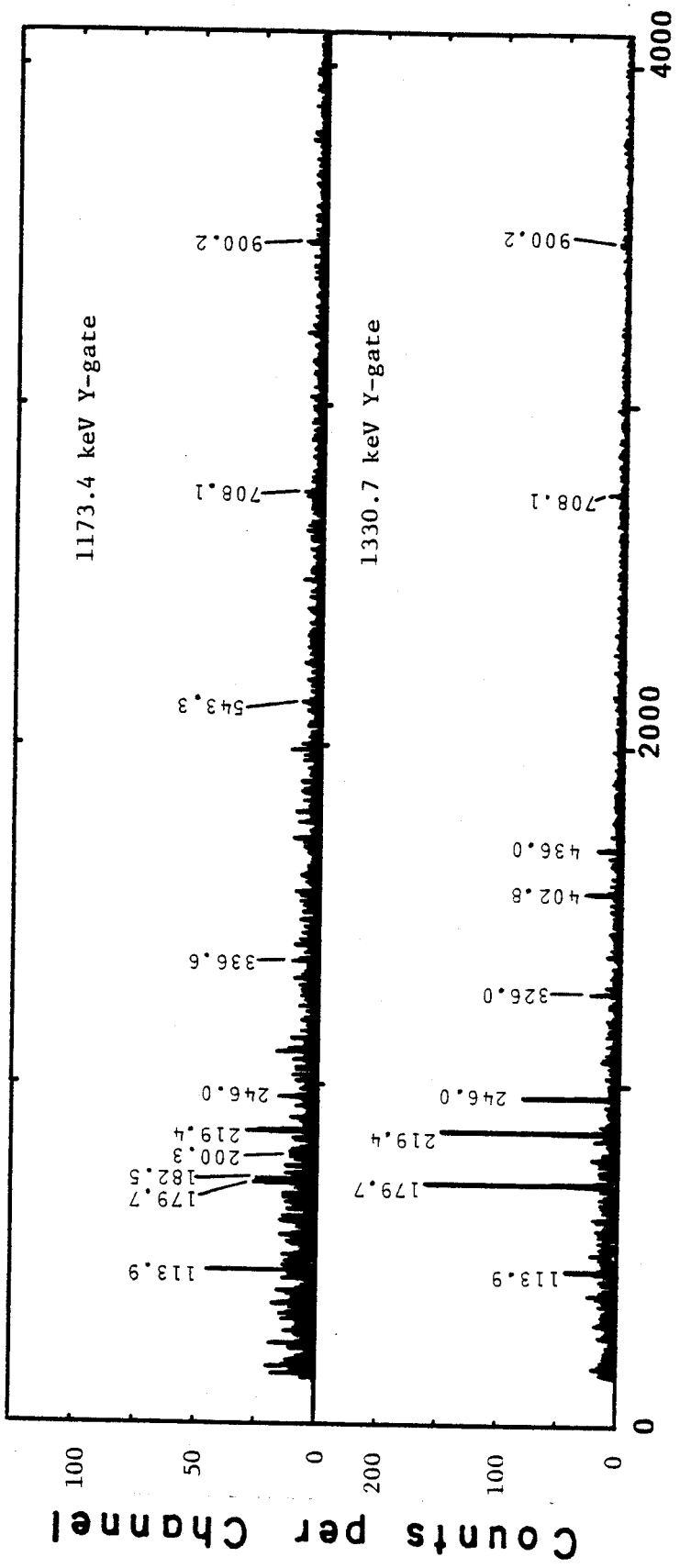

Figure I-2. (cont'd.).

APPENDIX J

Angular Distribution Plots of ^{139}Pr Transitions from $(\alpha,4n\gamma)$ Reaction.

Figure J. Angular distribution plots of ^{139}Pr transitions obtained from $(\alpha,4n\gamma)$ reaction. The data were taken in the 90-180° quadrant.

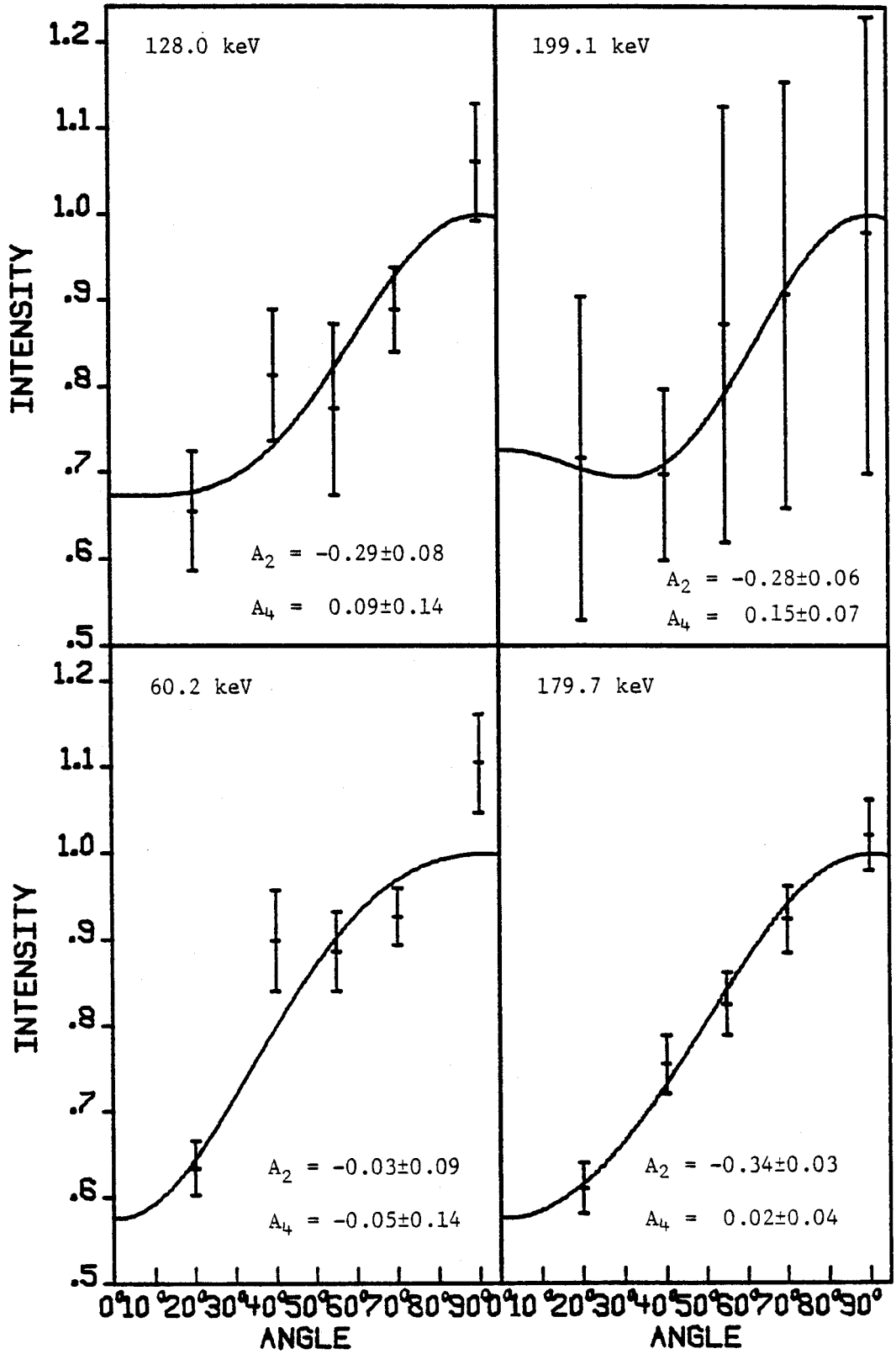
128.0 keV
A_2 = -0.29±0.08
A_4 = 0.09±0.14
199.1 keV
A_2 = -0.28±0.06
A_4 = 0.15±0.07
60.2 keV
A_2 = -0.03±0.09
A_4 = -0.05±0.14
179.7 keV
A_2 = -0.34±0.03
A_4 = 0.02±0.04
INTENSITY
INTENSITY
1.2
1.1
1.0
.9
.8
.7
.6
.5
0°10°20°30°40°50°60°70°80°90°
0°10°20°30°40°50°60°70°80°90°
ANGLE
ANGLE

Figure J.

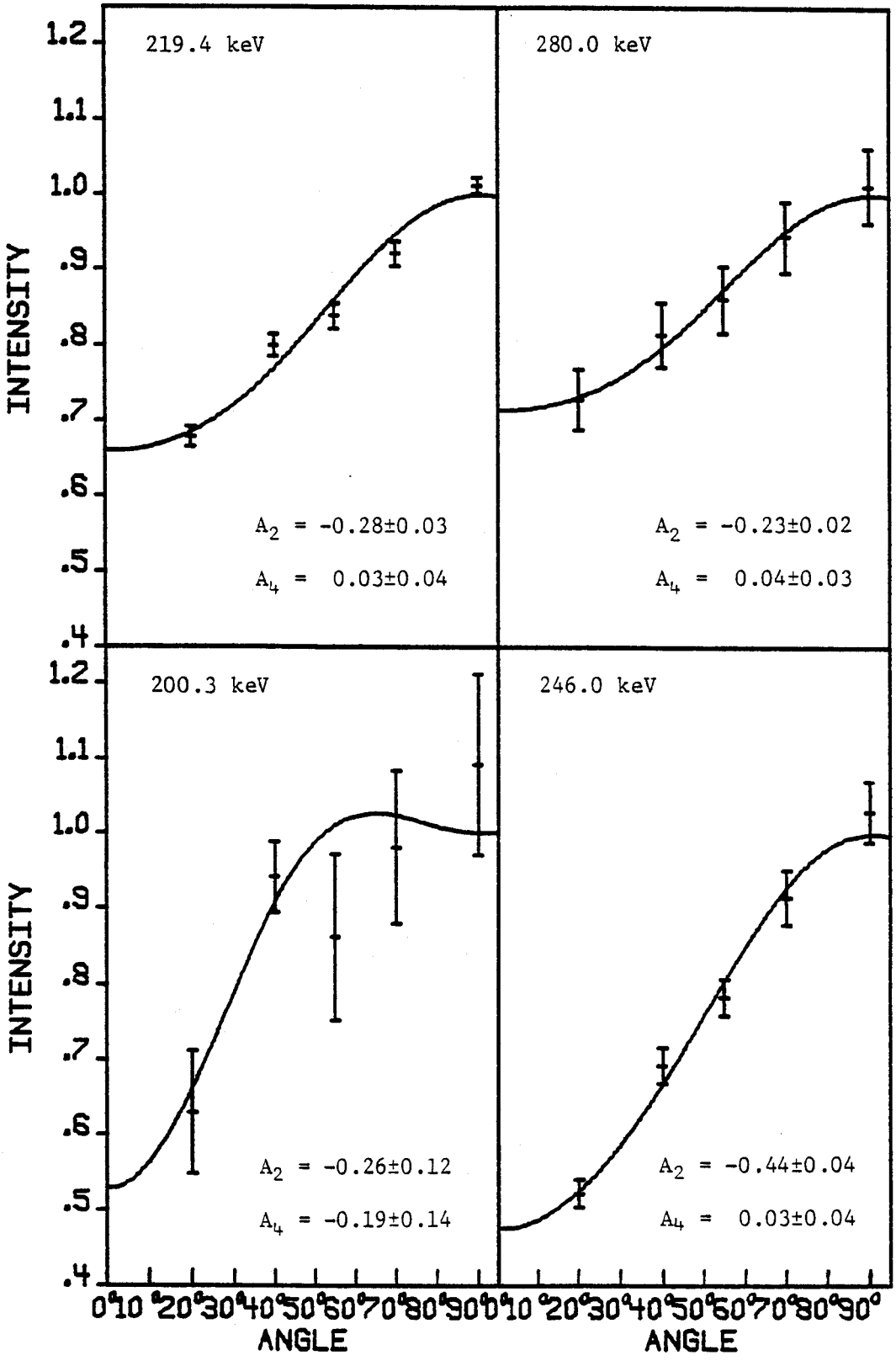

Figure J. (cont'd.).

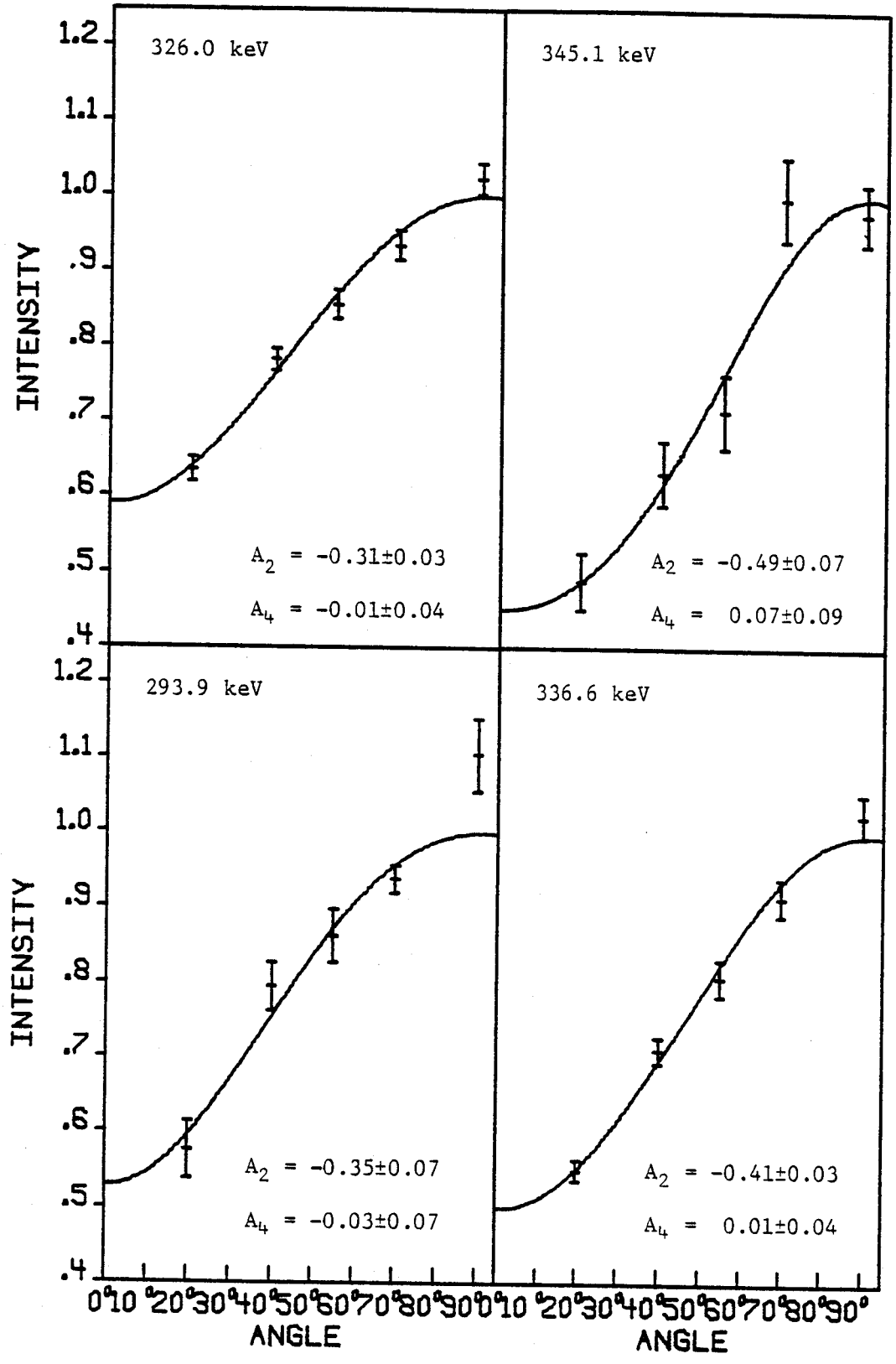

Figure J. (cont'd.).

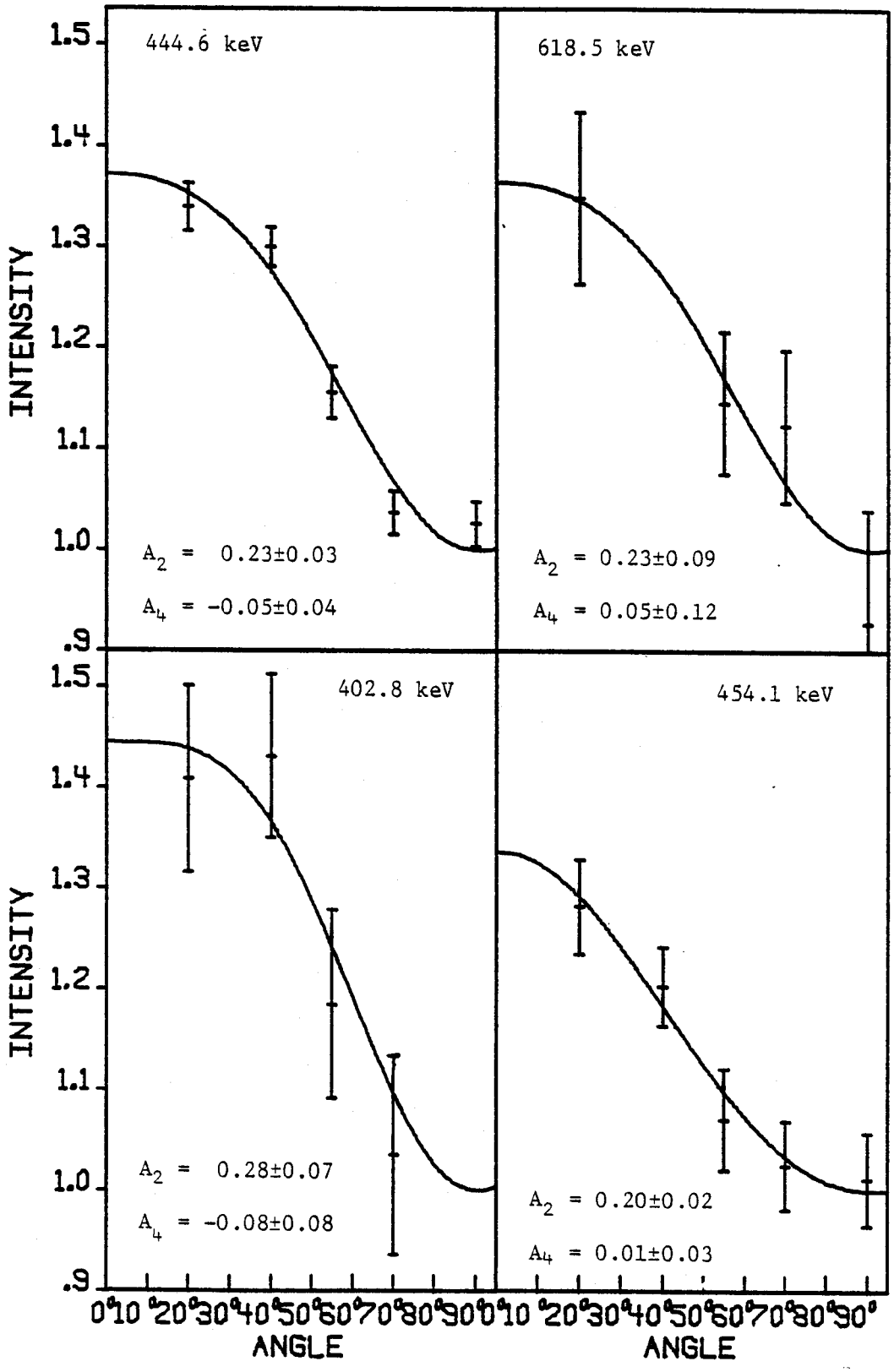

Figure J. (cont'd.).

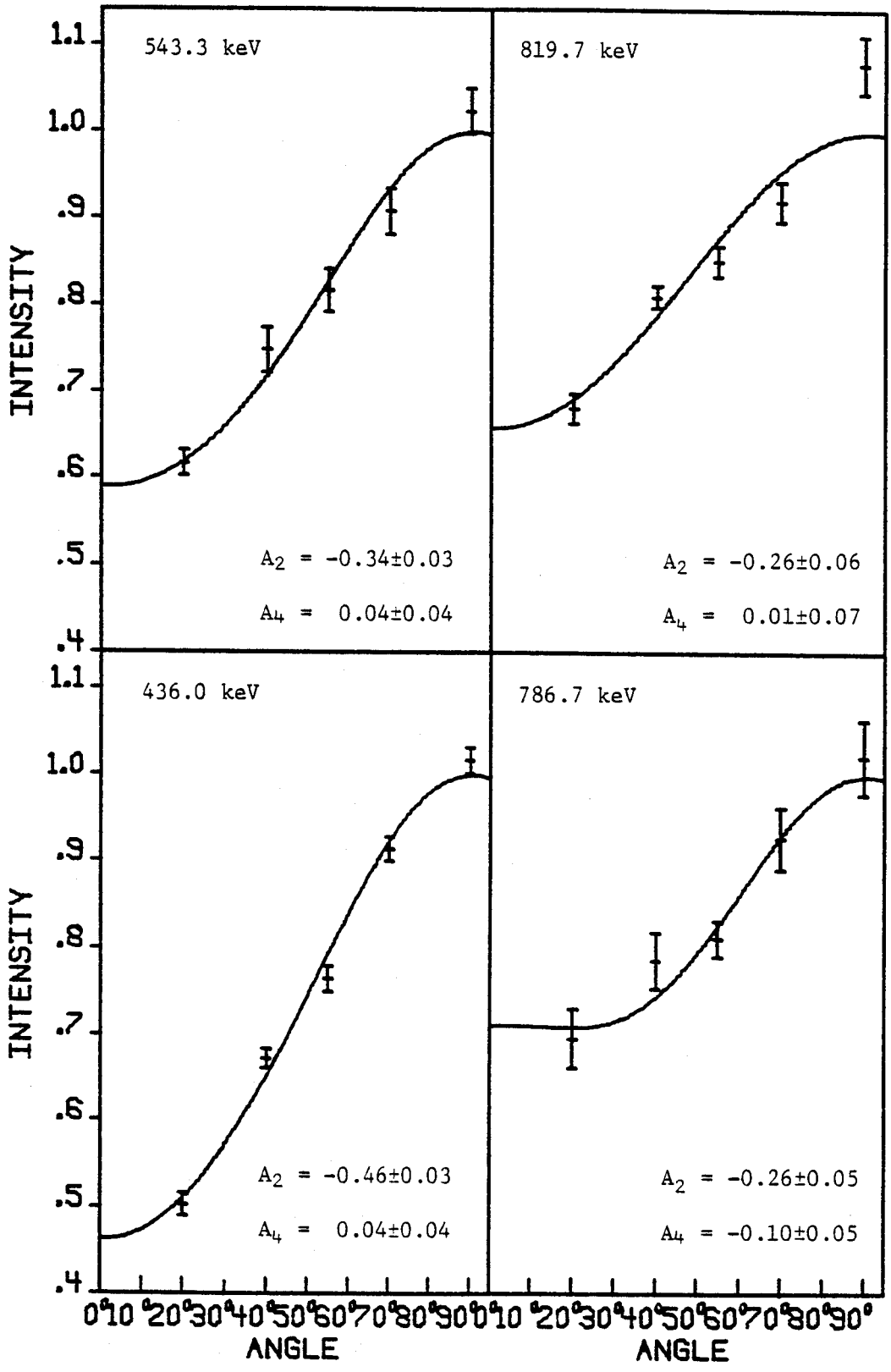

Figure J. (cont'd.).

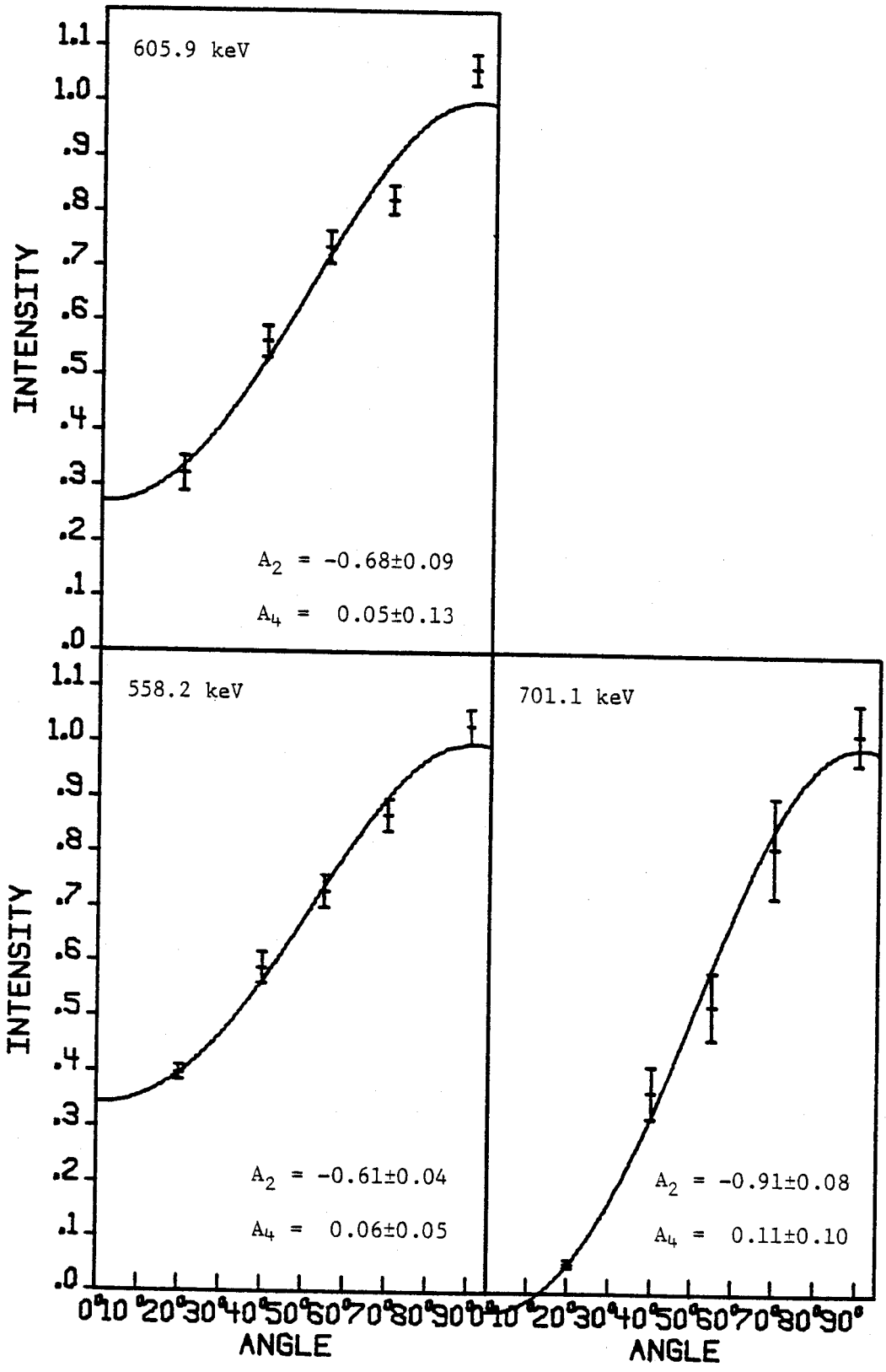

Figure J. (cont'd.).

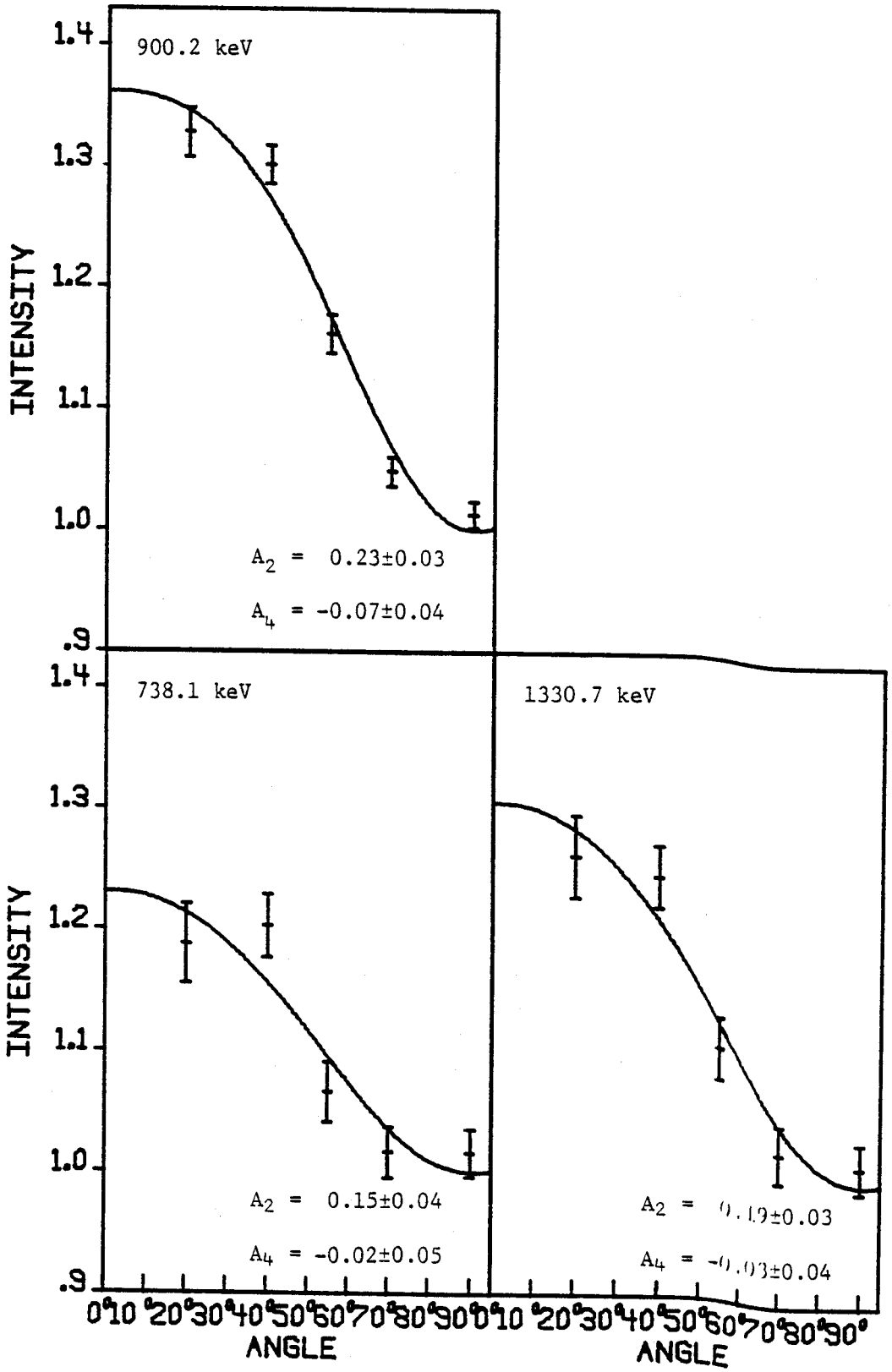

Figure J. (cont'd.).